UNIVERSITEIT VAN PRETORIA
UNIVERSITY OF PRETORIA
YUNIBESITHI YA PRETORIA

Textural Analysis and Plagioclase Grain Size Distribution of the Rooiberg Group, Bushveld Igneous Complex, South Africa.

Melissa Brown

14170435

Submitted in fulfilment of the requirement for the degree of Master of Philosophy in Geology in the Faculty of Agricultural and Natural Science at the University of Pretoria.

Supervisor: Professor Richard James Roberts

2024

Declaration

1. I understand what plagiarism entails and am aware of the University's policy in this regard.
2. I declare that this assignment is my own, original work. Where someone else's work was used (whether from a printed source, the Internet or any other source) due acknowledgement was given and reference was made according to departmental requirements.
3. I did not copy and paste any information directly from an electronic source (e.g., a web page, electronic journal article or CD ROM) into this document.
4. I did not make use of another student's previous work and submitted it as my own.
5. I did not allow and will not allow anyone to copy my work with the intention of presenting it as his/her own work.

Signature

3 January 2024

Date

ABSTRACT

The Rooiberg Group, occurring within the Kaapvaal craton at ~2,06 Ga, is a silicic large igneous province (SLIP), is a precursor to, and is synonymous with the Bushveld Igneous Province (BIC), the world's largest mafic body. The Rooiberg Group's volcanic successions, namely the Dullstroom, Damwal, Kwaggasnek, and Schrikkloof formations, were previously interpreted as largely consisting of lava flows, ranging from low- and high-Ti basalts to high-Mg rhyolites. Lenhardt et al. (2017) challenged the dominant lava-flow interpretations and proposed the Rooiberg Group is dominantly composed of highly welded, lava-like ignimbrites. In this study, petrographical and textural analysis was undertaken, and plagioclase grain size distributions studied throughout the Rooiberg Group formations to bring to light a clearer understanding of the Rooiberg Group's eruptional and emplacement styles, as well as the palaeoenvironment and volcanic origins. The Dullstroom and lower Damwal formations consist of lava flow sequences, whereas the upper Damwal, Kwaggasnek and Schrikkloof formations almost exclusively consist of ignimbrites originating from highly explosive pyroclastic eruptions, aligned with the increasingly siliceous composition of these formations. The Damwal, Kwaggasnek and Schrikkloof ignimbrites have various degrees of welding, ranging from non-welded ignimbrites displaying classic pyroclastic textures, to highly welded, lava-like and rheomorphic ignimbrites, that have often been misinterpreted as lava-flows due to the lava-like textures. The various degrees of welding reflect the welding continuum, where different degrees of welding may be found within a single pyroclastic flow cooling unit. The Rooiberg Group volcanics were emplaced in an alluvial to lacustrine palaeoenvironment, originating from caldera ring-fissure eruptions. Grain size distributions of the different formations possibly reveal that the remaining Rooiberg volcanic exposures are distal deposits, where the youngest formations (Kwaggasnek to Schrikkloof) reflect increasingly distal deposits. The Rooiberg Group occurs over an extensive area, where outcrops occur according to "fragments" or "packages", including the Nylstroom Package, Rooiberg Fragment, and Bothasberg Package.

Acknowledgements

I would like to first and foremost thank my supervisor, Professor James Roberts, for his constant support, guidance and patience. Prof. Roberts has never ceased to help and encourage me in my research endeavours. Thank you, James, for going out of your way to help me finish my master's degree. I would also like to thank Dr. Nils Lenhardt for allowing me to use some of his Rooiberg Group samples to work on, as well guiding me in the thin section work and lending his expertise regarding the Rooiberg Group rocks. A postgraduate degree is very difficult to achieve without support, so I would especially like to thank my very good friend, Sarita Downing, for supporting me constantly and not giving up on me. Immense gratitude is also expressed towards my husband, Kelvin Brown, for standing with me and continuously encouraging me. I extend a special thanks to my family, including my parents, sister, and mother-in-law, for their constant love and support. With my faith in the Lord and within His council and comfort in times of joy and difficulty alike, I was given strength and encouragement on numerous occasions, which pulled me through times of doubt. Without the Lord's interventions, this dissertation would not have been completed. The celebration of the completion of my master's degree, therefore, belongs to the Lord. Last but certainly not least, I would like to dedicate this thesis to my newborn son, Wren Kevin Brown. He spurred me on to finish what I started, and it is my hope that perhaps my labours would serve as inspiration to him one day.

Table of Contents

Chapter 5 - Discussion and Interpretation

List of Figures

List of Tables

Chapter 1 - Introduction

1.1. The Rooiberg Group Overview

The Rooiberg Group is an extensive, voluminous, felsic volcanic sequence with accompanying minor intercalated sediments deposited at ~ 2.06 Ga (Walraven, 1997) in northern central South Africa (figure 1). The Rooiberg Group terminates the Transvaal Supergroup (Willemse, 1969; Sharpe et al., 1982; Twist & French, 1983) and is a precursor to and felsic extrusive component of the Bushveld Igneous Complex, which is the largest intrusive layered igneous province in the world (Twist and French, 1983; Schweitzer & Hatton, 1995; Schweitzer et al., 1997; Ernst & Bell, 2010; Pankhurst et al., 2011; VanTongeren et al., 2016). The Rooiberg Group is conformably overlain by the sedimentary deposits of the Swaershoek Formation in the Nylstroom proto-basin, and by the Loskop Formation in the Cullinan-Witbank/ Middleburg Basin, initiating the sedimentary sequences of the Waterberg Supergroup (Martini, 1998; Mare et al., 2006).

The Rooiberg Group geochemistry has been well researched, but detailed mineralogical and textural analysis is lacking and the eruption styles, emplacement, and syn- and post-depositional processes of the Rooiberg Group volcanics are not yet well understood and are still debated today (Erickson & Cheney, 1992; Schweitzer et al., 1994; Schweitzer & Hatton, 1995; Lenhardt & Eriksson, 2012; Lenhardt et al., 2017). This can be attributed to the extensive alteration and age of the Rooiberg Group rocks, which can make accurate interpretations difficult. The major eruption style of the Rooiberg Group volcanics is also disputed, as many of the volcanic layers have previously been interpreted as lava flow deposits (Von Gruenewaldt, 1968; Clubley-Armstrong, 1977; Twist & French, 1983; Twist, 1985; Lenhardt and Eriksson, 2012), whereas Lenhardt et al. (2017) propose the majority of the Rooiberg Group volcanics are rather pyroclastic flow deposits that have undergone various degrees of welding. Highly welded and rheomorphic pyroclastic deposits are often misinterpreted as lava flow units, as rheomorphic ignimbrites have lava-like textures.

1.2. Aims

The aim of this study is to provide a more detailed textural analysis to further investigate the volcanic eruptional and emplacement styles in response to Lenhardt et al. (2017)'s study, as well as the syn- and post-depositional processes involved. Mineral textures will be studied to determine original volcanic textures and to distinguish original textures from alteration and overprinting textures. This will lead to a better understanding of emplacement processes and conditions of the Rooiberg volcanics, the extent of hydrothermal alteration, as well as distinguishing lava flow units from pyroclastic flow units.

The analysis of sedimentary and pyroclastic volcanic rock grains throughout a rock unit is a very useful sedimentological technique to determine overall grain sizes, how rounded or angular the grains or clasts are, and surface textures of grains; indicating textural maturity, the distribution of grain sizes, and sorting and grading of grain sizes (Krumbein and Sloss, 1963). This is important to establish palaeoenvironments in which the sediments were deposited, the nature and duration of transport of said sediments, as well as depositional processes and conditions (McManus, 1988).

Lateral grain size distribution analysis of tephra fallout deposits distinguishes vent and proximal lithofacies from medial to distal lithofacies, where larger grain sizes occur closer to the vent of the volcano, with decreasing grain sizes coinciding with furthering distances from the vent (Fisher, 1964). Sorting of volcanic grain sizes can indicate what type of deposit is being studied, for example, well sorted grains correspond with fallout deposits, whereas poorly sorted grains point to flow or surge deposits (Murai, 1961; Fisher, 1964). Regarding pyroclastic flow deposits, grain sizes may be graded vertically through a rock unit, where the basal zone of the deposit consists of coarse grains (Sohn, 1997), with decreasing grain size towards the top of the rock unit (Walker 1984).

Grain size distribution of plagioclase phenocrysts of the volcanic rocks of the Rooiberg Group is investigated to analyse any possible patterns that may exist. Analysis of plagioclase grain sizes may distinguish lava flow deposits, fallout deposits and pyroclastic flow deposits from each other. Variation of plagioclase grain sizes may also indicate proximal or distal deposits of the Rooiberg Group formations.

1.3. Hypotheses

It is proposed that the older formations of the Rooiberg Group, namely the Dullstroom and Lower Damwal formations, consist mainly of lava flow deposits, corresponding with their more mafic to intermediate chemical compositions (Schweitzer et al., 1995), resulting from more effusive eruptions. The younger Rooiberg Group formations, namely the Upper Damwal Formation, Kwaggasnek and Schrikkloof formations consist of predominantly to exclusively pyroclastic flow deposits as the chemical composition evolves to increasingly siliceous towards the top of the group. Volcanic textures of the upper Rooiberg Group formations have been previously misinterpreted as lava flow deposits due to welding of ignimbritic deposits, resulting in lava-like textures. This confirms Lenhardt, et al. (2017)'s research and conclusions. Grain size analysis of plagioclase crystals will show insight to depositional patterns of studied rock samples. Proximal versus distal deposits are likely not to be distinguished in this study, as pyroclastic flow deposits exhibit poor sorting textures.

Chapter 2 - Literature Review

2.1. The Rooiberg Group

2.1.1. Location and extent

The Rooiberg Group consists of extensively layered volcanic rock, approximately 3 to more than 5 km thick (Von Gruenewaldt, 1968), with an estimated volume of 350 000 km^3 erupted material (Twist and French, 1983; Eriksson et al., 1995; Cawthorn and Walraven, 1997). The Rooiberg Group is estimated to have once originally covered a surface area of more than 200 000 km^2 (Cawthorn and Walraven, 1997) across the Kaapvaal Craton, and currently covers an accumulated area of 50 000 to 67 000 km^2 (Willemse, 1969). Prominent outcrops of the Rooiberg Group fall within the confines of the Bushveld Igneous Complex (BIC) (Twist and French, 1983) and are found in three main locations in South Africa (figure 1). These include Mpumalanga from approximately Rust de Winter extending eastwards towards Loskop Dam and Dullstroom; Limpopo extending from Mokopane (previously Potgietersrus) south-westwards in an arc to Nylstroom and Bela-Bela (previously Warmbaths); and in the Rooiberg region, found directly West from Bella-Bella (Schweitzer et al., 1995).

The Rooiberg Group outcrops have been subdivided into “fragments” and “packages” by Schweitzer et al. (1995) according to the above mentioned geographic locations. They include the Rooiberg Fragment in the West (Rooiberg region), the Nylstroom Package (Mokopane to the Nylstroom and Bella-Bella regions) in the North, the Bothasberg Package (Loskop Dam region) in the East, and the Stavoren Fragment, further East close to Dullstroom, containing the basal Dullstroom Formation. This can be studied in figure 1 and figure 2. The location of this study includes the Loskop Dam and Dullstroom volcanics, which are estimated to be 3 520 m thick in the north to a maximum of 5 110 m towards the northeast (Clubley-Armstrong, 1977; Twist, 1985), forming part of the Bothasberg Package; as well as the Nylstroom volcanics, part of the Nylstroom Package.

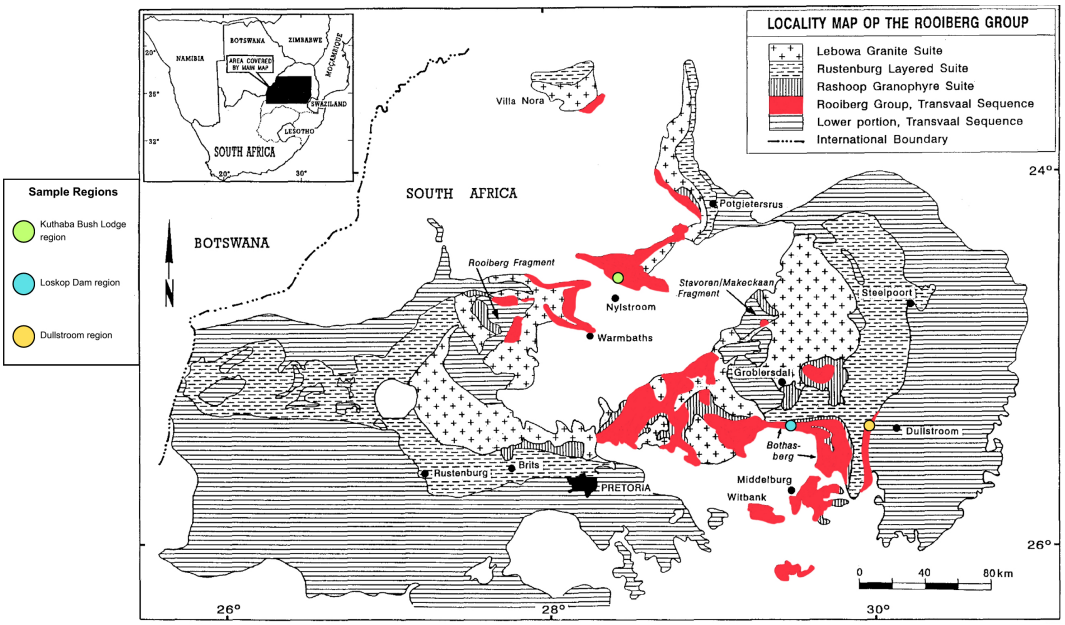

Figure 1. The distribution and extent of the remaining Rooiberg Group volcanic rocks, highlighted in red, outcropping within the bounds of the Bushveld Igneous Complex, north-central South Africa. Sample regions for this study are included, namely the Kuthaba Bush Lodge region, the Loskop Dam region, and the Dullstroom region (modified after Schweitzer, 1995, modified after Walraven, 1982).

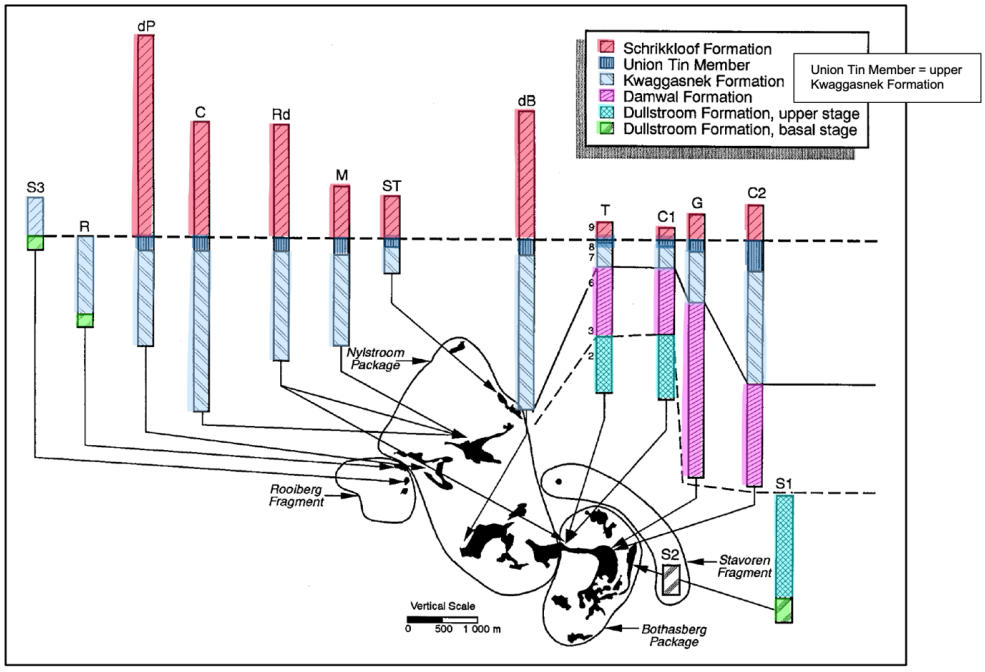

Figure 2. Diagram of the geographical distribution and stratigraphic thickness of each Rooiberg Group Formation. The abbreviations represent the literature and study undertaken by the following researchers: C1 & C2 - Clubley-Armstrong (1977); C – Coetzee (1970); dB – De Bruiyn (1980); dP – Du Plessis (1976); G – Von Gruenewaldt (1968); M – Menge (1969); Rd – Rhodes & Du Plessis (1976); R – Richards (1987); ST – Strauss (1954); S1-3 – Schweitzer et al. (1995); T – Twist (1985); (modified after Schweitzer et al., 1995).

2.1.2. Regional geology

The Rooiberg Group extrusions began at approximately 2071 +94/-65 Ma during the Early Palaeoproterozoic with deposition of first the Dullstroom and then the Damwal formations (Buchanan et al., 2004). These formations were deposited in the Transvaal intracratonic basin on the Kaapvaal Craton, terminating the volcano-sedimentary successions of the Transvaal Supergroup (Eriksson et al., 2005). The Transvaal Supergroup of ca. 2.7-2.1 Ga (Eriksson and Reczko, 1995; Eriksson et al., 1995; Walraven and Martini,1995) is one of the thickest Archaean-Palaeoproterozoic volcano-sedimentary basin-fills (Button, 1986). The Transvaal Supergroup was preceded by the Witwatersrand Supergroup (ca. 3.1-2.8 Ga), the Earth's most ancient sedimentary basin having formed syn-cratonisation and Kaapvaal terrane accretion (Robb and Meyer, 1995; Eriksson et al., 2005); and the Ventersdorp Supergroup of ~ 2.7 Ga (Armstrong et al., 1991) consisting predominantly of ultramafic to mafic volcanic rocks, possibly originating from a mantle superplume event (Eriksson et al., 2002; Eriksson et al., 2005). The volcano-sedimentary basins pre-dating the Rooiberg Group can be seen in figure 3 below:

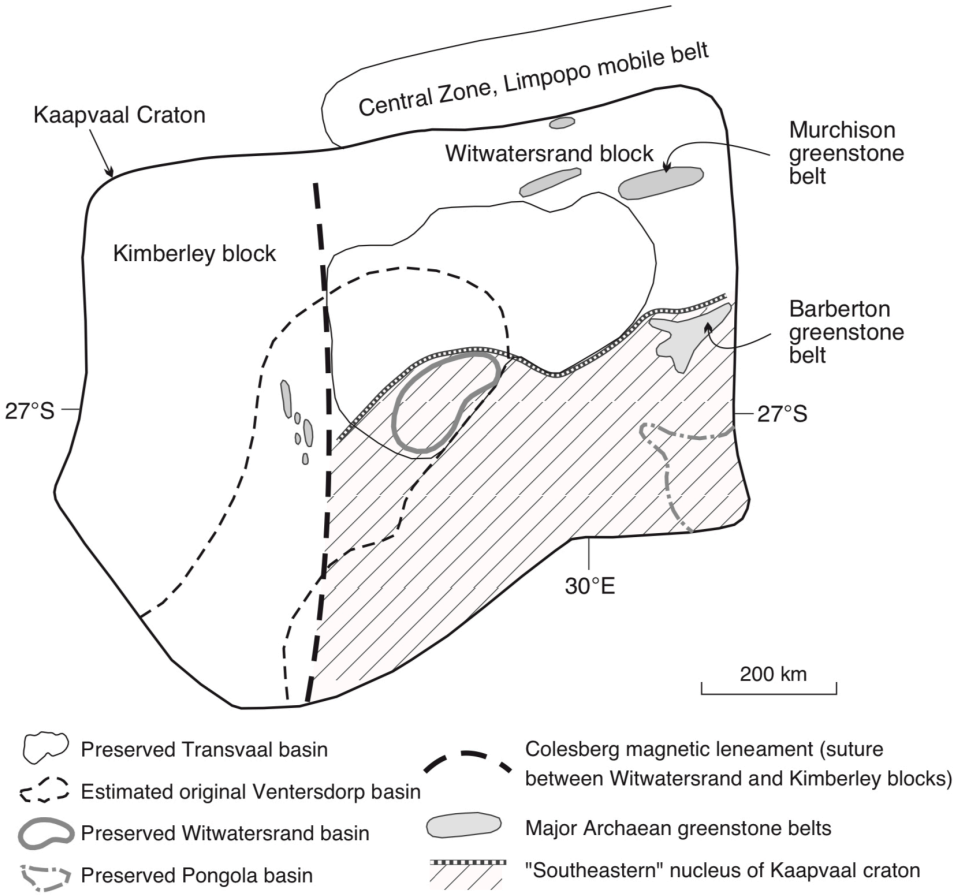

Figure 3. The regional depositional context of the Rooiberg Group on the Kaapvaal craton, including the preserved boundaries of the Witwatersrand and Transvaal basins, and the estimated original Ventersdorp Basin (Eriksson et al., 2005).

The Transvaal Supergroup begins with protobasinal volcanic rocks and fining upward siliciclastic rocks deposited in deep extensional basins (Eriksson and Reczko, 1995; Eriksson et al., 2005) of approximately Ventersdorp age (Eriksson et al., 1995), coeval with the Limpopo orogeny (Eriksson and Reczko, 1995). The protobasinal rocks are unconformably overlain by the Black Reef sandstones deposited in a sag basin related to thermal subsidence. Chemical sedimentation within an inland sea resulted in the Chuniespoort Group carbonates and banded iron formations (BIFs), uncomformably overlying the Black Reef Formation. A time gap of approximately 80 Ma along with an erosional angular unconformity follows the Chuniespoort Group and precedes the Pretoria Group (Bumby et al., 1998). The Pretoria Group was deposited in the central Transvaal Basin and precedes the ~ 2,06 Ga (Walraven, 1997) Rooiberg volcanics and is intruded by the ~ 2,05 Ga (Hatton, 1995) Bushveld layered intrusions (Bumby et al., 1998; Cawthorn et al., 1981; Eriksson and Reczko, 1995).

The Pretoria Group predominantly consists of alternating mudrock and quartz-rich sandstones, most of which have been metamorphosed to quartzite (Eriksson et al., 1993a, 1995; Eriksson and Reczko, 1995), with basaltic-andesitic lava flow interbeds, such as those from the subaerial Hekpoort Formation (Harmer and von Gruenewaldt, 1991), as well as minor conglomerates and carbonate rocks. The Pretoria Group depositional settings of alternating alluvial and lacustrine deposits to shallow and deep marine deposits (in an epeiric sea) are due to cyclical pre-rift uplift, extensional rift settings, and thermal subsidence (Eriksson et al., 1995, 2001b; Eriksson and Reczko, 1995), related to global eustacy of second-order sea level changes (Catuneanu and Eriksson, 1999; Eriksson et al., 2005). This can be studied in detail in figure 3.

Compressional tectonic activity occurred post-Pretoria Group and pre-Rooiberg volcanism and Bushveld magmatism, resulting in two different compressional events. This led to the folding of the Pretoria Group rocks. The first compressional event resulted in SE-NW trending folds, which were then re-folded by the second compressional event, resulting in ENE-SWS trending folds (Bumby et al., 1998). This signifies a significant change in tectonic setting during the time gap between the Pretoria Group and the unconformably overlying Rooiberg felsites (Eriksson et al., 2005).

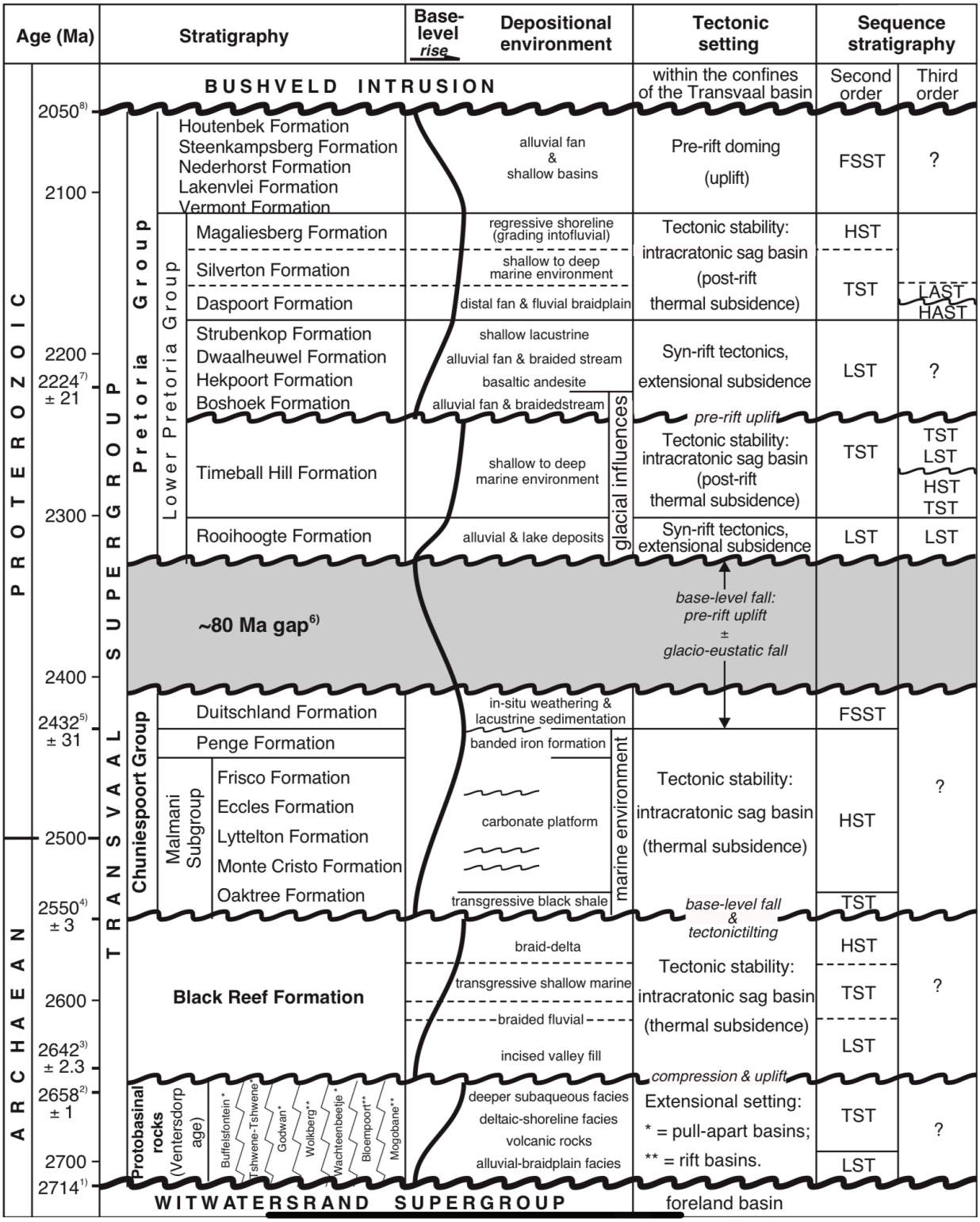

Figure 4. Summarised volcano-sedimentary successions and palaeo-environments of the Transvaal Supergroup, before the volcanic extrusions of the Rooiberg Group (Eriksson et al., 2001b, 2005).

2.1.3. Stratigraphic sequences

Stratigraphic sequences were initially difficult to decipher due to the massive nature and extensive thickness of the Rooiberg rocks, as well as limited geochemical data analysis. Different successions were originally established by relying on colour, texture and structural differences (Lombaard, 1932; Wolhuter, 1954; Twist and French, 1983; Twist, 1985). Twist (1985) subdivided the Rooiberg Group into nine consecutive units with minor intercalating sedimentary rock deposits, with the Rustenburg Layered Suite (RLS) from the BIC at the base of Unit 1 (figure 5). Initial established successions are not accurate due to colouring and texture attributes not being exclusive to one stratigraphic sequence (Eriksson et al., 1993; Schweitzer & Hatton, 1995; Schweitzer et al., 1995). This is due to ubiquitous hydrothermal alteration of the Rooiberg Group (Eriksson & Cheney, 1992; Eriksson et al., 1993; Schweitzer & Hatton, 1995).

With the advancement of geochemical analysis, the Rooiberg Group is subdivided into four formations, namely in chronological order: the Dullstroom Formation (oldest), Damwal Formation, Kwaggasnek Formation, and the Schrikkloof Formation (youngest and most siliceous). Outcrops of the lower formations of the Rooiberg Group occur in more localised regions, whereas the upper formations are more extensive and widespread (Hatton and Schweitzer, 1995; Schweitzer et al., 1995).

Schweitzer (1995) arranged the geographical distribution of the Rooiberg Group rocks according to the locations of the different formations, which includes the Rooiberg Fragment to the West (containing the basal stage of the Dullstroom Formation which is intercalated with the Smelterskop Formation, overlain by rhyolites of the Schrikkloof Formation), the Nylstroom Package (including the Kwaggasnek and Schrikkloof formations only, occurring in the North central location of the Rooiberg volcanics), and the Bothasberg Package to the East (containing all four formations) (Stear, 1977; Richards, 1987;Schweitzer, 1995). For a detailed account of the geographical distribution and thickness of each Rooiberg Group Formation, see figure 2.

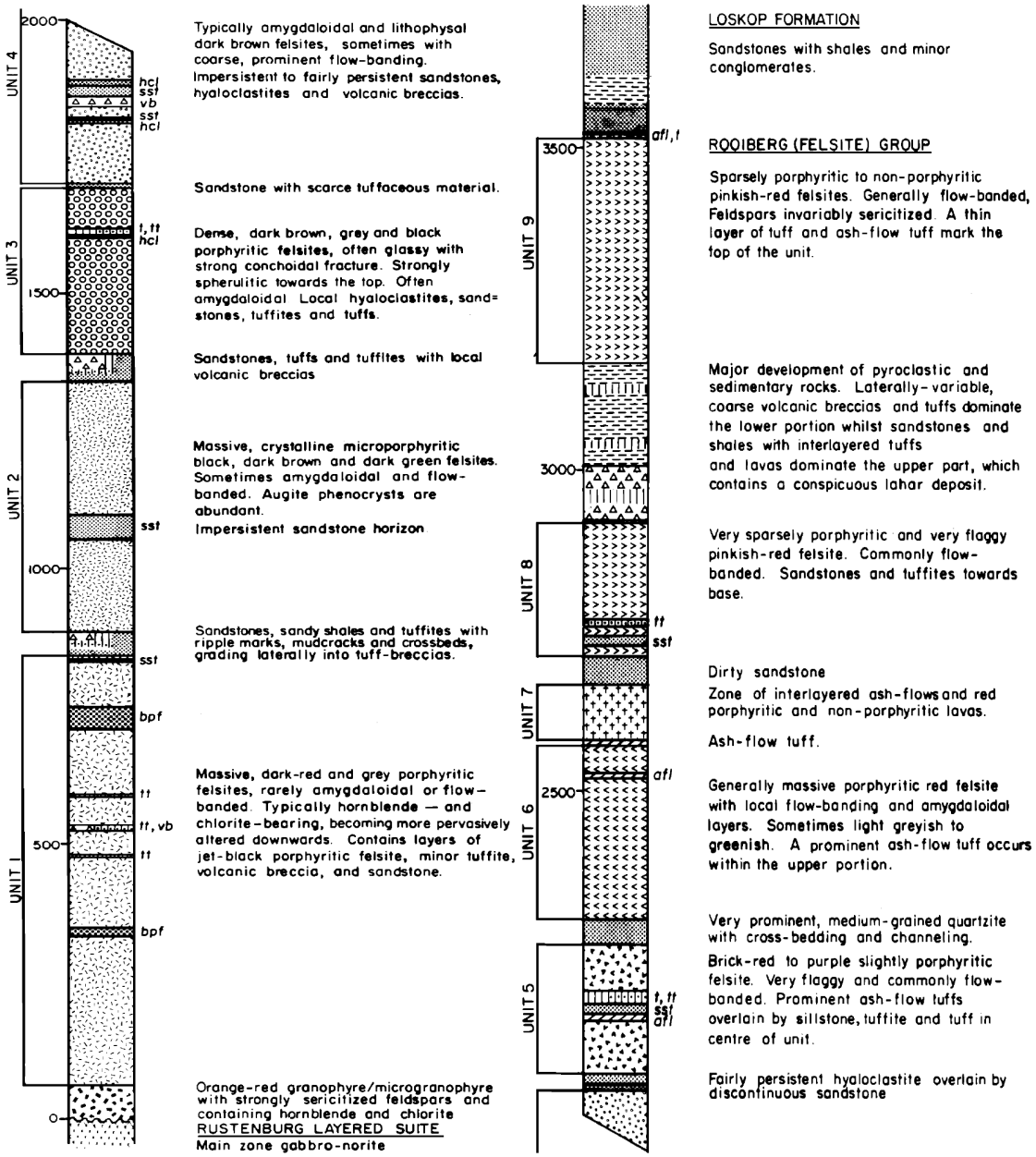

Figure 5. The Rooiberg Group initially subdivided into 9 consecutive units, based on rock studies from the Loskop Dam area (Bothasberg Package). Abbreviations are as follows: sst- sandstone; hcl- hyaloclastite; afl- ash-flow tuff; t- tuffite; vb- volcanic breccias; bpf- black porphyritic felsite. (Twist, 1985).

2.1.4. Geochemistry

The four formations of the Rooiberg Group each differ geochemically according to magma type. There are nine different magma types in total, where the Dullstroom Formation contains six of the nine magma types (Hatton and Schweitzer, 1995). The Dullstroom Formation comprises a Basal Stage and an Upper Stage. The Basal Stage is composed of low titanium (LTI) basaltic andesites, basal rhyolites, high magnesium felsites (HMF), where “felsite”- an older, outdated term- is rhyolitic and dacitic in composition (IUGS, 1989), and high titanium basalts (HTI) (Hatton and Schweitzer, 1995; Schweitzer et al., 1995). The Basal Dullstroom lava flow deposits contain sedimentary xenoliths, discontinuous, intercalated pyroclastic flow deposits and sedimentary rock (Schweitzer et al., 1995).

The Upper Dullstroom Formation consists of HTI basalts, high Ti-Fe-P andesites, high magnesium felsites and low magnesium felsites (LMF). The HMF of the Upper Stage are the equivalent of Units 1 and 2 studied and categorised by Twist (1985) (Schweitzer et al., 1995). The Upper Stage contains localised regions of intercalated sedimentary rock and pyroclastic deposits (Schweitzer et al., 1995). The LTI basaltic andesites and the HTI basalts are intercalated towards the bottom of the Dullstroom Formation. The LMF and HMF are more dominant than the high Ti-Fe-P andesites toward the top of the Dullstroom Formation (Hatton and Schweitzer, 1995; Schweitzer et al., 1995). The Basal and Upper Stage of the Dullstroom Formation are separated by the intruding RLS (figure 7). The Upper Dullstroom Formation and the remaining Rooiberg Group successions roof the BIC (Hatton and Schweitzer, 1995; Schweitzer et al., 1995).

The Damwal Formation consists of the high Ti-Fe-P andesites, the HMF and predominantly of the low magnesium rhyolites. The Kwaggasnek and Schrikkloof formations are compositionally entirely comprised of the low magnesium felsites with only small chemical variations. (Hatton and Schweitzer, 1995; Schweitzer et al., 1995). The lithologies and magma types of the Rooiberg Group formations can be studied in detail in figures 6 and 7.

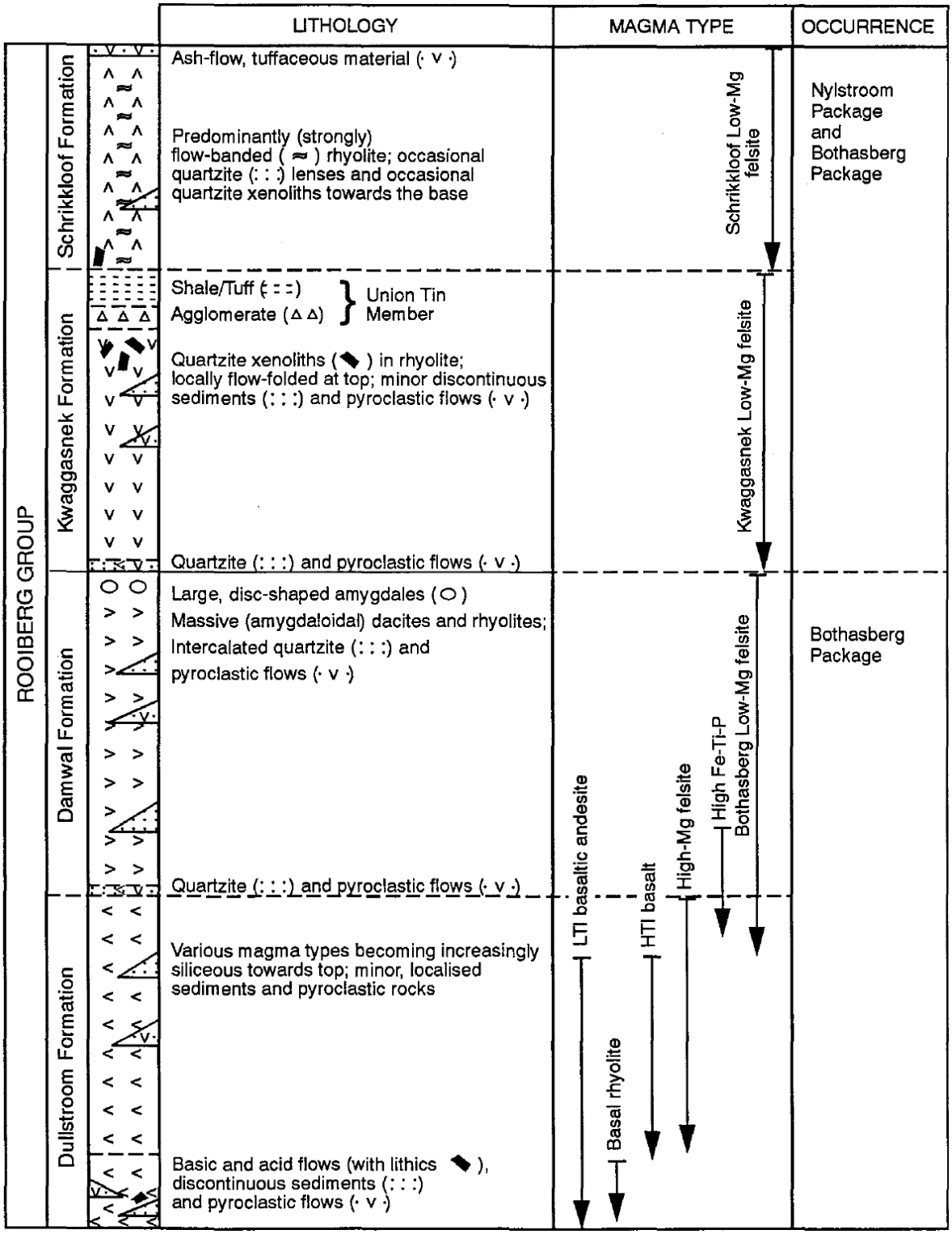

Figure 6. Stratigraphy and geochemistry of the Rooiberg Group formations, which includes the Dullstroom, Damwal, Kawaggasnek, and Schrikkloof formations. The Dullstroom floor rocks are also included in the Bothasberg Package (Schweitzer et al., 1995).

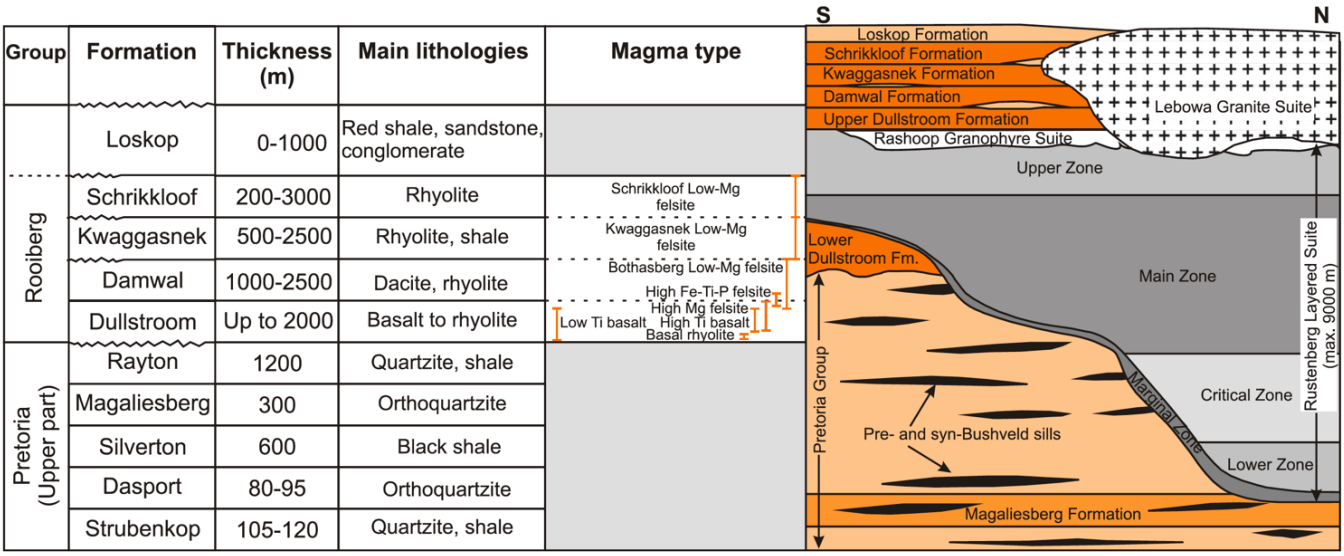

Figure 7. The thicknesses, lithologies, and magma types of the Rooiberg Group formations. The Rooiberg formations unconformably overly the Upper Pretoria Group of the Transvaal Supergroup and are overlain by the Loskop Formation of the Waterberg Group. The Rooiberg Group is intruded by the Bushveld Igneous Complex (Lenhardt, et al., 2017; modified after SACS, 1980; Walraven, 1982; Harmer and Sharpe, 1985; and Schweitzer et al., 1995).

Overall, the SiO_2 content increases from the basal rhyolites of the Dullstroom Formation towards the top of the Rooiberg Group succession (Buchanan et al. 1999, 2002, 2004; Lenhardt and Eriksson, 2012) and the MgO, Al_2O_3, TiO_2 and P_2O_5 contents decrease towards the top of the Rooiberg succession (Schweitzer et al., 1995; Hatton and Schweitzer, 1995; Buchanan et al., 2002; Lenhardt and Eriksson, 2012; Lenhardt et al., 2017). Na_2O and K_2O are prevalent in all the formations with somewhat haphazard trends, which can be attributed to the fact that Na_2O and K_2O predominantly make up feldspars, which occur as main mineral phases throughout the Rooiberg sequences (Lenhardt et al., 2017). This can be studied in figures 8 and 9.

The chemostratigraphy graph in figure 8 displays the distinct chemical signatures for each formation for the Loskop Dam area. The Damwal Formation has an average of 68 wt% SiO_2 content that only slightly increases towards the topmost sequences of the formation. TiO_2 decreases from 0,64 to 0,44 wt% from the bottom to the top of the formation and MgO distinctly decreases from approximately 0,9 to 0,1 wt%. P_2O_5 slightly increases from 0,07 to 0,23 wt% from the bottom to the top of the formation. The Damwal Formation is enriched in $Fe_2O_{3(total)}$ of 5,8 to 9,9 wt% and is relatively depleted in Lu (0,52-0,98 ppm), a compatible trace element (Joyalemi, 2015; Lenhardt et al., 2017).

The Kwaggasnek Formation increases in SiO_2 from the bottom to the top of the formation from 68,9 to 80,8 wt%. TiO_2 is relatively low and only slightly decreases from 0,42 to 0,36 wt%. MgO contents are very low consistently throughout the formation from 0,12 to less than 0,01 wt%. P_2O_5 decreases from the bottom to the top of the formation from 0,08 to 0,02 wt%. $Fe_2O_{3(total)}$ displays a more random trend with intermediate concentrations from 1,1 to 7,4 wt%. Lutetium increases from the bottom to the top of the formation from 0,2 to 0,97 ppm, possibly signifying an increase in amphibole crystallisation (Joyalemi, 2015; Lenhardt et al., 2017).

The Schrikkloof Formation contains the highest concentration of SiO_2, ranging from 73,5 to 79,5 wt%. TiO_2, P_2O_5, MgO concentrations are low, ranging from 0,21 to 0,29 wt%; 0,01 to 0,05 wt%; and 0,02 to 0,3 wt% respectively. Fe_2O_3 is relatively low, ranging from 3,37 to 4,38 wt%. Lutetium increases further from the bottom to the top of the formation from 0,61 to 1,22 ppm (Joyalemi, 2015; Lenhardt et al., 2017).

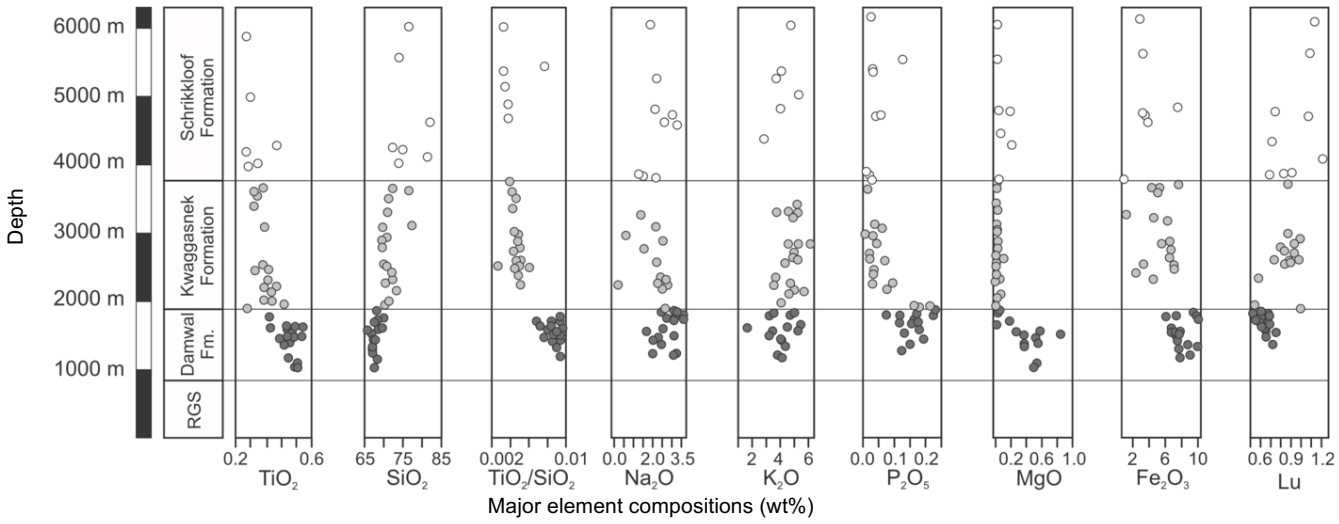

Figure 8. Major element compositions according to depth and corresponding formations (Damwal to Schrikkloof, with the underlying Rashoop Granophyre Suite [RGS] of the BIC) of the Rooiberg Group, based on the Loskop Dam area, (Lenhardt et al., 2017; data taken from Joyalemi, 2015).

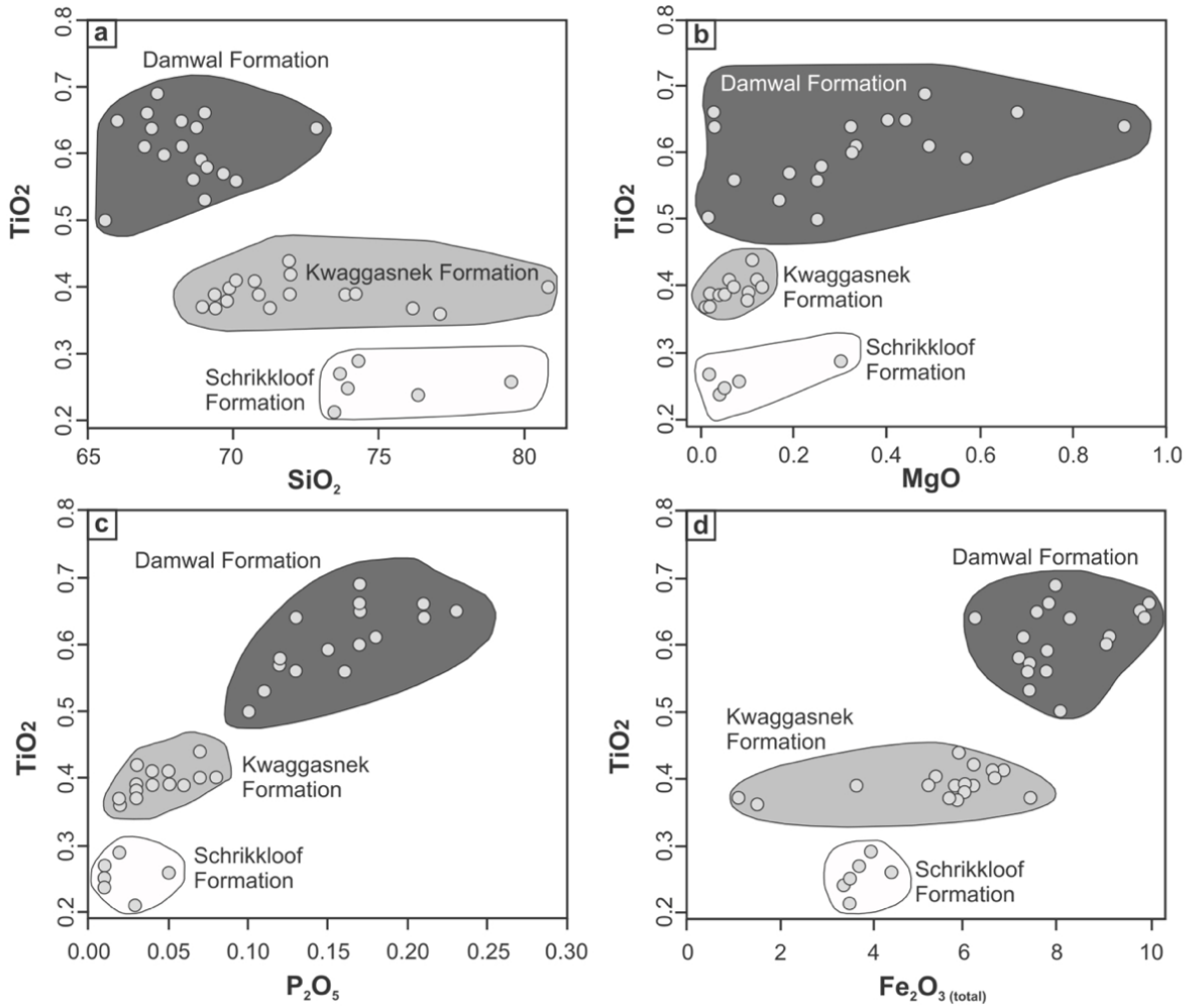

Figure 9. Major element bivariate plots by Lenhardt et al. (2017) of (a) TiO_2 vs. SiO_2, (b) TiO_2 vs. MgO, (c) TiO_2 vs. P_2O_5, and (d) TiO_2 vs. $Fe_2O_{3(total)}$, to chemically distinguish the different formations within the Rooiberg Group, (Lenhardt et al., 2017; boundaries by Schweitzer et al., 1995 & Hatton and Schweitzer, 1995).

In addition, Mathez et al. (2013) categorised the Rooiberg lavas into two distinct groupings- magnesian and ferroan lavas. The Dullstroom LTI and HMF lavas are magnesian, whereas the Dullstroom LMF, Damwal LMF, Kwaggasnek LMF, and Schrikkloof LMF lavas are all ferroan lavas. The magnesian lavas are also calcic to slightly calc-alkalic (figure 10), similar to that of calc-alkaline granitoids originating from subduction zone margins (Frost et al., 2001), and are suggested to have an upper mantle source previously influenced by Archaean subduction processes of the Kaapvaal craton (Mathez et al., 2013). Buchanan et al. (1999), however, propose that LTI and HMF Dullstroom rocks (magnesian lavas) originate from a lithospheric source with 20-30% upper continental crust assimilation accompanied by fractional crystallisation of pyroxene and plagioclase, signifying the onset of Bushveld magmatism.

The ferroan lavas are suggested to have a different source, that of basaltic liquids, synonymous to the Rustenberg Layered Suite of the BIC, that underwent fractional crystallisation (Mathez et al., 2013; Van Tongeren et al., 2010). The Dullstroom LMF and Damwal LMF ferroan lavas are calc-alkalic to alkali-calcic and are metaluminous, whereas the Kwaggasnek and Schrikkloof LMF ferroan lavas are calc-alkalic to alkali-calcic and are fairly peraluminous (Mathez et al., 2013).

Trace element compositions further distinguish the magnesian and ferroan lavas, where the magnesian lavas (figure 11a) are more enriched in the compatible trace elements and depleted in incompatible trace elements. The ferroan lavas (figure 11b) are depleted in compatible trace elements, specifically in scandium, vanadium, chromium, copper, nickel and strontium and are more enriched in incompatible trace elements.

Incompatible trace element trends, including the rare earth elements (REEs), can be studied in figure 12, showing an increase in concentration towards the top of the Rooiberg Group sequence. There is an increasingly pronounced negative Eu anomaly from the Upper Dullstroom to Schrikkloof formations (Buchanan, 2006; Mathez et al., 2013).

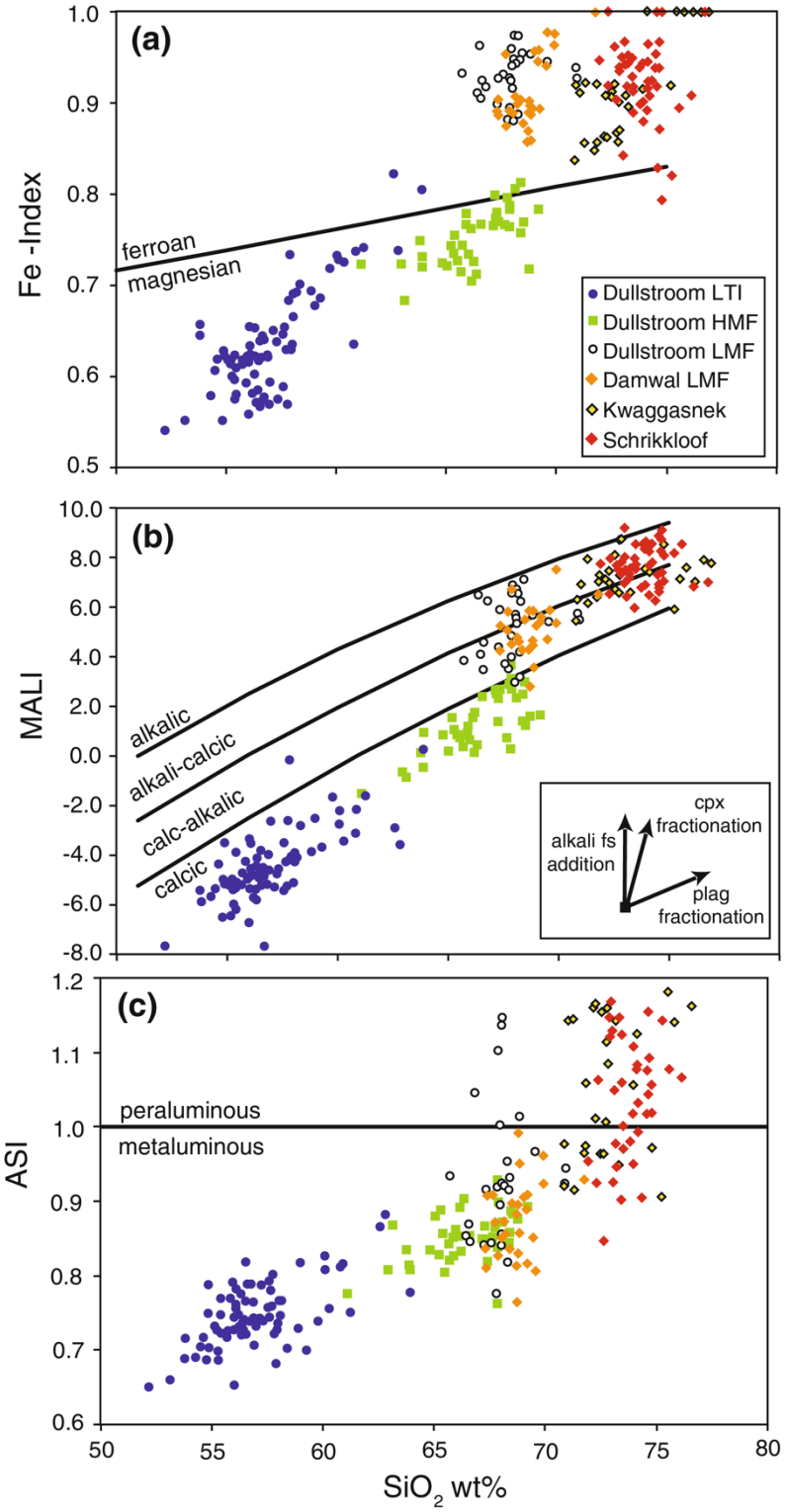

Figure 10. The Rooiberg Group magma types on bivariate plots of (**a**) Fe-Index (wt% of FeO_T/FeO_T + MGO) vs. SiO_2, (**b**) MALI (wt% of Na2O + K_2O – CaO) vs. SiO_2, and (**c**) ASI (atomic% of Al/[Ca – 1,67P + Na + K]) vs. SiO_2, distinguishing the ferroan and magnesian lavas; calcic, calc-alkalic to alkali-calcic; and metaluminous and peraluminous compositions from each other (Mathez et al., 2013).

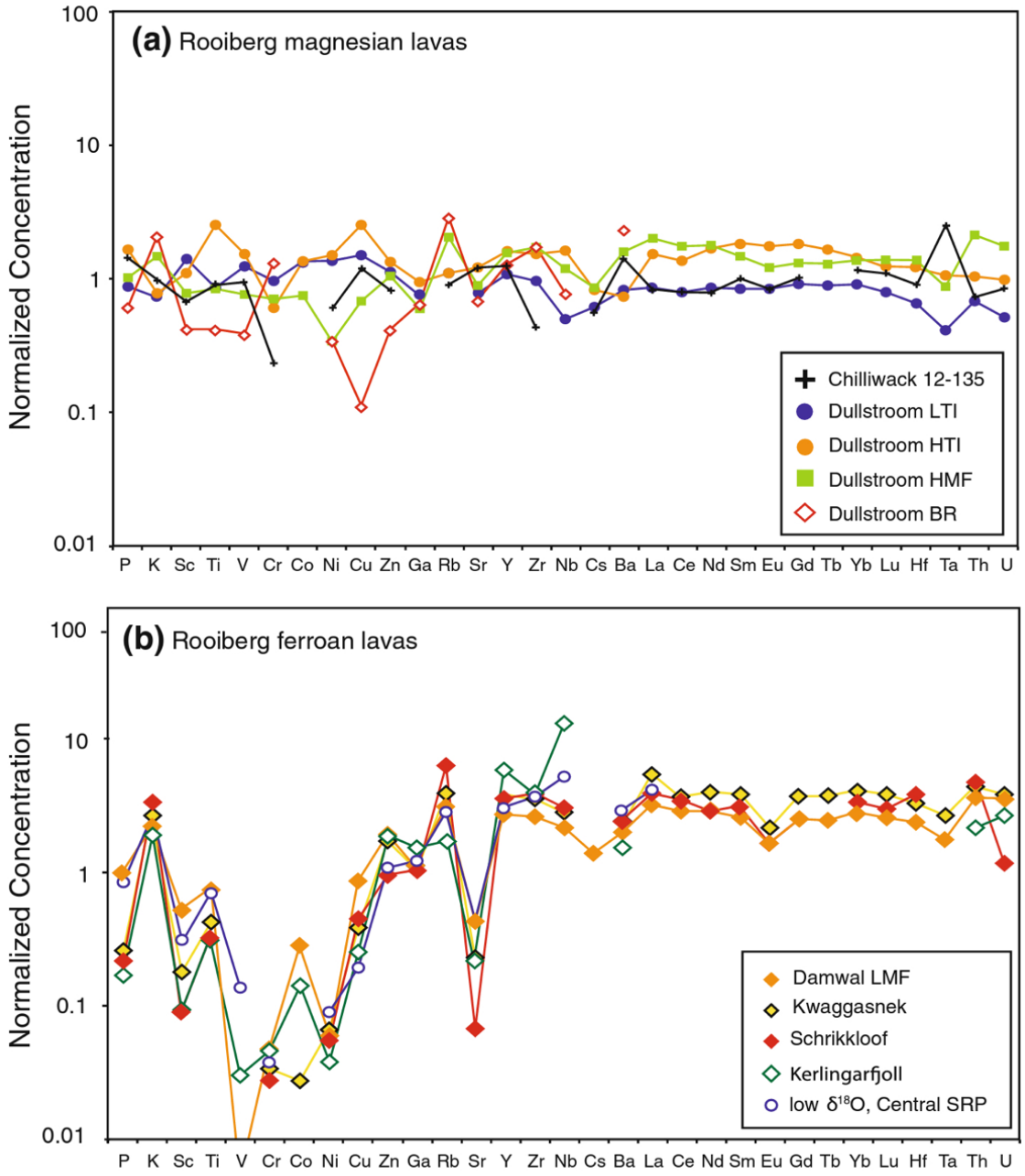

Figure 11. Trace element compositions normalised to the bulk continental crust (Rudnick and Gao, 2003) of the Rooiberg (a) magnesian and (b) ferroan lavas (Mathez et al., 2013).

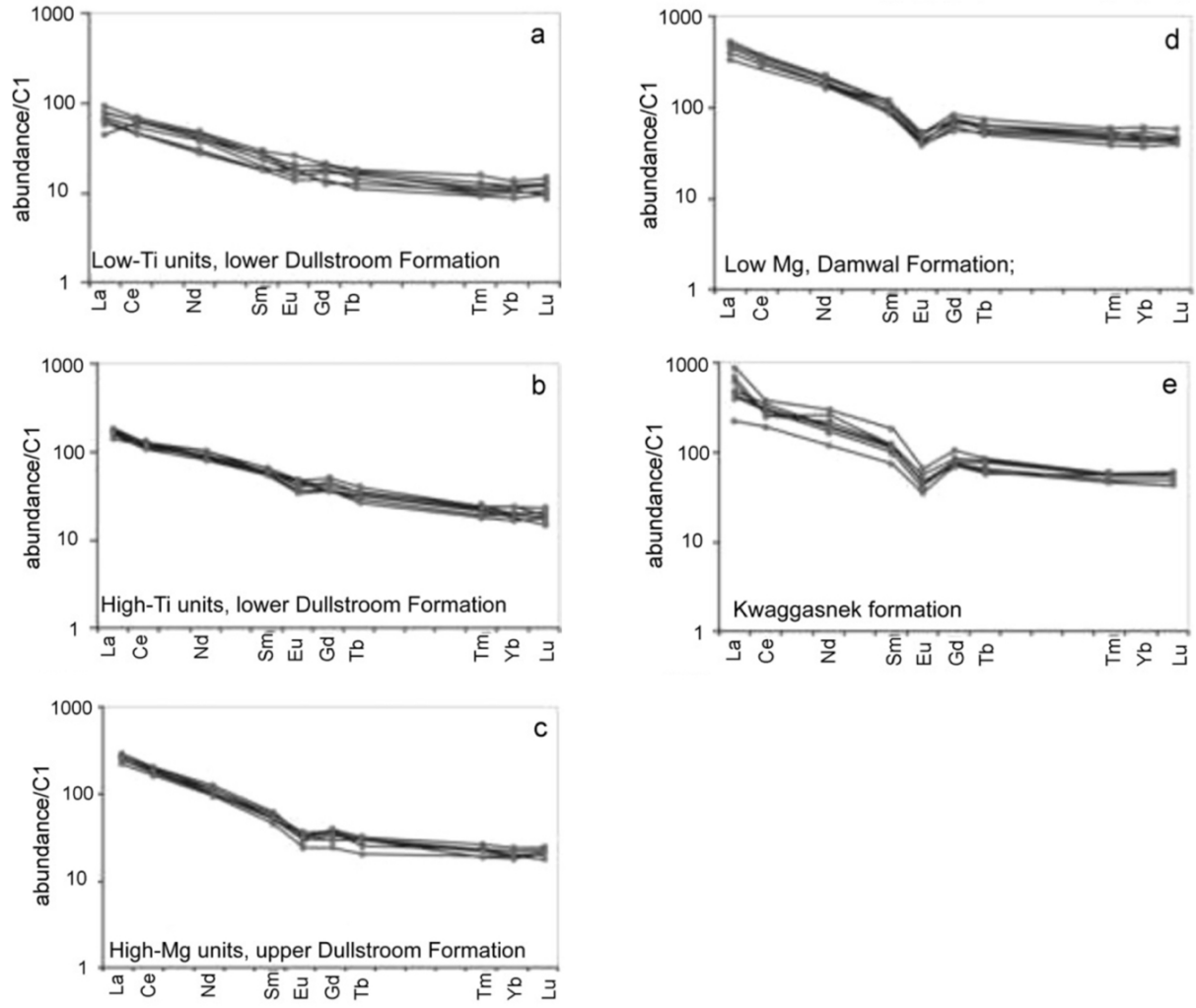

Figure 12. Rare Earth Element concentrations (normalised to chondrite) of (a) the LTI basaltic andesites of the lower Dullstroom Formation, (b) the HTI basalts of the lower Dullstroom Formation, (c) the HMF of the upper Dullstroom Formation, (d) the LMF of the Damwal Formation, and (e) the LMF of the Kwaggasnek Formation, (Lenhardt and Eriksson, 2012).

2.1.5. Connection to the Bushveld Igneous Complex (BIC)

The Rooiberg Group is widely accepted today to have originated from lithospheric and lower crustal partial melting of the Kaapvaal craton due to mantle plume activity, which is the equivalent source for the Bushveld Igneous Province (Sharpe et al., 1981; Sawkins, 1984; Hatton, 1995; Hatton and Schweitzer, 1995). The Rooiberg Group not only preceded the BIC but was synchronous with the BIC event (Schweitzer et al., 1995). The BIC consists of the Rustenburg Layered Suite, the Rashoop Granophyre Suite, and the Lebowa Granite suite (SACS, 1980). The Rustenburg Layered Suite is further subdivided into the Lower, Critical, Main, and Upper zones and has considerable economic significance (Von Gruenewaldt and Harmer, 1992).

2.1.6. Geochronology

Limited geochronological study of the entire Rooiberg Group, as well as hydrothermal alteration corresponding with the emplacement of the Lebowa Granite Suite of the BIC has resulted in imprecise age dates of the Rooiberg Group across the spectrum. Further age dating for each Rooiberg Group formation should be conducted to acquire a clear and accurate geochronological order of the Rooiberg Group volcanics.

Buchanan et al. (2004) dated the Dullstroom and Damwal formations to 2071 + 94 Ma/-65 Ma using Rb-Sr data of 28 samples, and the Kwaggasnek Formation to 1577 +620/ -1000 Ma using Rb-Sr data of 6 samples. The entire sequence from Dullstroom to Kwaggasnek formations are dated to 1837 +360/ -320 Ma using Sm-Nd data of 29 samples. Walraven (1997) dated the Kwaggasnek Formation (previously categorised as the Selons River Formation) to 2061 +/- 2 Ma using U-Pb data of 2 samples of rhyolite. Age dates between the Rustenberg Layered Suite (RLS) of the Bushveld Igneous complex, the Rooiberg Group rocks and overlying Waterberg Group rocks can be compared in figure 13 below.

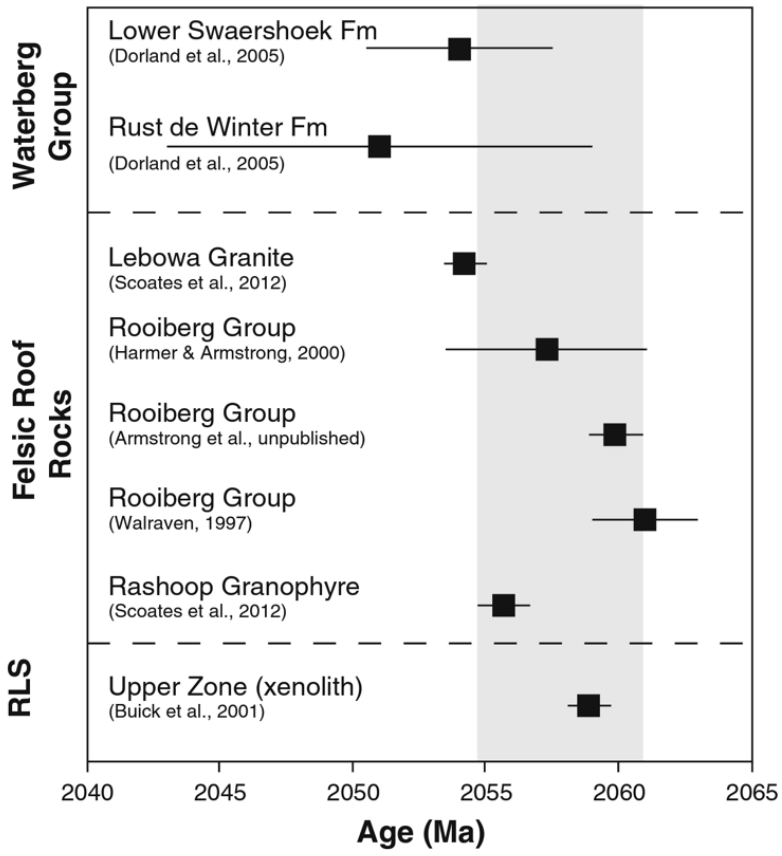

Figure 13. U-Pb age date comparison of the Rustenberg Layered Suite (RLS) of the Bushveld Complex, the felsic roof rocks of the Rooiberg Group (Upper Dullstroom to Schrikkloof Fm), and the overlying formations of the Waterberg Group (Mathez et al., 2013).

2.1.7. Silicic Large Igneous Provinces

Large Igneous Provinces (LIPs) are second to the most significant mafic intrusive and extrusive emplacements within the Earth's crust, the first being basaltic eruptions and intrusions of divergent boundaries at mid-ocean ridges (Coffin and Eldhom, 1992, 1994). LIPs constitute iron- and magnesium-rich intrusives and extrusives, not associated with mid-ocean ridge extension, and include continental and ocean basin flood basalts along with their plutonic counterparts, submarine ridges, seamounts, and oceanic plateaus, which are most commonly related to continental divergent boundaries. The LIP flood basalts comprise substantial aerial extents of more than 0,1 Mkm^2 and the crustal instrusives make up voluminous proportions of the Earth's crust (Coffin and Eldhom, 1994).

LIPs were revised by Bryan and Ernst (2008), since previous classifications largely overlooked associated ultramafic and silicic LIPs (often due to poorer exposure and erosion of such provinces), classification of duration of magmatism and emplacement was too broad, and previously LIPs were mainly classified according to aerial extent. LIPs have been redefined as follows: LIPs have aerial extents of more than 0,1 Mkm^2 and volumes of more than 0,1 Mkm^3. Emplacement of magmatic and volcanic fields occur due to igneous pulses over a shorter duration of time, approximately 1-5 Ma, and overall magmatic activity lasts for a maximum of 50 Ma. LIPs are associated with intraplate tectonic settings or have geochemical signatures linked to intraplate tectonic settings. LIPs have geochemistries that are dominantly mafic, however they can include ultramafic constituents and most often include considerable silicic provinces where some LIPs are dominated by silicic emplacements. LIPs no longer include sea mounts, sea ridges, and ocean floor crust creation. Mid-ocean ridge tectonics and associated volcanism are rather linked to occur after LIP events (figures 14 and 15).

Thus, Silicic Large Igneous Provinces (SLIPs) are included within the LIP definition (Bryan and Ernst, 2008). SLIPs are related to intraplate tectonics, continental margins, or arc-settings where significant crustal partial melting takes place, resulting in highly siliceous compositions (Bryan et al., 2002) and may precede ocean basin formation (Bryan et al., 2012). SLIPs obtain calc-alkaline and primitive isotopic geochemical signatures and include intermediate compositions along with the dominant siliceous compositions in their sequences (Bryan et al., 2013). A prime example of a SLIP is Sierra Madre Occidental- located in northwest Mexico, occurring 38-18 Ma, and consisting of mainly rhyolitic ignimbrites reaching thicknesses up to 55 km (Ferrari et al., 2002, 2007; Bryan et al., 2008, 2013).

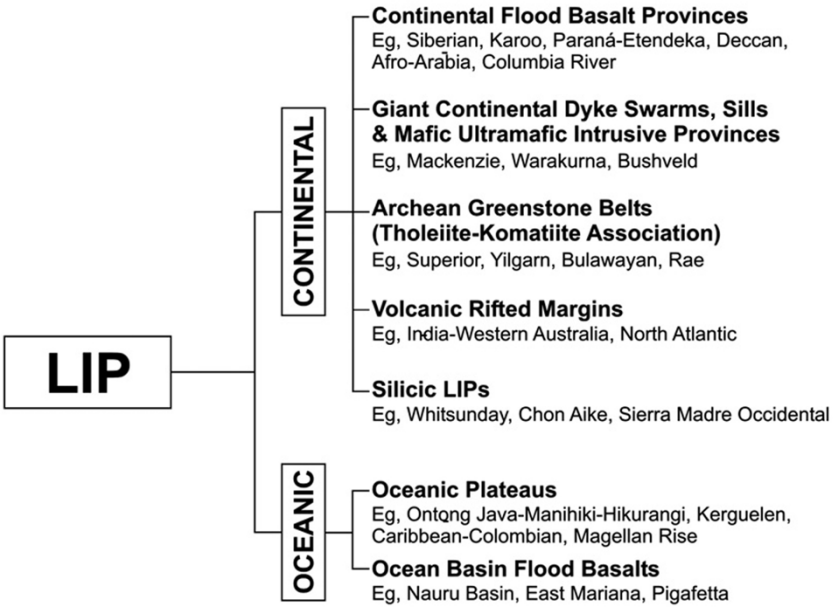

Figure 14. A visual revised classification of Large Igneous Provinces with examples by Bryan and Ernst (2008), building on from the work of Coffin and Eldhom (1994).

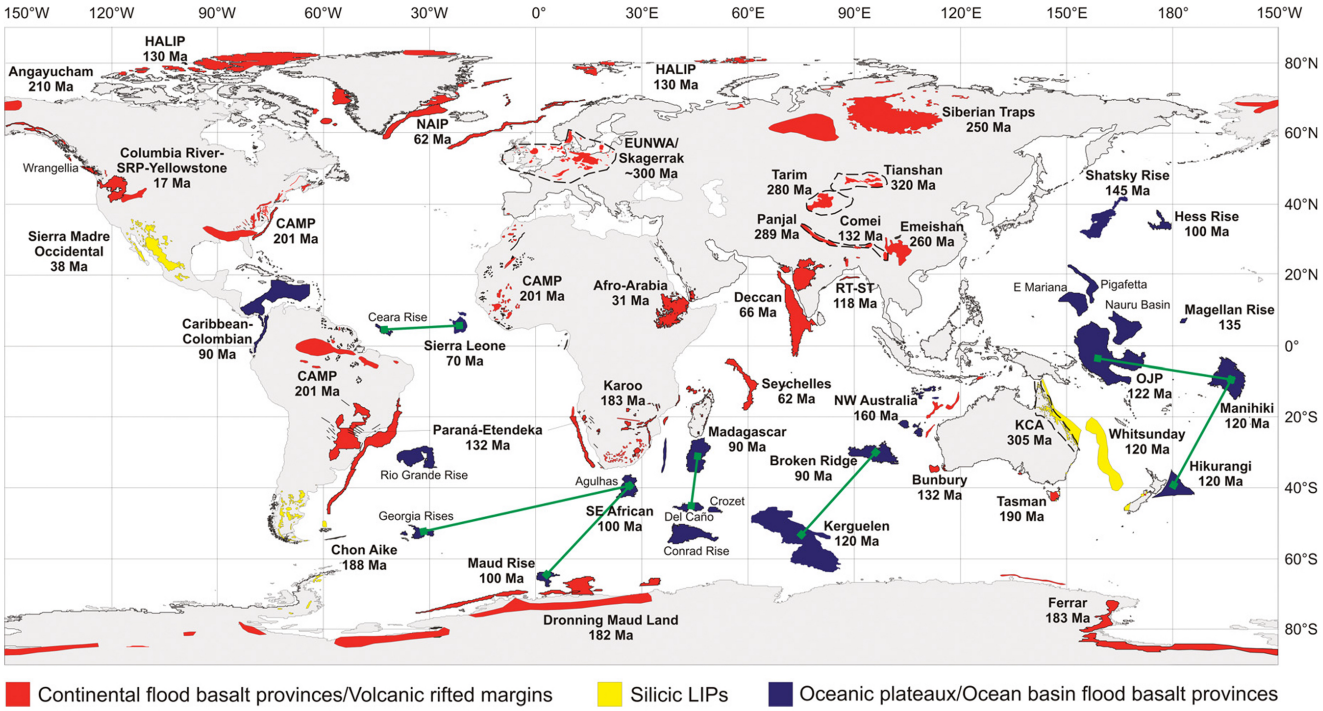

Figure 15. A revised map of the distribution of Large Igneous Provinces across the world, during the Mesozoic and Cenozoic, including continental flood basaltic provinces and volcanic rifted margins, ocean plateaus and ocean basin flood basaltic provinces, as well as silicic large igneous provinces. Green tie-lines link oceanic provinces that were rifted apart during seafloor spreading (Bryan and Ferrari, 2013; modified from Bryan and Ernst, 2008).

2.2. Pyroclastic Flow Deposits

2.2.1. Explosive eruptions and pyroclasts

Pyroclasts are volcanic and country rock fragments that originate from explosive eruptions. Magma within the crust ascends from higher temperature and pressure conditions towards the surface. Magmas of felsic composition, which often contain volatile gases that exsolve, expand and cause fragmentation as the magma ascends, and give rise to explosive and violent eruptions. The swift ascent and extrusion of this magma results in poor to no crystal growth. Fragmentation may also be caused by magma or lava coming into contact with water, glaciers, or saturated sediments, resulting in a hydroclastic eruption (Fisher and Schminke, 1984; Freundt and Schminke, 1992).

Pyroclasts include glass shards and pumice (vitric material), crystals, and lithic fragments (Fisher and Schminke, 1984; Cas and Wright, 1987). As these pyroclasts are ejected into air or water, according to the nature of the eruption and eruption column, they may fall back to the surface and become fallout deposits, or the eruption cloud may collapse and flow or surge across the surface to form pyroclastic flow deposits. Fallout deposits include the deposition of larger fragments from their initial trajectory, which are too heavy to be carried by wind or the eruption cloud and are deposited fairly close to the eruption centre. Less dense fragments are carried by the eruption cloud, which is buoyant and turbulent, and are carried further from the eruption centre. Fine fragments are carried by wind, which may be deposited a large distance from the eruption centre (Fisher, 1964; Fisher and Schminke, 1984; Houghton et al., 2000).

Pyroclastic flows result from either the collapse of dense eruption columns, “boiling over” eruptions, and lateral eruptions of pyroclastic material associated with dome collapse (Fisher, 1979; Fisher and Schminke, 1984). These eruptional processes and deposits can be studied in figure 16. Subaerial eruptions will only be discussed here, as the Rooiberg Group volcanics are subaerial and did not include subaqueous eruptions (Erikkson et al., 1994; Lenhardt & Eriksson, 2012; Lenhardt et al., 2017).

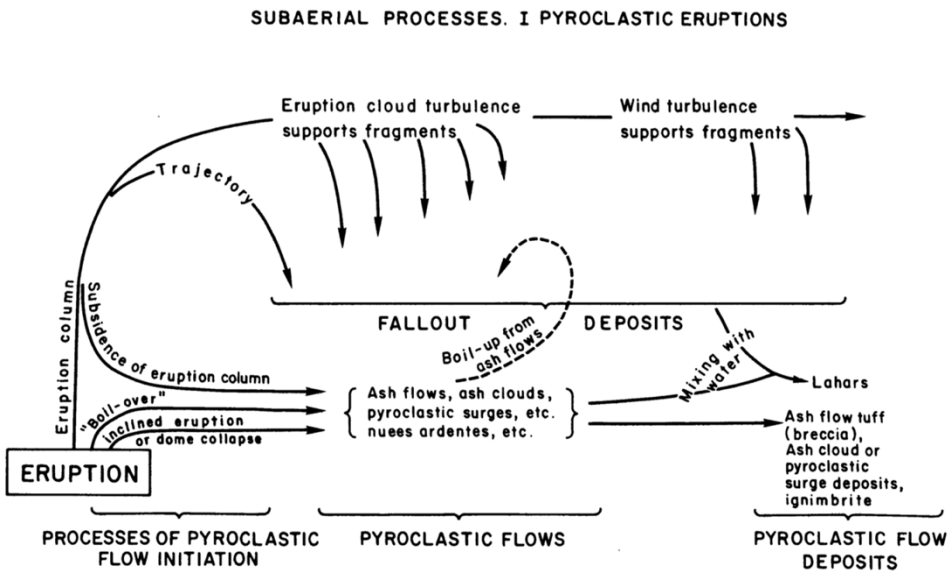

Figure 16. An illustration of the processes of pyroclastic eruptions (Fisher and Schminke, 1984).

2.2.2. Pyroclastic flow deposits and ignimbrites

Pyroclastic density currents are pyroclastic particles and volcanic gas of high temperatures that rapidly flow together as one system and can be transported far distances, in comparison to siliceous lava flows, which can be voluminous, but not extensive, due to their higher viscosity. Pyroclastic density currents give rise to two main types of deposits, including pyroclastic flow deposits and pyroclastic surge deposits (Freundt et al., 2000). Pyroclastic flow deposits tend to be poorly sorted and have no distinct structure or layering, whereas pyroclastic surge deposits are well sorted and tend to constitute of finer grains and thinner deposits (Fisher and Schminke, 1984). Ignimbrites, as defined by Walker (1983), are rock formations formed by the deposition and cooling of pyroclastic flows, which widely range geochemically from mafic to rhyolitic in composition and which are chiefly made up of pumiceous material.

The volume of a pyroclastic flow deposit may indicate the type of volcano and volcanic setting the deposit originates from. Small volumes (up to 1 km^3) often originate from small central vent volcanoes and are commonly linked to arc settings. Pyroclastic flows of small volume flow into depressions and valleys and are more controlled by the existing topography. Medium volumes (1-100 km^3) tend to originate from stratovolcanoes. Large volumes (100-1000 km^3) arise from large caldera volcanoes that produce substantial eruptions. Pyroclastic flows of large volumes may exceed and cover existing topography. When these pyroclastic flows are continuous, they result in very thick, sheet-like pyroclastic deposits which completely bury the terrain beneath and form plateaus of ignimbrite (Fisher and Schminke, 1984).

Small to medium volumes are linked to basaltic to rhyolitic chemical compositions, whilst larger volumes are derived from dacitic to rhyolitic chemical compositions and are composed largely of highly vesiculated materials, such as pumice (Fisher and Schminke, 1984). Furthermore, the larger the volume of the pyroclastic flow, the larger the distance the pyroclastic flow travels, thus the more extensive the pyroclastic flow deposit (Smith, 1960a).

An ignimbrite may be classified as a high aspect ratio ignimbrite (H.A.R.I.) or a low aspect ratio ignimbrite (L.A.R.I.). The aspect ratio is calculated by dividing the vertical thickness by the horizontal extent (V/H) of the ignimbrite. H.A.R.I. types are thicker with lower horizontal extents, which are topography controlled and are emplaced within valleys. L.A.R.I. types are thinner, but extensive deposits which originate from pyroclastic flows that are not topography controlled and have been found to climb and cover higher elevations, including mountains (Walker, 1983). L.A.R.I. types are emplaced by high velocity pyroclastic flows, which correspond to a high discharge rate during eruption (Wilson and Walker, 1981; Walker, 1983).

Pyroclastic flow deposits can be distinguished by flow and cooling units (Smith, 1960b). A flow unit is a single pyroclastic flow deposit, which can be divided into a ground and basal layer, followed by the main body of the deposit and may be topped with an ash-cloud deposit (once the ash settles from the pyroclastic cloud), which can be seen in figure 17. The ground layer (layer 1) of the ignimbrite is rich in coarse grained lithics and crystals. Layer 2, which comprises the main ignimbrite body is subdivided into two layers- 2a and 2b. Layer 2a is an ash basal layer that may be reversely graded and may or may not be present. Layer 2b is poorly sorted and may be variably graded. The bottom of layer 2b may be normally graded and the top of layer 2b may be reverse graded and enriched in pumice clasts (Freundt et al., 2000). Lapilli pipes, also known as fossil fumaroles or ignimbrite pipes (Walker, 1971), occur within the body of the ignimbrite and form post emplacement where gas escapes through the cooling & compacting pyroclastic flow deposit. Lapilli pipes are fines poor and are rich in lithic fragments and crystals. Layer 3 is a massive ash layer that may or may not be present (due to its susceptibility to erosion) and forms by the settling of ash particles from the ash cloud riding over the pyroclastic flow (Freundt et al., 2000).

Individual flow units differ from each other by their grading and overall grain sizes, concentration of pumice clasts, and the presence of cross-bedding. Flow units may be thin and only measure a few centimetres, or they may be more substantial, measuring a few metres thick. When individual flow units swiftly flow on top of one another and create a stack of hot pyroclastic flows and then cool together as a single unit, this would be classified as a cooling unit (Smith, 1960b; Fisher and Schminke, 1984).

A cooling unit cools according to different heat zones, according to how each zone cools and releases heat, which results in different welding zones (seen in figure 18). The non-welded zone occurs as the outer and basal layer of the cooling unit, where heat is rapidly released into the atmosphere or into the underlying, cool ground (Smith, 1960b). The central and lower-central zone of the cooling unit cools at the slowest rate and remains at a higher temperature for a longer period of time (Jaeger, 1968); therefore, this zone undergoes the most welding and becomes the densest zone. This dense welding zone grades into a partially welded zone going towards the outer, non-welded layer (Smith 1960b).

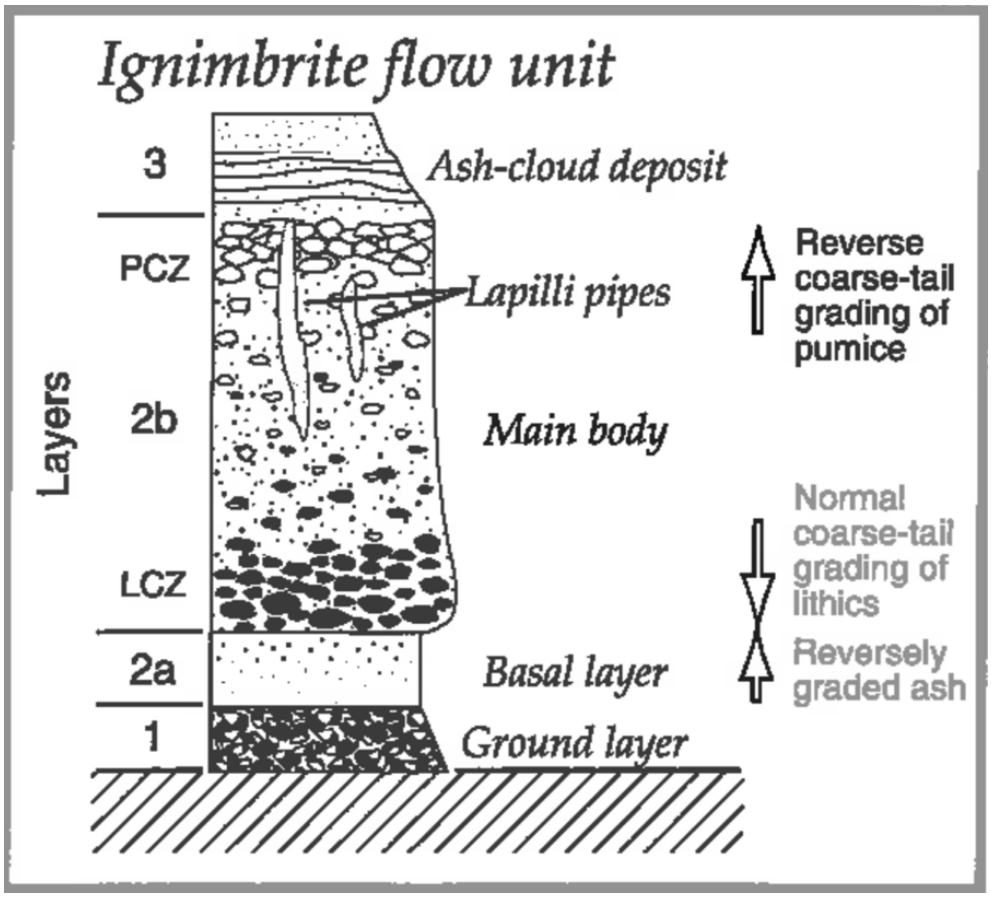

Figure 17. An idealised stratigraphic view of an ignimbrite flow unit, where LCZ stands for “Lithic Concentration Zone” and PCZ stands for “Pumice Concentration Zone” (Freundt et al., 2000).

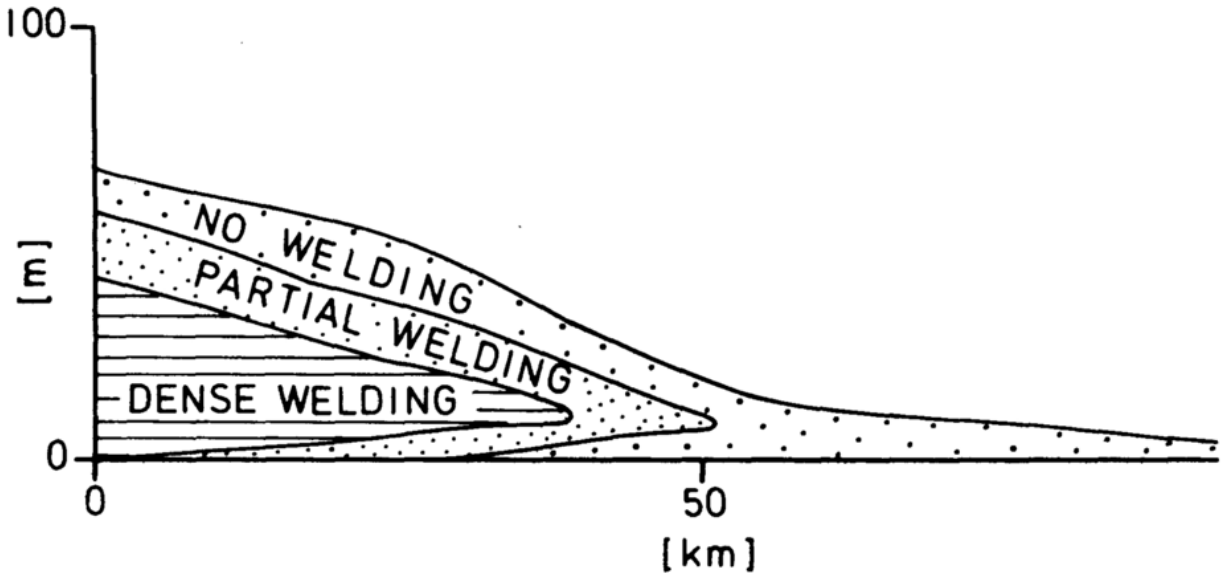

Figure 18. A cross-sectional view of a pyroclastic flow cooling unit according to its welding zones (Smith, 1960b; Fisher and Schminke, 1984).

Chapter 3 - Methodology

The following research is based on thin sections made from rock samples sampled at Kuthaba Bush Lodge, belonging to the Nylstroom package; Loskop Dam and Dullstroom, belonging to the Bothasberg Package, which can be referenced in figures 1 and 5. The study area consists of the upper Dullstroom, Damwal, Kwaggasnek and Schrikkloof formations. The research methodology to study the Rooiberg Group's mineral textures and grain size distribution (GSD) is listed below.

3.1. Field analysis

Field analysis of the Schrikkloof Formation was undertaken at Kuthaba Bush Lodge, in the Modimolle area. Each outcrop analysed was photographed. Observations were made according to texture of the groundmass; the presence of clasts, fragments and phenocrysts; the presence of flow banding, jointing and folding; and the presence of any sedimentary features. Based on this analysis, the rock type was preliminarily categorised, and the nature of formation and deposition of the rocks present is discussed.

3.2. Microscopy and Grain Size Distribution Analysis

1. Photographs of thin sections (from samples collected by Dr. Nils Lenhardt and Dr. Olutola O. Jolayemi from Khutaba Lodge and Loskop Dam) were taken under a polarising microscope, under plane polarised light (ppl) and crossed polarised light (xpl).
2. Observations of relevant thin sections were recorded. Observations include the phenocrysts present, groundmass texture, mineralogical composition and mineralogical textures. Observations primarily focus on the feldspar phenocrysts.
3. The software ImageJ was used to measure the diameter of feldspar phenocrysts from images taken by the polarising microscope. The feldspar size data was used to create frequency grain size distribution (GSD) histograms. Different populations of data were observed and used in interpretation of the magmatic, eruptive and depositional processes that were likely to have formed the rocks of the Rooiberg Group.

Chapter 4 – Observations & Results

4.1. Field Analysis – Kuthaba Bush Lodge

The following field analysis took place at Kuthaba Bush Lodge, Modimolle. The rocks examined form part of the Schrikkloof Formation and belong to the Nylstroom Package (see figure 5 for reference, Schweitzer et al., 1995), with minor intercalated sedimentary rock, namely outcrops 12 and 14. Figure 19 shows the locations of the outcrops observed and studied at Kuthaba Bush Lodge:

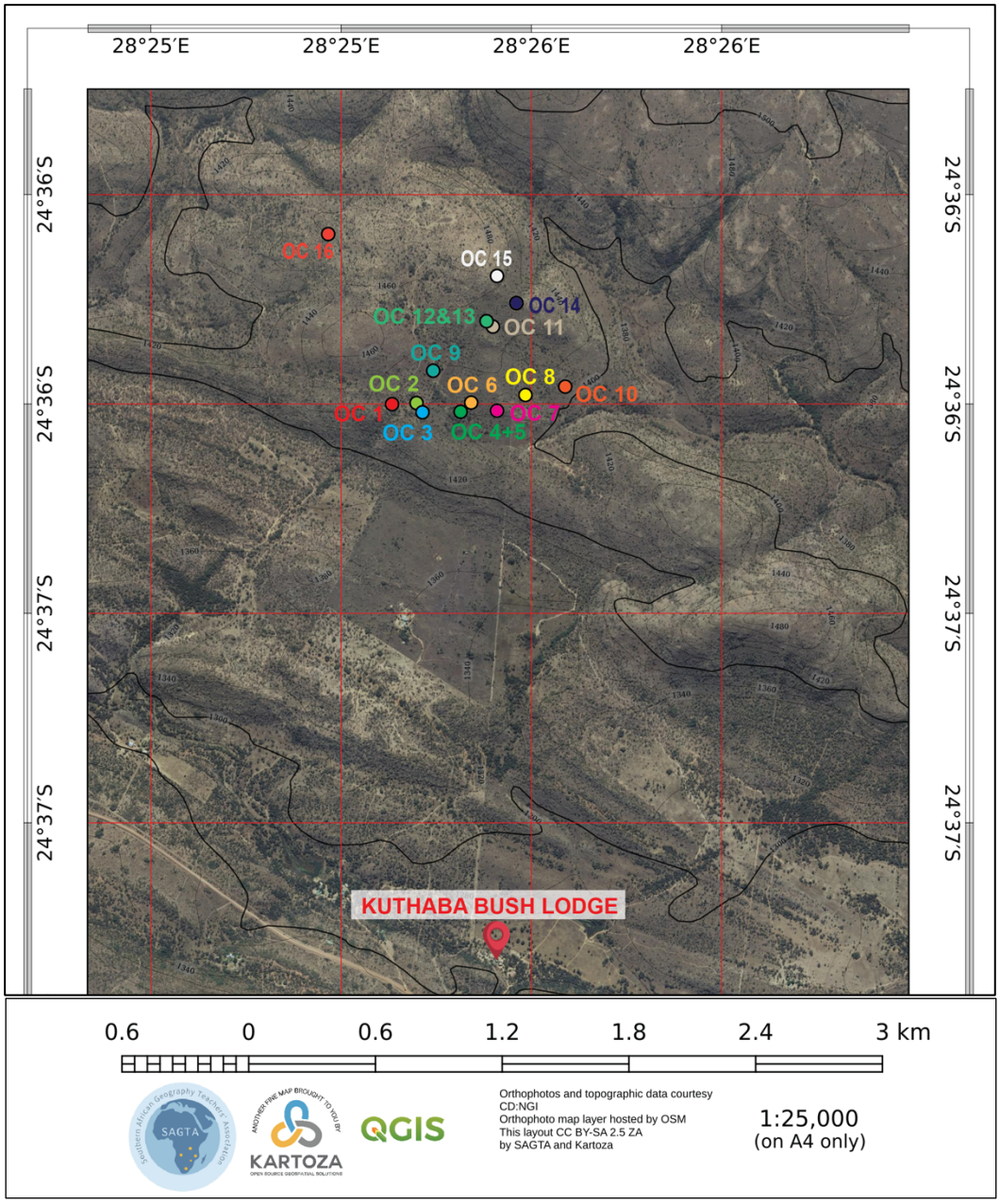

Figure 19. An orthophoto hybrid map of outcrop (OC) 1 to 16 investigated during the field analysis within Kuthaba Bush Lodge, Modimolle (SAGTA map downloader, Kartoza, 2021).

4.1.1. Outcrop 1 [24º 36' 30,3" S; 28º 25' 38,6" E]:

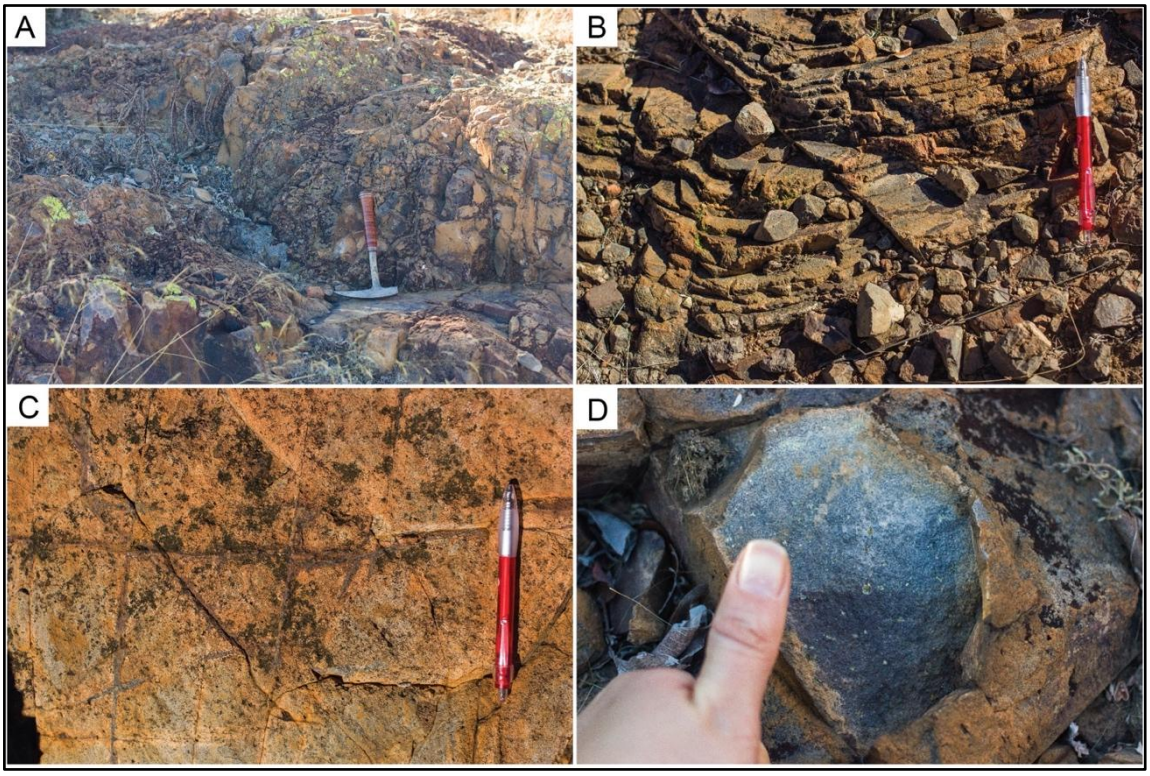

Figure 20. **A**) A blocky, lava-like ignimbrite. **B**) A rheomorphic lava-like ignimbrite displaying flow-banding. **C**) Hydrothermal alteration of Fe-rich precipitates along joints of an extremely high-grade welded ignimbrite. **D**) A fresh piece of extremely high-grade welded ignimbrite with massive, aphanitic textures with green crystals consisting of secondary minerals.

Outcrop 1 (figure 20) consists of blocky, lava-like ignimbrite (figure 20A), with localised flow-banding (figure 20B). The rock has undergone hydrothermal alteration, observed by the red colour of the outer layers of the rock as well as the joints, having a red to purple colour (figure 20C). The red colour of the rock and joints are precipitated hematite, originating from iron-rich hydrothermal fluids. A fresh piece of the ignimbrite (figure 20D) displays a grey to blue colour and an aphanitic texture with the presence of green crystals, which are possibly altered or recrystallised collapsed and compressed pumice clasts. These green crystals may consist of chlorite due to hydrothermal alteration post-deposition. Outcrop 1 is a lava-like ignimbrite forming part of the Upper Schrikkloof Formation, located close to the Waterberg Group contact (found just South of Outcrop 1).

4.1.2. Outcrop 2 [24º 36' 30,15" S; 28º 25' 42" E]:

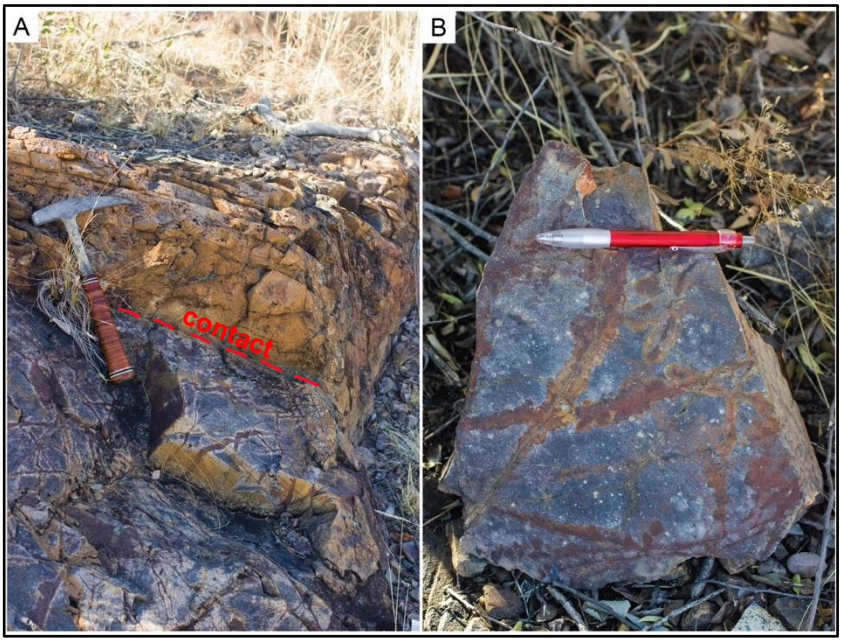

Figure 21. **A**) A contact between two different ignimbrites. **B**) A rock fragment of the lower, massive and highly hydrothermally altered ignimbrite.

Outcrop 2A (figure 21) displays the visible contact between two different ignimbritic deposits. The lower ignimbrite is lava-like and massive with jointing and is observed to be highly hydrothermally altered. This is deduced from the stark purple colour and hematite precipitates along the joints. An abundance of green secondary minerals, possibly chlorite, are observed. The upper ignimbrite is flow-banded or lineated and lava-like.

4.1.3. Outcrop 3 [24º 36' 30,96" S; 28º 25' 42,97" E]:

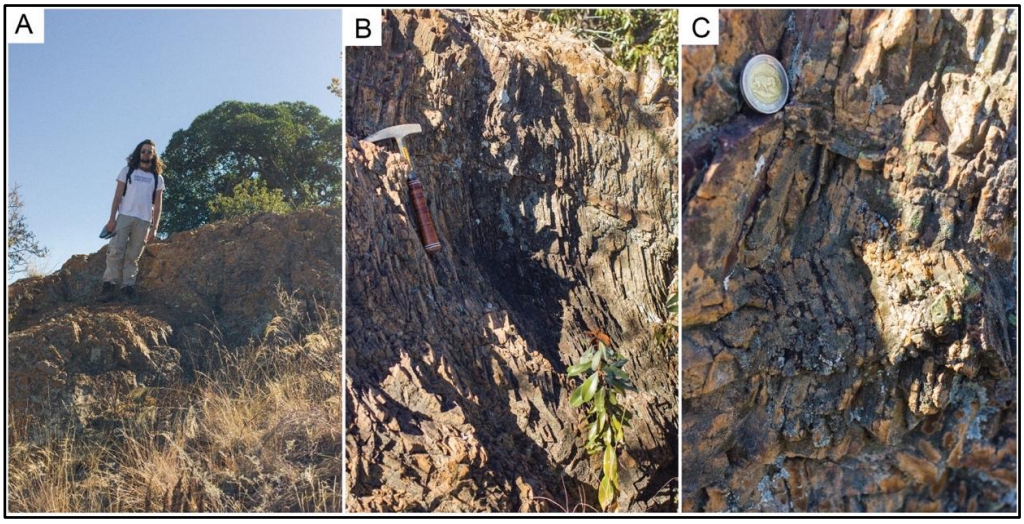

Figure 22. A highly flow-banded, lava-like ignimbrite. **A**) A large-scale, flow-banded and blocky ignimbrite, geologist as scale. **B**) Highly flow-banded and folded rheomorphic ignimbrite. **C**) A close-up of the folded, flow-banded ignimbrite.

Outcrop 3 (figure 22) consists of extensive ignimbrite deposits. The ignimbrite is meticulously flow-banded and folded (seen clearly in figures 22B and C). The interior rock texture is massive with secondary crystals, consisting of the same secondary minerals observed in outcrops 1 and 2. Outcrop 3 is a rheomorphic, lava-like ignimbrite.

4.1.4. Outcrop 4 [24º 36' 30,41" S; 28º 25' 49,46" E]:

Figure 23. An intricately flow-banded, lava-like ignimbrite.

4.1.5. Outcrop 5 [24º 36' 30,41" S; 28º 25' 49,46" E]:

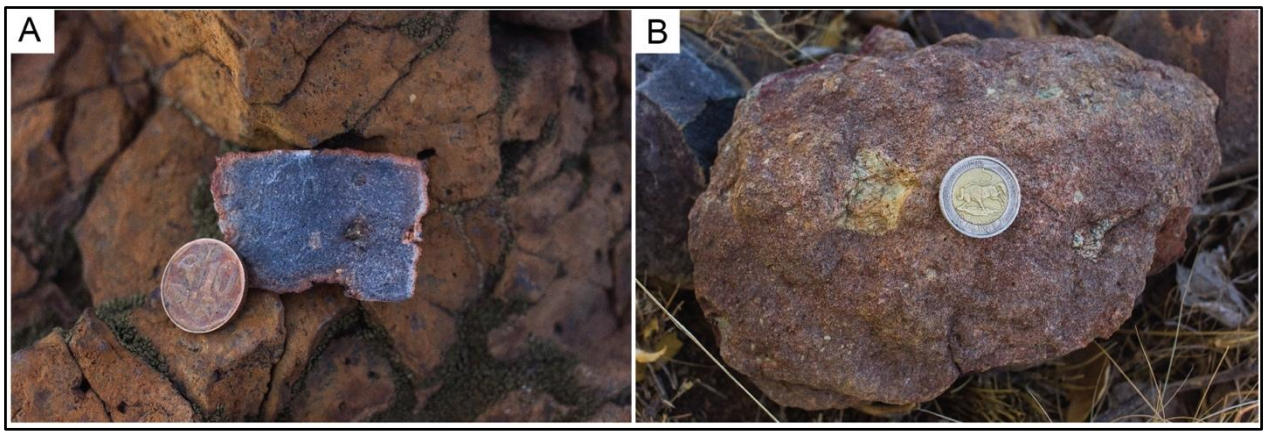

Figure 24. **A)** A fresh hand specimen of a flow-banded, lava-like ignimbrite. **B)** A non-welded ignimbrite rock fragment found with a coarse-grained matrix and large pumice clasts, not in-situ.

Outcrops 4 (figure 23) and 5 (figure 24) are likely a continuation of outcrop 3, consisting of extensive flow-banded lava-like ignimbrite. Outcrop 5 displays lava-like textures as seen in outcrops 1-3 with an aphanitic texture with secondary crystals, consisting of altered pumice clasts, altered plagioclase phenocrysts, or chlorite crystals due to hydrothermal alteration.

Outcrop 5 exhibits the same lava-like textures as outcrops 1 to 4, as seen in figure 24A. The defined middle phenocryst is angular and prismatic, which appears to be orthorhombic, monoclinic or triclinic, suggesting it could be an altered phenocryst crystal, such as a pyroxene, plagioclase, or hornblende that formed within the magma chamber or volcanic pipe during the magma ascent.

The rock fragment in figure 24B is a non-in-situ ignimbrite that is poorly welded. The groundmass is coarse grained encompassing a large, altered pumice clast, lithic fragments and crystal fragments. This rock fragment possibly belongs to the lower Schrikkloof Formation, to a poorly welded ignimbrite.

4.1.6. Outcrop 6 [24º 36' 29,92' S; 28º 25' 50,82" E]:

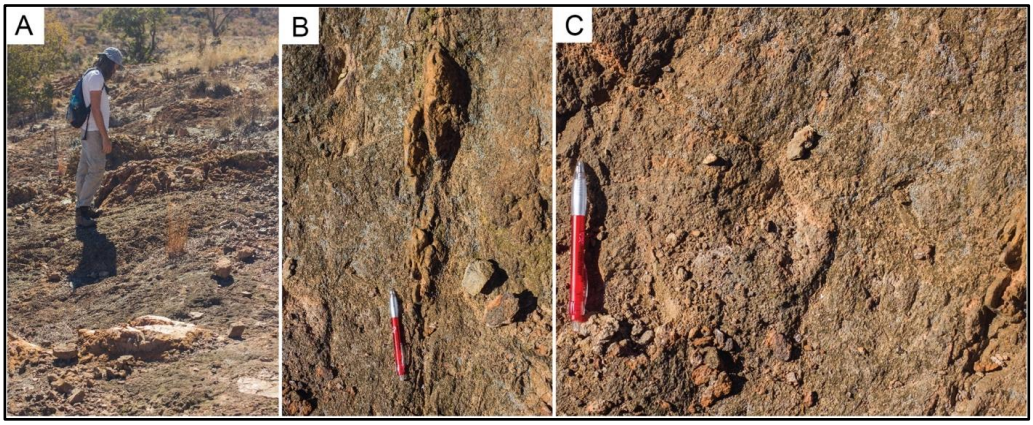

Figure 25. **A)** Intercalation of ignimbrites of varying degrees of welding. **B)** A welded ignimbritic layer jutting out from a non-welded ignimbrite or tuff. **C)** An non-welded ignimbrite or tuff of a friable and weathered texture.

Outcrop 6 (figure 25) consists of ignimbrites with different welding intercalated with one another, likely originating from different pyroclastic flows, or the intercalation of a low-grade, welded ignimbrite and a non-welded tuff. The jutting prominent outcrops seen in figures 25A and B consist of harder, denser ignimbrite that has undergone some degree of welding. The other ignimbrite or ash fallout deposit seen in figure 25C is more porous and coarser grained, indicating a non-welded ignimbrite or tuff, which has been more susceptible to weathering.

4.1.7. Outcrop 7 [24º 36' 30,73" S; 28º 25' 54,76" E]

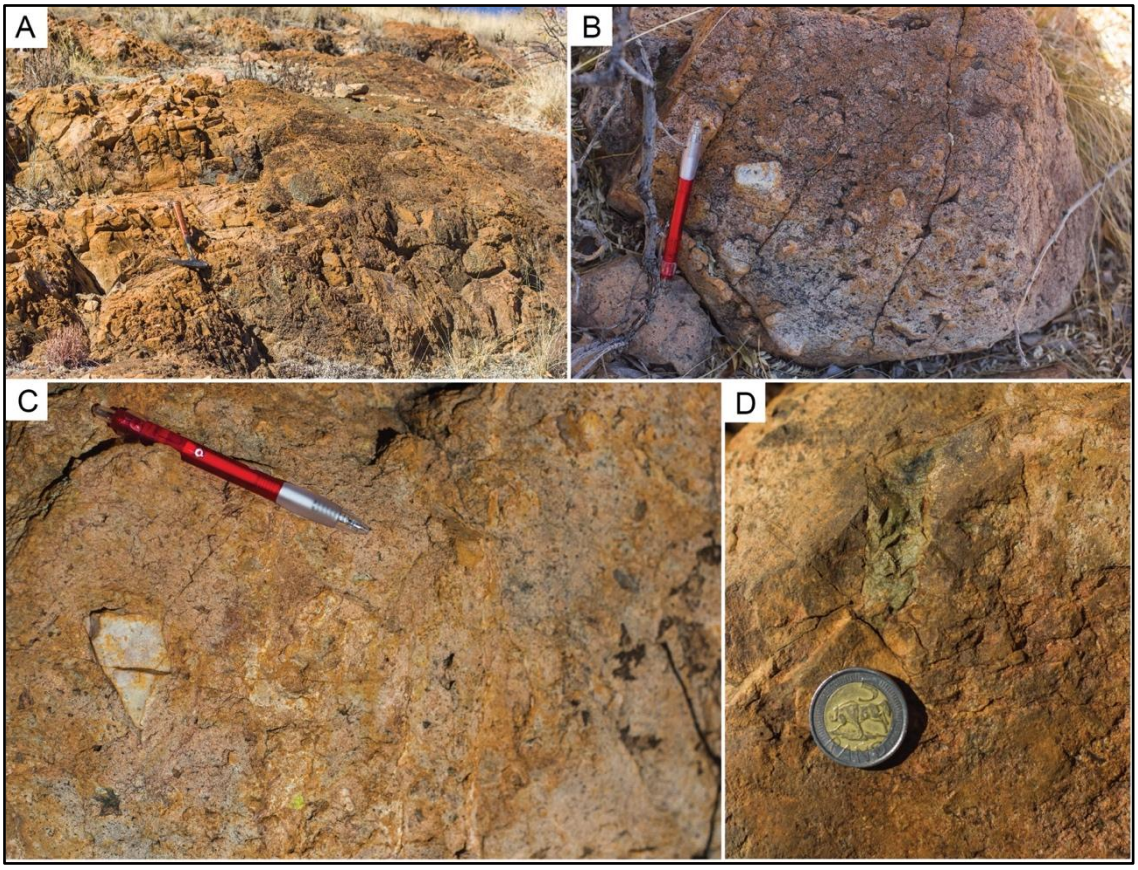

Figure 26. **A)** An ignimbrite deposit of low-grade welding, containing lithic **(B and C)** and altered pumice **(D)** clasts.

Outcrop 7 (figure 26) is an approximately 1,65 m thick, low-grade welded ignimbrite which is moderately dense and possesses a clastic groundmass texture with large (up to 5 cm in length) angular clasts of lithic and altered pumice clasts, which are matrix supported. Figure 26B exhibits moderate normal grading, with the largest observed lithic clast being quartzite. Figure 26D exhibits a collapsed and lengthened, pumice clast, which has been recrystallised to green secondary minerals, such as chlorite.

4.1.8. Outcrop 8 [24º 36' 28,98" S; 28º 25' 59,11" E]:

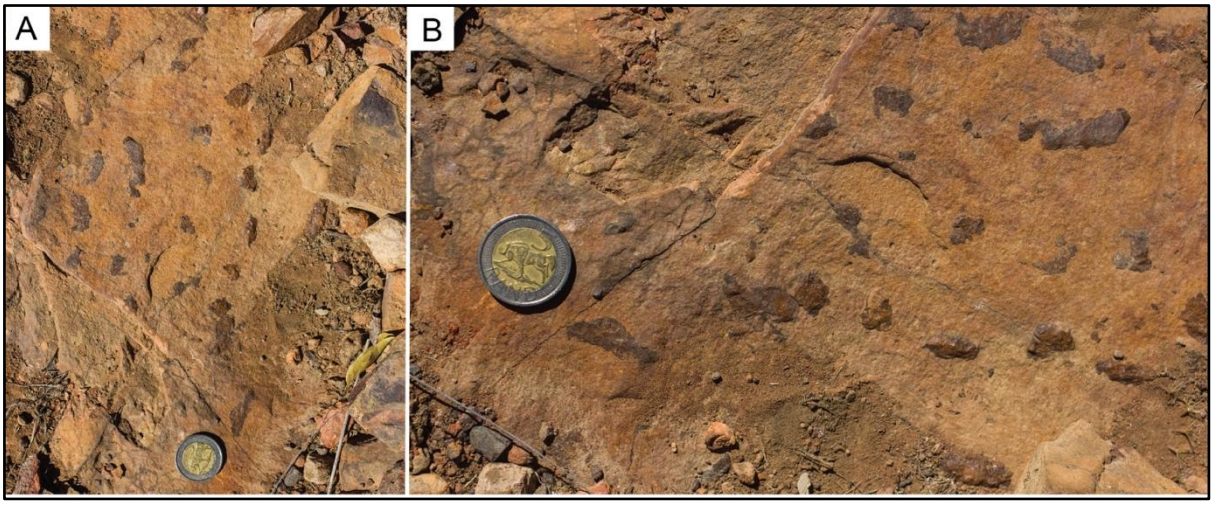

Figure 27. A welded ignimbrite of flattened and globular-shaped pumice clasts.

Outcrop 8 (figure 27) is a welded ignimbrite with a dense, retained pyroclastic groundmass texture. The brown elongated clasts are collapsed and elongated pumice clasts, with lengths varying from 0,5 cm to 3,5 cm. The pumice clasts are recrystallised and can be considered as fiamme, displaying the beginnings of a eutaxitic texture.

4.1.9. Outcrop 9 [24º 36' 25,01" S; 28º 25' 43,66" E]:

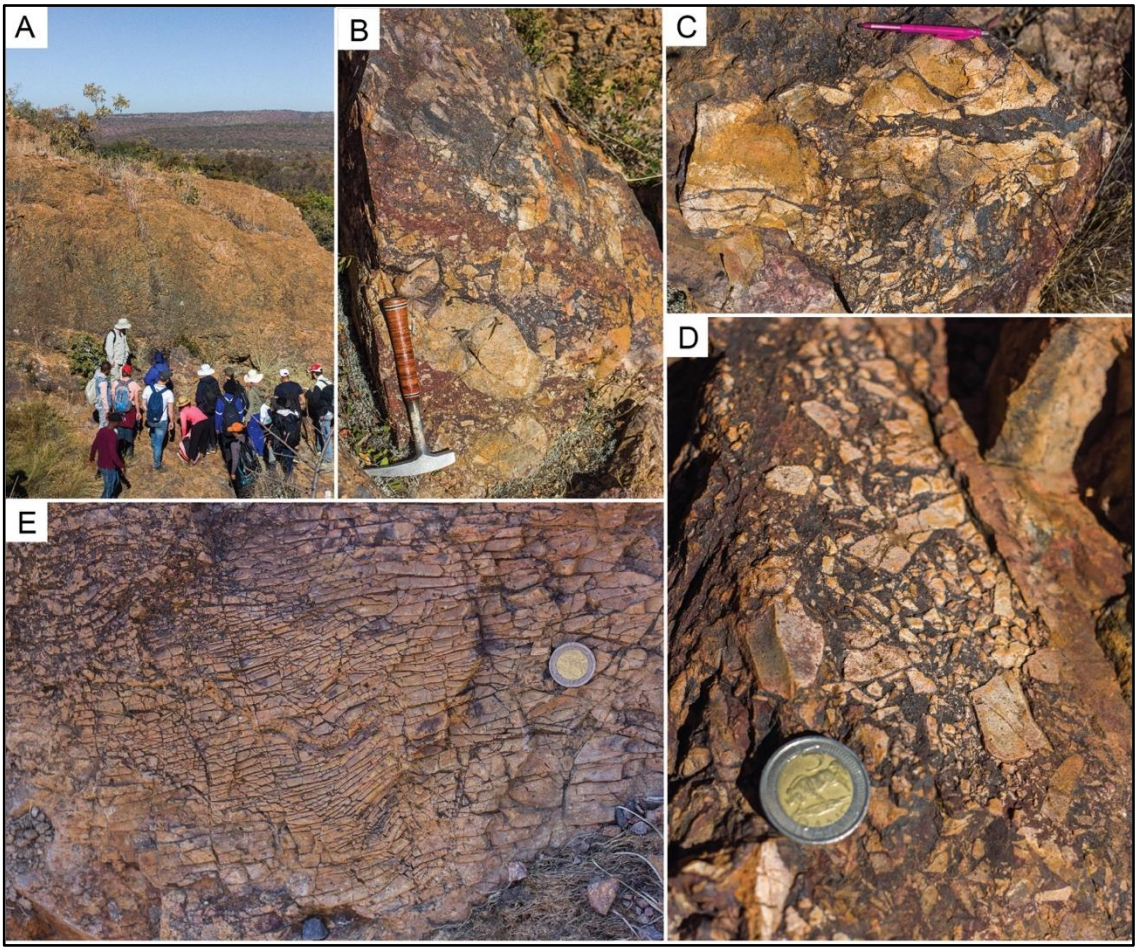

Figure 28. An extensive flow-banded and brecciated ignimbrite. **A)** A large-scale view of brecciated and flow-banded lava-like ignimbrite, geologists as scale. **B-D)** Brecciated and hydrothermally altered lava-like ignimbrite with fracture-filled iron precipitates. **E)** Highly flow-banded and fractured lava-like ignimbrite.

Outcrop 9 (figure 28) consists of an extensive area of rheomorphic lava-like ignimbrite that has been strongly hydrothermally altered, as evidenced by the red and purple colouring of the rocks, which are iron precipitates, such as hematite. Tracts of intricate flow banding (figure 28E) are found throughout this region. Pipe-like zones of brecciated ignimbrite (figures 28B, C & D), consisting of angular lava-like ignimbrite clasts set within a fine-grained matrix of iron precipitates, crosscut the monolithic exposures of the rheomorphic, lava-like ignimbrite.

4.1.10. Outcrop 10 [24º 36' 27,48" S; 28º 26' 04,43" E]:

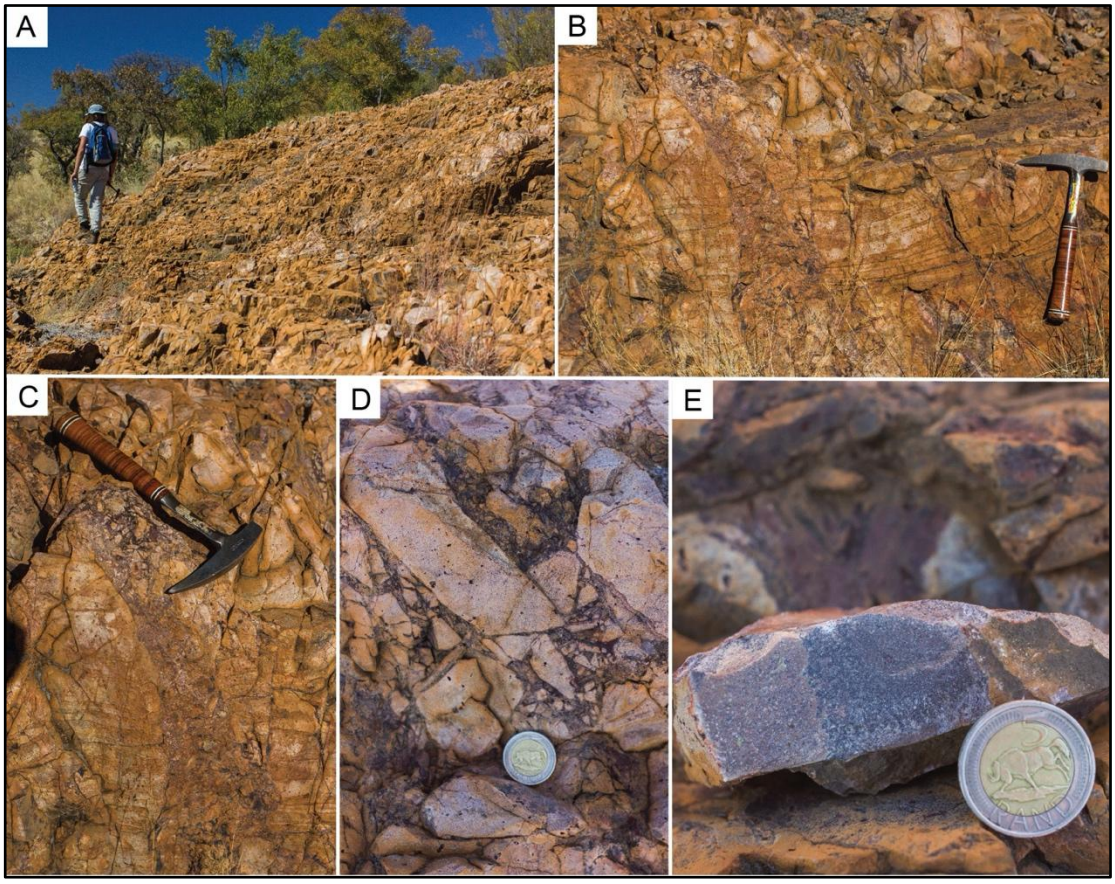

Figure 29. **A)** Extensive blocky lava-like ignimbrite, geologist for scale. **B & C)** A geyser pipe containing brecciated ignimbrite and Fe-precipitates cutting through a rheomorphic lava-like ignimbrite. **D)** Angular clasts of of dense, lava-like ignimbrite within the geyser pipe. **E)** Dense, aphyric texture of extremely high-grade welding of the observed ignimbrite.

Outcrop 10 (figure 29) signifies the continuation of the geyser zone of outcrop 9, directly eastsoutheast, 0,63 km away. Similar to outcrop 9, outcrop 10 consists of a massive to slightly flow-banded lava-like ignimbrite. A geyser pipe (figure 29C) of large, angular ignimbrite clasts (up to 13 cm in length) set within an iron-precipitate groundmass (figure 29D) cuts vertically through the highly welded ignimbrite. The massive lava-like texture of the ignimbrite is observed in figure 29E.

4.1.11. Outcrop 11 [24º 36' 19,77" S; 28º 25' 53,84" E]:

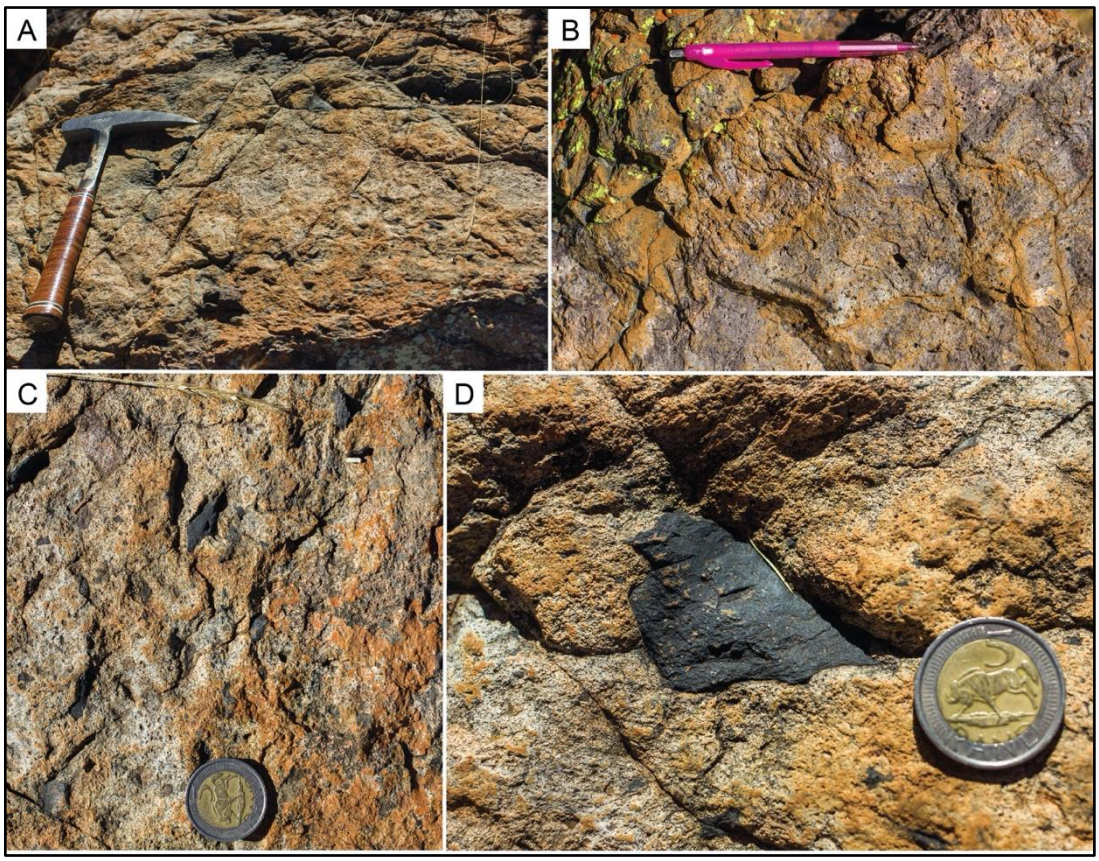

Figure 30. **A)** A non-welded ignimbrite. **B)** Clastic, sedimentary texture of the non-welded ignimbrite. **C)** Large lithic and pumice clasts within the non-welded ignimbrite. **D)** A large, angular clast within the non-welded ignimbrite.

Outcrop 11 (figure 30) comprises a non- to low-grade welded ignimbrite. The ignimbrite has a clastic, sandy-like texture with matrix-supported angular lithic fragments (figures 30C and D), which are siliciclastic. The lithic fragments range in length from 0,2 cm to 3,9 cm.

4.1.12. Outcrop 12 [24º 36' 18,95" S; 28º 25' 53,21" E]:

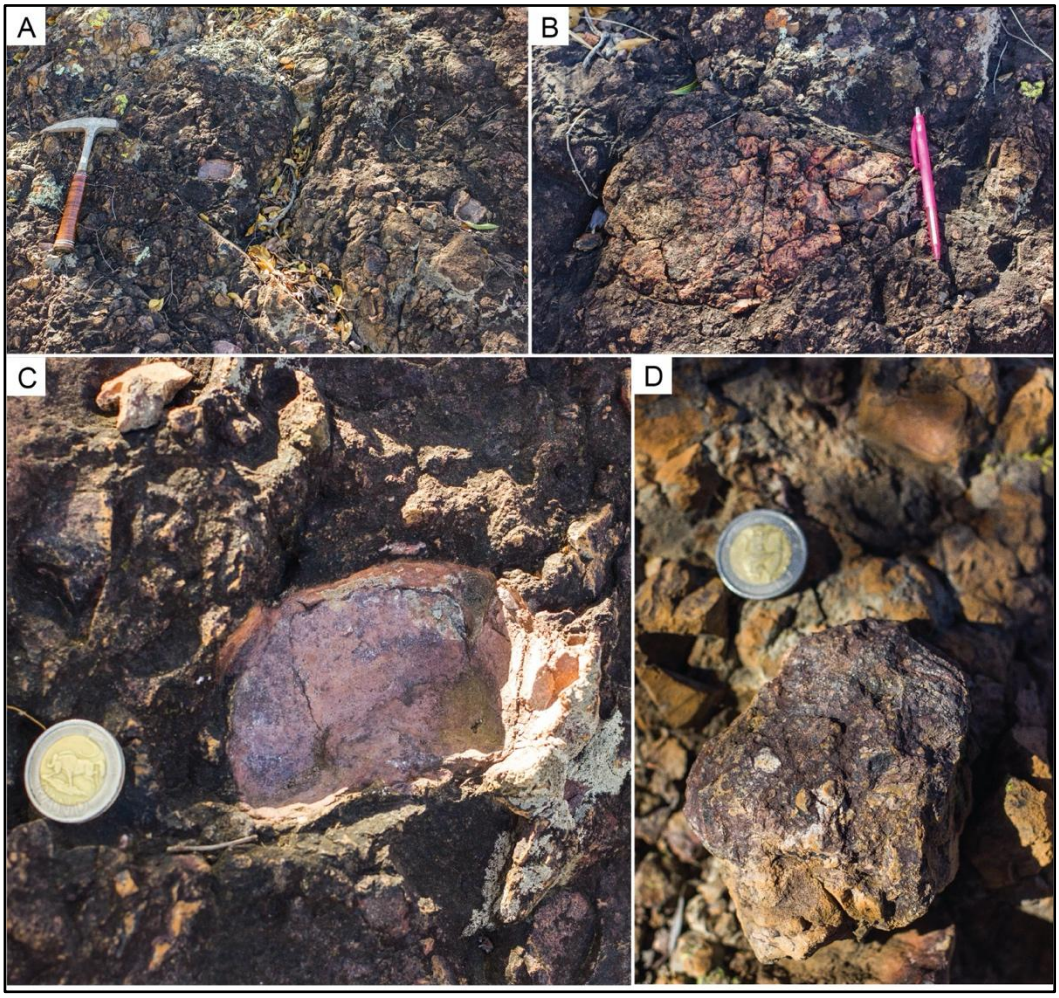

Figure 31. A) A lahar containing various sized lithic clasts. **B-D)** Clasts of various sizes and compositions set within a sandy matrix.

Outcrop 12 (figure 31) is a lahar, consisting of a coarse sandy groundmass which contains dominantly ignimbrite and minor siliciclastic clasts of various sizes. The clasts are angular to sub-angular (figure 31C) and measure between approximately 0,28 cm to 25,8 cm in diameter. The ignimbrite clasts range in welding from non-welded to welded.

4.1.13. Outcrop 13 [24º 36' 18,95" S; 28º 25' 53,21" E]:

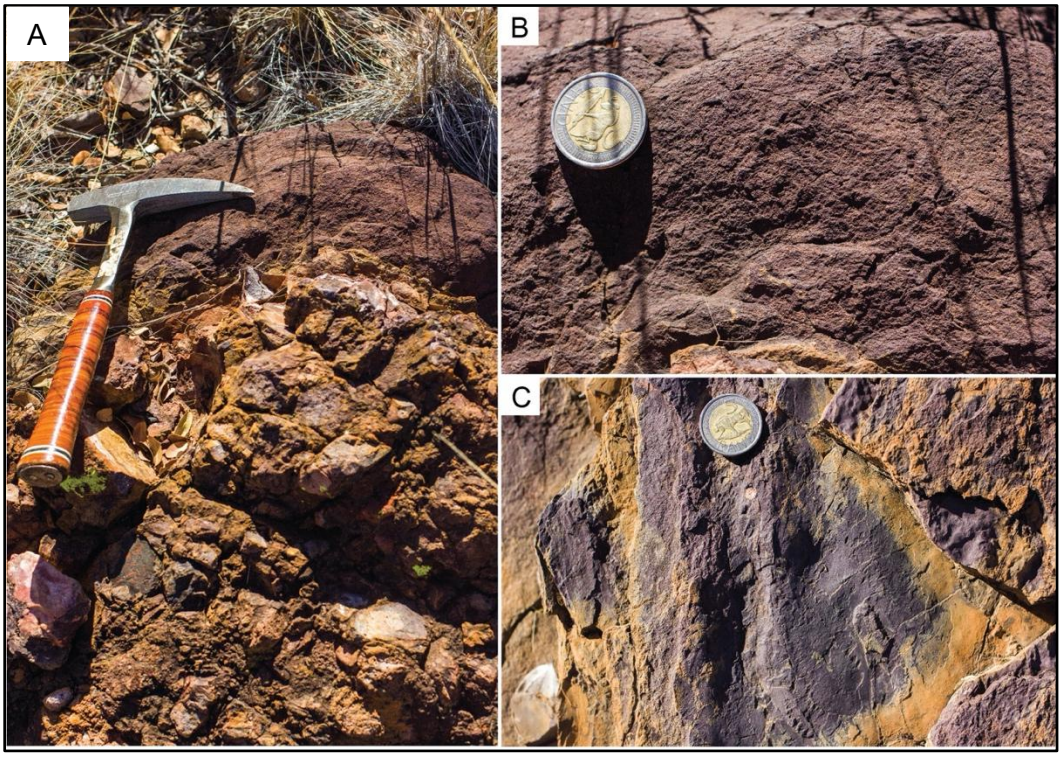

Figure 32. A) Contact between a lahar and sandstone. **B)** Hydrothermally altered sandstone. **C)** Ripple marks on observed sandstone.

Outcrop 13 (figure 32) exhibits the lahar from outcrop 12 overlying a sandstone. The debris flow likely came to rest and was deposited on top of sand sediments. The sandstone displays a deep purple colour, signifying hydrothermal alteration of iron-rich fluids. This hydrothermal alteration is likely the same hydrothermal event found across the Rooiberg ignimbrites of the sampled region. The sandstone in outcrop 13 (figure 32B) exhibits symmetrical ripple marks (figure 32C).

4.1.14. Outcrop 14 [24º 36' 16,66" S; 28º 25' 58,59" E]:

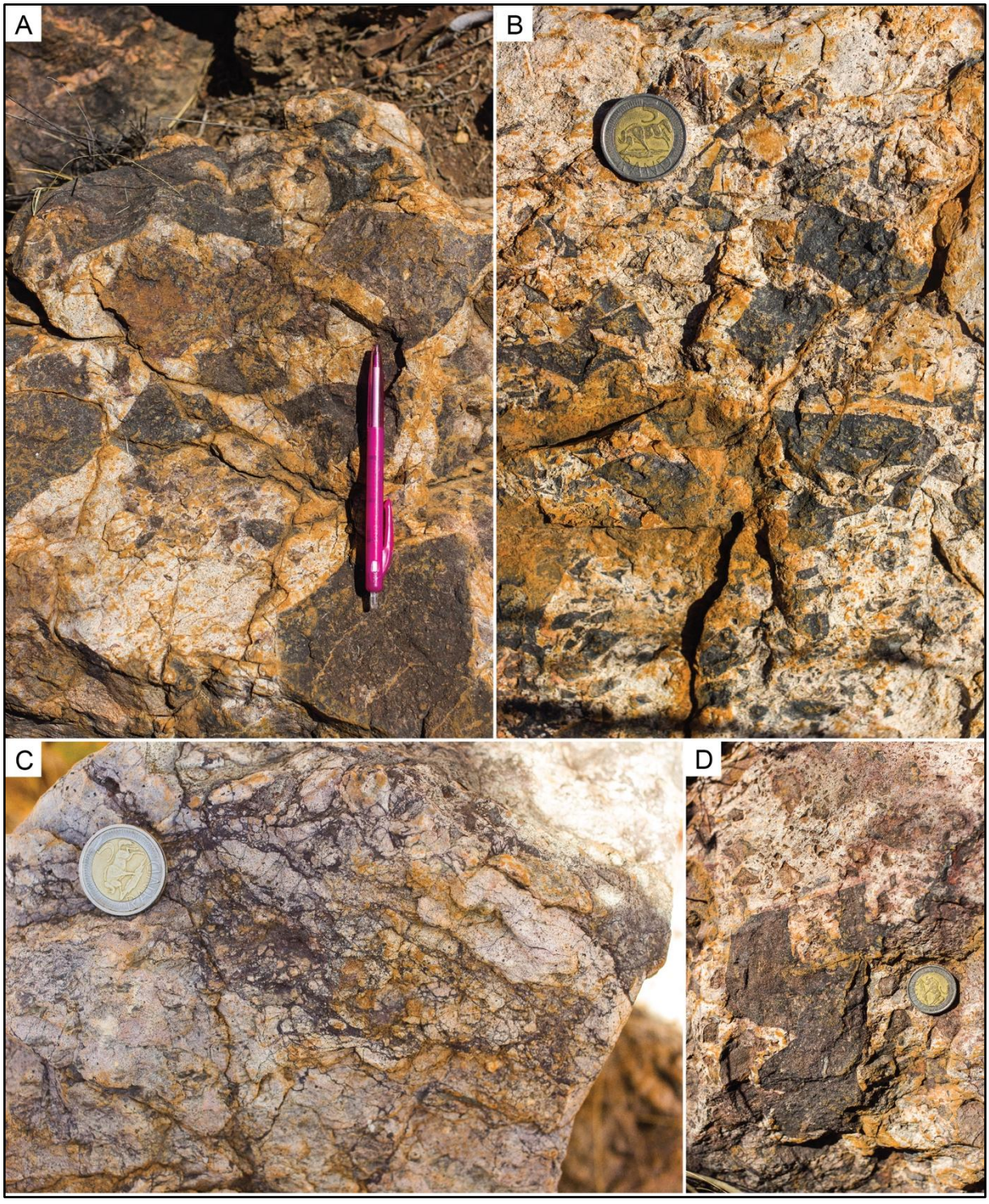

Figure 33. A) A peperite with a white, sandy groundmass containing large rhyolitic, angular clasts. **B & D)** Black angular and occasionally blob-like rhyolitic clasts of differing sizes. **C)** Brecciation of peperite in a vein-like structure with an Fe-filled matrix.

4.1.15. Outcrop 15 [24º 36' 12,71" S; 28º 25' 54,52" E]:

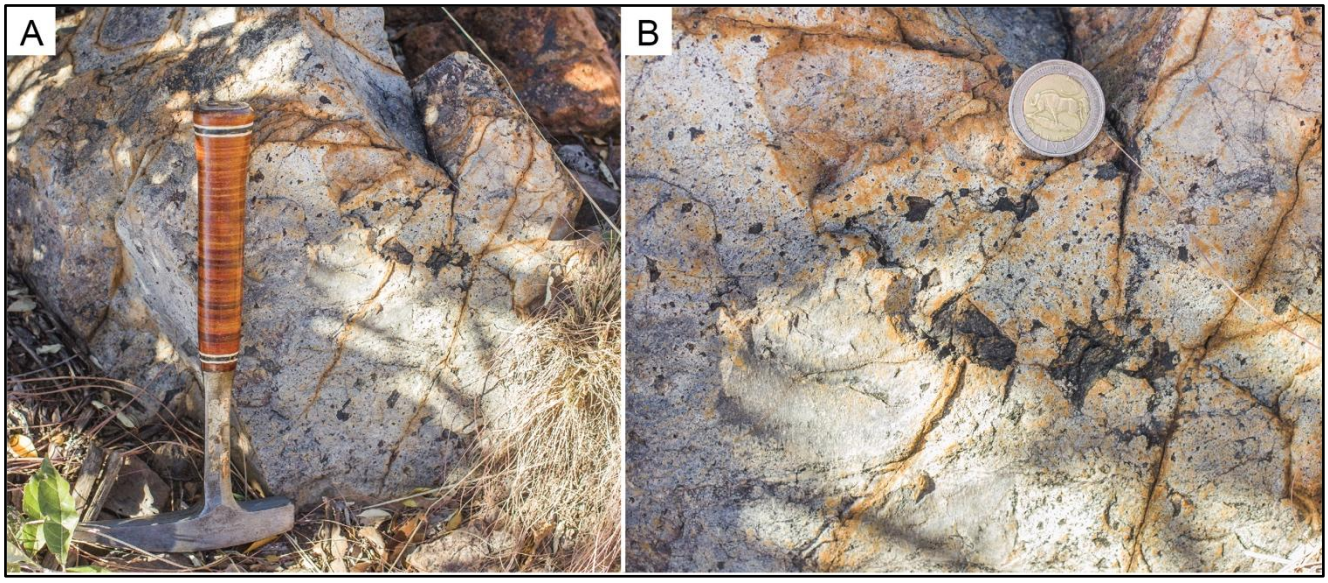

Figure 34. A) A peperite comprising dominantly sandy groundmass with scattered rhyolitic clasts. **B)** The black clasts range from angular to blob-like and are likely rhyolitic in composition.

Outcrops 14 (figure 33) and 15 (figure 34) consist of sandy peperite containing black, glassy clasts which are dacitic to rhyolitic in composition. The clasts are mostly angular, however blob-like and sub-angular clasts are also present. The clasts range in length from approximately 0,12 cm to 15 cm in outcrop 14 and 0,03 cm to 2,33 cm in outcrop 15. Figure 33C of outcrop 14 displays a vein of brecciation of the peperite rock set in an iron precipitate matrix. The brecciated vein is likely attributed to geyser activity, similar to or the same as the evidence of geyser and hydrothermal activity seen in outcrops 9 and 10. This geyser activity would have occurred post-peperite formation.

4.1.16. Outcrop 16 [24º 36' 6,95" S; 28º 25' 28,66" E]:

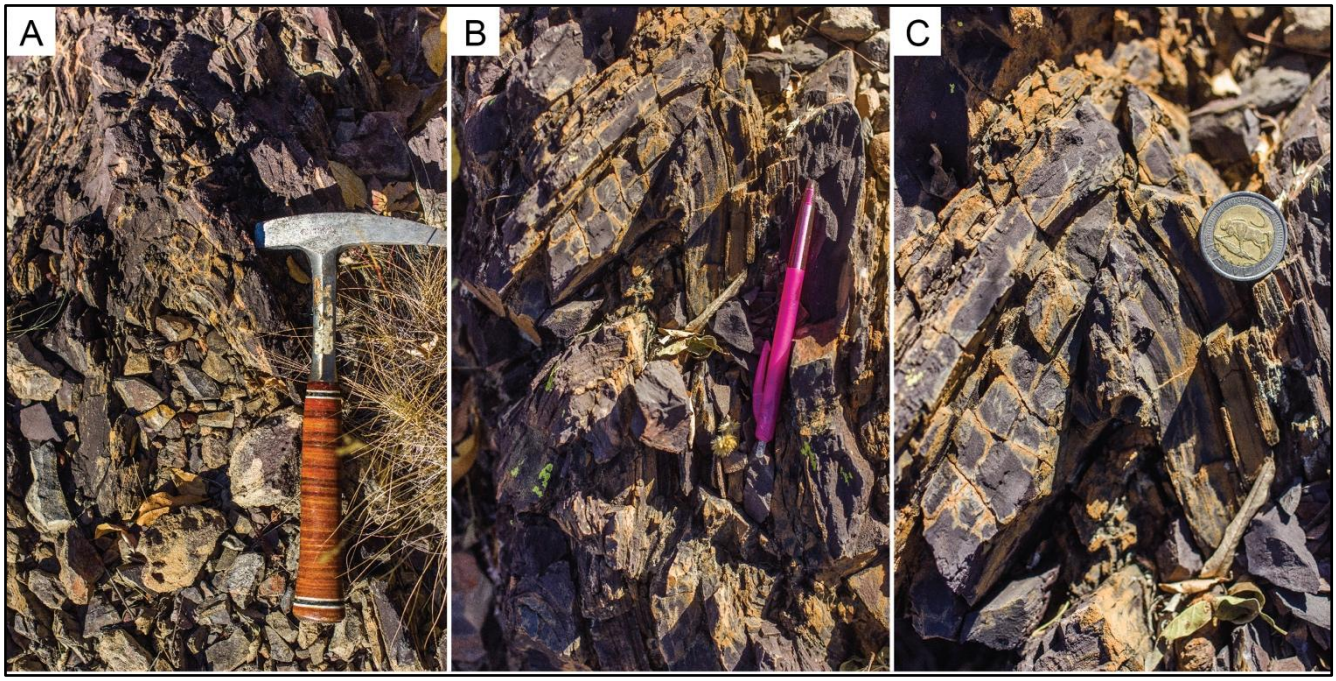

Figure 35. A) An extremely high-grade welded ignimbrite with sheath folding. **B &C)** A closer look at the sheath folding of the lava-like ignimbrite.

Outcrop 16 (figure 35) comprises an extremely high-grade, lava-like ignimbrite that has flow banding and sheath folds. The texture of the rock is completely aphyric. The ignimbrite is also strongly hydrothermally altered by iron-rich fluids, observed by the deep purple colour of the rock.

Table 1. A summary of the Rooiberg Group Field Analysis at Kuthaba Bush Lodge.

Outcrop	Formation	Rock type	Rock texture and mineralogy
1	Schrikkloof Formation	Ignimbrite	Blocky, lava-like with localised flow-banding. Groundmass is aphanitic with specks of green collapsed pumice clasts altered to secondary minerals. Hydrothermally altered with hematite precipitates.
2	Schrikkloof Formation	Ignimbrite	Lava-like and massive outcrop overlain by a flow-banded lava-like ignimbrite. Jointed and hydrothermally altered with hematite precipitates along the joints.
3	Schrikkloof Formation	Ignimbrite	Lava-like and extensively folded and flow-banded (rheomorphic). Massive texture with specks of secondary minerals.

Outcrop	Formation	Rock type	Rock texture and mineralogy
4	Schrikkloof Formation	Ignimbrite	Extensively folded and flow-banded (rheomorphic). Lava-like and aphanitic.
5	Schrikkloof Formation	Ignimbrite	Extensively folded and flow-banded (rheomorphic). Lava-like with an aphanitic groundmass. Rare phenocrysts of secondary minerals, which are recrystallised collapsed pumice clasts and/ or pyroxene, plagioclase, and hornblende.
6	Schrikkloof Formation	Ignimbrite	Intercalation of welded lava-like ignimbrite and non-welded, coarse, and porous ignimbrite.
7	Schrikkloof Formation	Ignimbrite	Low-grade welding with a clastic texture. Angular lithic (quartzite) clasts and altered (chlorite) pumice clasts present which are matrix supported.
8	Schrikkloof Formation	Ignimbrite	High-grade of welding with a fiamme and eutaxitic texture.
9	Schrikkloof Formation	Ignimbrite	Lava-like and flow-banded with localised brecciation. Strongly hydrothermally altered with hematite precipitates.
10	Schrikkloof Formation	Ignimbrite	Massive to slightly flow-banded. Localised brecciated pipes of angular ignimbrite clasts within an iron-precipitate groundmass.
11	Schrikkloof Formation	Ignimbrite	Low grade welding to no welding. Clastic, sandy texture. Matrix-supported angular siliciclastic fragments.
12	Schrikkloof Formation	Lahar	Coarse, sandy groundmass containing ignimbrite (major) and siliciclastic (minor) clasts of various sizes. Clasts are angular to sub-angular.
13	Schrikkloof Formation	Sandstone	Iron-rich (hydrothermal alteration). Symmetrical ripple marks.
14	Schrikkloof Formation	Peperite	Sandy groundmass containing glassy clasts, which range from angular to blob-like.
15	Schrikkloof Formation	Peperite	Sandy groundmass containing glassy clasts, which are angular to blob-like.
16	Schrikkloof Formation	Ignimbrite	Extremely high-grade welding. Lava-like with flow-banding and sheath folds. Aphyric texture. Strongly hydrothermally altered with iron precipitates.

4.2. Hand Specimen & Thin Section Analyses

The following Rooiberg Group rock samples were sampled from four locations, namely the Loskop Dam region, the Selons Rivier region, the Dullstroom region, and from Kuthaba Bush Lodge (figure 36). The Loskop Dam and Selons Rivier outcrops are continuous and can be considered the same sampling region. Therefore the "Loskop Dam region" will include samples sampled from both Loskop Dam and Selons Rivier. The Dullstroom region includes two samples from the Dullstroom Formation, namely RG 7 and RG 46. The Loskop Dam region includes samples from the Damwal Formation (LD 021 and RL 1), Kwaggasnek Formation (LD 002 and LD 004), and Schrikkloof Formation (SM 28.1). Kuthaba Bush Lodge includes the Schrikkloof Formation only and comprises the most samples, including PYR 1A and 1B, PYR 2, KTP 2, KT 9, KT 53, KT 57, KT 201, KT 202.1, and KT 210. The sample regions in relation to the Rooiberg Group extent across South Africa can be seen in Figure 1. Figures 37 to 39 are orthophotos of the sampled areas, displaying the locations of each sampled rock.

These samples were sampled by Dr. Nils Lenhardt and Dr. Olutola Jolayemi in previous years for different scientific studies. These samples are therefore not directly correlated with the outcrops in the field analysis (chapter 4.1) conducted in the present study. The field analysis contributes to the present study by field observations only. The Dr. Lenhardt and Dr. Jolayemi samples in this study have been used for the thin section analyses and grain size distribution analyses.

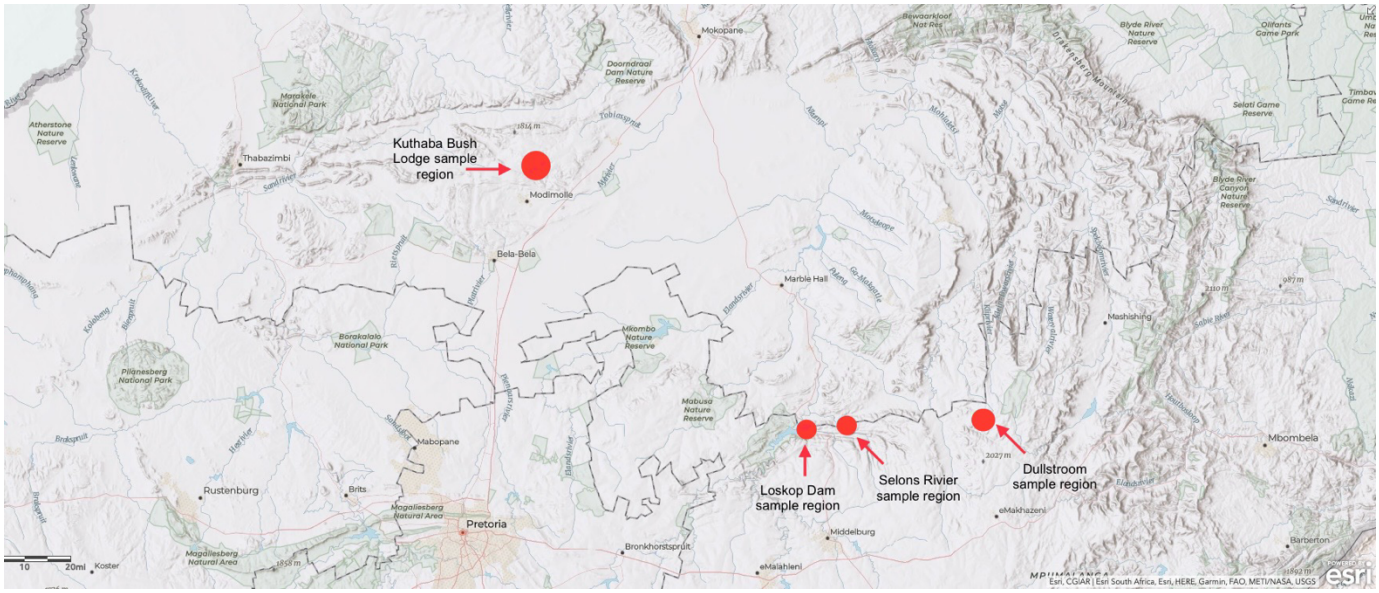

Figure 36. An annotated terrain map of the sample regions, namely the Kuthaba Bush Lodge region, the Loskop dam region, the Selons Rivier region, and the Dullstroom region. Map by National Geographic Map Maker, Esri (2022).

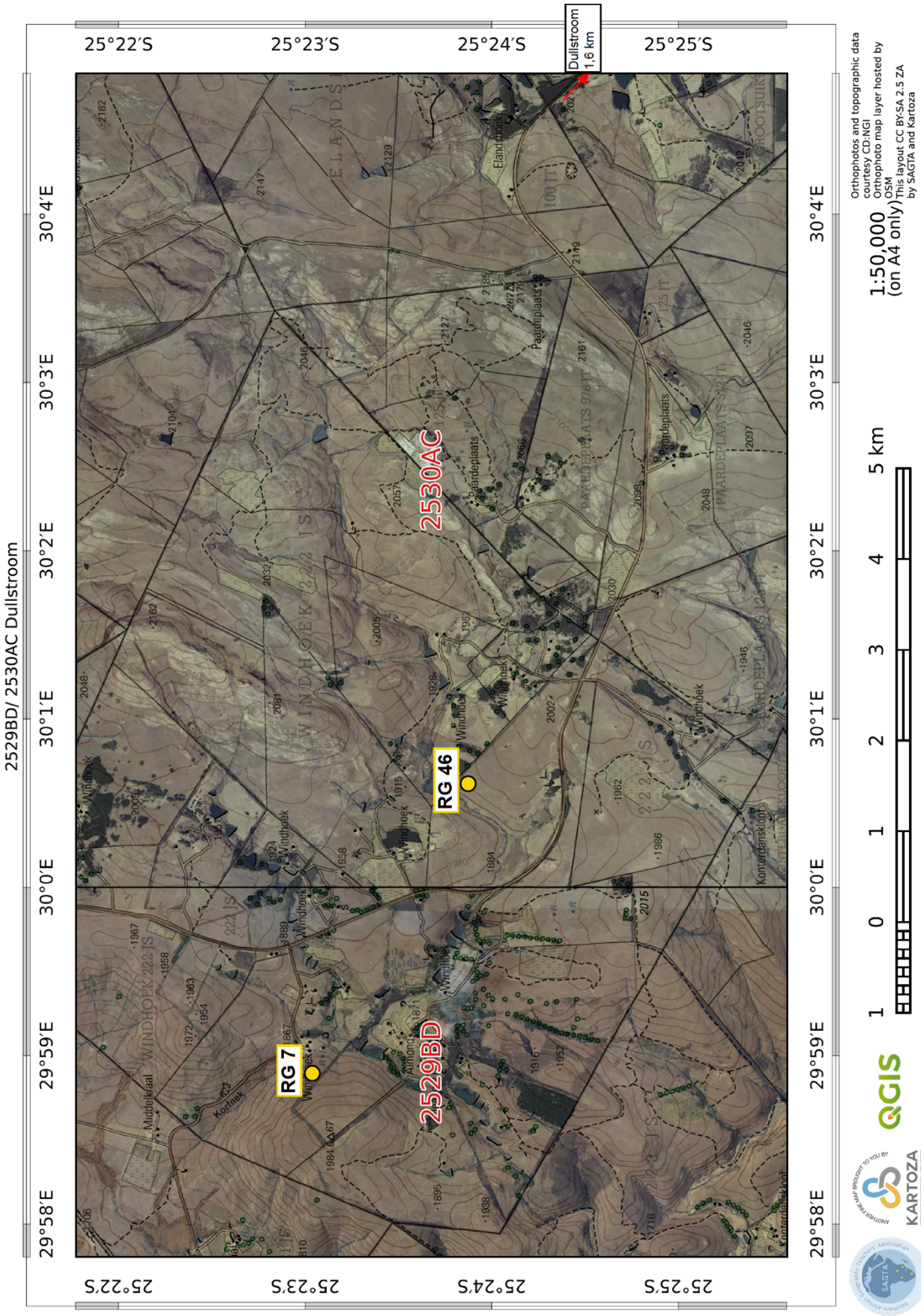

Figure 37. Orthophoto hybrid map of the Dullstroom sample region. Samples included are from the Dullstroom Formation (highlighted in yellow). Map by SAGTA, Kartoza, 2023.

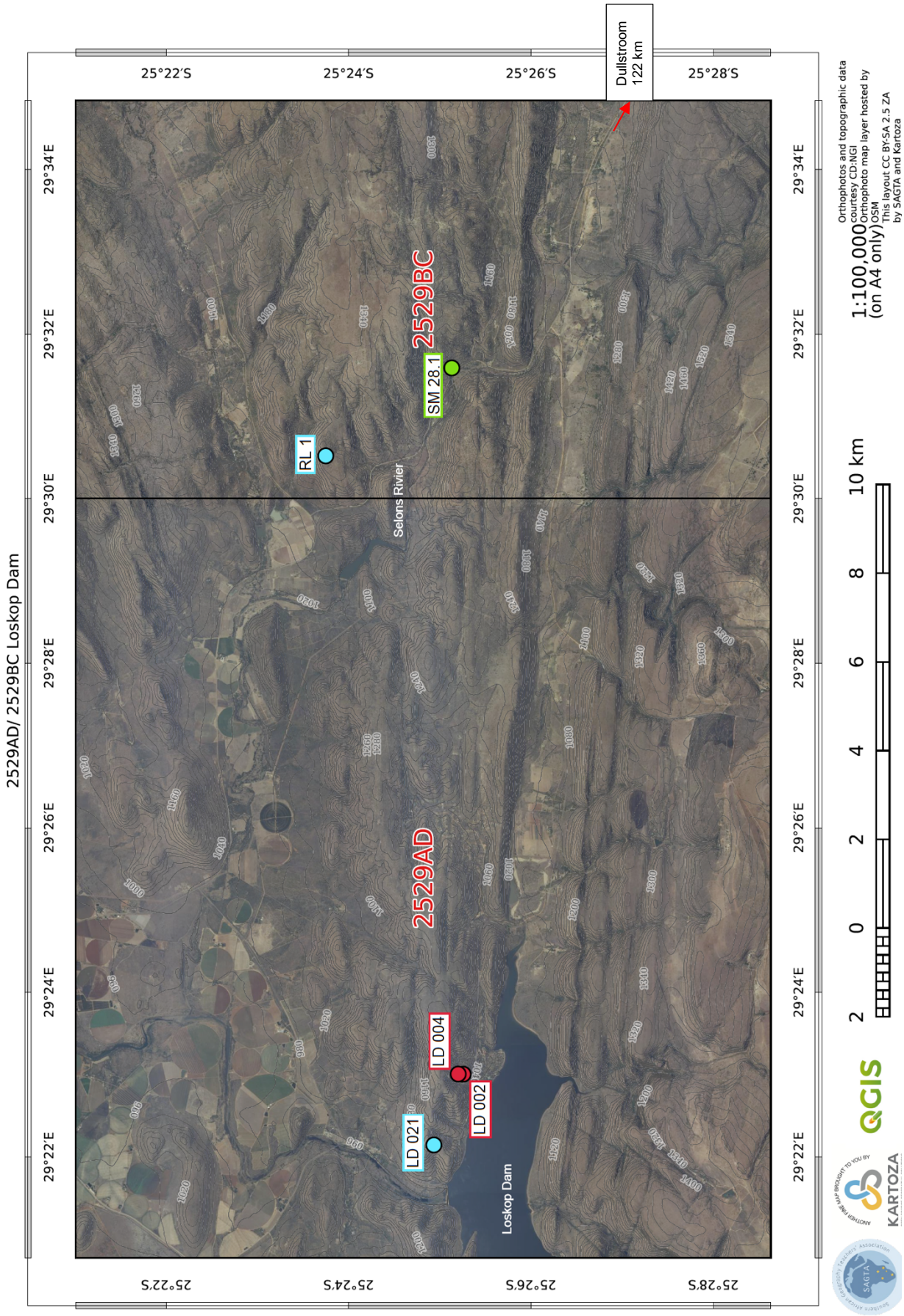

Figure 38. Orthophoto of the Loskop Dam sample region. Samples included are from the Damwal Formation (highlighted in blue), Kwaggasnek Formation (highlighted in red), and the Schrikkloof Formation (highlighted in green). Map by SAGTA, Kartoza, 2023.

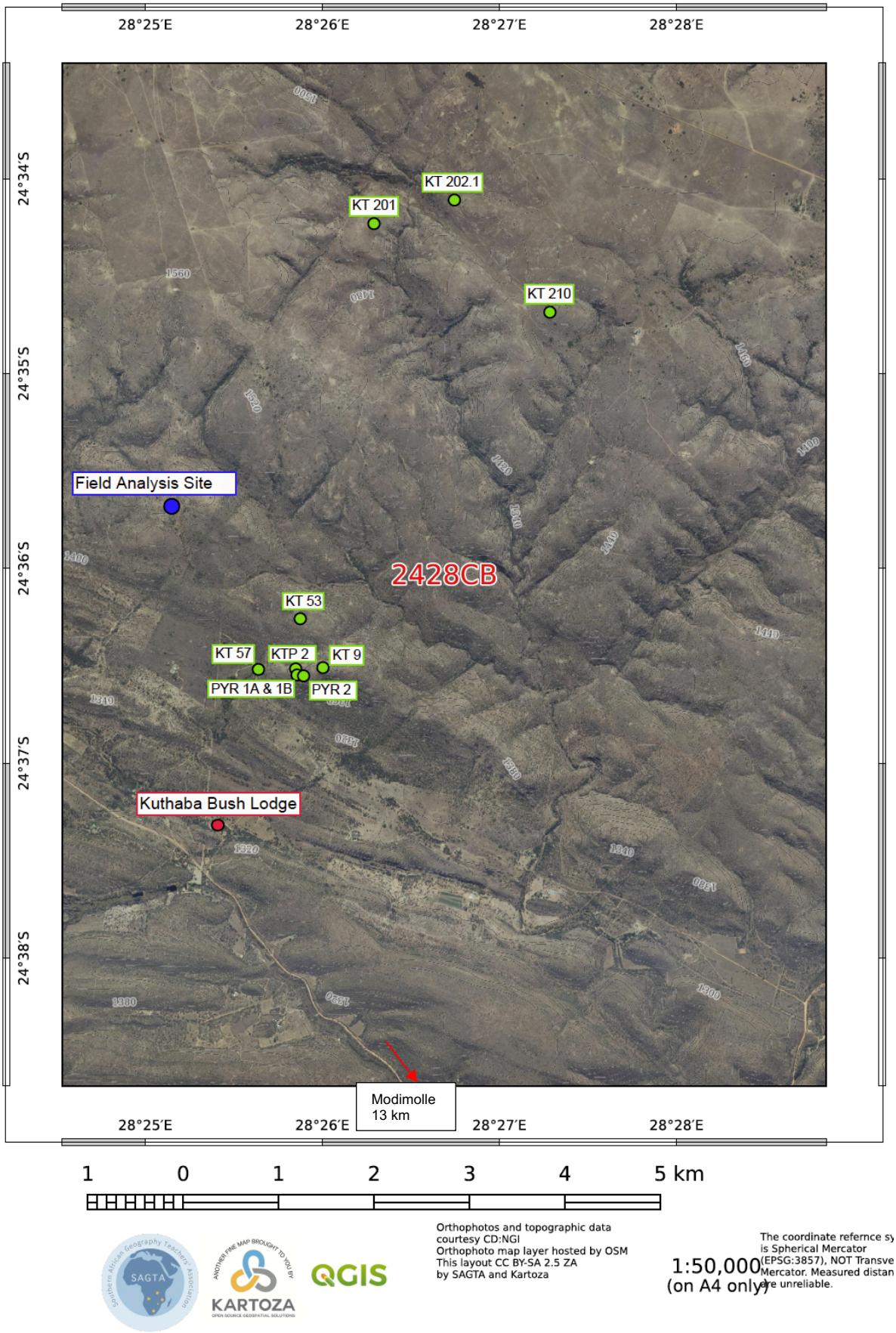

Figure 39. Orthophoto of the Kuthaba Bush Lodge sample region. All Kuthaba samples are from the Schrikkloof Formation (seen in green). Map by SAGTA, Kartoza, 2023.

4.2.1. The Dullstroom Sampling Site

The Dullstroom Formation:

RG 7 [25°23'02.0" S; 29°58'54,2" E]:

Figure 40. Hand sample of an aphanitic, darkly coloured rock with occasional elongated amygdules.

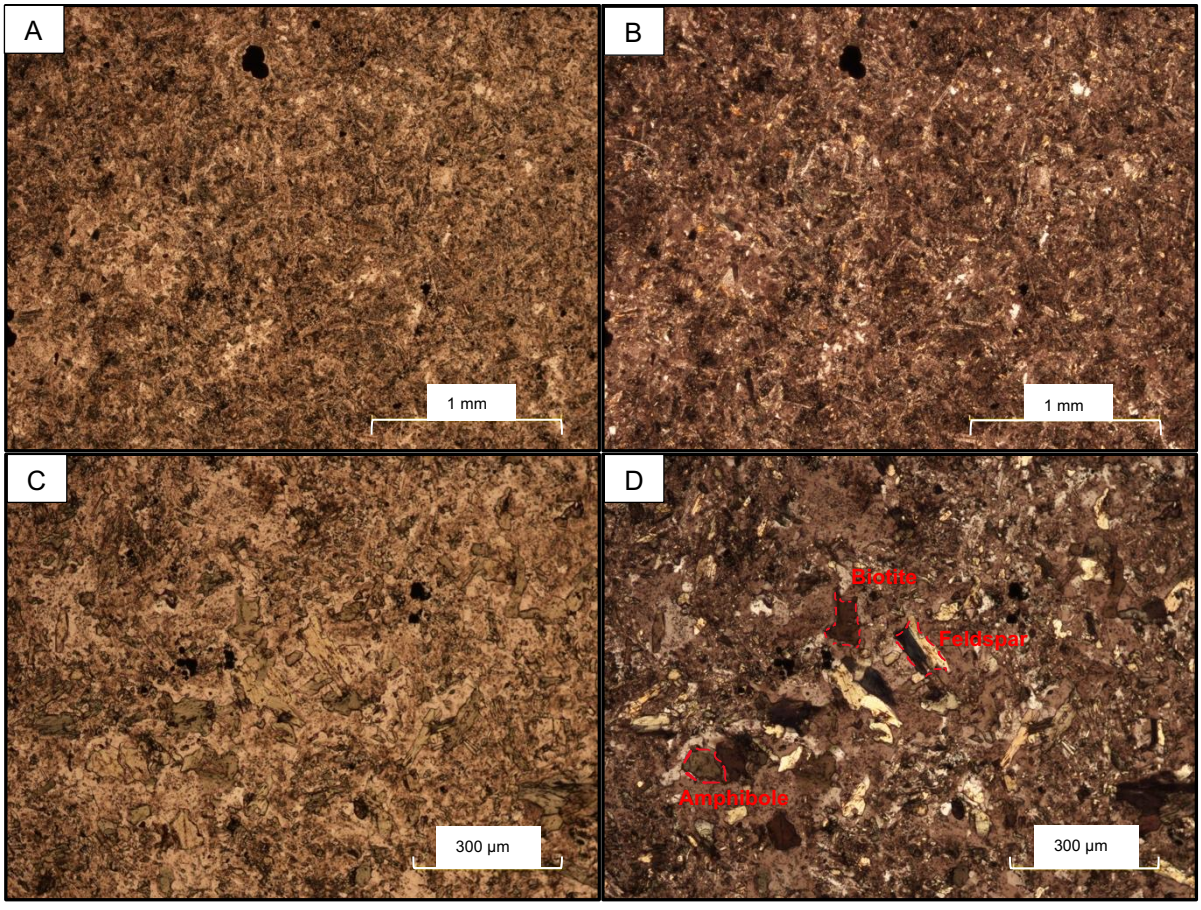

Figure 41. A polarised microscope photograph of rock sample RG7: **A- PPL and B- XPL** cryptocrystalline texture with larger opaque crystals distributed throughout the sample. **C- PPL and B- XPL** at 10X magnification displaying a glassy groundmass, containing crystals of feldspar, amphibole and biotite.

Rock sample RG 7 (figures 40 and 41) has a cryptocrystalline, devitrified groundmass containing microlites of plagioclase or apatite, laths of hornblende and biotite, and specks of opaque minerals (up to 190 µm in length) which are likely to be magnetite or titanomagnetite and can be seen in figures 41A and B. Hornblende and biotite crystals range from approximately 50 µm to 170 µm, as seen in figures 41C and D. The opaque minerals are anhedral and interstitial, which may be overgrowths and may be secondary minerals. The very fine-crystalline and glassy groundmass signifies rapid cooling and eventual quenching. Fine flow banding, not seen in the magnified thin section as it is too large, is observed by eye in the cut rock sliver. RG 7 is likely a basaltic andesite crystallised from a lava flow.

RG 46 [25°23'53.3" S; 30°00'37.1" E]:

Figure 42. Hand sample of an aphanitic and compact darkly coloured rock, similar to rock sample RG 7.

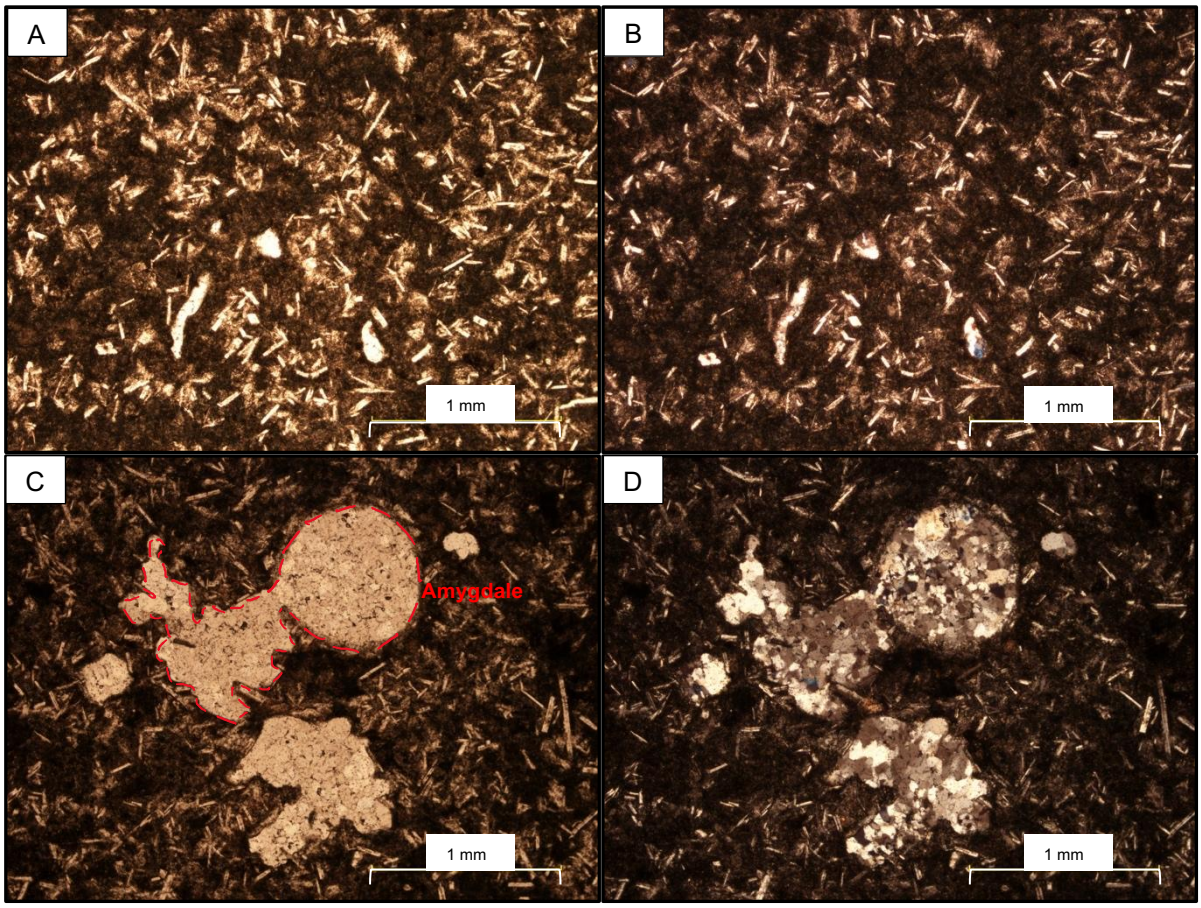

Figure 43. A polarised microscope photograph of rock sample RG 46: **A- PPL** and **B- XPL** displaying a hypocrystalline texture containing abundant plagioclase crystals in a glassy groundmass. **C- PPL** and **D- XPL** exhibit amygdales infilled with secondary quartz.

Rock sample RG 46 (figures 42 and 43) is composed of a devitrified glassy groundmass containing numerous euhedral to subhedral plagioclase crystals, which range in length from approximately 0,05 mm to 0,45 mm (50-450 µm) and are randomly orientated, as observed throughout the sample. RG 46 can be considered micro-porphyritic containing micro-phenocrysts of plagioclase. Rounded to anhedral amygdules are largely present, which are filled with secondary quartz crystals, as seen in figures 43C and D. The plagioclase crystals were crystallised during magma ascent and eruption, which was followed by rapid cooling and quenching of erupted lava, resulting in a glassy matrix. RG 46 is interpreted to represent an andesite.

4.2.2. The Loskop Dam Sampling Site

The Damwal Formation:

RL 1 [25°23'44,0" S; 29°30'30,5" E]:

Figure 44. Hand sample of a porphyritic and dense darkly coloured rock. This rock is crystallised from a lava flow, being an andesite or dacite in composition.

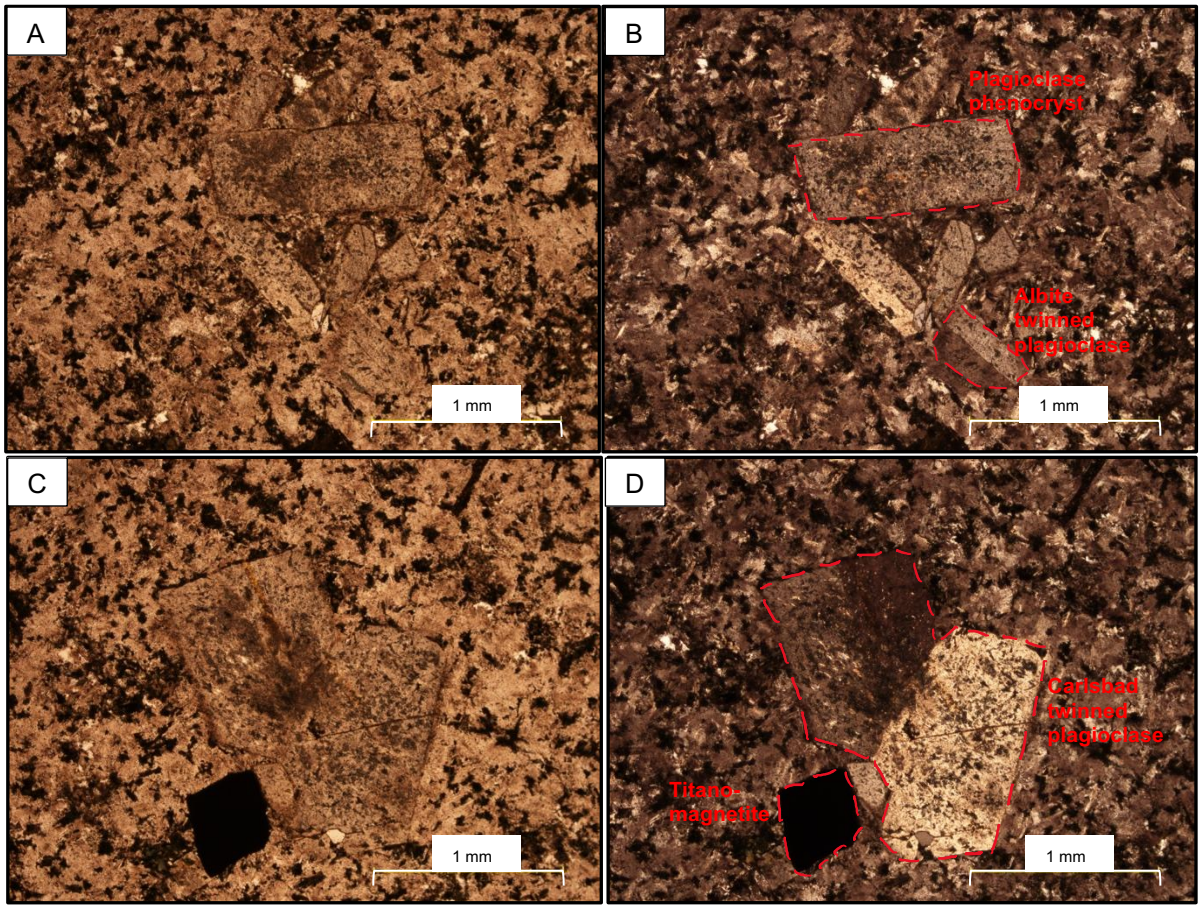

Figure 45. A polarised microscope photograph of rock sample RL 1: **A- PPL** and **B- XPL** a glomeroporphyritic texture of plagioclase phenocrysts. **C- PPL** and **D- XPL** twinned plagioclase and a large opaque phenocryst.

Rock sample RL 1 (figures 44 and 45) is porphyritic and consists of a devitrified glassy groundmass surrounding euhedral to subhedral plagioclase phenocrysts, which range from 0,22 mm to 1,22 mm in length. The plagioclase phenocrysts (of albite composition) occur as clusters forming glomerocrysts, having accreted during early crystallisation, shortly before eruption occurred. The plagioclase phenocrysts also have sieve textures and appear to be partially sericitised, associated with hydrothermal alteration. This can be seen in figure 45. Albite twinning of some of the plagioclase crystals can be seen in figure 45B and Carlsbad twinned plagioclase crystals can be seen in figures 45C and D. Magnetite or titanomagnetite are copious, observed throughout the section, and are interstitial, however a distinct titanomagnetite crystal is observed in figures 45C and D. This represents two different crystal growth periods of the titanomagnetite crystals, namely early and late-stage crystallisation. Rock sample RL1 originates from a lava flow where plagioclase crystal growth occurred before eruption. RL 1 is interpreted to be andesitic to dacitic in composition.

LD 021 [25°24’55,1” S; 29°22’09,4” E]:

Figure 46. Hand sample of an aphanitic, lightly coloured rock of intermediate composition, such as andesitic to dacitic.

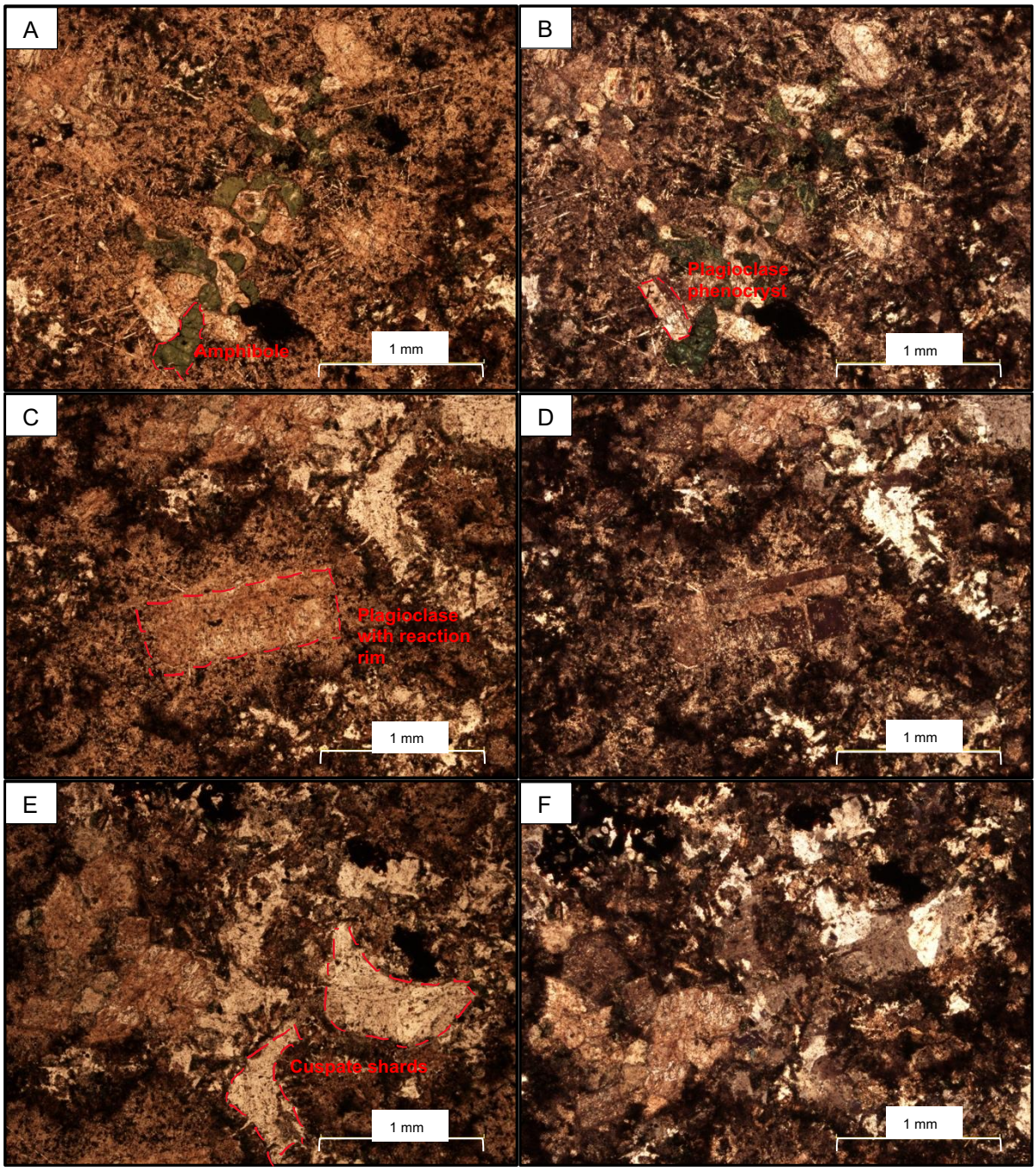

Figure 47. A polarised microscope photograph of rock sample LD 021: **A- PPL** and **B-XPL** displaying a microporphyritic to porphyritic texture containing plagioclase phenocrysts surrounded by a devitrified glassy groundmass. **C- PPL** and **D- XPL** display a plagioclase phenocryst with a reaction rim, and **E- PPL** and **F-XPL** show recrystallised cuspate shards within the devitrified groundmass.

Rock sample LD021 (figures 46 and 47) consists of a devitrified cryptocrystalline groundmass containing needle-like crystals or microlites, consisting of quartz and/ or feldspar (seen in figures 47A-D), specks and laths of titanomagnetite, as well as plagioclase phenocrysts. Oftentimes the plagioclase phenocrysts occur as glomerocrysts, such as that observed in figures 47A and B. Albite twinning of some

plagioclase crystals can be seen in figures 47B and D. The plagioclase crystals range in length from 0,16 mm to 1,3 mm. A green anhedral mineral, seen in figures 47A and B, surrounds the plagioclase crystals in their cluster, and is likely to be hornblende. A reaction rim surrounds the plagioclase phenocryst in figures 47C and D, with polycrystalline quartz needles radiating out from the plagioclase crystal. The plagioclase crystals have albite twinning and contain titanomagnetite inclusions. Sickle-shaped structures are observed in figures 47C-F, with clear examples in figures 47E and F. These sickle-shaped structures may be glass shards, which have been recrystallised to quartz. LD 021 is intermediate in composition and is likely to be andesitic to dacitic. It is possible LD 021 was crystallised from a lava flow or perhaps is a low to medium grade welded ignimbrite, considering the recrystallised glass shards observed in figures 47E and F.

The Kwaggasnek Formation

LD 002 [25°25'16,6" S; 29°22'59,9" E]:

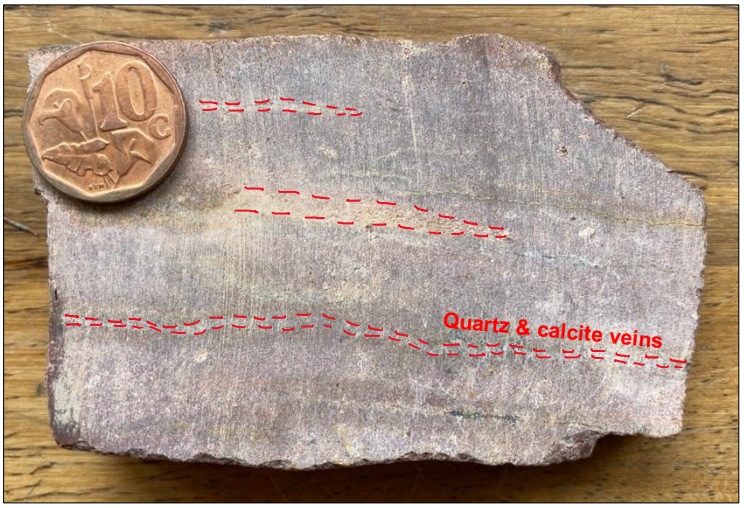

Figure 48. Hand sample of a fine-grained, reddish coloured rock. Cracks and veins run across the hand sample, infilled with secondary minerals such as quartz or calcite. Occasional phenocrysts are observed throughout the sample. LD 002 is a medium welded ignimbrite of rhyodacite composition.

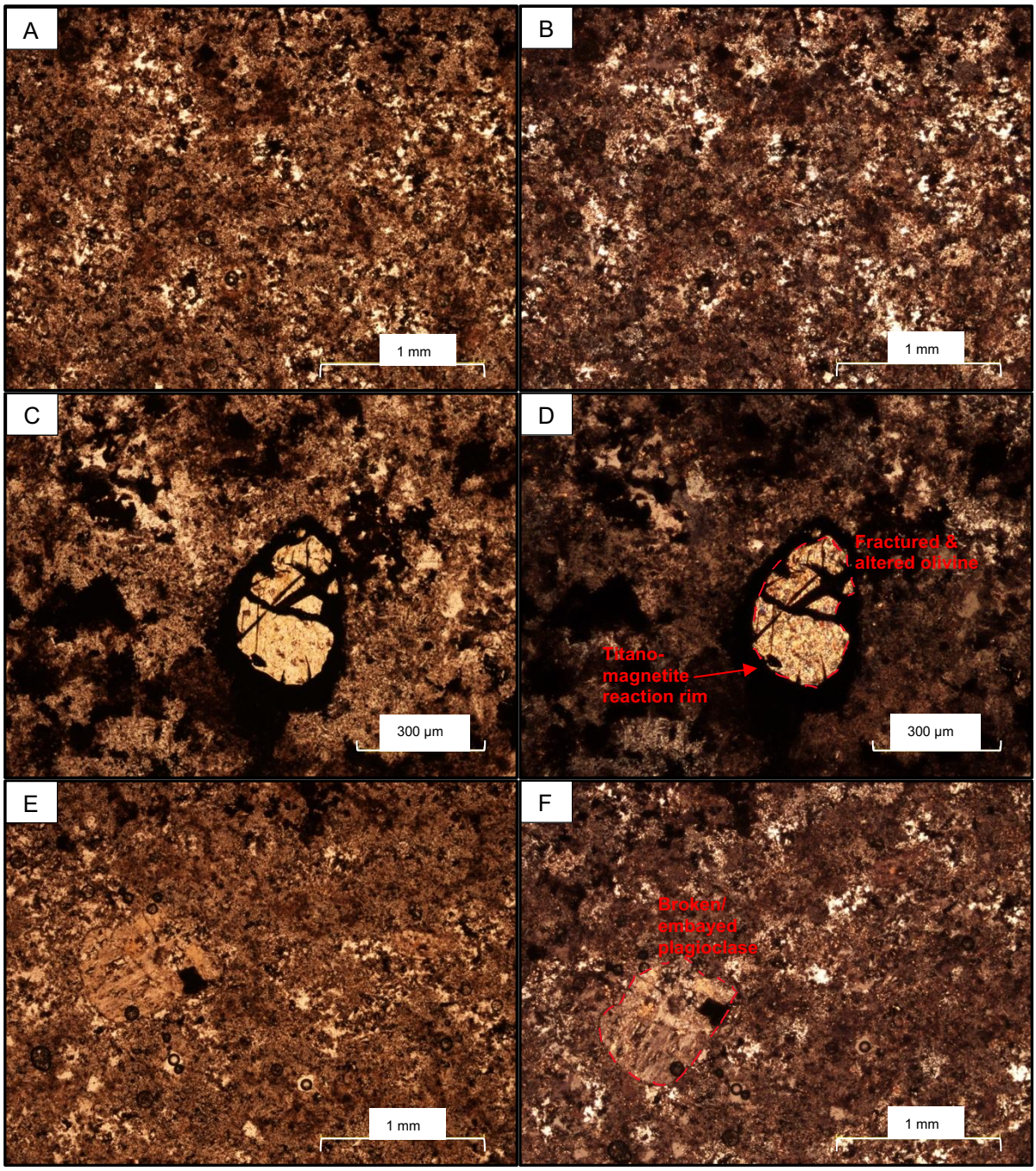

Figure 49. A polarised microscope photograph of rock sample LD 022: **A- PPL** and **B- XPL** displaying a devitrified, glassy groundmass of spherulitic texture. **C- PPL** and **D- XPL** at 10X magnification, showing a heavily fractured olivine phenocryst or xenocryst- likely to be originally fayalitic in composition and altered to possibly serpentine. **E- PPL** and **F- XPL** displays a seemingly broken subhedral plagioclase crystal.

Rock sample LD 002 (figures 48 and 49) consists of a devitrified, glassy groundmass with numerous spherical micro-spherulites. Titanomagnetite, plagioclase or quartz microlites, and secondary quartz are identified in the matrix. This can be seen in figures 49A and B. Figures 49C and D show an altered olivine crystal, recrystallised to numerous fine-crystalline minerals, which are possibly bowlingite or chlorophaeite.

A magnetite or titanomagnetite reaction rim occurs around the olivine crystal and fills the olivine's fractures, further resulting in embayment of the olivine. The olivine phenocryst is either an early formed crystal or a xenocryst. Figures 49E and F display a broken subhedral plagioclase phenocryst. The plagioclase crystal may also have been embayed and reacted with the matrix, resulting in half of the crystal being left behind instead of it being broken. The plagioclase phenocryst contains inclusions of an opaque mineral (such as titanomagnetite) and glass. Phenocrysts within this section are slightly rarer, making up approximately 5% of the rock sample. The veins running across the hand sample of LD 002 seen in figure 49 are composed of secondary quartz. LD 002 is a welded ignimbrite of rhyodacitic to rhyolitic composition.

LD 004 [25°25'14,0" S; 29°22'59,9" E]:

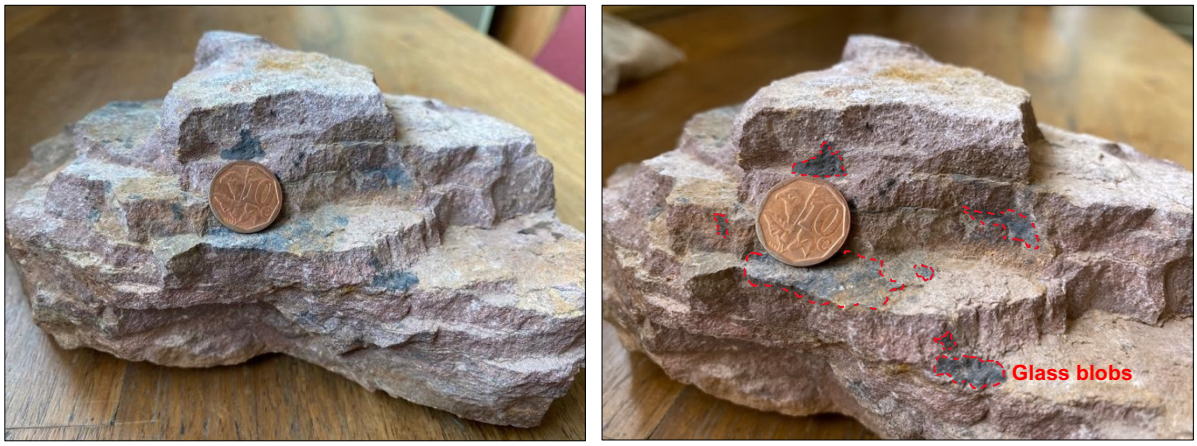

Figure 50. Hand sample of a fine grained, reddish coloured rock with small phenocrysts and blobs of glass fragments. LD 004 is a low to medium welded ignimbrite of rhyolitic composition.

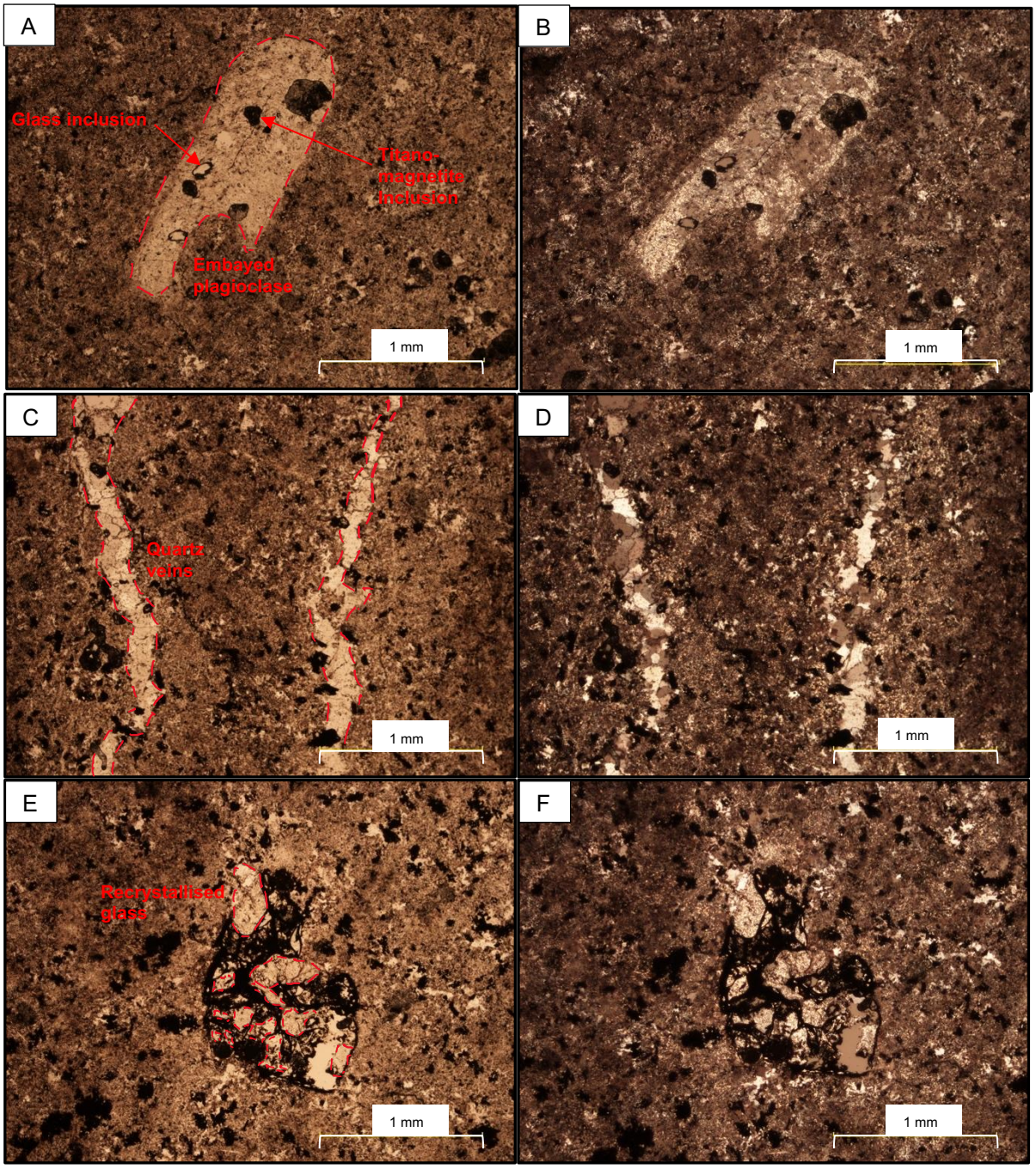

Figure 51. A polarised microscope photograph of rock sample LD 004: **A- PPL** and **B- XPL** displaying an embayed plagioclase phenocryst encompassed in a glassy, devitrified groundmass. **C- PPL** and **D- XPL** show quartz veins running through the thin section. **E- PPL** and **F- XPL** display a cluster of altered anhedral minerals or recrystallised glassy blobs surrounded by an interstitial opaque mineral or reaction rim.

Rock sample LD 004 comprises a devitrified groundmass, consisting of quartz, feldspar, opaques (such as magnetite or titanomagnetite) and sericite or saussurite. The groundmass also contains micro-spherulitic textures in some sections, such as in figures 51A and B. Plagioclase phenocrysts are present, such as the one seen in figures 51A and B, however it is more clearly seen at 10X magnification.

This plagioclase is embayed, contains glass and magnetite inclusions, and is sericitised. There are occasional quartz veins, such as those observed in figures 51C and D. Blobs of recrystallised glass (similar to that of the groundmass) are seen in figures 51E and F, which are surrounded by an opaque mineral (such as magnetite or titanomagnetite). LD 004 is a low welded ignimbrite of rhyolitic composition.

The Schrikkloof Formation

SM 28.1 [25°25'07,0" S; 29°31'32,1" E]:

Figure 52. Hand sample of a clastic and porphyritic pyroclastic rock, including lithic and glassy fragments, of a deep red colour, displaying a hypocrystalline texture. SM 28.1 is a low welded ignimbrite of rhyolitic composition.

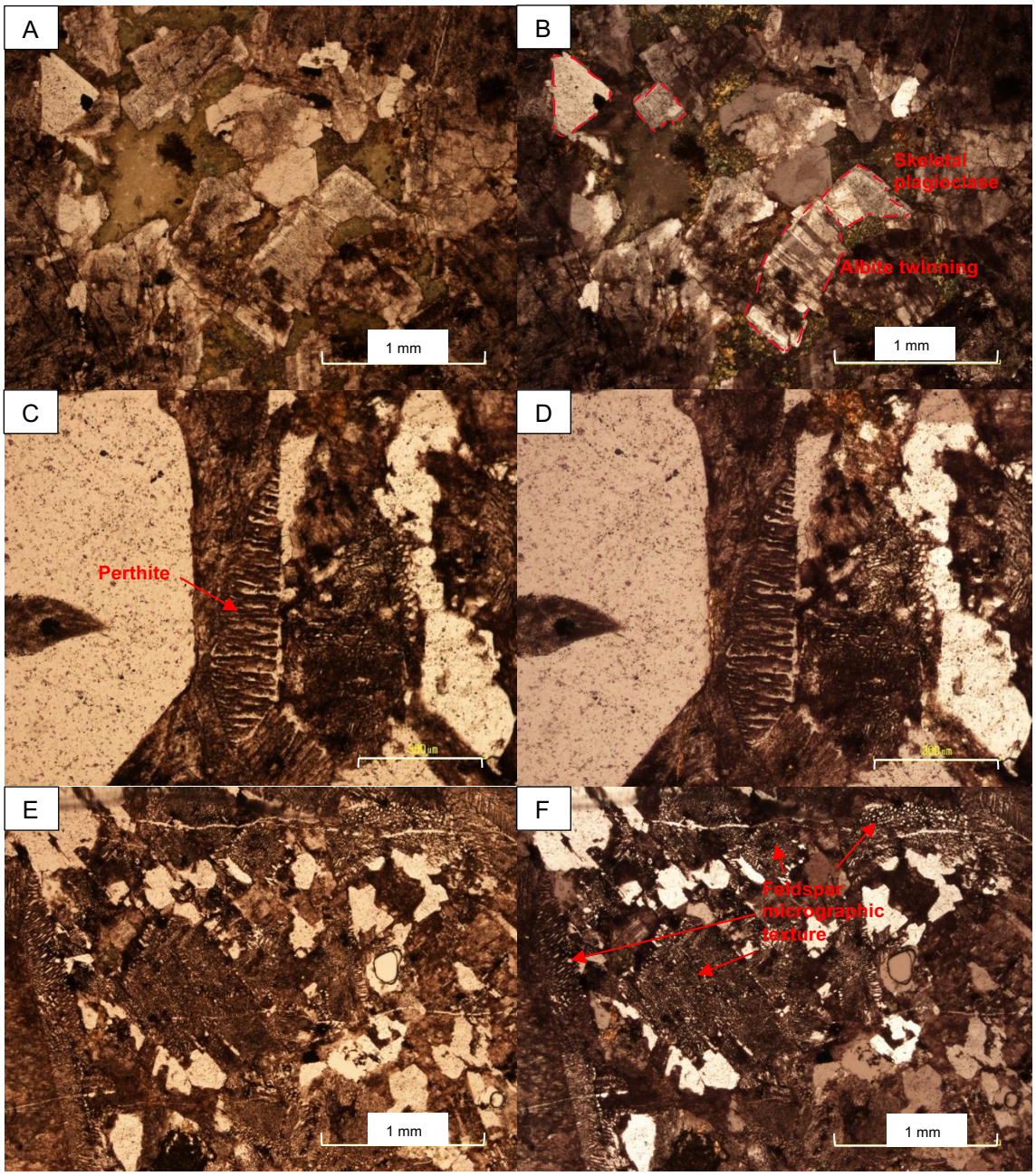

Figure 53. A polarised microscope photograph of rock sample SM 28.1: **A- PPL** and **B- XPL** displaying skeletal plagioclase, some displaying albite twinning, and quartz phenocrysts with interstitial green secondary minerals and a glassy groundmass surrounding the crystals. **C- PPL** and **D- XPL** at 10X magnification display perthite in the centre, some micrographic texture, interstitial quartz, and a large euhedral quartz phenocryst to the left. **E- PPL** and **F- XPL** include more micrographic texture, skeletal plagioclase, and quartz.

Rock sample SM 28.1 is characterised by a devitrified groundmass with numerous large phenocrysts, resulting in a hypocrystalline texture. Phenocrysts include plagioclase and quartz, seen throughout figure 53. Plagioclase phenocrysts tend to be skeletal (seen in figures 53A and B), some displaying albite twinning (figure 53B), and some displaying perthite exsolution, likely the unmixing of orthoclase and

albite. This can be seen in figures 53C and D and in figures 53E and F. Micrographic texture of quartz and feldspar intergrowths is seen throughout the section. This is particularly clear in figures 53E and F. The abundant presence of perthite, quartz and feldspar micrographic texture, and skeletal plagioclase suggests rapid cooling and instability of quartz and plagioclase crystal growth. SM 28.1 is a low welded ignimbrite that underwent rapid cooling during and after emplacement.

4.2.3. The Kuthaba Bush Lodge Sampling Site

The Schrikkloof Formation

KT 9 [24°36'30,8" S; 28°26'00,4" E]:

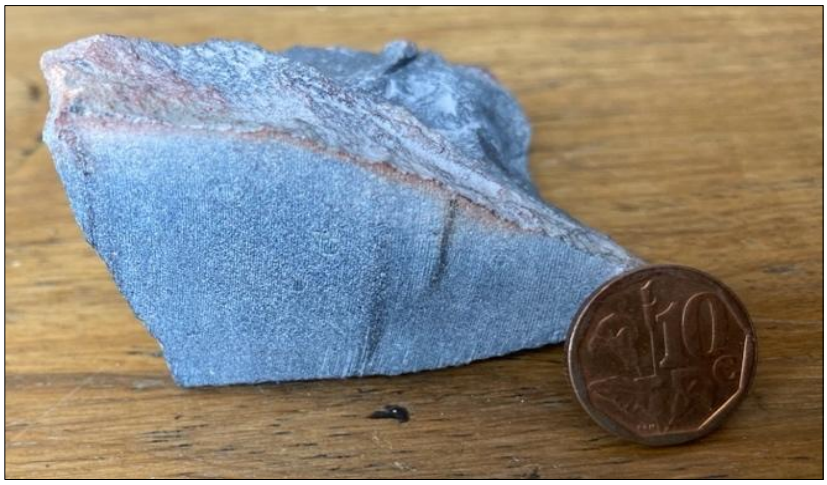

Figure 54. Hand sample of an aphanitic rock of a grey-blue colour, with minor (~5%) phenocryst content. KT 9 is a highly welded ignimbrite of rhyolitic composition.

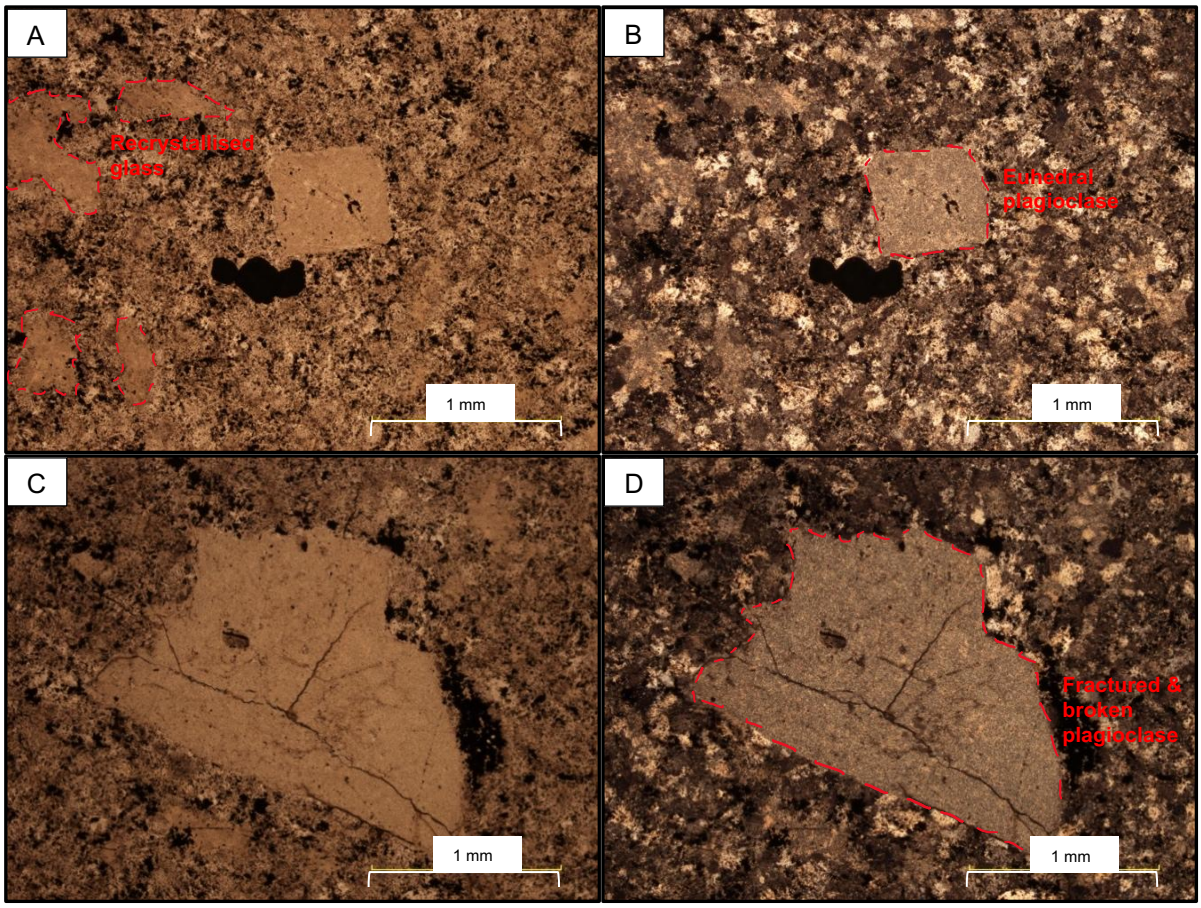

Figure 55. A polarised microscope photograph of rock sample KT 9: **A- PPL** and **B- XPL** display a completely devitrified groundmass with a euhedral plagioclase crystal and anhedral titanomagnetite or magnetite phenocryst. **C- PPL** and **D- XPL** show a fractured and broken plagioclase phenocryst encompassed in a devitrified matrix.

Sample KT 9 is hypocrystalline, consisting of a completely devitrified groundmass. The groundmass consists of inter-locking crystals of quartz, plagioclase, titanomagnetite and sericite, which can be seen in figure 55. KT 9 has sparse (~5%) phenocrysts, which include plagioclase that have been altered to fine sericite, often containing titanomagnetite inclusions, which can be seen in figures 55A-D. The plagioclase phenocrysts are most often subhedral with fuzzy outlines, suggesting a reaction with the groundmass. Blobs of original glass or pumice, recrystallised to match the groundmass (however finer crystalline than the groundmass), can be seen to the left in figures 55A and B. KT 9 is similar to and found close to the field analysis outcrops 2 and 5 seen in chapter 4.1.2 and 4.1.5. KT 9 is a lava-like, highly welded ignimbrite.

KT 53 [24°36’14,9” S; 28°25’53,9” E]:

Figure 56. Hand sample of a darkly coloured, aphanitic rock, with a lava-like texture. KT 53 is a highly welded, lava-like ignimbrite of rhyolitic composition.

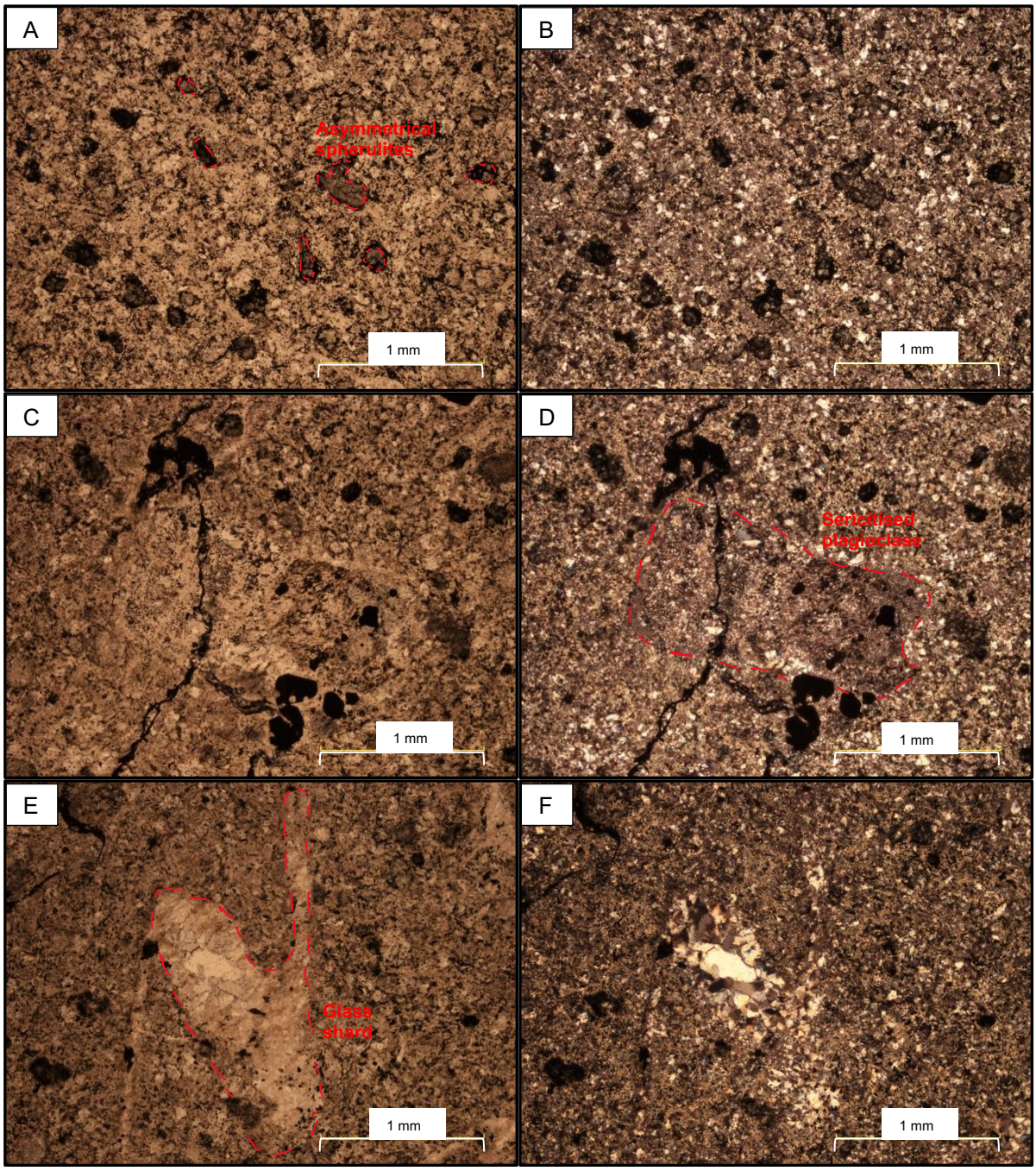

Figure 57. A polarised microscope photograph of rock sample KT 53: **A- PPL** and **B-XPL** display a completely devitrified groundmass with spherulitic texture. **C-PPL** and **D-XPL** show a recrystallised plagioclase phenocryst. **E-PPL** and **F-XPL** show a glass shard recrystallised to quartz within a devitrified, spherulitic groundmass.

Sample KT 53 consists of a microcrystalline, devitrified matrix with a micro-spherulitic texture. The spherulites are spherical to asymmetrical, which can be seen in figures 57A and B, and range in diameter from 0,1 mm to 0,4 mm. The groundmass consists of recrystallised quartz, plagioclase, magnetite or titanomagnetite, and sericite. Titanomagnetite and magnetite are found within the matrix, as well as occurring as phenocryst speckles, and infilling of fractures, as seen in figures 57C and

D. Plagioclase phenocrysts are present throughout the section, however they only have an approximate 1-5% presence within the section. The plagioclase phenocrysts are completely sericitised and often have opaque inclusions, such as the one observed in figures 57C and D, and range in length from 0,25 mm to 1,7 mm. A preserved glass shard can be seen in figures 57E and F, which has been recrystallised to quartz. KT 53 is an intensely welded ignimbrite of rhyolitic composition.

KT 57 [24°36'30,2" S; 28°25'38,5" E]:

Figure 58. Hand sample of a light grey rock with an aphanitic groundmass containing numerous glassy specks and phenocrysts. KT 57 is a rheomorphic lava-like ignimbrite.

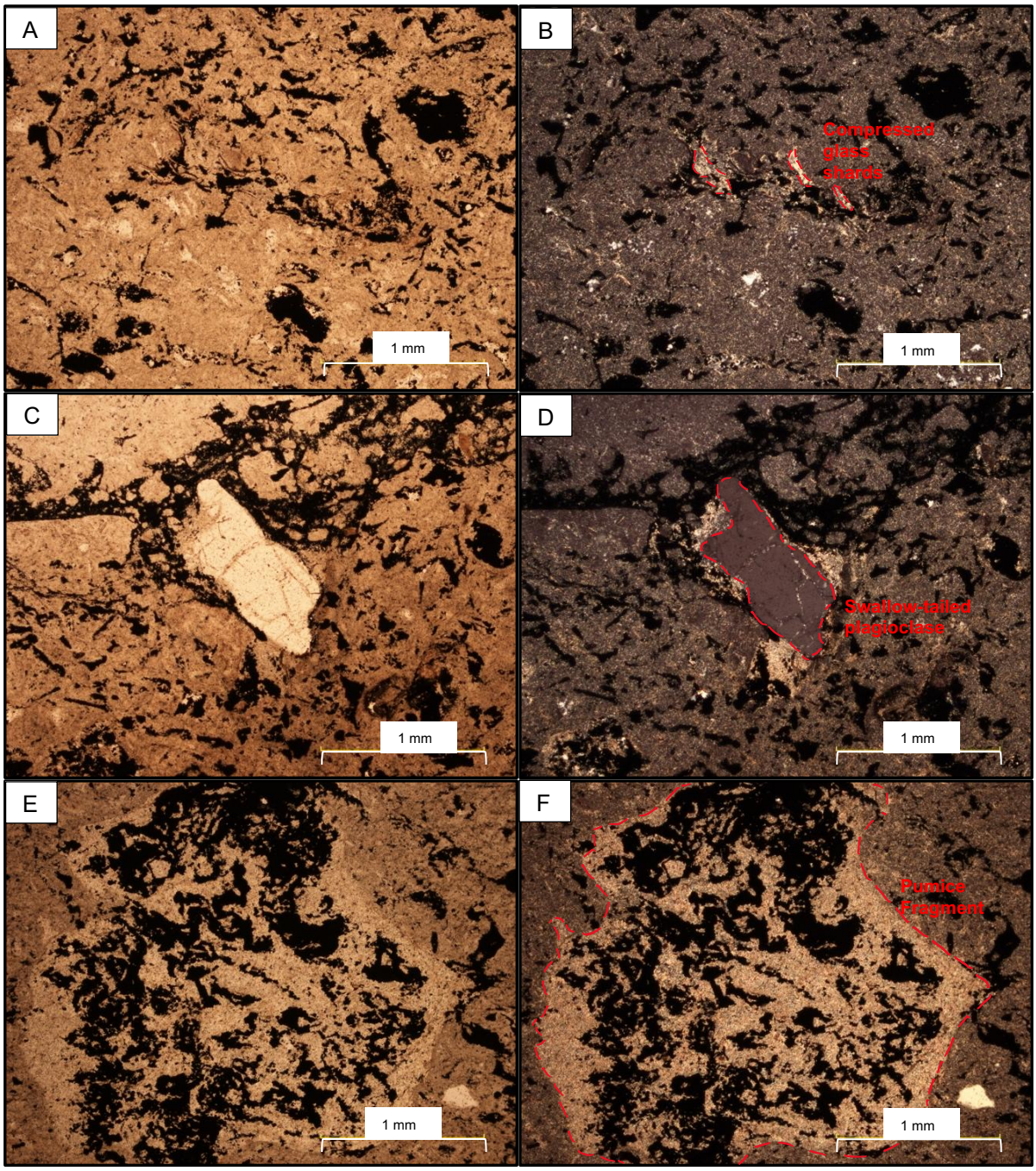

Figure 59. A polarised microscope photograph of rock sample KT 57: **A- PPL** and **B- XPL** display a devitrified, glassy groundmass with opaque minerals, likely titanomagnetite or magnetite, emulating flow patterns. Compressed and elongated recrystallised glass shards are also present. **C- PPL** and **D- XPL** display a fractured plagioclase phenocryst that is slightly swallow-tailed. **E- PPL** and **F- XPL** feature a large pumice fragment, recrystallised to minerals similar to that of the groundmass.

Sample KT 57 comprises a microcrystalline, devitrified groundmass containing magnetite or titanomagnetite displaying flow textures, however they do not have a particular flow direction, and they seem to be interstitial and secondary. This can be seen throughout figure 59. Figures 59A and B display small (approximately 0,05 mm

to 0,36 mm in length) compressed and elongated glass shards, which have been recrystallised to secondary minerals, such as sericite. Other glass shards within this section are recrystallised to quartz. Plagioclase phenocrysts make up approximately 2-5% of the section and are most often completely sericitised. Plagioclase phenocrysts range in length from 0,3 mm to 1,2 mm. Figures 59C and D display a plagioclase phenocryst with slight swallow-tail terminations, indicating quench textures. Collapsed pumice fragments are seen throughout the section, which are recrystallised to microcrystalline secondary minerals, such as sericite, zeolite, and opaques (such as magnetite or titanomagnetite). Some pumice fragments are slightly elongated, displaying flow textures. A large pumice fragment, which is completely replaced by sericite or zeolite and magnetite or titanomagnetite, is seen in figures 59E and F. KT 57 is a sample taken from outcrop 1 in chapter 4.1.1. KT 57 is a highly altered and intensely welded ignimbrite, showing the beginnings of rheomorphism.

KT 201 [24°34’13,8” S; 28°26’18,1” E]:

Figure 60. Hand sample of a grey rock with a fine crystalline groundmass containing phenocrysts and quartz veins. KT 57 is a highly welded ignimbrite.

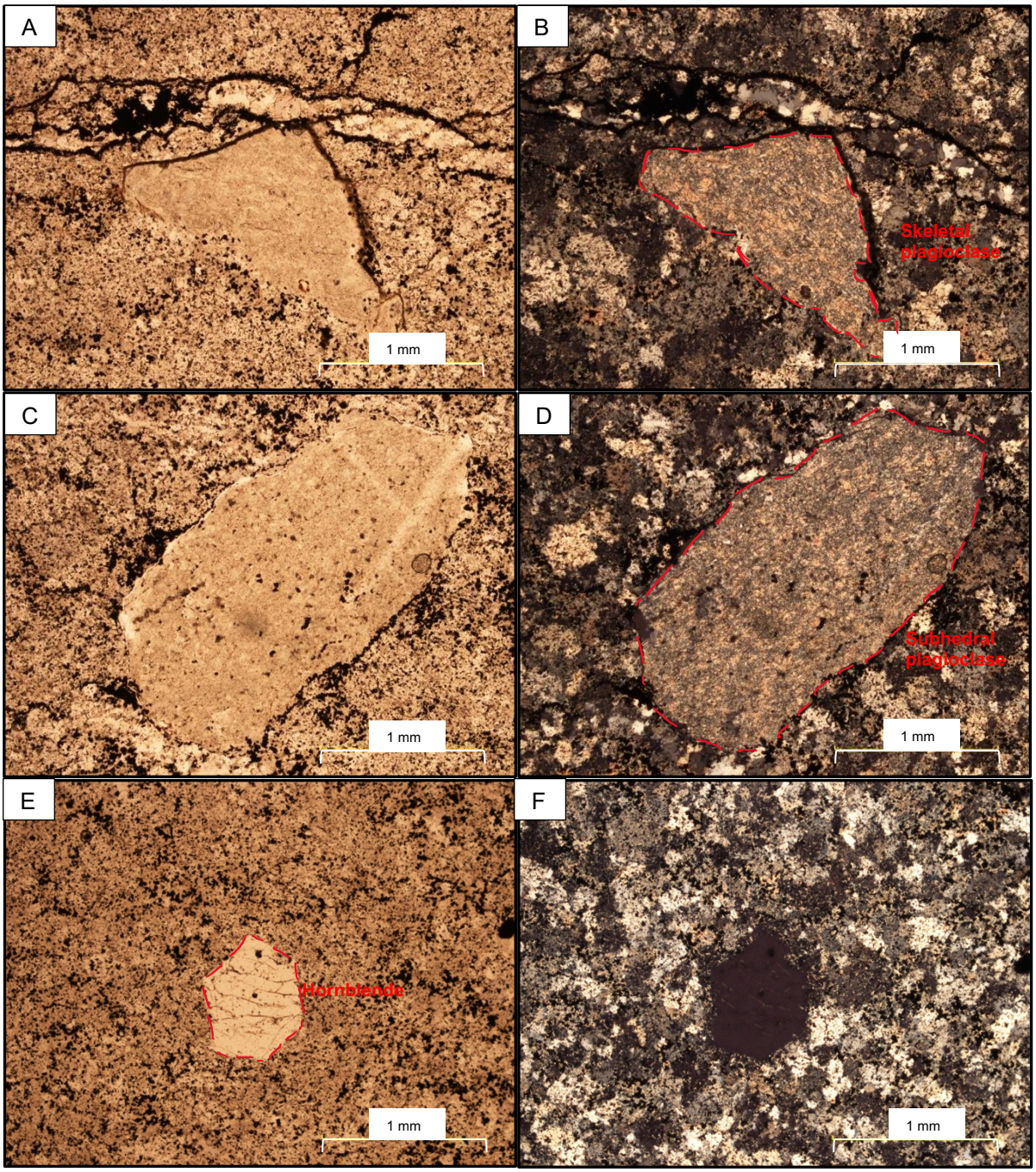

Figure 61. A polarised microscope photograph of rock sample KT 201: **A- PPL** and **B- XPL** display a broken and sericitised plagioclase phenocryst surrounded by a completely devitrified groundmass. **C- PPL** and **D- XPL** contain a large (2,4 mm long) sericitised plagioclase phenocryst. **E- PPL** and **F- XPL** contain fractured hornblende.

Rock sample KT 201 consists of a completely devitrified groundmass containing opaques, likely magnetite or titanomagnetite, quartz, and plagioclase. KT 201 is very similar in mineralogy and texture to rock sample KT 9. Phenocrysts, which make up approximately 2-5% of the mineralogical distribution, consist of sericitised plagioclase, often with opaque reaction rims and eaten borders, seen in figures 61A-D, revealing instability between the plagioclase phenocrysts and the groundmass. The plagioclase

phenocrysts also contain opaque mineral and glass inclusions (figures 61C and D) where some seem to be broken, or they may have a skeletal structure, such as the one seen in figures 61A and B. Other phenocrysts include hornblende (figures 61E and F) which are fractured and have opaque inclusions. Secondary quartz veins are occasionally seen throughout the section. KT 201 is a highly welded ignimbrite of rhyolitic composition.

KT 202.1 [24°34'6,9" S; 28°26'44,9" E]:

Figure 62. Hand sample of a dark, purplish rock comprising an overall aphanitic texture with sparse (1%) phenocrysts. KT 202.1 is a highly welded, lava-like ignimbrite.

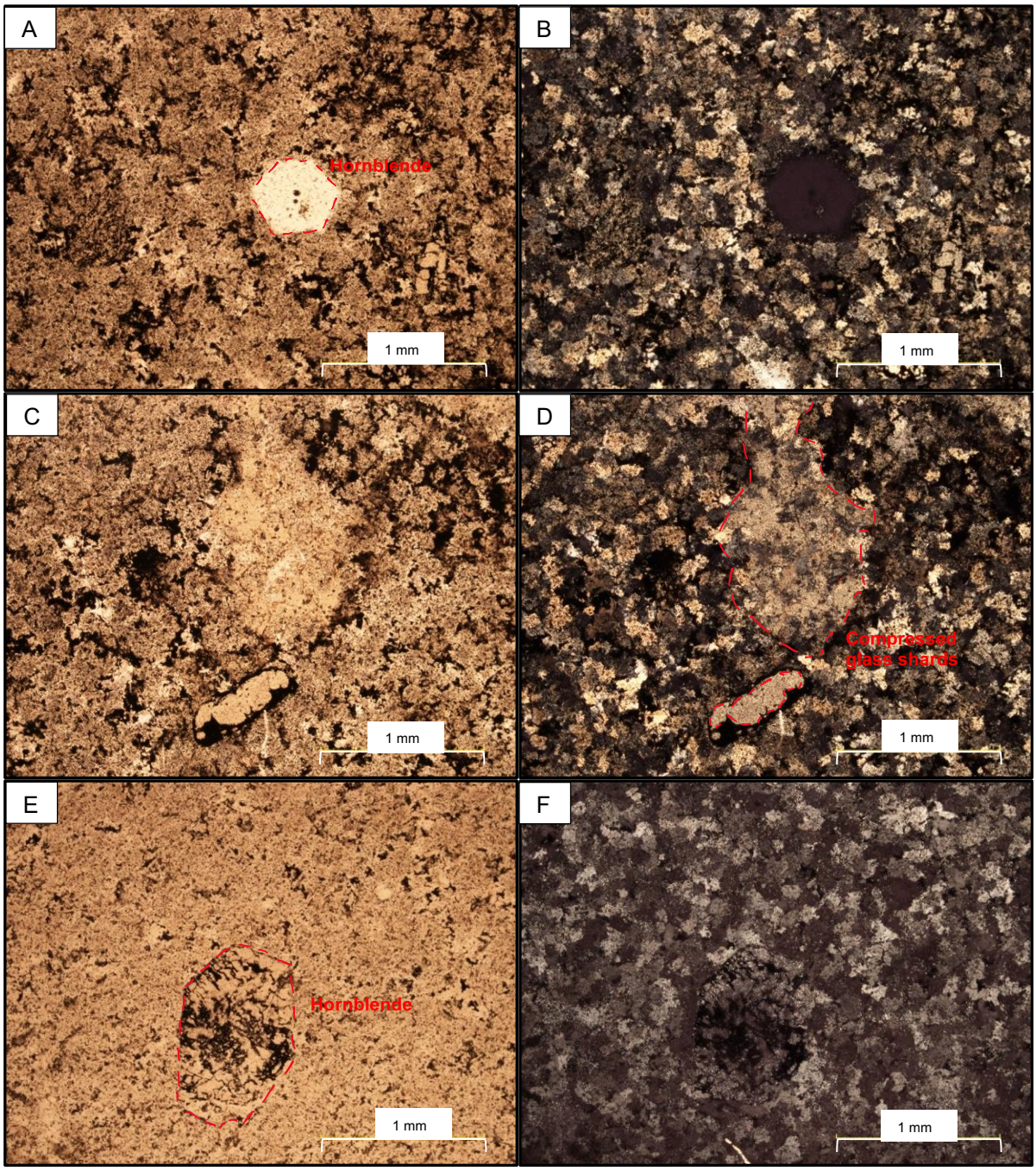

Figure 63. A polarised microscope photograph of rock sample KT 202.1: **A- PPL** and **B- XPL** display an altered, devitrified groundmass containing a hexagonal phenocryst, which is likely hornblende. **C- PPL** and **D- XPL** include two possible recrystallised glass shards which have been recrystallised to a similar material as the groundmass. **E- PPL** and **F- XPL** display a hexagonal mineral which has completely reacted with the groundmass and recrystallised to the same material as the groundmass, with only opaques that have preserved the original mineral shape.

Rock sample 202.1 is very similar in texture and mineralogy to KT 201. KT 202.1 is aphanitic with a completely devitrified groundmass, consisting of quartz, opaques, and sericite. Phenocrysts are rare and make up approximately 1-2% of the rock.

Phenocrysts include sericitised plagioclase, hornblende (seen in figures 63A, B, E and F), and quartz. Quartz veins are also present within this section. Possible compressed and preserved glass shards are seen in figures 63C and D, which have also been devitrified to material very similar to that of the groundmass. The phenocryst mineral seen in figures 63E and F is originally hexagonal and possibly hornblende, which has been completely altered to material similar to that of the groundmass. Opaque minerals (such as magnetite and titanomagnetite) make up the borders and cracks of the original hornblende mineral. KT 202.1 is a highly welded, lava-like ignimbrite.

KT 210 [24°34'40,7" S; 28°27'17,5" E]:

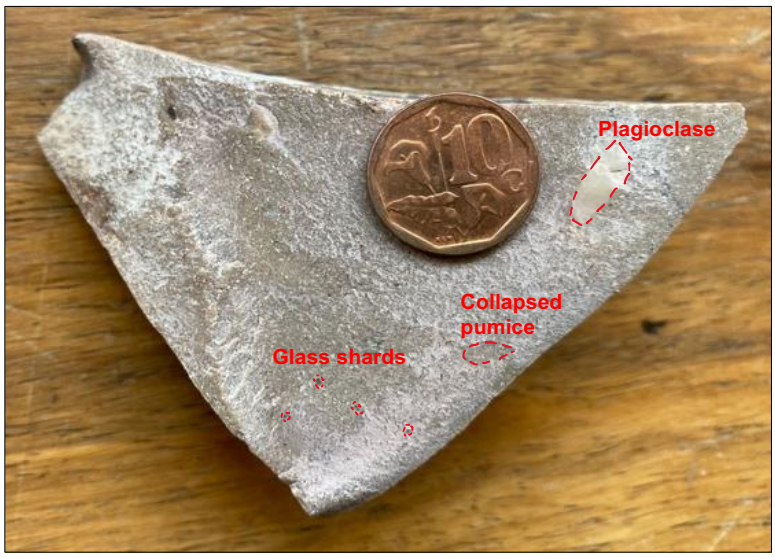

Figure 64. Hand sample of a fine grained, light grey rock, which includes specks of glass shards, possible lithic fragments and collapsed pumice fragments. KT 210 is a non-welded ignimbrite of rhyolitic composition.

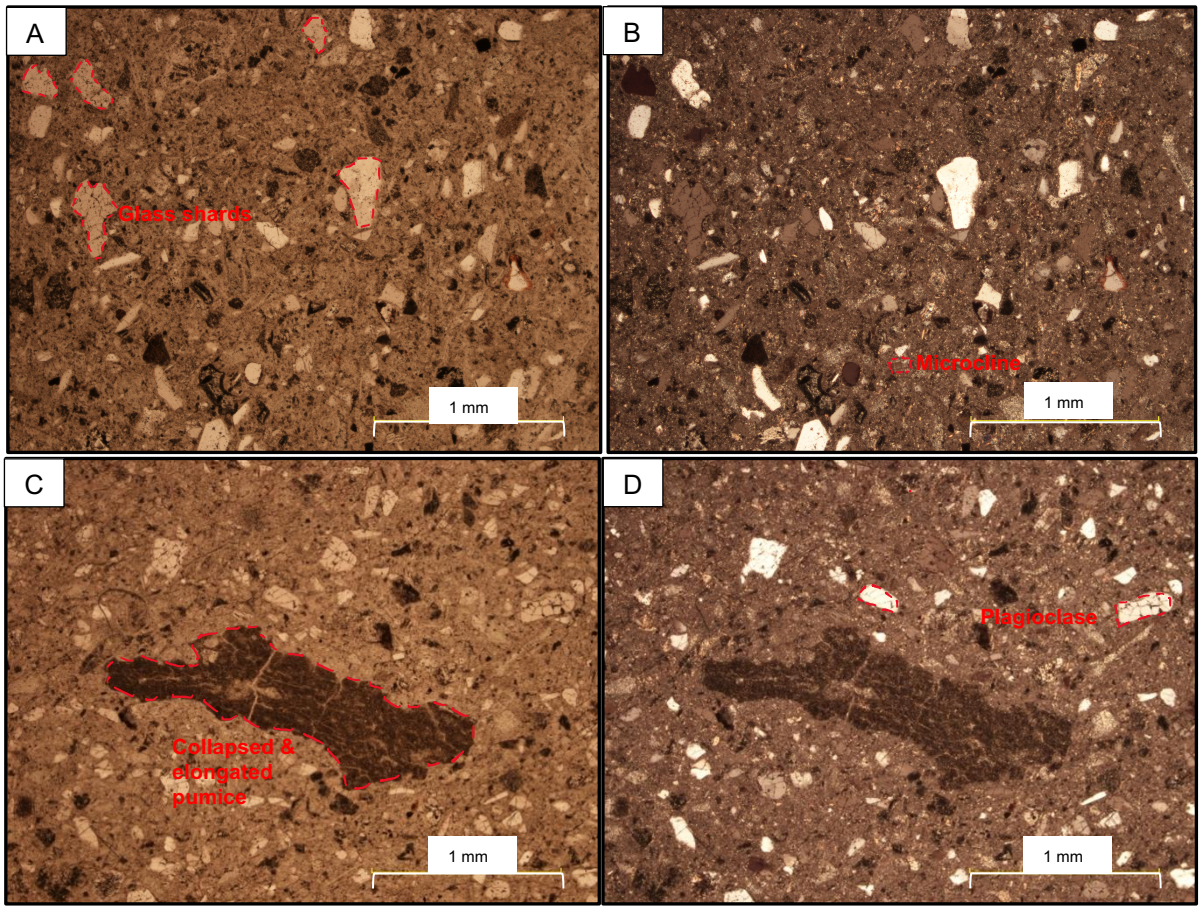

Figure 65. A polarised microscope photograph of rock sample KT 210: **A- PPL** and **B- XPL** display a clastic texture with glass shards, recrystallised to quartz, small, compressed pumice fragments which have been altered to sericite, all surrounded by a glassy matrix. **C- PPL** and **D- XPL** display a collapsed and elongated pumice fragment surrounded by a sea of glassy groundmass, glass shards and broken plagioclase crystals.

Rock sample KT 210 is composed of a glassy groundmass with numerous (80-90%) fragments of mostly glass shards, followed by collapsed pumice fragments and then broken crystals, seen across figure 65. KT 210 displays a classic pyroclastic texture. Glass shards are recrystallised to quartz and collapsed pumice fragments are altered to secondary clay minerals, such as sericite. This can be seen by the 2 mm long pumice fragment in figures 65C and D. Small plagioclase crystals (0,1-0,3 mm in length) can be seen in figure 65C and D. A small microcline crystal (0,12 mm) is also observed in figures 65A and B. Minor micro-spherulites can also be observed in figures 65A and B. KT 210 is a non-welded ignimbrite of rhyolitic composition.

KTP 2 [24°36'31,7" S; 28°25'52,3" E]:

Figure 66. Hand sample of a light grey rock with a fine-grained matrix, containing glassy specks and pumice fragments. KTP 2 is a low to non-welded rhyolitic ignimbrite.

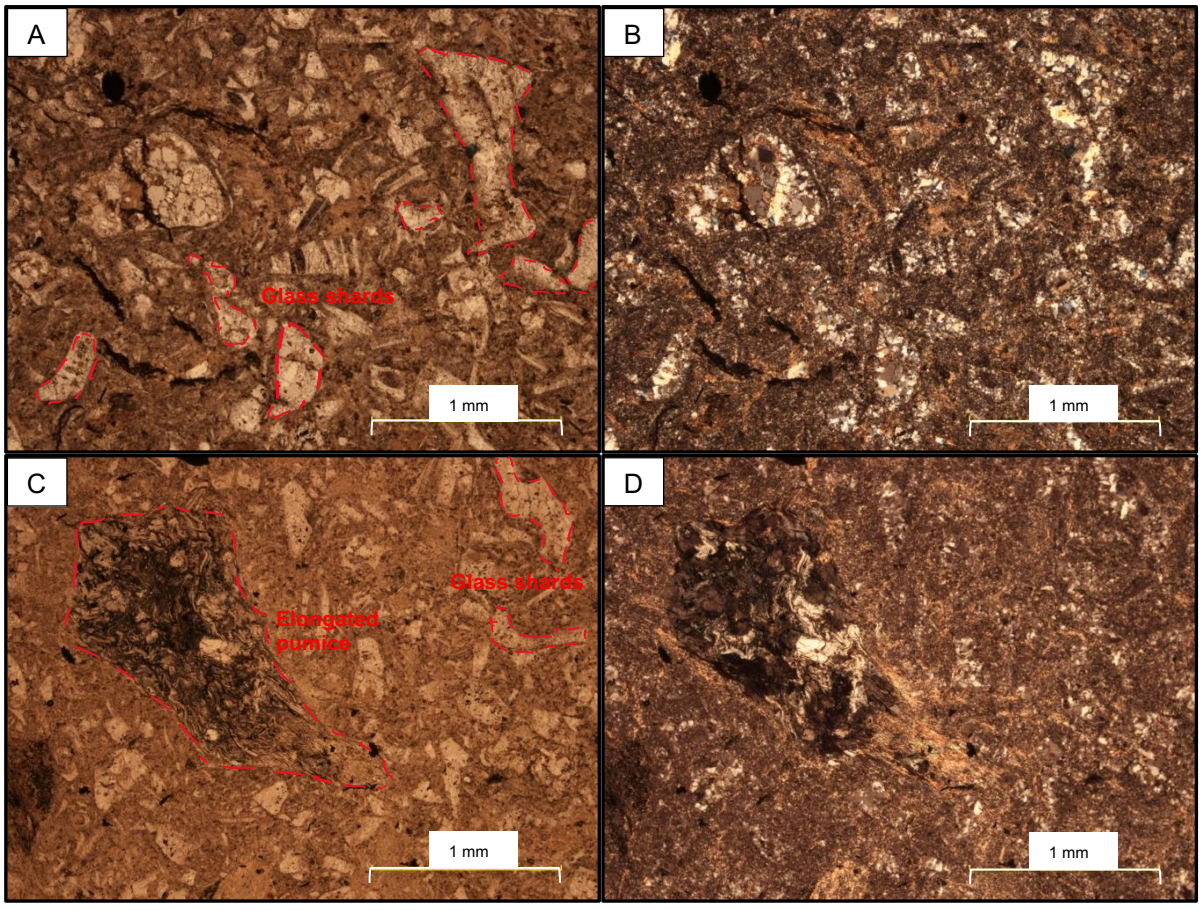

Figure 67. A polarised microscope photograph of rock sample KTP 2: **A- PPL** and **B- XPL** display numerous recrystallised glass shards situated in a devitrified, glassy groundmass, with opaque minerals present as well. **C- PPL** and **D- XPL** include a collapsed and elongated pumice fragment, recrystallised to opaques, quartz, and secondary clay minerals, surrounded by recrystallised glass shards and a glassy matrix.

Rock sample KTP 2 consists of scores of glass shards, ranging in length from approximately 0,7 mm to 1,1 mm, which are mostly recrystallised to quartz but also include alteration to secondary clay minerals, such as sericite or saussurite. The glassy groundmass is altered mostly to clay minerals. Opaque minerals, likely magnetite and titanomagnetite, are also present. This can be seen in figures 67A-D. Compressed pumice fragments are frequent throughout the section and are also recrystallised to quartz, clay minerals, and opaques. The opaque minerals within the pumice particularly display flow patterns. The pumice fragments are elongated, appear as dark lenses, and display fiamme textures. Some glass shards in different sections show slight preferred orientation, aligning with the orientation of the pumice lenses. This can be seen in figures 67C and D. KTP 2 correlates with outcrop 7 in chapter 4.1.7 and is a medium to highly welded ignimbrite displaying micro-fiamme texture.

PYR 1A [24°36'31,6" S; 28°25'51,9" E]:

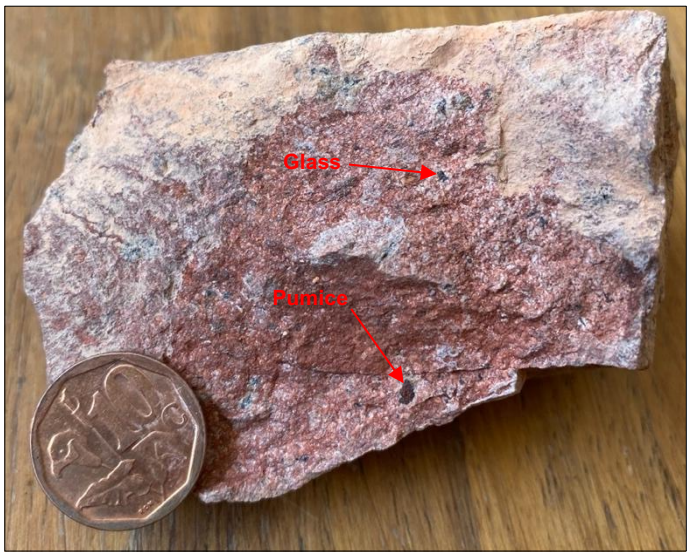

Figure 68. Hand sample of a red coloured, fine crystalline rock, containing specks and shards of glass and pumice. PYR 1A is a medium to highly welded ignimbrite of rhyolitic composition.

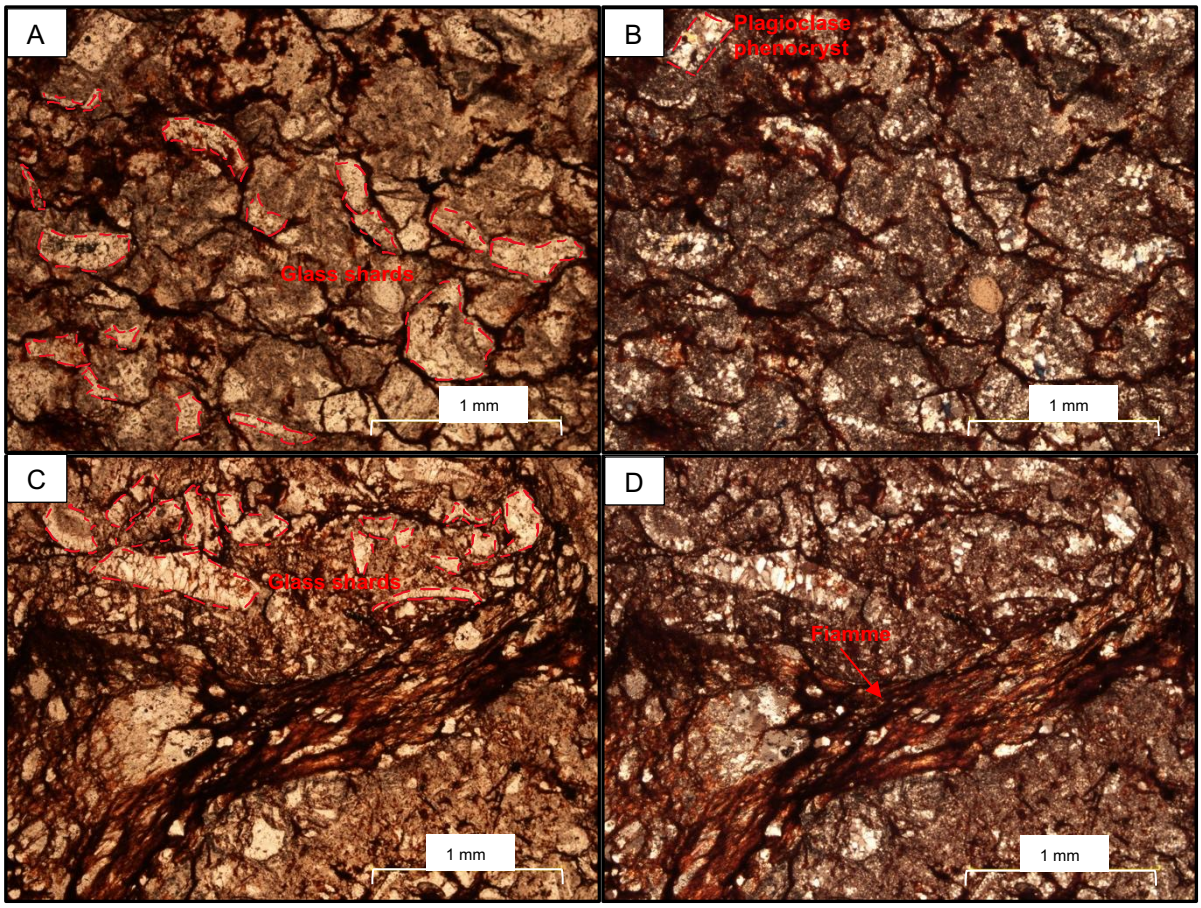

Figure 69. A polarised microscope photograph of rock sample PYR 1A: **A- PPL** and **B- XPL** display recrystallised glass shards that have preferred orientation, set in a devitrified, glassy matrix. Interstitial opaques and hematite overgrowths are also present. **C- PPL** and **D- XPL** include an elongated, compressed pumice, which can be considered a fiamme. Numerous glass shards, recrystallised mainly to quartz are clearly seen and are set in a preferred orientation, aligned with the fiamme.

PYR 1A consists of numerous glass shards, which have been recrystallised mainly to quartz. The groundmass is devitrified, glassy, and displays perlitic cracks. The groundmass has been recrystallised to quartz and secondary clay minerals, such as sericite. Interstitial opaque minerals, such as magnetite or titanomagnetite are largely present. The deep red colouring throughout the section is attributed to secondary hematite, likely precipitated during hydrothermal alteration. This can be seen throughout figure 69. Figures 69C and D include a collapsed and elongated pumice lens, displaying fiamme texture. The pumice lens has been recrystallised to magnetite or titanomagnetite, quartz, sericite, as well as hematite. The glass fragments throughout the section have a slight preferred orientation and align to the pumice lenses. PYR 1A is similar to outcrop 8 in chapter 4.1.8 and is a medium welded ignimbrite displaying the beginnings of rheomorphism and micro-fiamme texture, and has been highly altered, largely due to iron-rich hydrothermal alteration.

Sample PYR 1B [24°36'31,6" S; 28°25'51,9" E]:

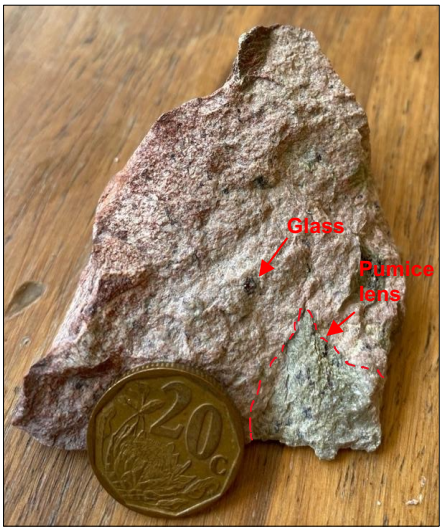

Figure 70. Hand sample of a light grey to red coloured rock with a fine crystalline matrix containing specks of glass and altered small to large pumice lenses. PYR 1B is a low to medium welded ignimbrite of rhyolitic composition.

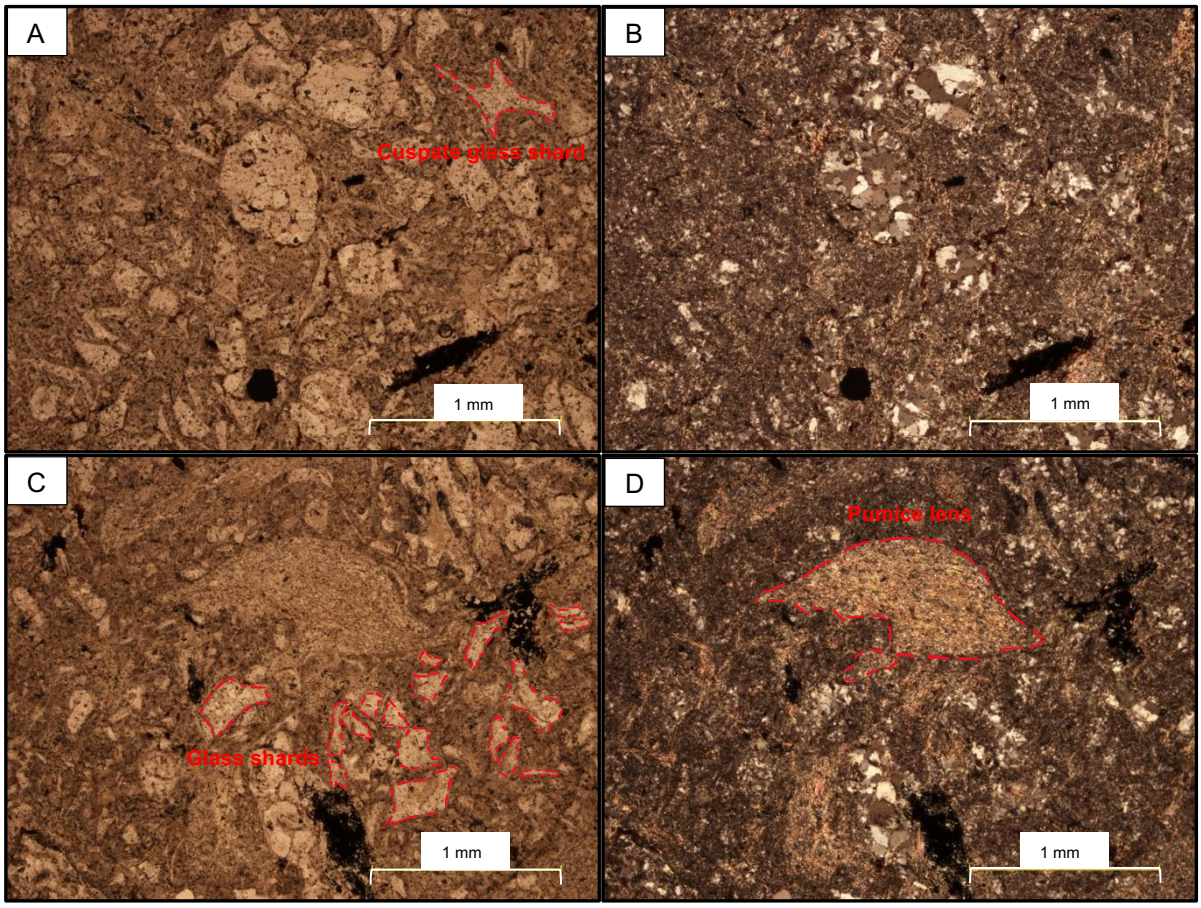

Figure 71. A polarised microscope photograph of rock sample PYR B: **A- PPL** and **B- XPL** display recrystallised glass shards and opaque minerals set in a fine devitrified, glassy matrix. **C- PPL** and **D- XPL** include collapsed pumice lenses, recrystallised to sericite.

Rock sample PYR 1B occurs in the same location as PYR 1A (24°36'31,6" S; 28°25'51,9" E), however displays slightly different textures and a lower level of iron-rich hydrothermal alteration. This suggests PYR A and PYR B belong to different pyroclastic flow units. PYR 1B consists of glass shards recrystallised mainly to quartz. Glass shards are sub-angular to rounded, with a few remaining angular, and are often C- and Y- shaped. The glass shards do not seem to have a preferred orientation, such as those seen in PYR 1A. The groundmass is devitrified and glassy, made up of microcrystalline quartz and secondary clay minerals, such as sericite and saussurite. This can be seen throughout figure 71. Pumice lenses are also observed throughout the section, such as the eye-shaped pumice lens seen in figures 71C and D. The pumice lenses are mainly altered to secondary clay minerals, the same as observed in the groundmass. Opaque minerals are distributed throughout the section and occur interstitially as well as phenocrysts and inclusions within the glass shards. PYR 1B is similar to and found close to outcrop 11 in chapter 4.1.11 and is a low welded ignimbrite.

PYR 2 [24°36'32,2" S ; 28°25'53,0" E]:

Figure 72. Hand sample of an aphanitic, grey to green coloured rock. Specks of glass and magnetite or titanomagnetite crystals can be seen. Small lenses and elongated pumice fiamme are also observed. PYR 2 is a medium welded ignimbrite of rhyolitic composition.

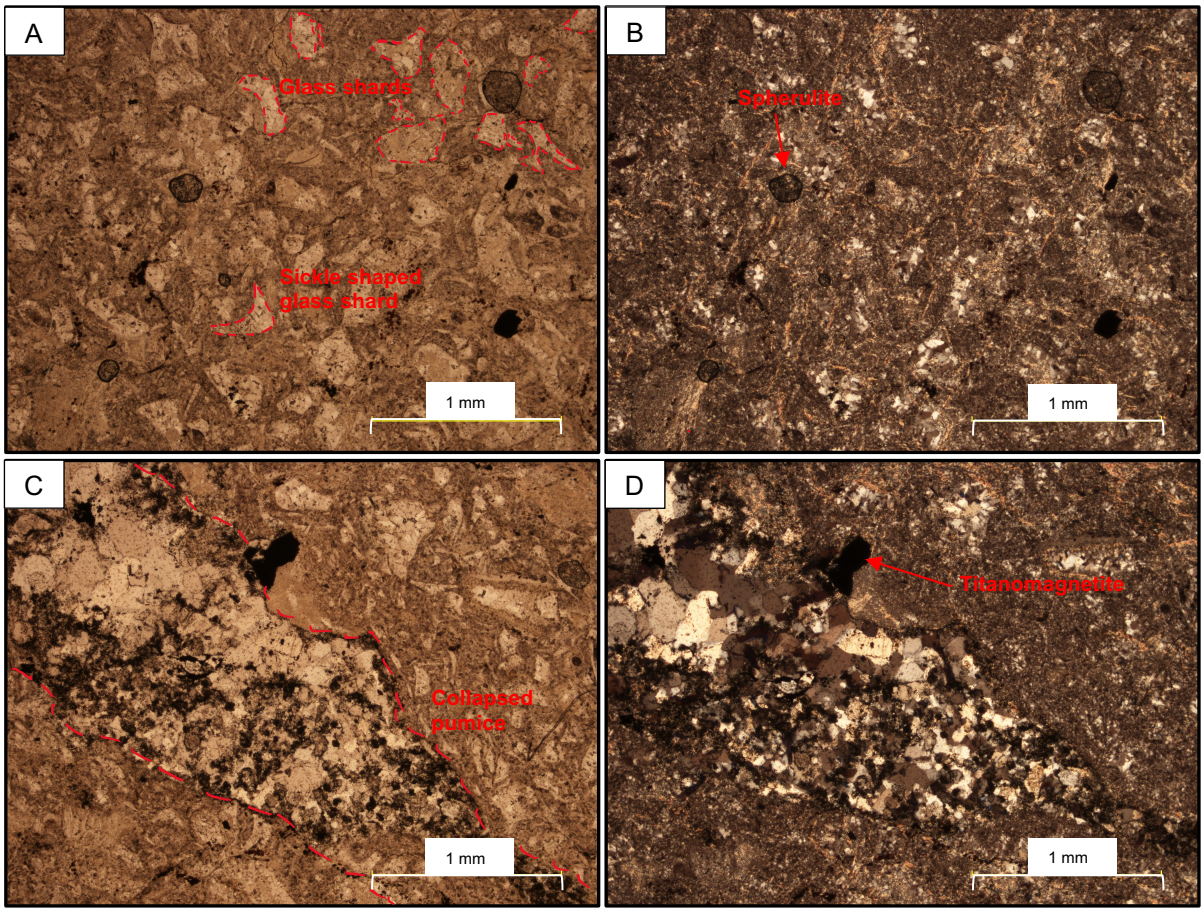

Figure 73. A polarised microscope photograph of rock sample PYR 2: **A- PPL** and **B- XPL** contain glass shards, mainly recrystallised to quartz, opaque specks, and phenocrysts set in a devitrified, glassy matrix. Rare spherulites are also present. **C- PPL** and **D- XPL** include a large compressed and elongated pumice fragment, recrystallised dominantly to quartz. Recrystallised glass shards and opaques are also present, all set within a devitrified, glassy matrix.

Rock sample PYR 2 is texturally and mineralogically similar to PYR 1B. PYR 2 consists of a devitrified, glass groundmass recrystallised to quartz, opaques (titanomagnetite), and secondary clay minerals (sericite). There are occasional spherulites (figures 73A and B) within the section, ranging in diameter from 0,06 mm to 0,2 mm, most of which are spherical, whereas some are asymmetrical. Abundant glass shards are seen throughout figures 72 and 73. The glass shards are cuspate, sickle, Y- and C- shaped, most of which are sub-angular. The glass shards are recrystallised mostly to quartz, but also contain clay minerals. Collapsed pumice fragments (seen in figures 73C and D) are abundantly distributed throughout the section, are lens-like and elongated, and are recrystallised to quartz and clay minerals (such as sericite). A particularly large and elongated pumice fiamme is observed across figures 73C and D. Specks of titanomagnetite phenocrysts are found throughout the sample. PYR 2 is a low to medium welded ignimbrite.

Table 2. A summary of the above rock samples' mineralogy, texture, and composition.

	Rock Sample	Volcanic texture	Minerals present	Additional Microscopic structures & textures	Overall rock composition
Dullstroom Formation	**RG 7**	Cryptocrystalline + glassy GM	Biotite, hornblende, plagioclase &/or apatite, & titanomagnetite	Fine flow banding	Basaltic andesite
	RG 46	Hypocrystalline	Plagioclase & secondary quartz (infilling of amygdales)	Amydaloidal, random orientation of crystals	Andesite
Damwal Formation	**RL 1**	Porphyritic + devitrified, glassy GM	Plagioclase phenocrysts and titanomagnetite	Random orientation of crystals, plagioclase clusters (glomerocrysts)	Andesite to dacite
	LD 021	Porphyritic + devitrified, glassy GM	Plagioclase, hornblende, titanomagnetite, polycrystalline quartz, possible recrystallised glass shards	Random orientation of crystals, plagioclase clusters (glomerocrysts)	Andesite to dacite
Kwaggasnek Formation	**LD 002**	Spherulitic with a devitrified, glass groundmass + 5% phenocrysts	Plagioclase, rare olivine, magnetite or titanomagnetite, quartz	Spherulitic, possibly welded	Rhyodacite to rhyolite
	LD 004	Devitrified, glassy groundmass, micro-spherulitic texture + plagioclase phenocrysts + blobs of glass clasts	Plagioclase, quartz, magnetite or titanomagnetite, secondary sericite or saussurite	Micro-spherulitic, low to medium welding	Rhyodacite to rhyolite
Schrikkloof Formation	**SM 28.1**	Hypocrystalline + devitrified groundmass + numerous phenocrysts	Plagioclase, perthite, quartz, magnetite or titanomagnetite	Micrographic texture, skeletal plagioclase, perthite exsolution, low-medium grade welding	Rhyolite
	KT 9	Hypocrystalline + completely devitrified groundmass + 5% phenocrysts + recrystallised pumice fragments	Quartz, plagioclase, magnetite or titanomagnetite, sericite	Compressed pumice fragments, highly welded	Rhyolite
	KT 53	Microcrystalline, devitrified groundmass + 1-5% phenocrysts + occasional glass shards	Quartz, plagioclase, magnetite or titanomagnetite, sericite	Micro-spherulitic, completely sericitized plagioclase phenocrysts, highly welded	Rhyolite

	Rock Sample	Volcanic texture	Minerals present	Additional Microscopic structures & textures	Overall rock composition
Schrikkloof Formation	**KT 57**	Microcrystalline, devitrified groundmass + 2-5% phenocrysts + recrystallised pumice, eutaxitic texture	Quartz, plagioclase, magnetite or titanomagnetite, sericite	Completely sericitised, swallow-tailed plagioclase displaying quench textures; collapsed + elongated pumice fragments; opaques displaying flow textures; early rheomorphism; highly welded	Rhyolite
	KT 201	Aphanitic, completely devitrified groundmass + 2-5% phenocrysts	Quartz, plagioclase, hornblende, magnetite or titanomagnetite, sericite	Broken & skeletal plagioclase phenocrysts with reaction rims, secondary quartz veins, highly welded	Rhyolite
	KT 202.1	Aphanitic, completely devitrified groundmass + 1-2% phenocrysts	Sericitised plagioclase, hornblende, quartz, magnetite or titanomagnetite, sericite	Compressed & recrystallised glass shards, secondary quartz veins, highly welded	Rhyolite
	KT 210	Glassy groundmass + 80-90% glass & pumice fragments, rare phenocrysts, clastic texture	Quartz, plagioclase, magnetite or titanomagnetite, sericite, microcline	Numerous sub-angular glass shards, compressed pumice fragments, non-welded	Rhyolite
	KTP 2	Glassy groundmass + numerous recrystallised glass shards & pumice fragments, rare phenocrysts, eutaxitic texture	Quartz, sericite or saussurite, magnetite or titanomagnetite	Compressed & elongated pumice fragments- micro-fiamme texture, slight preferred orientation of pumice and glass shards, opaques displaying flow textures, medium to high welding	Rhyolite
	PYR 1A	Glassy, perlitic groundmass, numerous recrystallised glass shards, collapsed & elongated pumice fragments	Quartz, sericite, magnetite or titanomagnetite, secondary hematite	Perlitic cracks, collapsed & elongated pumice fragments- fiamme texture, slight preferred orientation of glass & pumice- rheomorphic	Rhyolite

	Rock Sample	Volcanic texture	Minerals present	Additional Microscopic structures & textures	Overall rock composition
Schrikkloof Formation	**PYR 1B**	Devitrified, glassy groundmass + numerous recrystallised glass shards, lens-like recrystallised pumice fragments, interstitial & phenocrysts of opaque minerals, clastic texture	Quartz, sericite, magnetite or titanomagnetite	Cuspate, C- and Y-shaped glass shards, no preferred orientation of fragments & shards, low welding	Rhyolite
	PYR 2	Devitrified, glassy groundmass, numerous recrystallised glass shards, abundant collapsed & recrystallised pumice fragments, specks & phenocrysts of opaque minerals, clastic texture	Quartz, sericite, magnetite or titanomagnetite	Cuspate, C- and Y-shaped glass shards which are angular to sub-angular, collapsed & elongated pumice fragments, rare micro-spherulites- mostly spherical, slight preferred orientation of glass shards & pumice, low to medium welding	Rhyolite

Additional thin section microphotographs not included in the above results section can be studied in Appendix A.

4.3. Plagioclase grain size distribution results

The Dullstroom Formation contains a small range of plagioclase diameter sizes, ranging from 8 to 52 µm. Most of the plagioclase crystals have a diameter between 15 to 30 µm, and are relatively evenly spread out between this range. Overall, the Dullstroom Formation plagioclase phenocrysts are fine crystalline with a mean of 22,5 µm, which can be seen in the grain size distribution (GSD) histogram in figure 74 below.

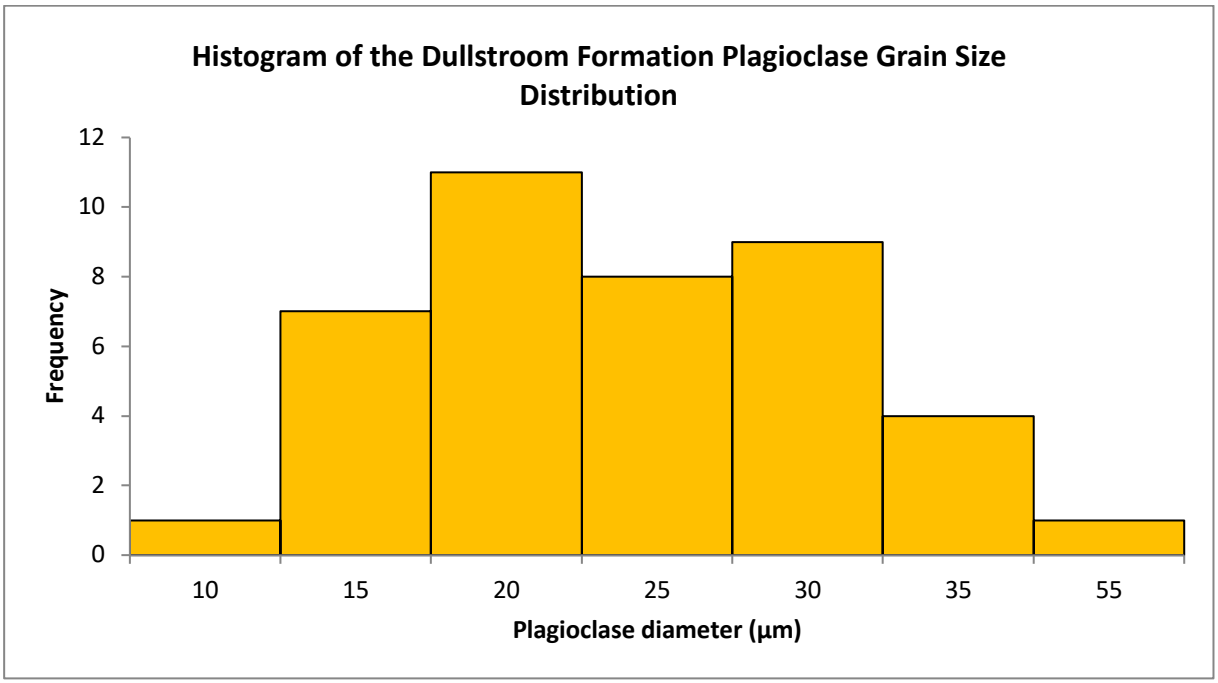

Figure 74. A plagioclase GSD histogram of the Dullstroom Formation found in the Dullstroom and Loskop Dam sampling regions.

The Damwal Formation contains a large range of plagioclase diameter sizes, ranging from 32 to 862 µm. Most of the plagioclase crystals have a diameter between 100 to 300 µm, with a distinction in crystal population size with diameters of 151 to 200 µm. Although the plagioclase diameter range is large, few crystals have a diameter larger than 350 µm. Overall, the Damwal Formation plagioclase phenocrysts are fine to moderate in size with a mean of 232,4 µm (figure 75).

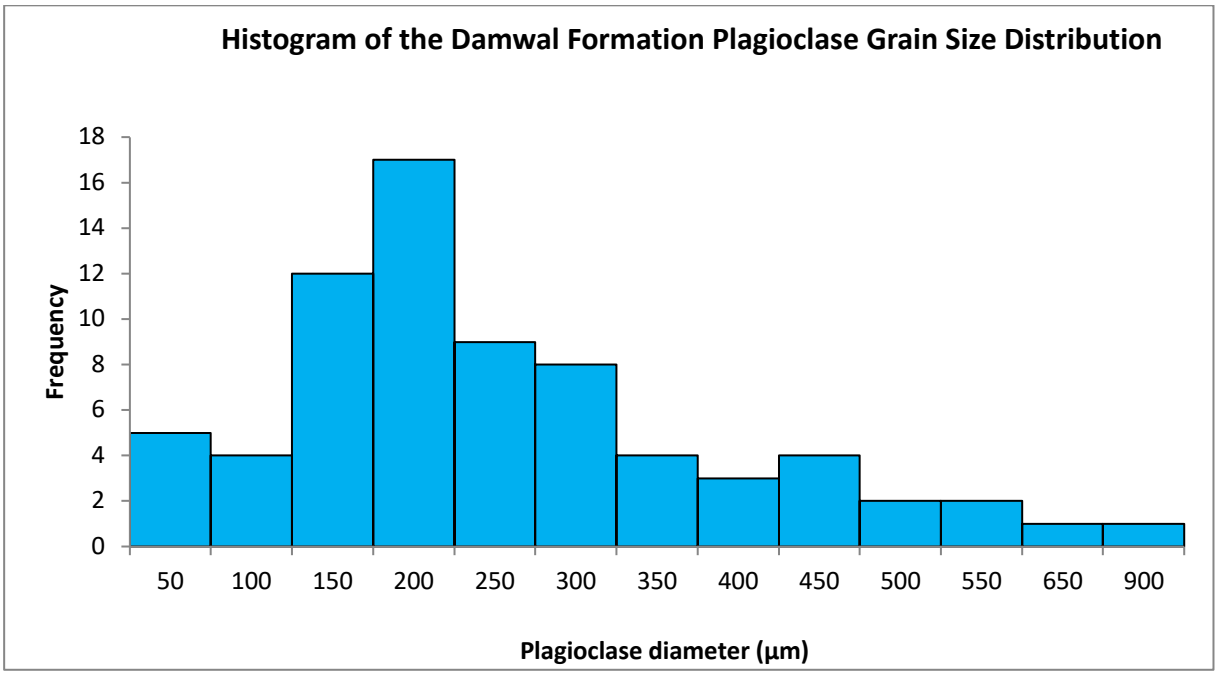

Figure 75. A plagioclase GSD histogram of the Damwal Formation found in the Loskop Dam sampling region.

The Kwaggasnek Formation (figure 76) contains a relatively large range of plagioclase diameter sizes, ranging from 174 to 774 µm and are distinctively lacking in finer crystal sizes compared to the rest of the Rooiberg Group formations. Most of the plagioclase crystals have a diameter between 250 to 350 µm. Diameters larger than 350 µm are rare. Overall, the Kwaggasnek Formation plagioclase phenocrysts are moderate to large in size with a mean of 364,07 µm. It is noted that the Kwaggasnek Formation contains the smallest data set size. If a larger sampling region and more samples would have been collected, the Kwaggasnek Formation might show slightly different results.

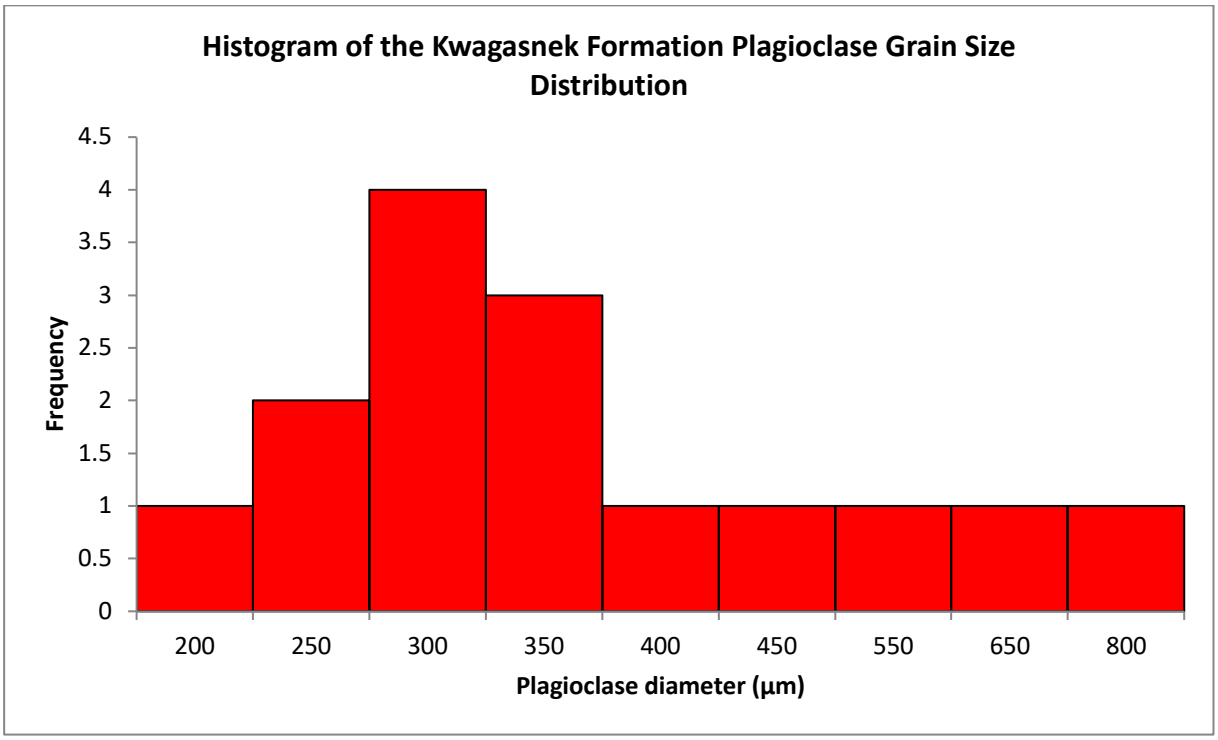

Figure 76. A plagioclase GSD histogram of the Kwaggasnek Formation found in the Loskop Dam sampling region.

The Schrikkloof Formation (figure 77) contains the largest range of plagioclase diameter sizes, ranging from 23 to 1902 µm. Most of the plagioclase crystals have a diameter between 23 to 150 µm. There are slight increases in crystal population size with diameters between 250 to 300 µm, 350 to 400 µm, and 950 to 1902 µm. Overall, the Schrikkloof Formation is rich in finer plagioclase diameter sizes, with a mean of 282,4 µm. The Schrikkloof Formation contains the largest data set size, revealing a more reliable GSD pattern.

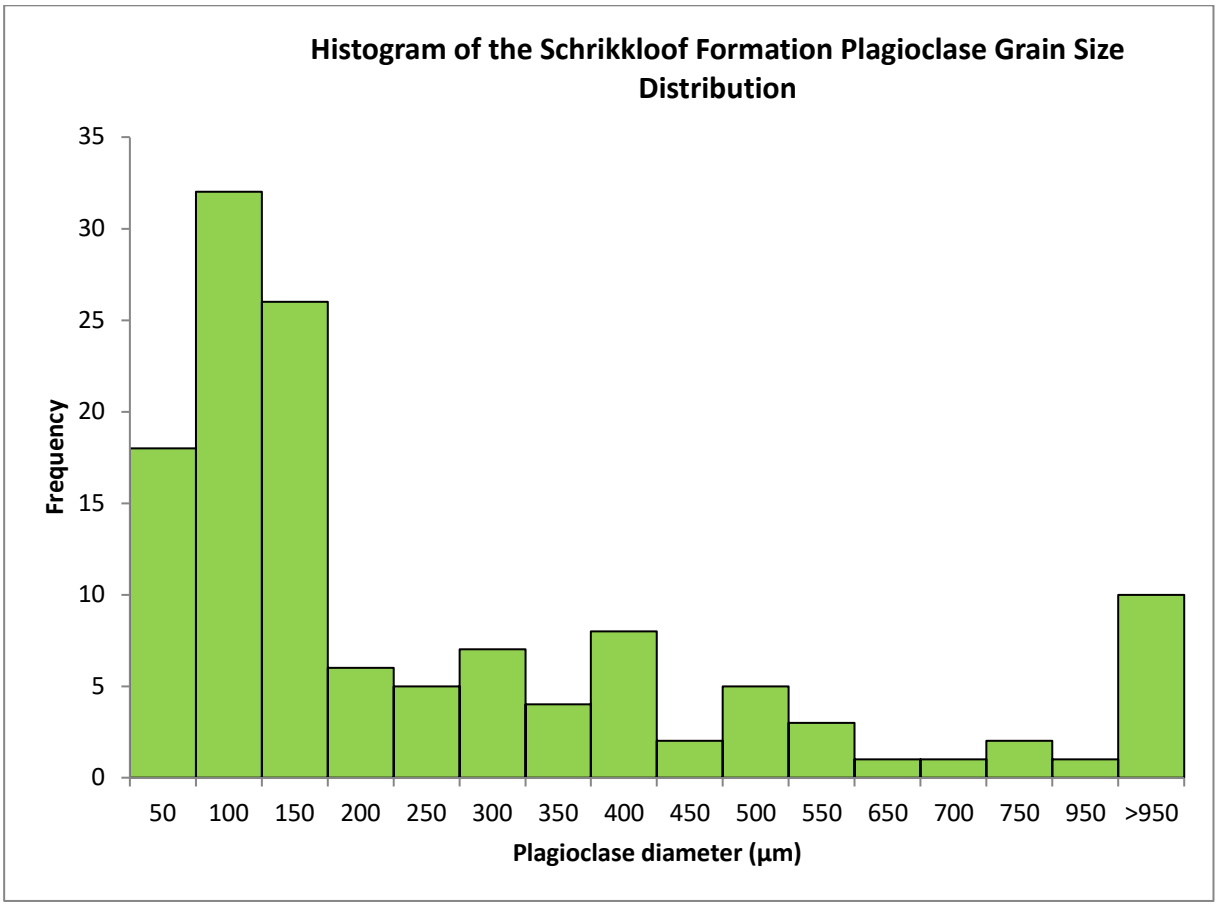

Figure 77. A plagioclase GSD histogram of the Schrikkloof Formation found in the Loskop Dam and Kuthaba Bush Lodge sampling regions.

Figure 78 and table 3 below can be studied to compare the plagioclase phenocryst sizes and GSD patterns between the four Rooiberg Group formations. It is observed that there are different frequency GSD patterns for each Rooiberg Group Formation. The most distinct difference is between the Dullstroom Formation, which is fines-rich (10-35 µm) with a very small range in plagioclase sizes (8-52 µm), when compared to the remainder of the Rooiberg Group formations. The Damwal (32-862 µm), Kwaggasnek (174-774 µm) and Schrikkloof formations (23-1902 µm) all have larger ranges of plagioclase phenocryst sizes, with the Schrikkloof Formation containing the largest range. The Damwal and Kwaggasnek have mostly moderate plagioclase crystal sizes, whereas the Schrikkloof Formation is rich in fine plagioclase crystal sizes (50-150 µm). The Kwaggasnek Formation displays the most unreliable GSD pattern due to its small sample size, whereas the Schrikkloof Formation displays the most reliable GSD pattern, as it contains the largest sample and data set size.

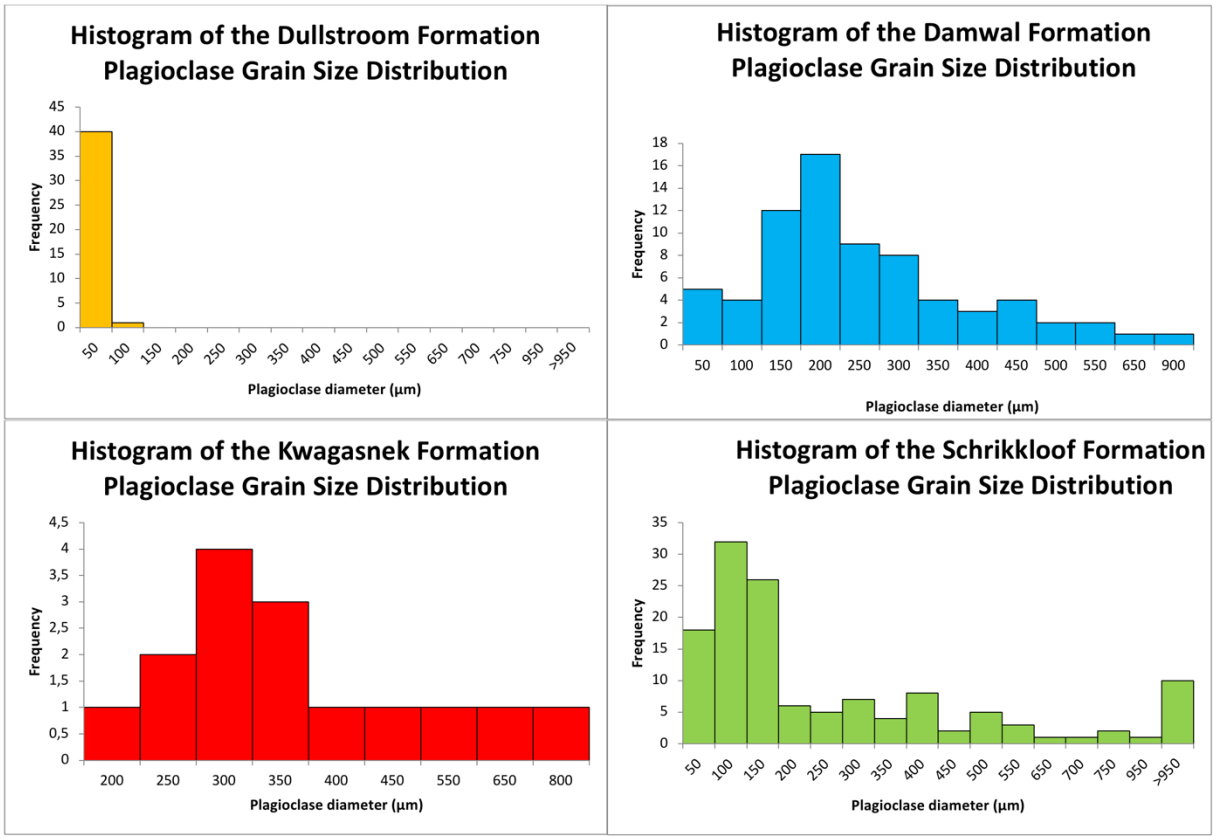

Figure 78. A comparison of the histogram GSD patterns between the four Rooiberg Group formations.

Table 3. Comparing statistical values of the plagioclase GSD of the Rooiberg Group formations.

Formation	Dullstroom	Damwal	Kwaggasnek	Schrikkloof
Plag. minimum diameter (µm)	8	32	174	23
Plag. maximum diameter (µm)	52	862	774	1902
Diameter range (µm)	44	830	600	1879
Median (µm)	21	193	328	128
Mode (µm)	27	129	337	71
Sum of all diameters (µm)	908	16 733	5 461	36 994
No. of values in data set	41	72	15	131
Mean (µm)	22,15	232,40	364,07	282,40

The Schrikkloof Formation was sampled in two very different locations, namely the Loskop Dam region and Kuthaba Bush Lodge. It is noted that there are possibly different GSD patterns between the different sampling sites. The Schrikkloof plagioclase crystal sizes in the Loskop Dam region have a slightly larger range compared to Kuthaba Bush Lodge's plagioclase crystals, with more of the crystal sizes occurring between 650 and 750 µm. The Loskop Dam sample size is, however, very small, and may not be displaying a reliable GSD pattern. The Kuthaba Bush Lodge plagioclase crystal sizes have a slightly smaller range and are enriched in finer crystal sizes, namely 23 to 150 µm. This can be studied in figures 79 and 80, as well as table 4.

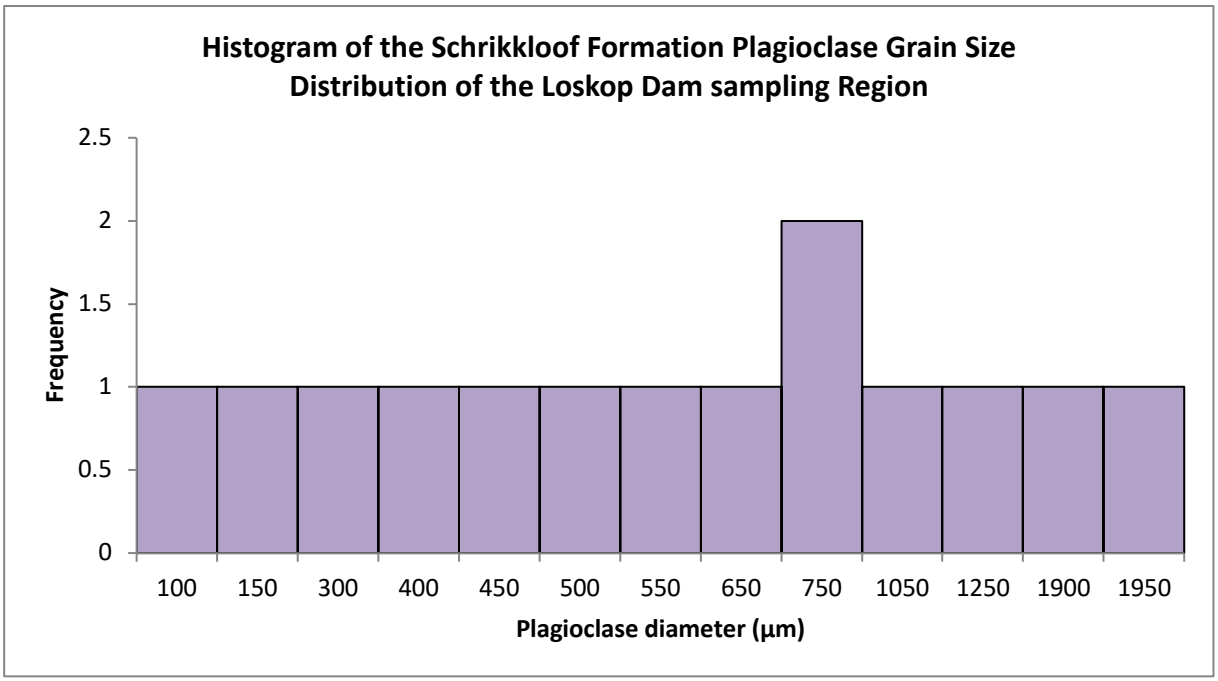

Figure 79. A plagioclase GSD histogram of the Schrikkloof Formation found in the Loskop Dam sampling region.

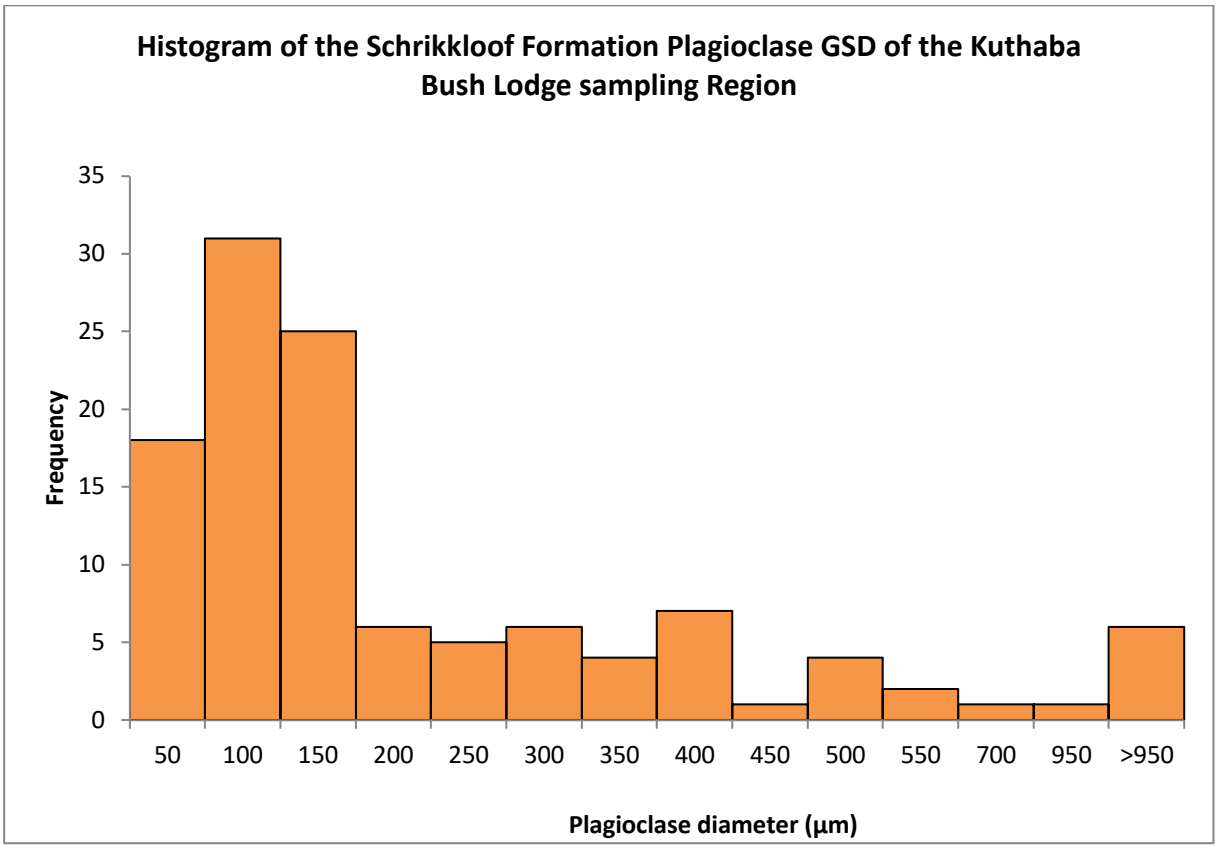

Figure 80. A plagioclase GSD histogram of the Schrikkloof Formation found in the Kuthaba Bush Lodge sampling region.

Table 4. Comparing statistical values of the plagioclase GSD of the Schrikkloof Formation between the two different sampling sites, Kuthaba Bush Lodge and Loskop Dam.

Sampling Site	Kuthaba Bush Lodge	Loskop Dam
Plag. minimum diameter (µm)	23	83
Plag. maximum diameter (µm)	1624	1902
Diameter range (µm)	1601	1819
Median (µm)	109	560,5
Mode (µm)	71	N/A
Sum of all diameters (µm)	26 622	10 372
No. of values in data set	117	14
Mean (µm)	227,54	740,86

Frequency GSD histograms have been drawn up to compare the GSD patterns for the individual rock samples of the Schrikkloof Formation at the Kuthaba Bush Lodge sample region (figure 81). Degree of welding for each rock sample is included. GSD patterns seem to be random with no distinction or particular similarity between rock samples found in the same locations. There might be a slight correlation of GSD patterns between rock samples of the same or similar degree of welding. Low to medium welded rock samples seem to have fines skewed GSD patterns with a smaller grain size range, whereas highly welded rock samples tend to display a larger range of GSDs and are neither fines nor coarse-grained skewed. Highly welded samples, however, contain less plagioclase phenocrysts and therefore have less grain size data. An increased number of collected data is needed, and results would need to be duplicated to confirm if there are predictable GSD patterns between highly welded and low welded ignimbrites. Raw plagioclase diameter data for this study can be found in Appendix B for reference.

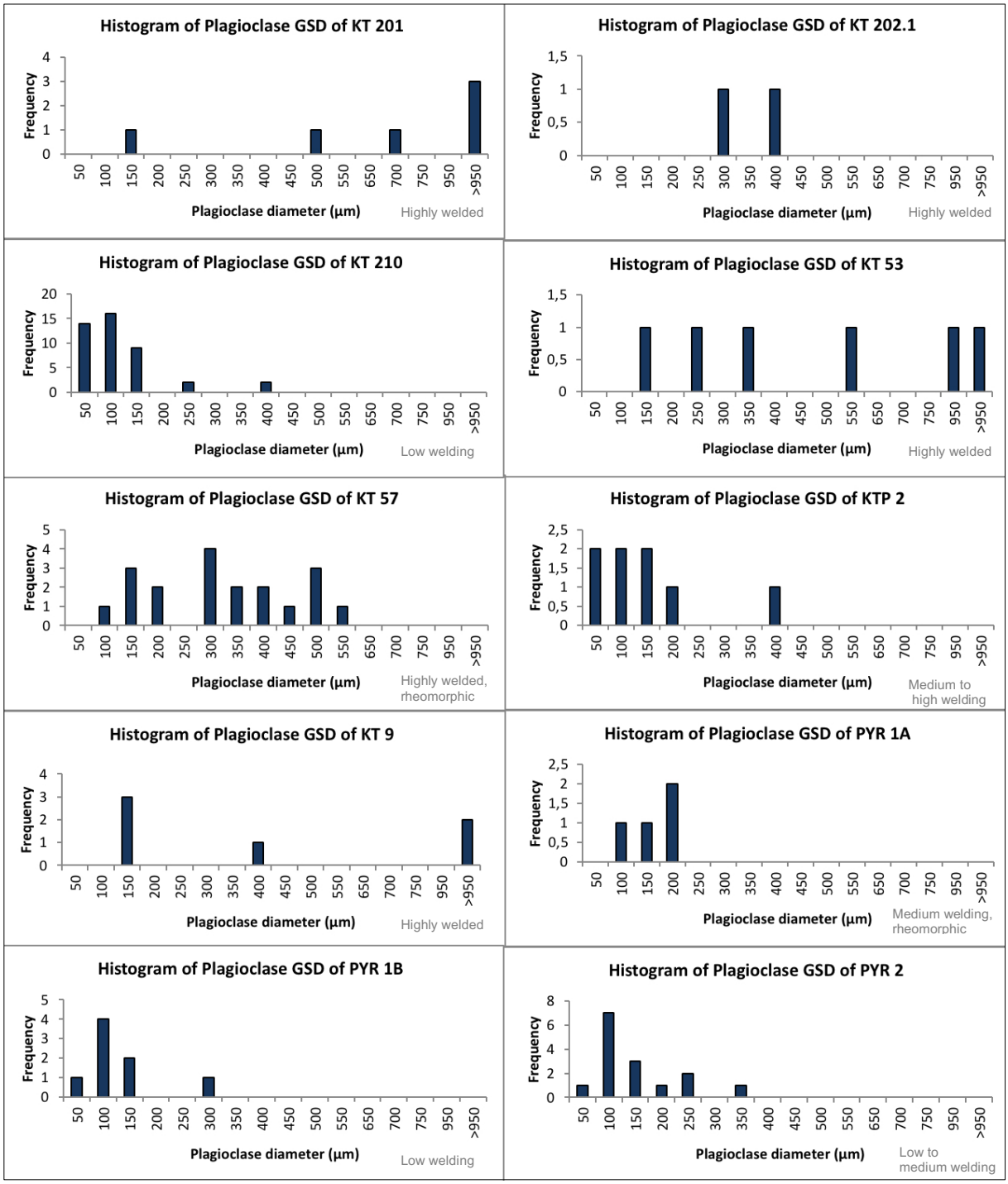

Figure 81. Plagioclase GSD frequency histograms of the Kuthaba Bush Lodge volcanic rock samples, all of which belong to the Schrikkloof Formation.

Chapter 5 - Discussion & Interpretation

5.1. Textural and welding analysis, in accordance with Lenhardt et al. (2017)

5.1.1. Differentiating Characteristics of lava-like to non-welded ignimbrites.

There are distinguishing characteristics that separate a solidified lava flow (e.g., rhyolite) from a solidified pyroclastic flow deposit (e.g., ignimbrite). However, there is an overlap of some characteristics for rhyolite and ignimbrite, as well as a phenomenon called welding (Iddings, 1899) to take into consideration (Walker, 1983), which often results in misinterpretation of a volcanic deposit, i.e. a lava flow deposit versus a pyroclastic deposit (example, Bonnichsen and Kauffman, 1987). Therefore, these volcanic deposits and their distinguishing characteristics are described and categorised below, which can also be studied in figure 82.

Branney et al. (1992) and Branney & Kokkelaar (1992) suggest that pyroclastic flows can be progressively and gradually deposited over time to form thick masses of ignimbrite, instead of a pyroclastic deposit and the process of welding occurring as one event at one point in time. They suggest welding takes place during the gradual deposition over a longer period of time, resulting in the welding continuum. A single flow unit may grade from non-welded (pyroclastic-textured) through to extremely high-grade welding (lava-like) vertically through an ignimbrite, as single pyroclastic flows are deposited gradually over time, or laterally across an ignimbrite, from the source to distal portions of the ignimbrite.

Lava-like ignimbrites are on the “extremely high-grade” welding continuum and have undergone the greatest possible amount of welding to the extent where the ignimbrite is texturally identical to that of a lava flow (Ekren et al., 1984; Branney et al., 1992). Lava-like ignimbrites are aphyric and are fully crystallised and/or devitrified (Schmincke and Swanson, 1967), having a low particle viscosity flow during the pyroclastic flow emplacement and may have developed vesicles syn- and post-emplacement (Branney et al., 1992). Lava-like ignimbrites result from a pyroclastic eruption with a low eruption column height, therefore the pyroclastic flow preserves its internal heat and has greater emplacement temperatures (Branney et al., 1992).

Non-particulate flow occurs during deposition and may materialise after deposition (as a secondary flow), resulting in possible eutaxitic textures, fiamme, flow folds and lineations (Branney et al., 1992; Branney and Kokkelaar, 1992). The lineated textures and flow folds are given the term “rheomorphic”, where Wolff and Wright (1981) state that rheomorphism only occurs during post-emplacement non-particulate flow. Branney et al. (1992), however, highlight that flow structures may also develop during syn-emplacement of viscous non-particulate flows, as is the case with lava-like ignimbrites, making the distinction between primary and secondary flows (Chapin and Lowell, 1979) obsolete. One of the most prominent ways of distinguishing lava-like ignimbrites from lava flows is the presence of the basal and/or upper autobreccia of

the ignimbrite, which may or may not be exposed or preserved (Branney et al., 1992). The summarised models theorising the non-particulate flow, agglutination, deposition, and welding processes, as well as the formation of rheomorphic textures and structures can be studied in figure 83.

Ignimbrites along the welding continuum grade from extremely welded, lava-like textures to increasingly clastic in texture towards the non-welded spectrum. A high-grade rheomorphic ignimbrite is dominantly welded with zones of intense welding and rheomorphism (Branney and Kokkelaar, 1992). The rheomorphism of high-grade rheomorphic ignimbrites are widespread and are considered to be primary structures, having formed during the mass, laminar, and viscous flow, during which the pyroclastic flow degassed and collapsed (Schmincke and Swanson, 1967; Branney and Kokkelaar, 1992; Sumner and Branney, 2002). The textural structures include lineations, flow folds and flow banding, flattened pumice and shards (fiamme), rotated crystals and clasts in the direction of flow, and imbrication. High-grade rheomorphic ignimbrites may also be vitrophyric with a devitrified groundmass (Schmincke and Swanson, 1967).

A non-rheomorphic welded ignimbrite has low-grade welding where the pumice clasts are flattened and darkened (where intensely welded and flattened pumice fragments are black and obsidian-like) and devitrification of the ash groundmass may have taken place. Clastic and fragmental texture, however, can still be observed microscopically and no rheomorphic structures are present (Ross and Smith, 1961). A non-welded ignimbrite simply has retained its original pyroclastic texture with no welding and eutaxitic texture present. This includes granular consolidation of pumice clasts, lithic fragments, glass shards and ash (Ross and Smith, 1961).

The rock samples analysed in this study range across the entire welding spectrum (seen in figure 82). The Dullstroom Formation studied rocks, rock samples RG 7 and 48, consist of basaltic andesite and andesite respectively, originate from a fountain-fed lava flow. The Damwal Formation samples are from two different eruptional origins, namely rock sample RL 1 is an andesite to dacite, originating from a lava-flow. Rock sample LD 021 is a lava-like ignimbrite of high-grade welding with rare preserved glass shards. The Kwaggasnek Formation (rock samples 002 and 004) consists of non-rheomorphic ignimbrites of low- to medium-grade welding. The Schrikkloof Formation (rock samples SM 28.1, KT 9, KT 53, KT 57, KT 201, KT 202.1, KT 210, KTP 2, PYR 1A, PYR 1B, and PYR 2) consists of ignimbrites spread across the welding spectrum, including high aspect ratio non-welded ignimbrites, non-rheomorphic welded ignimbrites, rheomorphic ignimbrites, and lava-like ignimbrites of extremely high-grade welding.

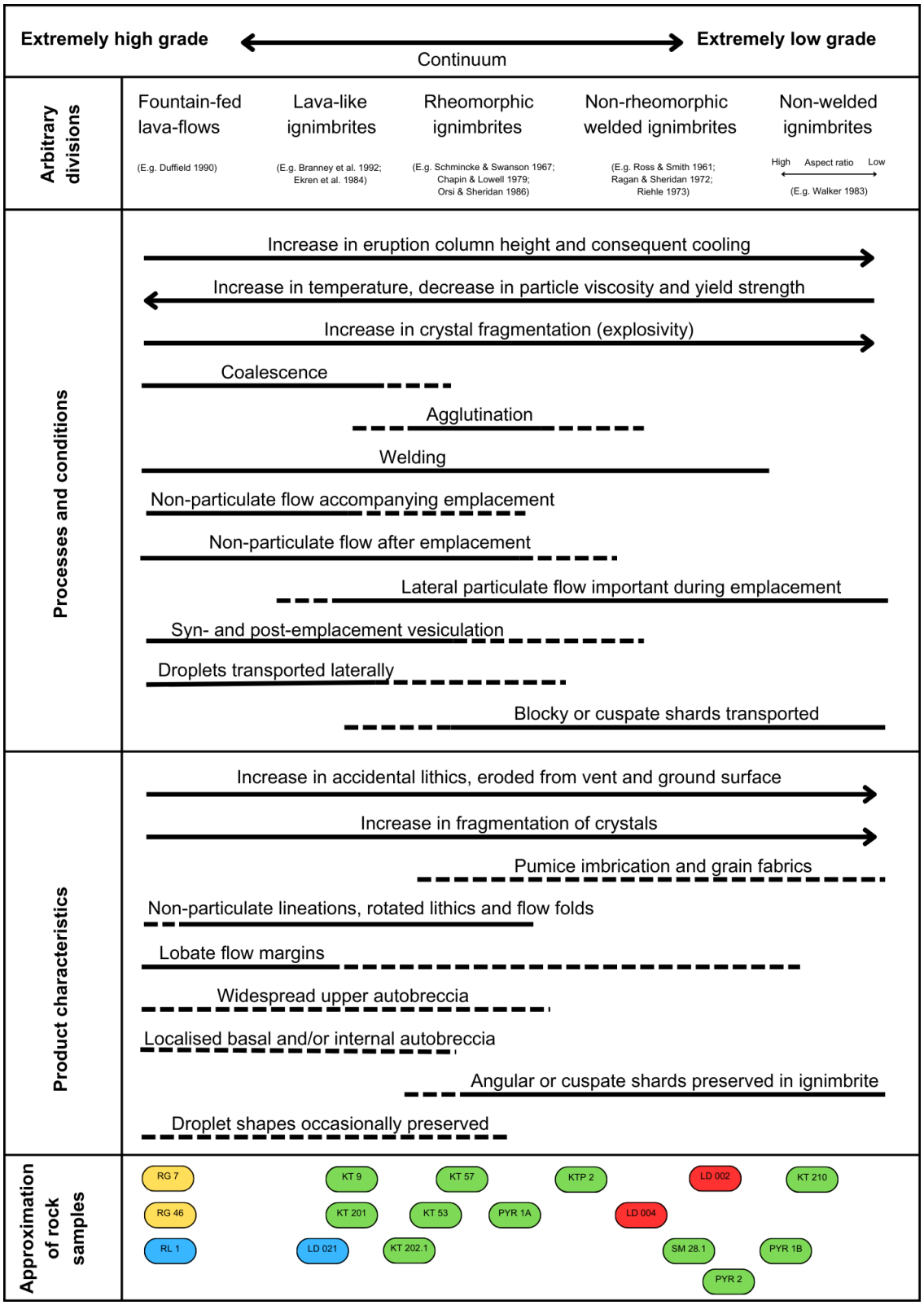

Figure 82. The welding continuum of ignimbrites and the processes and products thereof. The solid lines shown within the "processes" and "products" rows signify distinguishing attributes within that continuum. Dotted lines suggest possible attributes that may be found at that welding continuum. Rock samples of this study are included and are colour coded according to each formation: Dullstroom Formation- yellow, Damwal Formation- blue, Kwaggasnek Formation- red, and the Schrikkloof Formation- green (Modified after Branney & Kokkelaar, 1992).

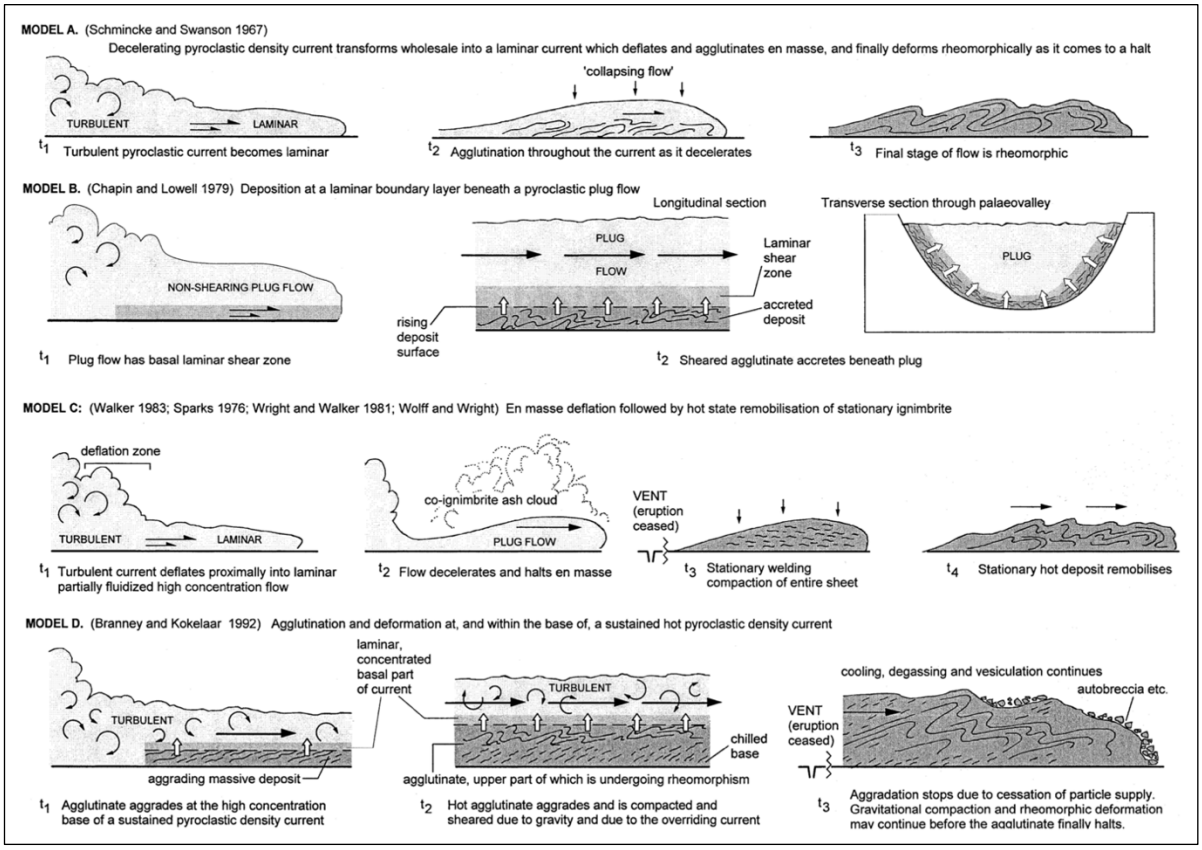

Figure 83. Different theories proposing the flow, agglutination, emplacement processes, and formation of rheomorphic structures in extremely high-grade lava-like ignimbrites (Sumner and Branney, 2002).

5.1.2. Predominant pyroclastic flow deposits of the Rooiberg Group volcanics

The Rooiberg Group rock samples studied constitute lava flow deposits in the Dullstroom and Damwal formations, as they exhibit lava flow textures without clastic or welded pyroclastic textures. This includes aphyric, cryptocrystalline to hypocrystalline textures in the Dullstroom Formation (figures 40 and 42) and micro-porphyritic to porphyritic textures with a devitrified, glassy groundmass in the Damwal Formation (figures 44 and 46). The Dullstroom and Damwal formations also exhibit amygdaloidal textures (figures 39 and 42), occasional flow banding (rock sample RG 7, too large to observe in thin section), and are mafic to intermediate in composition (being more so intermediate) (IUGS, 1989; Hatton and Schweitzer, 1995). The porphyritic rock samples constitute mainly plagioclase phenocrysts, which often occur as glomerocrysts, and do not occur as broken crystals. This suggests the Dullstroom Formation comprises mostly lava flow deposits. One Damwal rock sample (LD 021 in figures 46C to F) contains sickle-shaped glass shards, which indicates pyroclastic origin. The Damwal Formation, therefore, consists of both lava flow deposits and pyroclastic flow deposits, signifying a transition from lava flows of intermediate

compositions to pyroclastic flow deposits as compositions start to become more siliceous towards the top of the formation.

The Kwaggasnek and Schrikkloof formations constitute pyroclastic flow deposits, which have varied degrees of welding, most especially across the Schrikkloof Formation. The Kwaggasnek Formation constitutes spherulitic to micro-spherulitic textures (figures 48A and B) with devitrified groundmasses and minor phenocryst contents (figures 48C to F and 50A, B, E and F). Elongated glass blobs or small pumice clasts are also identified (figures 48E and F), signifying a preservation of pyroclastic texture and a medium to high welding (Branney et al., 1992). The Schrikkloof Formation, which has been the predominant focus of this study, ranges from non-welded ignimbrites to highly welded, lava-like ignimbrites. The non-welded to low welded ignimbrites are associated with numerous glass shards (figures 64, 70, and 72). The low to non-welded ignimbrites contain angular to sub-angular glass shards and broken or fragmented crystals, displaying preserved pyroclastic textures.

The medium to high welded ignimbrites contain compressed and elongated pumice shards and start displaying fiamme and rheomorphic textures (figures 58, 66, and 68). The highly welded, lava-like ignimbrites have lava-like textures and do not have traces of glass shards and fragments (figures 60 and 62). The lava-like ignimbrites consist of aphanitic, completely devitrified groundmasses containing phenocrysts and completely compressed pumice fragments (Branney et al., 1992). The non-welded and low to highly welded ignimbrites scattered across the Kuthaba Sample Region reflect the welding continuum as stipulated by Branny and Kokkelaar (1992) (figure 82) and may display grading of welding and rheomorphism vertically through sustained pyroclastic flows. This also suggests prolonged pyroclastic eruptions. Rheomorphism would have taken place until the agglutinate had ceased its lateral movement, with most of the rheomorphism taking place across mid to upper sections of the pyroclastic flow agglutinate, according to Branney and Kokkelaar (1992)'s agglutinate and deformation model (figure 82). Welding would have taken place syn- and post-deposition as the hot agglutinate cooled, collapsed, and degassed. Most severe welding would have taken place in the centre of the cooling agglutinate, with lower degrees of welding taking place along the margins, as seen in figure 19 (Smith, 1960b; Fisher and Schminke, 1984).

Lenhardt et al. (2017) propose that the volcanics of the Damwal to Schrikkloof formations to comprise almost exclusively of highly welded to rheomorphic ignimbrites. This study confirms and supports this theory; however, it is suggested that the Damwal Formation is rather a transitional formation of lava flow deposits to pyroclastic flow deposits. Furthermore, Lenhardt et al. (2017) state that the Damwal to Schrikkloof volcanism resulted from highly explosive, boil-over eruptions originating from fissures,

likely associated with calderas, with low eruption columns. A low eruption column generated hot pyroclastic flows as it restricted air flow into the pyroclastic cloud, thus limiting the transfer of heat out of the system (Branney et al., 1992).

Eruption temperatures of the Dullstroom and Damwal formations have been calculated to be approximately 840-1120 ^{o}C and the upper, more siliceous formations were calculated to be more than 1000 ^{o}C (Lenhardt and Eriksson, 2012). The eruption temperatures along with the presence of anhydrous phenocrysts in the Rooiberg Group volcanic successions suggests the volcanic eruptions were very hot (Lenhardt and Eriksson, 2012). The hot eruption temperatures along with boil-over type eruptions would ensure widespread welding and would result in dominantly highly-welded, lava-like ignimbrites (Lenhardt et al., 2017). Low aspect ratios (Twist and French, 1983) of the Rooiberg Group volcanic rocks, between 1:100 to 1:1000, further support the ignimbrite theory (Lenhardt et al., 2017).

Aphanitic to cryptocrystalline textures of the lower Rooiberg Group formations suggest that the Dullstroom and Damwal volcanics were a result of the eruption of hot lava which rapidly cooled and solidified, not allowing for significant crystal growth. Micro-porphyritic to porphyritic textures along with quench mineral textures (such as skeletal, figures 52A and B, and swallow-tailed, figures 58C and D, plagioclase crystals) and glassy groundmasses suggest phenocryst mineral growth occurred during magma ascent, followed by rapid cooling and quenching as the lava was erupted. Glomeroporphyritic texture, more often seen in lavas when compared to pyroclastic deposits (McPhie et al., 1993), seen in the Damwal Formation likely occurred during slower magma ascent, where the plagioclase crystals accreted heterogeneously on a preexisting mineral, such as clinopyroxene or plagioclase, before eruption (Kirkpatrick, 1977).

It is noted that the Schrikkloof Formation sample from the Dullstroom sample region is distinctly different from those sampled at the Kuthaba Bush Lodge sample region. The Loskop Dam Schrikkloof sample is an older pyroclastic flow deposit, being sampled closer to the Kwaggasnek Formation, being emplaced in a slightly different palaeoenvironment, whereas the Kuthaba Schrikkloof samples are younger pyroclastic deposits, being sampled closer to the Waterberg Group. The Loskop Dam Schrikkloof sample contains large lithic fragments and phenocrysts, micrographic texture, and perthite. This may signify longer magma ascent periods, allowing for adequate phenocryst growth before eruption of porphyritic magma. Larger lithic fragments may indicate the Loskop Dam sample region contains more proximal pyroclastic deposits compared to the Kuthaba Bush Lodge region. The micrographic texture and perthite in sample SM 28.1 could be a result of the disequilibrium of feldspar during rapid cooling.

5.2. Palaeoenvironment of the Rooiberg Group volcanics

Lenhardt et al. (2017) identifies seven Rooiberg Group lithofacies in the Loskop Dam area, which are subdivided into syn-eruptive and inter-eruptive lithofacies. The syn-eruptive lithofacies include the highly explosive pyroclastic deposits, resulting in the ignimbrites of predominantly high-grade welding, as well as sedimentary deposits occurring at the same time as the explosive eruptions and emplacements. The inter-eruptive lithofacies include the sedimentary deposits of the Rooiberg Group occurring during the periods of volcanic dormancy. The syn-eruptive deposits include the coherent volcanic lithofacies (cv) and peperitic breccia lithofacies (Gp). The inter-eruptive lithofacies include the planar cross-bedded sandstone lithofacies (Sp), the horizontally bedded sandstone lithofacies (Sh), the low-angle cross-bedded sandstone lithofacies (Sl), the horizontally-bedded conglomerate lithofacies (Gm), and the bedded chert lithofacies (bc). The Rooiberg Group lithofacies can be studied in figure 84 below.

Table 5. The seven lithofacies and interpreted processes and palaeoenvironments of the Rooiberg Group, identified in the Loskop Dam region (Lenhardt and Eriksson, 2012; Lenhardt et al., 2017) with the addition of two new lithofacies (transitional volcanic lithofacies- tv and volcaniclastic lithofacies- vc) proposed by this study.

Lithofacies	Lithology and texture	Sedimentary structures	inferred process	Interpreted setting
cv	Aphyric, vesicular to porphyritic, non-vesicular	None	Lava flows	Subaerial deposits, near braided streams and/or lakes
tv	Aphyric, vesicular to porphyritic, non-vesicular, eutaxitic to parataxitic textures	Possible structures overprinted by welding and rheomorphism	Lava flows, pyroclastic density current; various amounts of syn- to post-depositional welding	Subaerial deposits, near braided streams and/or lakes
vc	Aphyric, porphyritic, spherulitic, eutaxitic to parataxitic textures	Possible structures overprinted by welding and rheomorphism	Pyroclastic density current; various amounts of syn- to post-depositional welding	Subaerial deposits, near braided streams and/or lakes, calderas and caldera ring fissures
Gp	Clast- to matrix-supported, jigsaw texture of angular to shard-like clasts in silty, sandy matrix	Non-stratified	Mingling of magma with poorly consolidated wet sediments, at the margins of intrusions or bases of lavas	Subaerial to shallow water deposits, possibly near lakes, ponds and rivers
SP	Poorly sorted, moderately rounded grains of medium to coarse sand	Planar cross-bedding	Straight-crested dunes under lower flow regime conditions	Braided stream
Sh	Poorly sorted, fining upwards grains of medium to fine sand	Horizontal bedding	Large linguoid bars or channel-filled sand deposits under upper flow regime conditions	Braided stream and/or flash flood
Sl	Poorly to moderately sorted, with grains of fine to coarse sand	Low-angle cross-bedding	Dunes that formed near the upper stage plane bed boundary	Sandy bed-load channel in braided stream
Gm	Poorly sorted, matrix-supported, angular to subrounded clasts showing fining upwards	Horizontal bedding	Gravel-capped longitudinal bars	Low-sinuosity braided stream
bc	Thin-bedded layers interbedded between coherent volcanic rocks and sandstones	Horizontal bedding	Inorganic precipitation of silica gel	Closed lake basin

All volcanic rocks sampled and described in this study belong to the coherent volcanic lithofacies (cv). It is suggested, however, that this lithofacies should be subdivided into the “coherent volcanic lithofacies” (cv), which only should include the lava flow deposits of the Dullstroom Formation, the “transitional volcanic lithofacies” (tv), which includes the Damwal Formation volcanics that transition from lava flow deposits to pyroclastic deposits as the chemical compositions become more silicic towards the top of the formation, and the “volcaniclastic lithofacies” (vc), which includes the pyroclastic deposits of the Kwaggasnek and Schrikkloof formations (table 5).

Sedimentary outcrops identified and described in the field analysis (chapter 4.1) at Kuthaba Bush Lodge display similar characteristics to the seven lithofacies described by Lenhardt et al. (2017). Outcrop 13 (figure 32 on page 56) comprises a fine- to medium-grained horizontally bedded sandstone with approximate symmetrical ripple marks, which is made up of eroded Pretoria Group siliciclastic rock (Lenhardt and Eriksson, 2012) and may have formed on the shore of a tidal shallow epeiric sea (Twist, 1983) or floodplains of sandy braided rivers (Lenhardt and Eriksson, 2012).

Outcrop 12 (figure 31 on page 55) comprises a lahar consisting of small to large ignimbritic clasts set in a sandy matrix, which conformably overlies sandstone in outcrop 13. The lahar indicates that the Rooiberg Group volcanics were deposited in a water-rich subaerial environment, which includes rivers, lakes, and the occurrence of rainfall. The lahar may also indicate the possibility of pyroclastic eruptions through crater lakes, however this may be ruled out, as there is no microscopic textural evidence for hydroclastic eruptions. The sandstone in outcrop 13 displays ripple marks that are approximately symmetrical, suggesting the ripples formed under tidal conditions. This could indicate the presence of a shallow epeiric sea. Additionally, Outcrop 9 (figure 28 on page 52), which consists of strongly hydrothermally altered rheomorphic lava-like ignimbrite and brecciated ignimbrite, signifies a water-rich palaeoenvironment during the cooling of the Schrikkloof pyroclastic flows.

Outcrops 12 and 13 do not perfectly fit in one of the seven lithofacies by Lenhardt et al. (2017), however the sandstone is congruent with the rippled sandstone lithofacies (Sr) described by Lenhardt and Eriksson (2012). Outcrops 14 (figure 33 on page 57) and 15 (figure 34 on page 58) consist of peperites and would belong to the syn-eruptive peperitic breccia lithofacies (Gp). The formation of these peperites likely occurred when hot pyroclastic flows came into contact with saturated sand particles, causing the explosive fragmentation and quenching of the fluid pyroclastic material, which then intermixed with the sandy sediment (Kokelaar 1989; Skilling et al., 2002). The sediment is likely related to braided streams (Lenhardt et al., 2017).

Lenhardt and Eriksson (2012)'s Rooiberg Group palaeoenvironment model (figure 84) includes a volcanic basin dominated by lava fissure and subdominant fountain eruptions with occasional and small explosive eruptions, resulting in stretches of dacite to rhyolite layers with smaller, occasional pyroclastic deposits. Sandy braided rivers meander across the landscape (Lenhardt and Eriksson, 2012; Lenhardt et al., 2017), where the accumulated sediment is eroded from proximal Pretoria Group siliciclastic rock sources (Eriksson et al., 1994). Peperites form as lava flows come into contact with the saturated sandy sediment at the braided river sites. Other isolated water bodies are present, including lakes and ponds, resulting in the formation of chert and shale (Lenhardt and Eriksson, 2012). Lenhardt et al. (2017) proposes the palaeoenvironment is rather dominated by successive highly explosive fissure eruptions resulting in a landscape dominated by layers of ignimbrite instead of lava flows and layers of rhyolite, which this study is in accordance with. Peperites therefore also rather form at the contacts between hot pyroclastic density currents and saturated sandy sediment (Kokelaar, 1989; Lenhardt et al., 2017).

Highly explosive eruptions resulting in thick, extensive pyroclastic deposits, such as those belonging to the Rooiberg Group volcanics, are linked to caldera crater and ring fissure eruptions (Fisher and Schminke, 1984). Lenhardt et al. (2017) correspondingly link the Rooiberg Group ignimbrites to highly explosive, hot eruptions originating from fissures, likely associated with calderas. Correspondingly, it is suggested that the Rooiberg Group ignimbrites of variable welding originate from highly explosive, rapid and hot eruptions from calderas and caldera ring fissures. Lateral caldera eruptions are also a possibility. Short periods of volcanic dormancy occur more frequently towards the upper Rooiberg Group formations (Eriksson et al., 1994; Lenhardt and Eriksson, 2012) and result in inter-eruptive sedimentary deposits (Lenhardt et al., 2017).

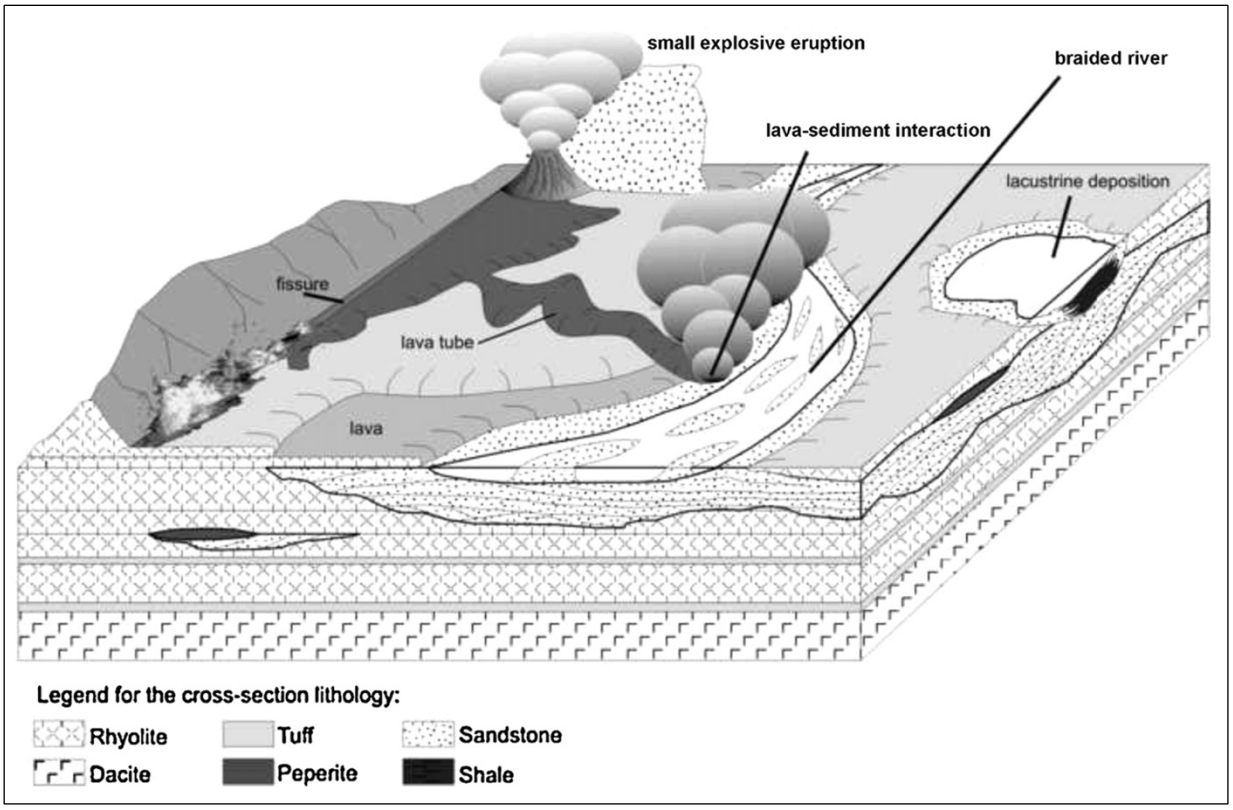

Figure 84. Palaeoenvironment model for the Rooiberg Group, including large expanses of land covered in lava flow deposits which are carved by braided sandy rivers and contain other bodies of water, such as lakes and ponds (Lenhardt and Eriksson, 2012).

5.3. Grain Size Distribution of plagioclase phenocrysts in the Rooiberg Group volcanic rocks

GSD analyses on pyroclastic deposits are computed to deduce different eruption and transport characteristics of the deposit's origin, such as the explosive strength of the volcanic eruption (Fisher, 1964) and the transport and deposition of pyroclastic material (Walker 1971; Wohletz, 1989). A pyroclastic flow deposit may contain the following components: pumice, glass shards, crystals, and lithic fragments- all of which have their own GSD signatures within the same rock sample (Fisher and Schminke, 1984). Grain sizes of the different pyroclastic components depend on the initial eruption itself, where crystal sizes are determined before eruption as phenocryst growth occurs within the ascending magma, which depends on the magmatic conditions. Pumice and glass shard grain sizes are initially determined by the fragmentation and quenching of explosively erupting lava, and lithic fragment sizes depend on the shattering of country rock during the explosive eruption. Grain sizes within a deposit are then determined by the particles' fall velocities, which depend on the grains' size, shape, density, and surface roughness (Walker, 1971).

In fallout deposits grain sizes are well sorted, as large and dense particles will settle closer to the volcanic vent, resulting in proximal lithofacies, whereas finer, more buoyant particles, such as ash, will settle out further away from the vent, resulting in distal lithofacies. The exception, however, is during a weak eruption with a large volcanic vent, when finer material may accumulate close to the vent because the vent is so large that only suspended ash particles are transported and deposited past the vent. Therefore, only coarse-grained material can reliably indicate proximal deposits (Fisher, 1964). The presence and strength of wind will affect the GSD pattern of fallout deposits, as suspended material will be carried and deposited in the direction of the wind. Other factors influencing GSD of fallout deposits include rain flushing and intermixing of overlying fine ash with underlying coarser grained deposits (Walker, 1971).

Pyroclastic flow deposits and ignimbrites have distinct GSD patterns, at least when the body of the ignimbrites are homogenous and poorly sorted with particles ranging from large volcanic bombs to fine ash that are erratically mixed. Sorting is poor within the body of an ignimbrite in both proximal and distal facies from the volcanic vent or fissure. Poor sorting is a result of the turbulence and *en masse* transportation of the volcanic material within the pyroclastic flow (Murai, 1961). There is an exception, however, for tapering distal ends of pyroclastic flows that display good sorting (fines enriched) and may show flow structures (Kuno, 1941; Murai, 1961). The ignimbrite body may be graded, as described in chapter 2.2.2 and seen in figure 18. The basal layer and ignimbrite pipes or fossil fumaroles of the ignimbrite are well sorted, enriched in coarser grained material and are often heterogenous (Murai, 1961; Walker, 1971).

A schematic log through a highly welded ignimbrite of the Rooiberg Group can be seen in figure 85 below. The Rooiberg Group ignimbrite constitutes a basal crystal rich layer followed by the body of the ignimbrite, which is massive and vitrophyric and becomes more vesicular towards the top. The ignimbrite may grade into a flow-banded zone at the top of the flow unit if rheomorphism has taken place (Lenhardt et al., 2017). The crystal rich basal layer may have formed by the removal of ash by the rushing of air in the density current during transport (Walker, 1971). Original grading of the Rooiberg ignimbrite likely was overprinted by welding. Sorting of the ignimbrite body would be poor if the rock was non-welded.

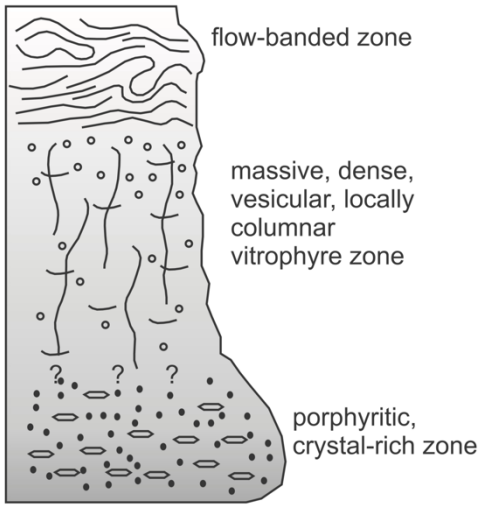

Figure 85. A cross-sectional view of a Rooiberg Group highly welded rheomorphic ignimbrite (Lenhardt et al., 2017).

The Rooiberg Group formations each have a unique frequency GSD pattern (figure 78). Crystal frequency GSD histograms may be used to distinguish different types of volcanic deposits, such as lava flow deposits from lava-like, highly welded pyroclastic flow deposits.

The Dullstroom Formation is well sorted, consisting of the smallest diameter size range with the smallest diameter sizes (with a mode of 27 µm and a mean of 22 µm). The Dullstroom Formation consists of andesitic lava flow deposits (Hatton and Schweitzer, 1995; Schweitzer et al., 1995). This is also reflected in the distinctly different GSD of plagioclase in the Dullstroom Formation compared to the rest of the Rooiberg formations. The Dullstroom Formation has good sorting and is enriched in fine crystaline plagioclase phenocrysts, whereas the rest of the formations have poor sorting and overall contain coarser plagioclase phenocrysts. The plagioclase phenocryst sizes in the Dullstroom Formation reflect quick and limited crystal growth during magma ascent and eruption. This may mean the Dullstroom magmas ascended and erupted quickly and crystallised at high temperatures, ranging between 840 to 1200 ^{o}C (Lenhardt and Eriksson, 2012).

The Damwal Formation GSD more closely resembles the Kwaggasnek and Schrikkloof GSDs, suggesting the Damwal Formation may dominantly consist of highly welded ignimbrites instead of lava flow deposits, as proposed by Lenhardt et al. (2017). Therefore, the Damwal Formation likely marks a transition where the lower portion of the formation transitions from lava flows to explosive eruptions yielding pyroclastic deposits, which dominate the rest of the formation.

The Damwal Formation is very poorly sorted with a mode of 129 µm and a mean of 232,4 µm (table 3). The Kwaggasnek and Damwal formations have GSD patterns that are the most similar out of the four formations, suggesting their eruption and transport processes are similar. The Kwaggasnek Formation is also poorly sorted, but

less so than the Damwal and Schrikkloof formations and has a mode of 337 µm and a mean of 364,07 µm (table 3). The Kwaggasnek plagioclase phenocrysts likely had slightly more time for crystal growth in the magma before eruption compared to the rest of the formations. This may have been a result of slower magma ascent compared to the rest of the Rooiberg Group formations.

The Schrikkloof Formation plagioclase GSD displays poor sorting and contains the largest range of plagioclase diameter sizes, with a mode of 71 µm and a mean of 282,4 µm (table 3). The poor sorting may reflect a higher explosive strength of the Schrikkloof eruptions and a greater turbulence within the pyroclastic flows during transport. The Schrikkloof Formation plagioclase GSD is skewed towards the fines, possibly suggesting rapid magma ascent and rapid, highly explosive eruptions, with insufficient time for adequate crystal growth in the magma. Alternatively, the fine crystal sizes may also reflect distal end deposits. The Damwal to Schrikkloof formations all contain mostly fine plagioclase crystal sizes, which may reflect overall quick magma ascents and highly explosive eruptions, or may suggest the remaining Rooiberg Group volcanic exposures are all distal deposits with the Schrikkloof Formation, specifically located in the Kuthaba Bush Lodge sample region, being the most distal.

Chapter 6 - Conclusions

The Rooiberg Group volcanic rocks have been analysed in this study to gain a better understanding of the eruption, transport and emplacement processes of the Rooiberg Group, which includes the Dullstroom, Damwal, Kwaggasnek, and Schrikkloof formations. Microscopic textural analysis reveals that the Dullstroom Formation constitutes lava flow textures, which includes aphyric, cryptocrystalline and hypocrystalline textures to micro-porphyritic and glomeroporphyritic textures with occasional flow banding and amygdales. The Damwal Formation displays lava flow microscopic textures similar to the Dullstroom Formation as well as lava-like ignimbritic microscopic texture, suggesting the Damwal volcanics consist of both dacitic lava flows as well as pyroclastic flow deposits, marking a transition from predominantly effusive to increasingly explosive eruptions. Additionally, GSD patterns for the Damwal Formation suggest volcanism consists of predominantly explosive eruptions, resulting in the emplacement of ignimbrites that have been variably welded.

The Kwaggasnek and Schrikkloof formations consist of non-welded to highly welded rheomorphic ignimbrites of rhyodacitic to rhyolitic composition, displaying a lava-like microscopic texture, which includes a completely devitrified groundmass, flattened and recrystallised pumice clasts, fiamme textures, and occasionally includes spherulites and perlitic cracks. Non-welded to medium welded ignimbrites display preserved pyroclastic texture and composition, which includes broken phenocrysts, preserved and recrystallised glass shards, pumice clasts and lithic fragments, where glassy material has been recrystallised to secondary minerals. This is in accordance with research presented by Lenhardt et al. (2017). Welding ranges from low-grade to extremely high-grade, reflecting the welding continuum and model of agglutination, deformation and transport of hot pyroclastic density currents presented by Branny and Kokelaar (1992).

The Rooiberg Group volcanism predominantly consists of highly explosive, sustained eruptions with high magmatic temperatures and periods of volcanic dormancy, as stipulated by Lenhardt and Eriksson (2012) and Lenhardt et al. (2017). The palaeoenvironment of the Rooiberg Group is subaerial on tracts of land covered in volcanic material, which is interrupted by bodies of water (such as lakes and possibly an epeiric sea) and is carved by sandy, braided rivers. The Rooiberg Group volcanism became increasingly explosive as compositions became increasingly siliceous. Explosive pyroclastic eruptions likely originated from caldera ring fissures, resulting in hot boil-over eruptions.

Plagioclase Grain Size Distribution patterns of the four Rooiberg formations, as exhibited by the GSD frequency histograms, distinguish the lava flow deposits of the Dullstroom Formation from the pyroclastic flow deposits of the Damwal, Kwaggasnek, and Schrikkloof formations. The Dullstroom GSD displays well sorted, fines enriched plagioclase crystal sizes, reflecting rapid and limited plagioclase growth during magma ascent and eruption before quenching of the lava flow. The Damwal, Kwaggasnek and Schrikkloof formations display poor sorting with peaks of fine to medium crystalline plagioclase sizes. The Schrikkloof Formation displays the poorest sorting of plagioclase crystal sizes, enriched more so in fine crystalline plagioclase sizes compared to the Damwal and Kwaggasnek formations. This suggests eruptions become increasingly violent with time with the Schrikkloof Formation representing rapid magma ascent before eruption. The remaining outcrops of the Nylstroom and Bothasberg packages (which includes the Kuthaba Bush Lodge, Loskop Dam and Dullstroom sample regions) are likely distal deposits, with the Schrikkloof Formation of the Kuthaba Bush Lodge sample region containing the most distal deposits.

Chapter 7 - References

Armstrong, R.A., Compston, W., Retief, E.A., Williams, I.S., Welke, H.J. (1991). Zircon ion microprobe studies bearing on the age and evolution of the Witwatersrand Triad. *Precambrian Research*, **53**, 243-66.

Bonnichsen, B. and Kauffman, D.F. (1987). Physical features of rhyolite lava flows in the Snake River Plain volcanic province, south- western Idaho. *Geological Society of America Special Paper*, **212**,119-145.

Branney, M.J. and Kokelaar, P. (1992). A reappraisal of ignimbrite emplacement: progressive aggradation and changes from particulate to non-particulate flow during emplacement of high-grade ignimbrite. *Bulletin of Volcanology*, **54**, 504-520.

Branney, M.J., Kokelaar, P., McConnell, B.J. (1992). The Bad Step Tuff: A lava-like rheomorphic ignimbrite in a calc-alkaline piecemeal caldera, English Lake District. *Bulletin of Volcanology*, **54**, 187-199.

Bryan, S.E. and Ernst, R.E. (2008). Revised definition of Large Igneous Provinces (LIPs). *Earth-Science Reviews*, **86**, 175-202.

Bryan, S.E., Ferrari, L., Réiners, C.M., Petrone, C.M., Ramos-Rosique, A., Campbell, I.H. (2008). New insights into crustal contributions to large volume rhyolite generation at the mid-Tertiary Sierra Madre Occidental Province, Mexico, revealed by U-Pb geochronology. *Journal of Petrology*, **49**, 47–77.

Bryan, S.E. Cook, A., Allen, C.M., Siégel, C. (2012) Early-mid Cretaceous tectonic evolution of eastern Gondwana: From silicic LIP magmatism to continental rupture. *Episodes*, **35**, 142–152.

Bryan, S.E., Orozco-Esquivel, T., Ferrari, L., López-Martínez, M. (2013). Pulling apart the Mid to Late Cenozoic magmatic record of the Gulf of California: is there a Comondú Arc? *Geological Society London Engineering Geology Special Publications*, **385**, 389-407.

Buchanan, P.C., Reimold, W.U., Koeberl, C., Kruger, F.J. (2004). Rb-Sr and Sm-Nd isotopic compositions of the Rooiberg Group, South Africa: early Bushveld-related volcanism. *Lithos*, **29**, 373-388.

Bumby, A.J., Eriksson, P.G., van der Merwe, R. (1998). Compressive deformation in the floor rocks to the Bushveld Complex (South Africa): evidence from the Rustenburg Fault Zone. *Journal of African Earth Sciences*, **27**, 307-330.

Button, A. (1986). The Transvaal sub-basin of the Transvaal Sequence. In: Anhaeusser, C.R., Maske, S. (Eds.), *Mineral Deposits of Southern Africa*. *Geological Society of South Africa, Johannesburg*, pp. 811–817.

Chapin, C.E. and Lowell, G.R. (1979). Primary and secondary flow structures in ash-flow tufts of the Gribbles Run Palaeovalley, central Colorado. In: Chapin, C.E., Elston, W.E. (eds) Ash flow turfs. *Geological Society of America Special Papers*, **180**, 137-154.

Cas, R.A.F. and Wright, J.V. (1987). *Volcanic Successions: Modern and Ancient*. Chapman & Hall, London.

Cawthorn, R.G. and Walraven, F. (1997). The Bushveld Complex: A Time to Fill and a Time to Cool. EGRI Information Circular, University of Witwatersrand, p. 307.

Cawthorn, R.G., Davies, G., Clubley-Armstrong, A., McCarthy, T.S. (1981). Sills associated with the Bushveld Complex, South Africa: an estimate of parental magma composition. *Lithos*, **14**, 1-15.

Coetzee, G.L. (1970). The Rooiberg Felsite series north of Nylstroom. *Symp. On the Bushveld Igneous Complex and other layered intrusions, Spec. publ., Geol. Soc. S. Afr.,* **1**, 312-325.

Coffin, M.F., and Eldholm, O. (1992). Volcanism and continental break-up: A global compilation of large igneous provinces. In Storey, B.C., Alabaster, T., and Pankhurst, R.J., eds., Magmatism and the causes of continental break-up: *Geological Society [London] Special Publication*, **68**, 17–30.

Coffin, M.F., and Eldholm, O. (1994). Large Igneous Provinces: Crustal structure, dimensions, and external consequences. *Reviews of Geophysics*, **32**, 1–36.

Clubley-Armstrong, A.R. (1977). The Geology of the Selonsrivier Area, North of Middelburg, Transvaal, with Special Reference to the Structure of the Regions southeast of the Dennilton dome, MSc Thesis (unpublished), University of Pretoria, 107pp.

De Bruiyn, H. (1980). The Geology of the acid phase of the Bushveld Complex, north of Pretoria – a Geochemical Statistical Approach. PhD thesis (unpublished), University of the Orange Free State, 171pp.

Du Plessis, M.D. (1976). The Bushveld Granites and Associated Rocks in the area north-west of Warm Baths, Transvaal. MSc thesis (unpublished), University of Pretoria, 85pp.

Ekren, E.B., Mcintyre, D.H., Bennett, E.H. (1984). High-temperature large-volume, lavalike ash-flow tuffs without calderas in southwestern Idaho. *US Geological Survey Professional Paper*, **1272**, 1-76.

Eriksson, P.G., Schweitzer, J.K., Bosch, P.J.A., Schereiber, U.M., Van Deventer, J.L., Hatton, C.J. (1993a). The Transvaal Sequence: an Overview. *Journal of African Earth Sciences,* **16**, 25-51.

Eriksson, P.G., Schreiber, U.M., Reczko, B.F.F., Snyman, C.P. (1994). Petrography and geochemistry of sandstones interbedded with the Rooiberg Felsite Group (Transvaal Sequence, South Africa): implications for provenance and tectonic setting. *Journal of Sedimentary Research*, **64**, 836–846.

Eriksson, P.G., Hattingh, P.J., Altermann, W. (1995). An overview of the geology of the Transvaal Sequence and Bushveld Complex, south Africa. *Mineralium Deposita*, **30**, 98-111.

Eriksson, P.G. and Reczko, B.F.F. (1995). The sedimentary and tectonic setting of the Transvaal Supergroup floor rocks to the Bushveld complex. *Journal of African Earth Sciences*, **21(4)**, 487-504.

Eriksson, P.G., Altermann, W., Octavian, C., van der Merwe, R. (2001b). Major influences on the evolution of the 2.67–2.1 Ga Transvaal basin, Kaapvaal craton. *Sedimentary Geology*, **141-142**, 205-31.

Eriksson, P.G., Condie, K.C., van der Westhuizen, W., van der Merwe, R., de Bruin, H., Nelson, D.R., Altermann, W., Catuneanu, O., Bumby, A.J., Lindsay, J., Cunningham, M.J. (2002). Late Archaean superplume events: a Kaapvaal–Pilbara perspective. *Journal of Geodynamics*, **34**, 207– 47.

Eriksson, P.G., Catuneanu, O., Els, B.G., Bumby, A.J., van Rooy, J.L., Popa, M. (2005). Kaapvaal craton: Changing first- and second-order controls on sea level from c. 3.0 Ga to 2.0 Ga. *Sedimentary Geology*, **176**, 121-148.

Ernst, R.E. and Bel, K. (2010). Large Igneous Provinces (LIPs) and carbonatites. *Mineralogy and* Petrology, **98**, 55-76.

Ferrari, L., López-Martínez, M., Rosas-Elguera, J. (2002). Ignimbrite flare up and deformation in the southern Sierra Madre Occidental, western Mexico: Implications for the late subduction history of the Farallon plate. *Tectonics*, **21**, 17-24.

Ferrari, L., Valencia-Moreno, M., Bryan, S. (2007). Magmatism and tectonics of the Sierra Madre Occidental and its relation with the evolution of western margin of North America. *Geological Society of America Special Paper,* **422**, 1–39.

Fisher, R.V. (1964). Maximum size, median diameter, and sorting of tephra. *Journal of Geophysical Research*, **69(2)**, 341-355.

Fisher, R.V. (1979). Models for pyroclastic surges and pyroclastic flows. *Journal of Volcanology and Geothermal Research*, **6**, 305-318.

Fisher, R.V. and Schminke, H.-U. (1984). *Pyroclastic Rocks*. Springer-Verlag, Berlin, Heidelberg, 465pp.

Freundt, A. and Schmincke, H.-U. (1992). Abrasion in pyroclastic flows. *Geologische Rundschau*, **81(2)**, 383‑389.

Freundt, A., Wilson, C.J.N., Carey, S.N. (2000). Ignimbrites and Block-and-Ash flow deposits. *Encyclopedia of Volcanoes.* Academic Press, New York, 581-599.

Frost, B.R., Barnes, C.G., Collins, W.J., Arculus, R.J., Ellis, D.J., Frost, C.D. (2001). A geochemical classification of granitic rocks. *Journal of Petrology*, **42**, 2033–2048.

Harmer, R.E. and von Gruenewaldt, G. (1991). A review of magmatism associated with the Transvaal Basin – implications for its tectonic setting. *South African Journal Geology*, **94**, 104-122.

Hatton, C.J. (1995). Mantle plume origin for the Bushveld and Ventersdorp magmatic provinces. *Journal of African Earth Sciences,* **21**, 571–577.

Hatton, C.J. and Schweitzer, J.K. (1995). Evidence for synchronous extrusive and intrusive Bushveld magmatism. *Journal of African Earth Sciences,* **21**, 579–594.

Houghton, B.F., Wilson, C.J.N., Pyle, D.M. (2000). Pyroclastic fall deposits. *In: SIGURDSSON, H. (ed.) Encyclopedia of Volcanoes.* Academic Press, London, 555‑570.

Iddings, J.P. (1899). The rhyolites. *Hague A, Iddings JP, Werd WH, Walcott CD, Girty GH, Stanton TW, Knowlton FH: Geology of the Yellowstone National Park, part II*, USGS Monograph, **32**, 356-432.

IUGS (International Union of Geological Sciences). (1989). A Classification of Igneous Rocks. Subcommittee on systematics of igneous rocks. *Blackwell Science Publishers*, pp. 35-139.

Jolayemi, O.O. (2015). *Chemical Evolution of the Paleoproterozoic Rooiberg Group, Kaapvaal Craton, South Africa: New Insights into the Formation of a Silicic Large Igneous Province (SLIP)*. PhD thesis, University of Pretoria.

Kirkpatrick, J.R. (1977). Nucleation and growth of plagioclase, Makaopuhi and Alae lava lakes, Kilauea Volcano, Hawaii. *Geological Society of America Bulletin*, **88**, 78-84.

Kokelaar, B.P. (1989). Fluidization of wet sediments the emplacement and cooling of various igneous bodies. *Journal of the Geological Society*, **139**, 21-33.

Krumbein, W.C. and Sloss, L.L. (1963). *Stratigraphy and Sedimentation*, 2nd edition. San Francisco: W. H. Freeman, 660pp.

Kuno, H. (1941). Characteristics of deposits formed by pumice flows and those by ejected pumice. *Tokyo Univ. Earthq. Res. Bull.*, **19**, 144-149.

Lenhardt, N. and Eriksson, P.G. (2012). Volcanism of the Palaeoproterozoic Bushveld Large Igneous Province: The Rooiberg Group, Kaapvaal Craton, South Africa. *Precambrian Research*, **214-215**, 82-94.

Lenhardt, N., Masango, S.M., Jolayemi, O.O., Lenhardt, S.Z., Peeters, G., Eriksson, P.G. (2017). The Palaeoproterozoic (~2,06 Ga) Rooiberg Group, South Africa: Dominated by extremely high-grade lava-like and rheomorphic ignimbrites? New observations and lithofacies analysis. *Journal of Africa Earth Sciences*, **131**, 213-232.

Lombaard, B.V. (1932). *Felsites and their relations in the Bushveld Complex*. PhD Thesis (unpublished), University of Zurich, 106pp.

Mare, L.P., Eriksson, P.G., Améglio, L. (2006). A palaeomagnetic study of the lower part of the Palaeoproterozoic Waterberg Group, South Africa. *Journal of African Earth Sciences*, **44**, 21-36.

Martini, J.E.J. (1998). The Loskop Formation and its relationship to the Bushveld Complex, South Africa, *Journal of African Earth Sciences*, **27**, 193-222.

Mathez, E.A., VanTongeren, J.A., Schwertzer, J. (2013). On the relationships between the Bushveld Complex and its felsic roof rocks, part 1: petrogenesis of Rooiberg and related felsites. *Contrib. Mineral. Petrol.*, **166 (2)**, 435-449.

McPhie, J., Doyle, M., Allen, R. (1993). *Volcanic textures – a guide to the interpretation of textures in volcanic rocks*. Centre for Ore Deposit and Exploration Studies, University of Tasmania, 211pp.

McManus, J. (1988). Grain size determination and interpretation. In Tucker, M. E. (Ed.)., *Techniques in sedimentology*. Oxford: Blackwell Scientific, pp. 63-85.

Menge, G.F. (1963). The Cassiterite Deposits on Doornhoek 342 KR and Vicinity, West of Naboomspruit Transvaal. MSc thesis (unpublished), University of Pretoria, 56pp.

Murai, S. (1961). A study of the textural characteristics of pyroclastic flow deposits in Japan. *Earthquake Research Institute*, **39**, 133-248.

Pankhurst, M.J., Schaefer, B.F., Betts, P.G. (2011). Geodynamics of rapid voluminous felsic magmatism through time. *Lithos*, **123**, 92-101.

Rhodes, R.C. and Du Plessis, M.D. (1976). Notes on some Stratigraphic Relations in the Rooiberg Felsite. *Trans. Geol. Soc. S. Afr.,* **79**, 183-185.

Richards, R.J. (1987). A Geological Investigation of Upper Transvaal Sequence Rocks in the northern Portion of the Rooiberg Fragment. MSc thesis (unpublished), University of Pretoria, 82 pp.

Robb, L.J. and Meyer, F.M. (1995). The Witwatersrand Basin, South Africa: geological framework and mineralization processes. *Economic Geology Research Insitute*, *Information Circular, University of Witwatersrand*, **293**, 37pp.

Ross, C.S. and Smith, R.L. (1961). *Ash-Flow Tuffs: Their origin geologic relations and identification*. Geological Survey Professional Paper 366, United States Government Printing Office, 366pp.

SACS (South African Committee for Stratigraphy). (1980). Stratigraphy of South Africa. Part 1 (Compiled by Kent, L.E.). Lithostratigraphy of the Republic of South Africa, South West Africa/ Namibia, and the Republic of Bophuthatswana, Transkei and Venda. *Handbk. Geol. Surv. S. Afr.,* **8**, 690pp.

Sawkins, F.J. (1984). *Metal deposits in relation to plate tectonics* (edited by Wyllie, P.J.), Springer-Verlang, Berlin, pp158-176.

Schmincke, H. and Swanson, D.A. (1967). Laminar Viscous Flowage Structures in Ash-Flow Tuffs from Gran Canaria, Canary Islands. *The Journal of Geology*, **75(6)**, 641-644.

Schweitzer, J.K. (1998). The Dullstroom basalt formation and the Rooiberg Group: Volcanic rocks associated with the Bushveld Complex, PhD Thesis, University of Pretoria.

Schweitzer, J.K., Hatton, C.J., de Waal, S.A. (1995). Regional Lithochemical Stratigraphy of the Rooiberg Group, upper Transvaal Supergroup: A Proposed New Subdivision. *South African Journal of Geology*, **98(3)**, 245-255.

Schweitzer, J.K. and Hatton, C.J. (1995). Chemical Alteration within the Volcanic Roof Rocks of the Bushveld Complex. *Economic Geology*, **90(8)**, 2218-2231.

Sharpe, M.R., Bahat, D., Von Gruenewaldt, G. (1981). The concentric elliptical structure of feeder sites to the Bushveld Complex and possible economic implications. *Trans. Geol. Soc. S. Afr.* **84**, 239–244.

Sharpe, M.R., Brits, R., Engelbrecht, J.P. (1982). Rare Earth and Trace Element Evidence Pertaining to the Petrogenesis of 2.3 Ga Old Continental Andesites and Other Volcanic Rocks from the Transvaal Sequence, South Africa. *Inst. Geol. Res. Bush. Compl. Res. Rep.* **40**, 63pp.

Skilling, I.P., White, J.D.L., McPhie, J. (2002). Peperite: a review of magma–sediment mingling. *Journal of Volcanology and Geothermal Research*, **114**, issues 1–2, 1-17.

Smith, R.L. (1960a). Ash flows. *Geological society of America Bulletin,* **71**, 795-842.

Smith, R.L. (1960b). Zones and zonal variations in welded ash flows. *U.S. Geological Survey, Prof. Paper 354F*, **8,** 149-159.

Sohn, Y.K. (1997). On traction–carpet sedimentation. *Journal of Sedimentry Petrology,* **67(3)**, 502–509.

Stear, W.M. (1977). The stratigraphy and sedimentation of the Pretoria Group at Rooiberg, Transvaal. *Transactions of the Geological Society of South Africa*, **80**, 53-65.

Strauss, C.A. (1954). The Geology and Mineral Resources of the Potgietersrus tin-fields. *Mem. Geol. Surv. S. Afr.,* **46**, 241 pp.

Sumner, J.M., and Branney, M.J. (2002). The emplacement history of a remarkable heterogeneous, chemically zoned, rheomorphic and locally lava-like ignimbrite: 'TL' on Gran Canaria. *Journal of Volcanology and Geothermal Research*, **115**, 109-138.

Twist, D. and French, B.M. (1983). Voluminous Acid Volcanism in the Bushveld Complex: A review of the Rooiberg Felsite. *Bull. Volcanol.* Volume **46-3**, 225-242.

Twist, D. (1983). An Economic Evaluation of the Rooiberg Felsite. *Inst. Geol. Res. Bushveld Complex, Univ. Pretoria, Res. Rep*. **41**, 25pp.

Twist, D. (1985). Geochemical evolution of the Rooiberg silicic lavas in the Loskop Dam area, southeastern Bushveld. *Economic Geology*, **80**, 1153-1165.

VanTongeren, J.A., Zirakparvar, N.A., Mathez, E.A. (2016). Hf isotopic evidence for a cogenetic magma source for the Bushveld Complex and associated felsic magmas. *Lithos*, **248-251**, 469-477.

Von Gruenewaldt, G. (1968). The Rooiberg Felsite north of Middleburg and its relation to the layered sequence of the Bushveld Complex. *Trans. Geol. Soc. S. Afr.*, **71**, 153-172.

Von Gruenewaldt, G. and Harmer, R.E. (1992). Tectonic setting of Proterozoic layered intrusions with special reference to the Bushveld Complex. *Proterozoic Crustal Evolution (Edited by Condie, K.C.),* pp181-213. Elsevier Scientific Publishers, Amsterdam.

Walraven, F. and Martini, J. (1995). Zircon Pb-evaporation age determinations for the Oak Tree Formation, Chuniespoort Group. Transvaal Sequence; implications for Transvaal-Griqualand West basin correlations. *South African Journal of Geology,* **98**, 58–67.

Walraven, F. (1997). Geochronology of the Rooiberg Group, Transvaal Supergroup, South Africa. *Information Circular 316, Economic Geology Research Unit*. University of the Witwatersrand, Johannesburg, South Africa, 21pp.

Walker, G.P.L. (1971). Grain-size characteristics of pyroclastic deposits. *Journal of Geology*, **79**, 696-714.

Walker, G.P.L. (1983). Ignimbrite types and ignimbrite problems. *Journal of Volcanology and Geothermal Research*, **17**, 64-88.

Walker, G.P.L. (1984). Characteristics of dune-bedded pyroclastic surge bedsets. *Journal of Volcanology and Geothermal Research*, **20**, 281–296.

Willemse, J. (1969). The Geology of the Bushveld Igneous Complex, the Largest Repository of Magmatic Ore Deposits in the World. *Econ. Geol. Monogr.*, **4**, 1-22.

Wilson, C.J.N. and Walker, G.P.L. (1981). *Violence in pyroclastic flow eruptions*. Tephra Studies (S. Self and R.S.J. Sparks, Editors). Reidal Dordrecht. 441-448pp.

Wolhuter, L.E. (1954). The Geology of the Country Surrounding Loskop Dam, Transvaal, MSc Thesis (unpublished), University of Pretoria, 66pp.

Appendix A

A complete assemblage of the rock samples' photomicrographs

The Dullstroom Sampling Site

The Dullstroom Formation:

RG 7 [25°23'02.0" S; 29°58'54,2" E]:

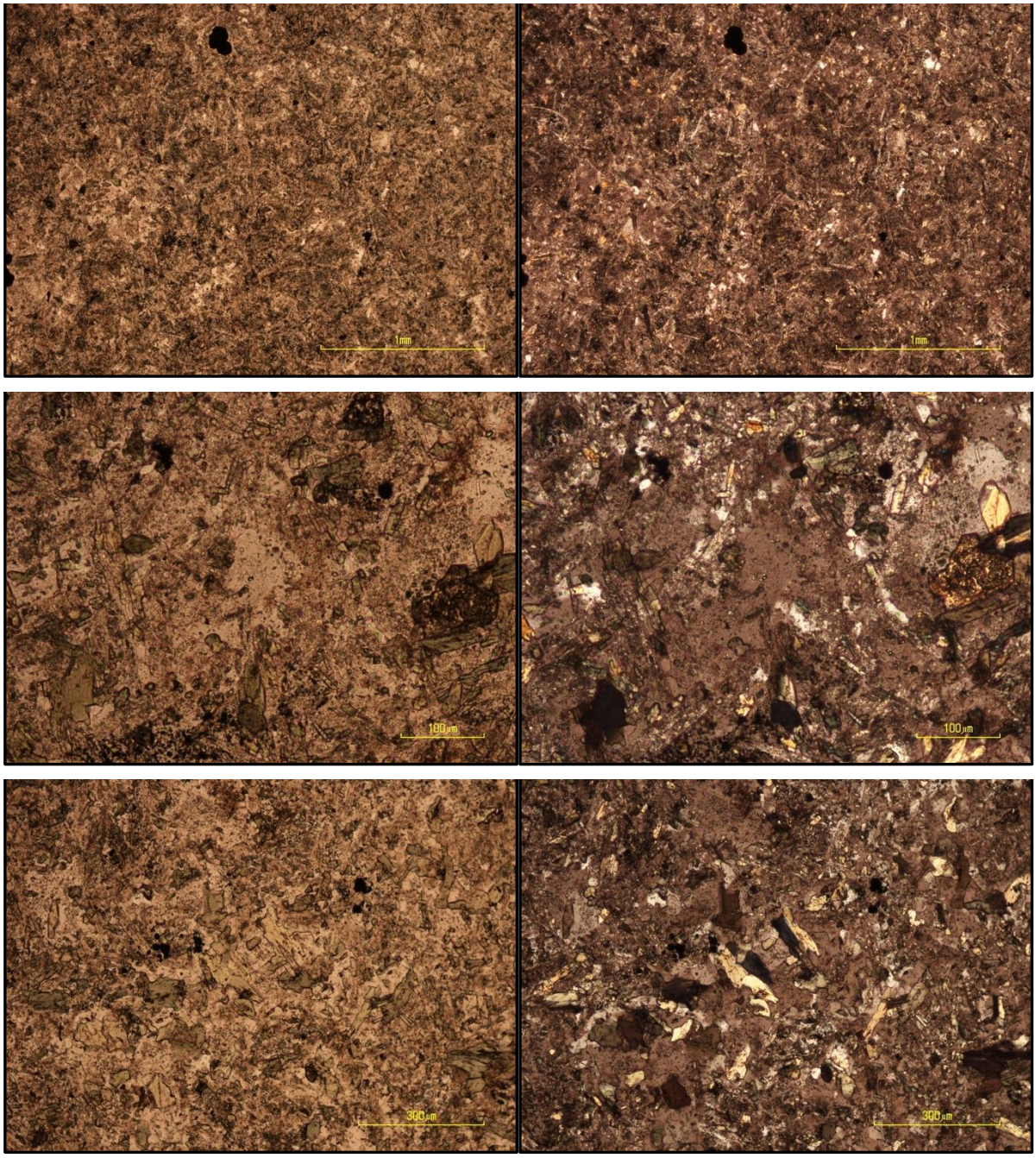

RG 46 [25°23'53.3" S; 30°00'37.1" E]:

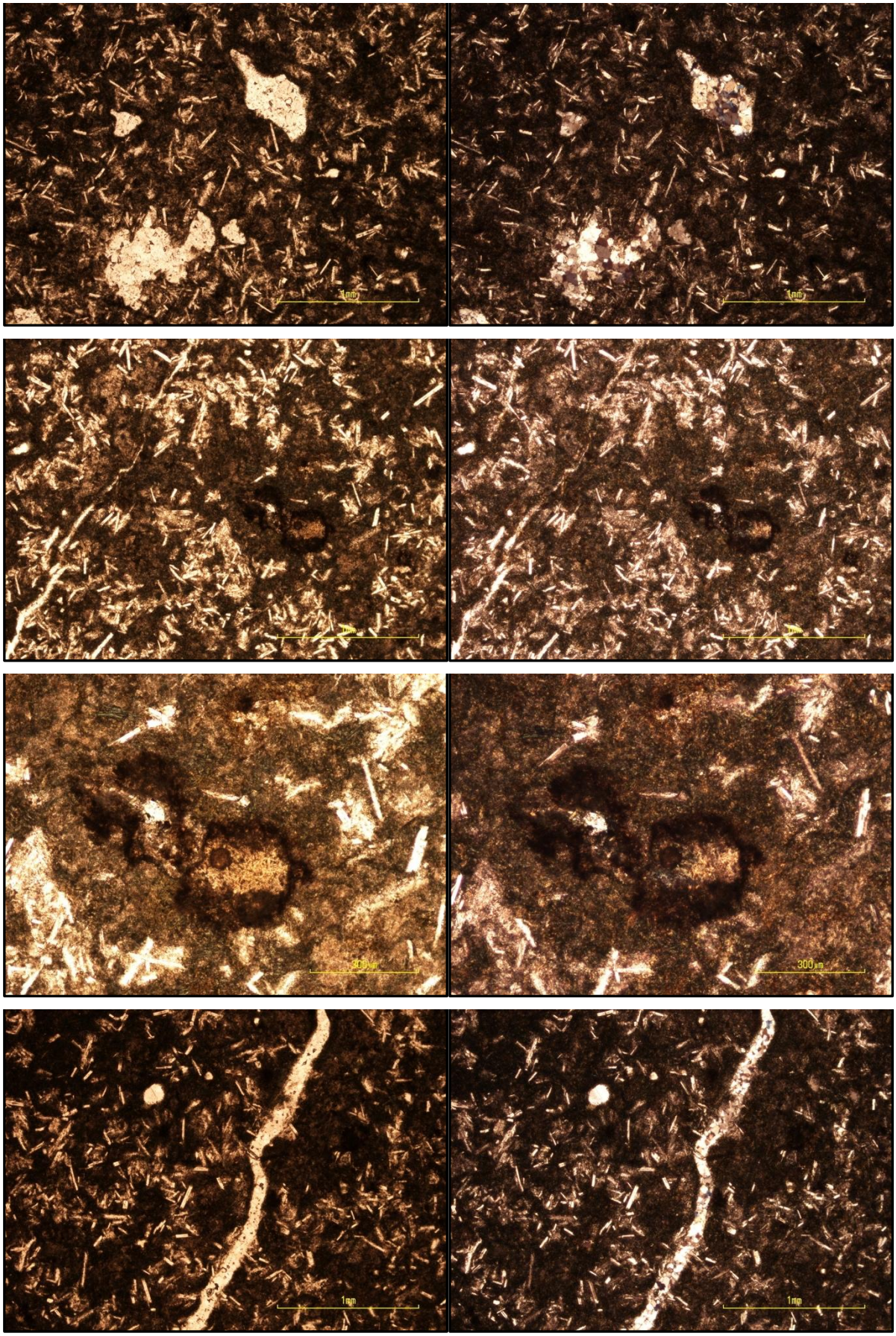

The Loskop Dam Sampling Site

The Damwal Formation:

RL 1 [25°23'44,0" S; 29°30'30,5" E]:

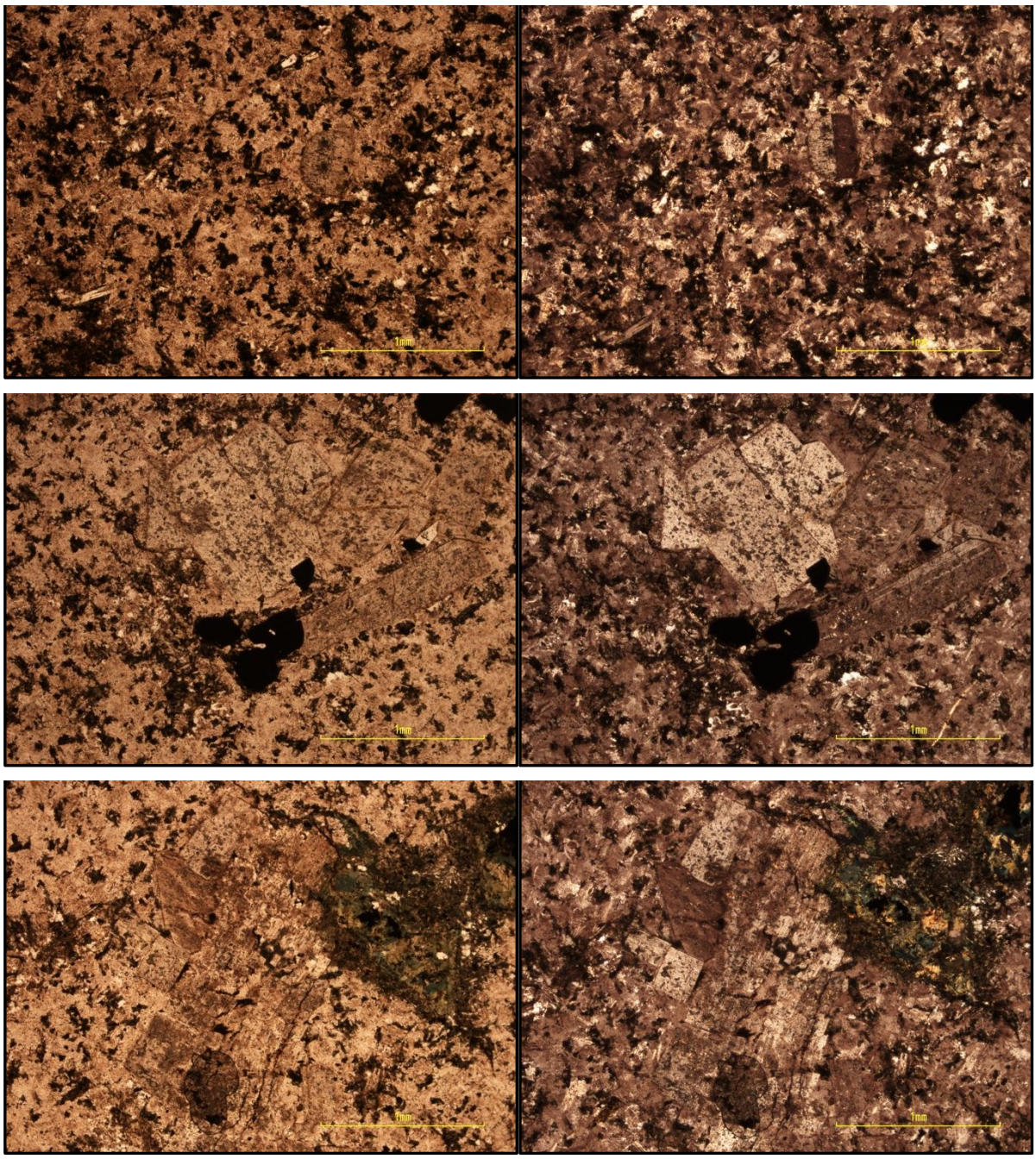

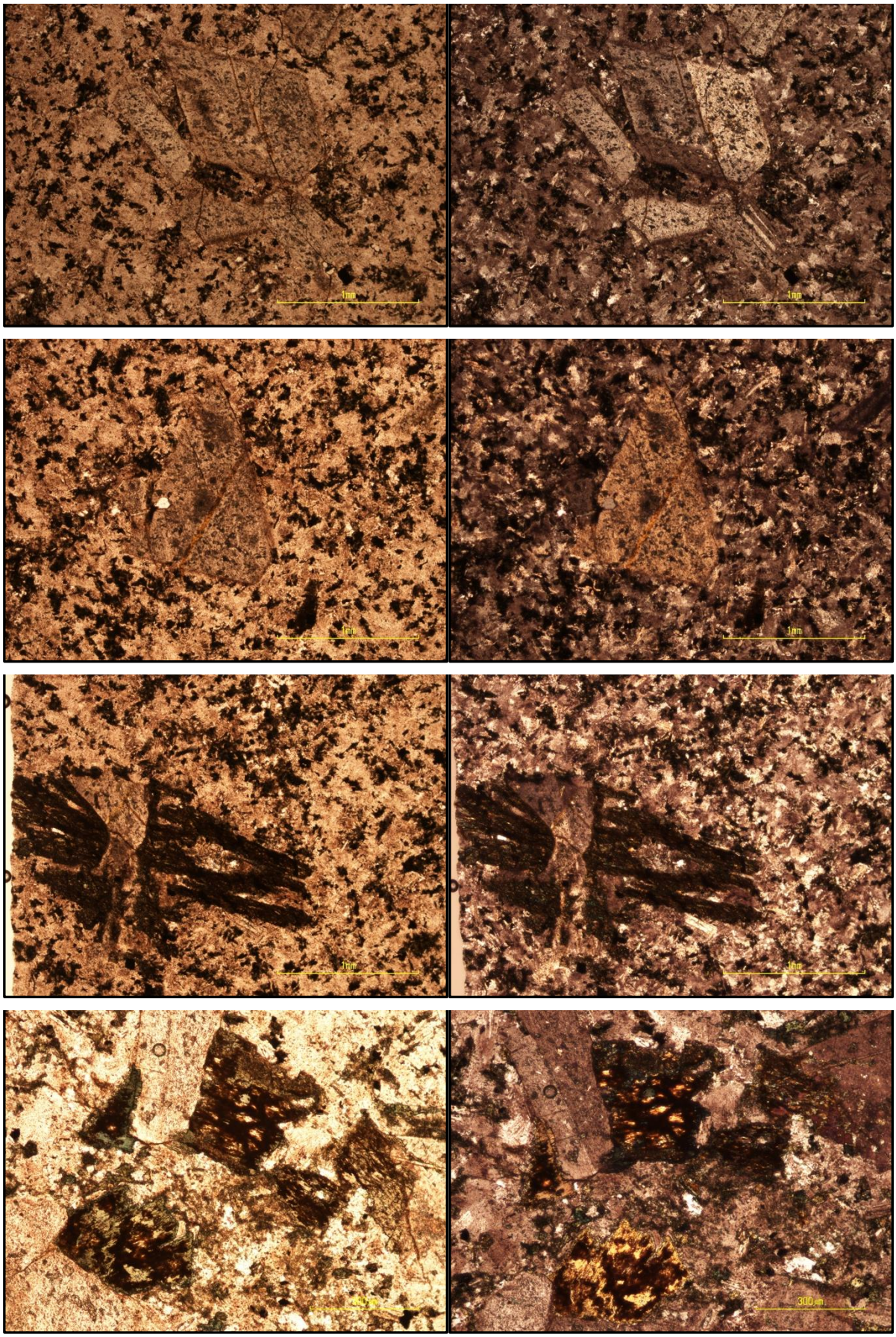

LD 021 [25°24'55,1" S; 29°22'09,4" E]:

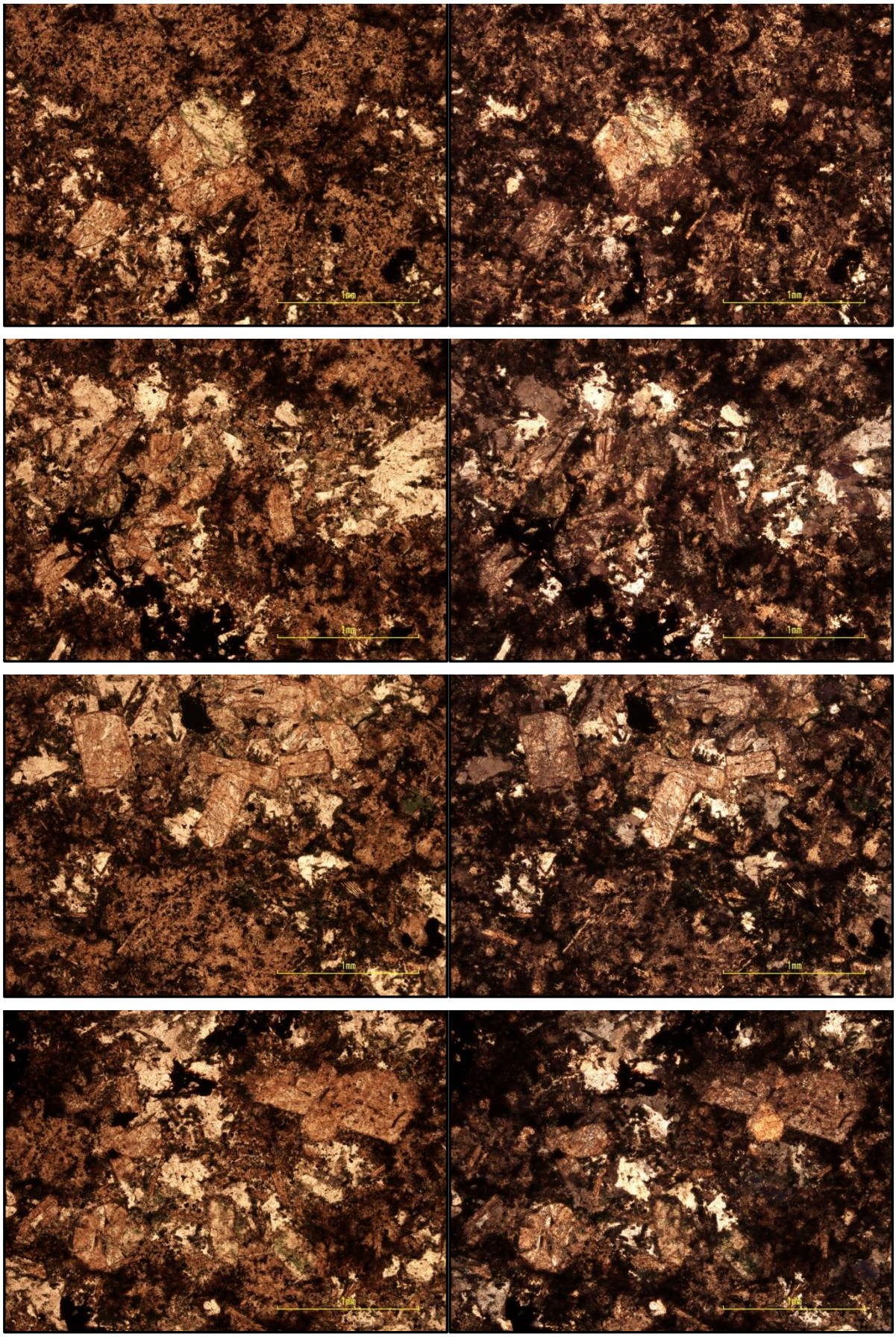

The Kwaggasnek Formation

LD 002 [25°25'16,6" S; 29°22'59,9" E]:

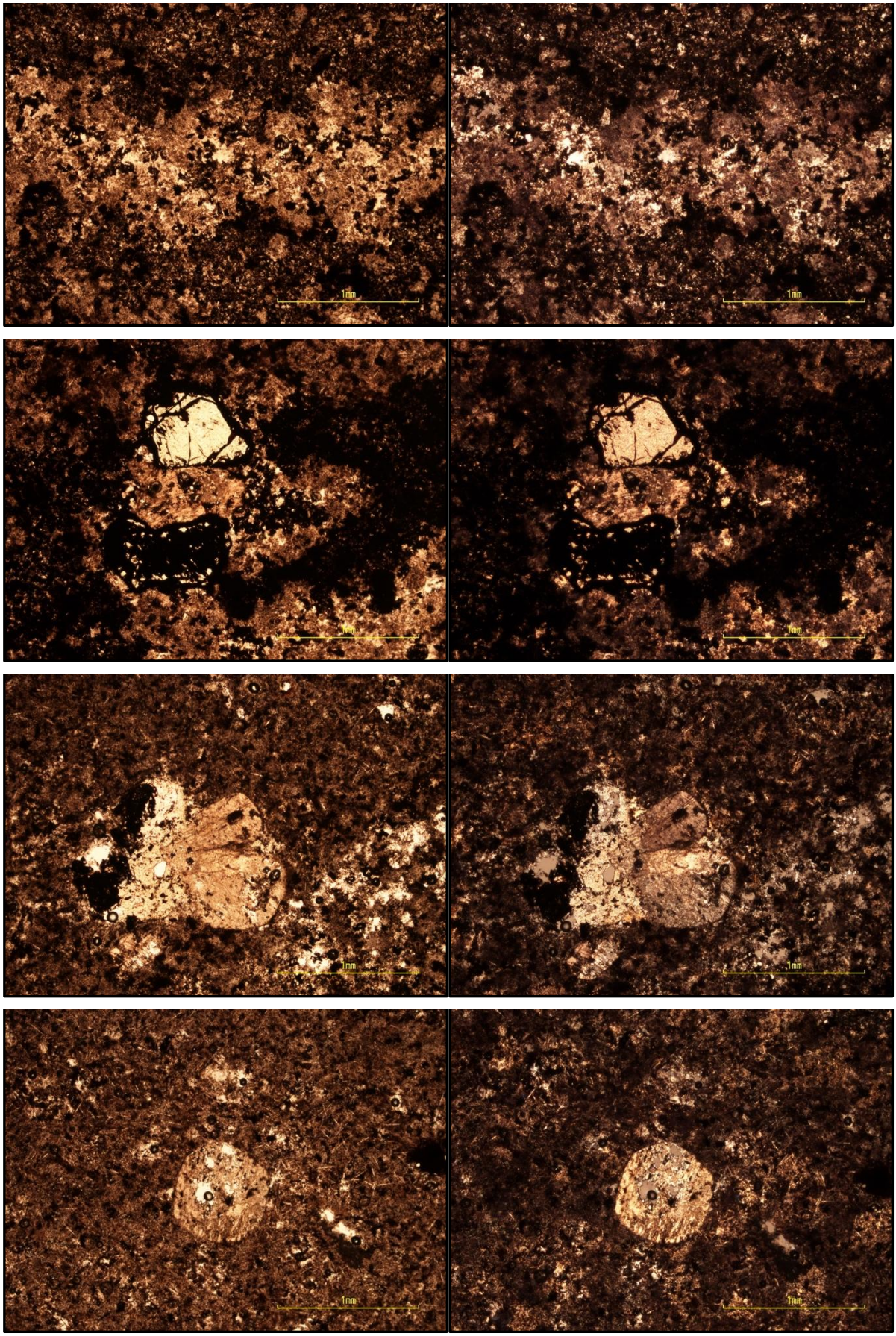

LD 004 [25°25'14,0" S; 29°22'59,9" E]:

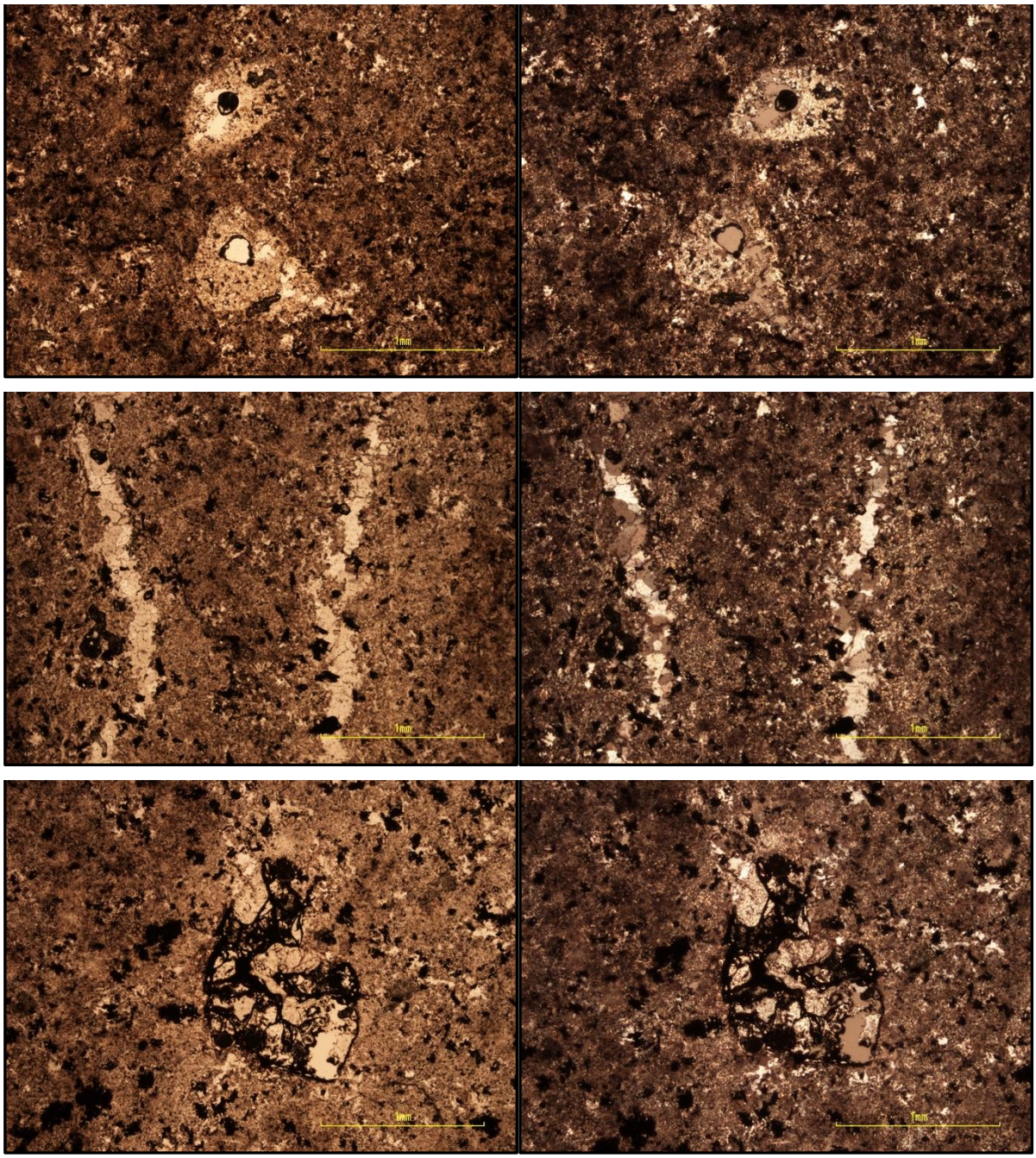

The Schrikkloof Formation

SM 28.1 [25°25'07,0" S; 29°31'32,1" E]:

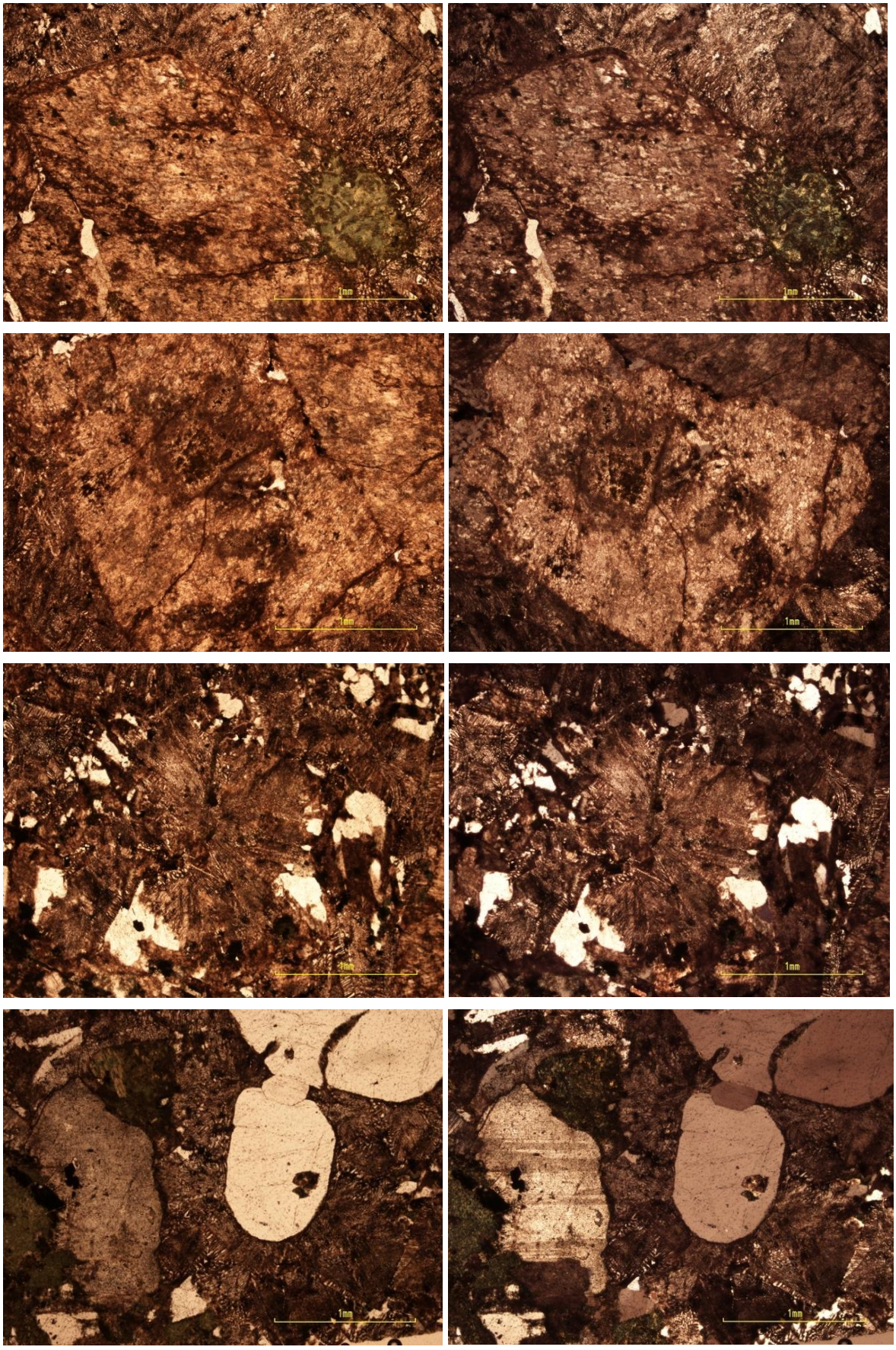

The Kuthaba Bush Lodge Sampling Site

The Schrikkloof Formation

KT 9 [24°36'30,8" S; 28°26'00,4" E]:

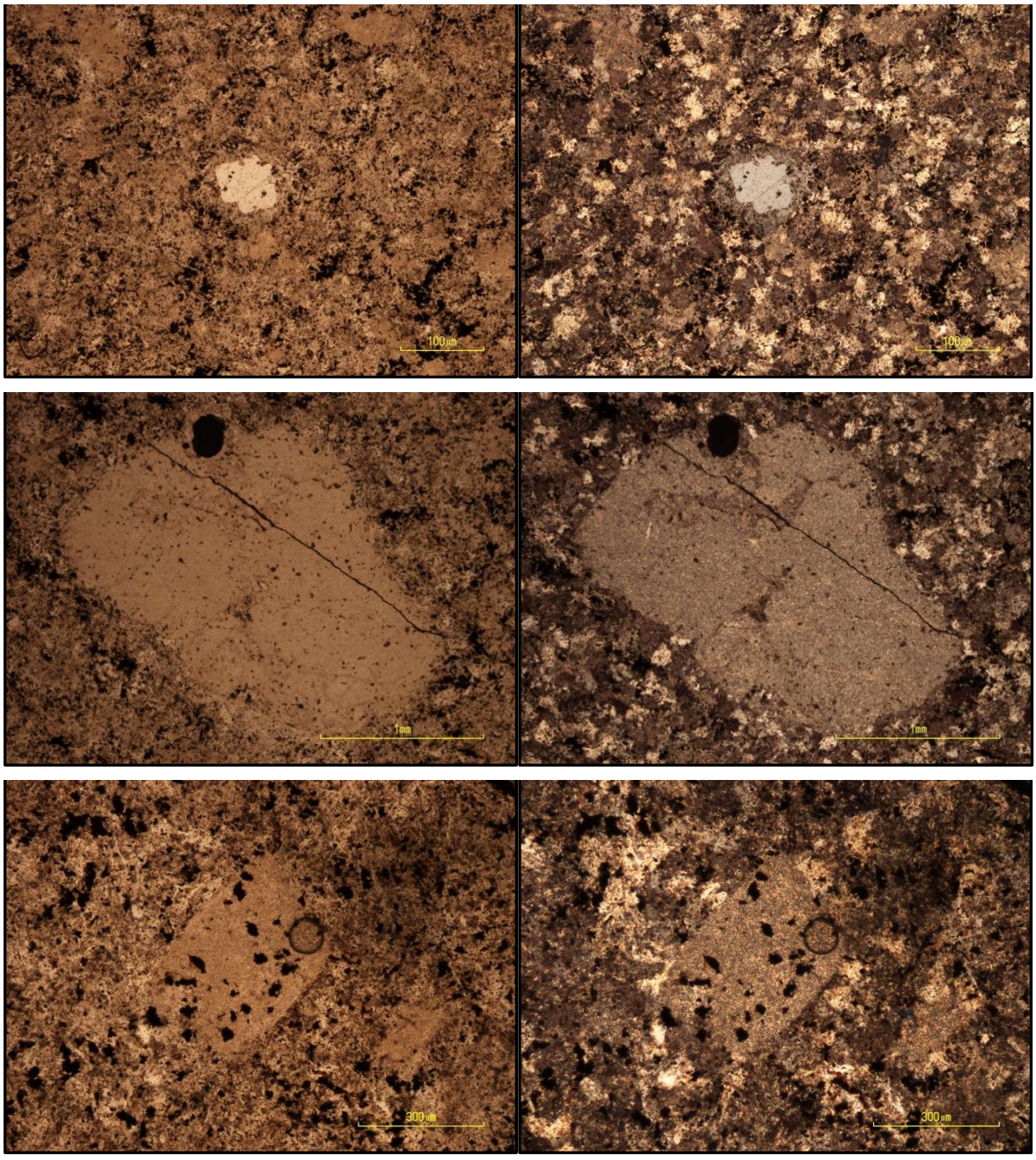

KT 53 [24°36'14,9" S; 28°25'53,9" E]:

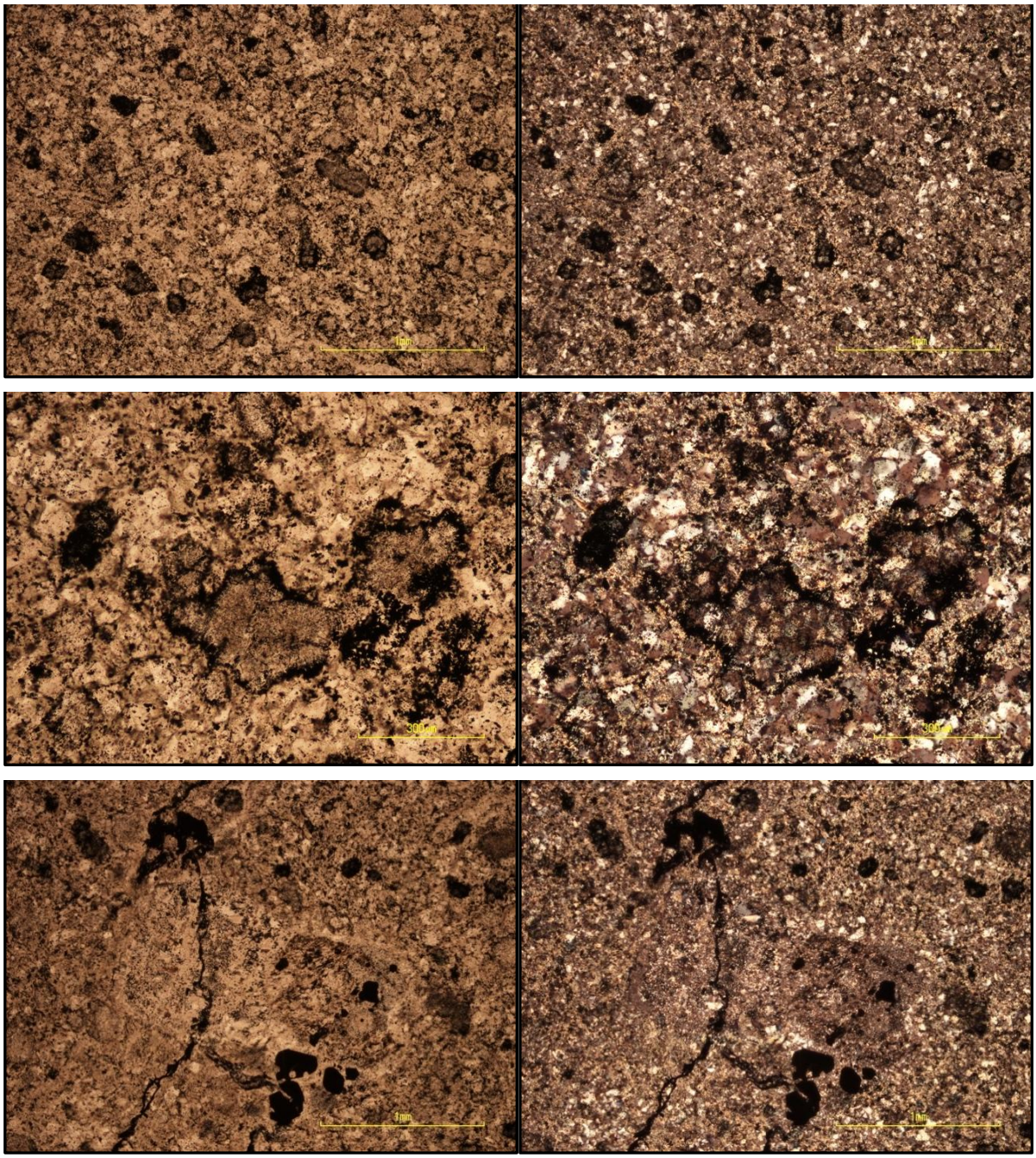

KT 57 [24°36'30,2" S; 28°25'38,5" E]:

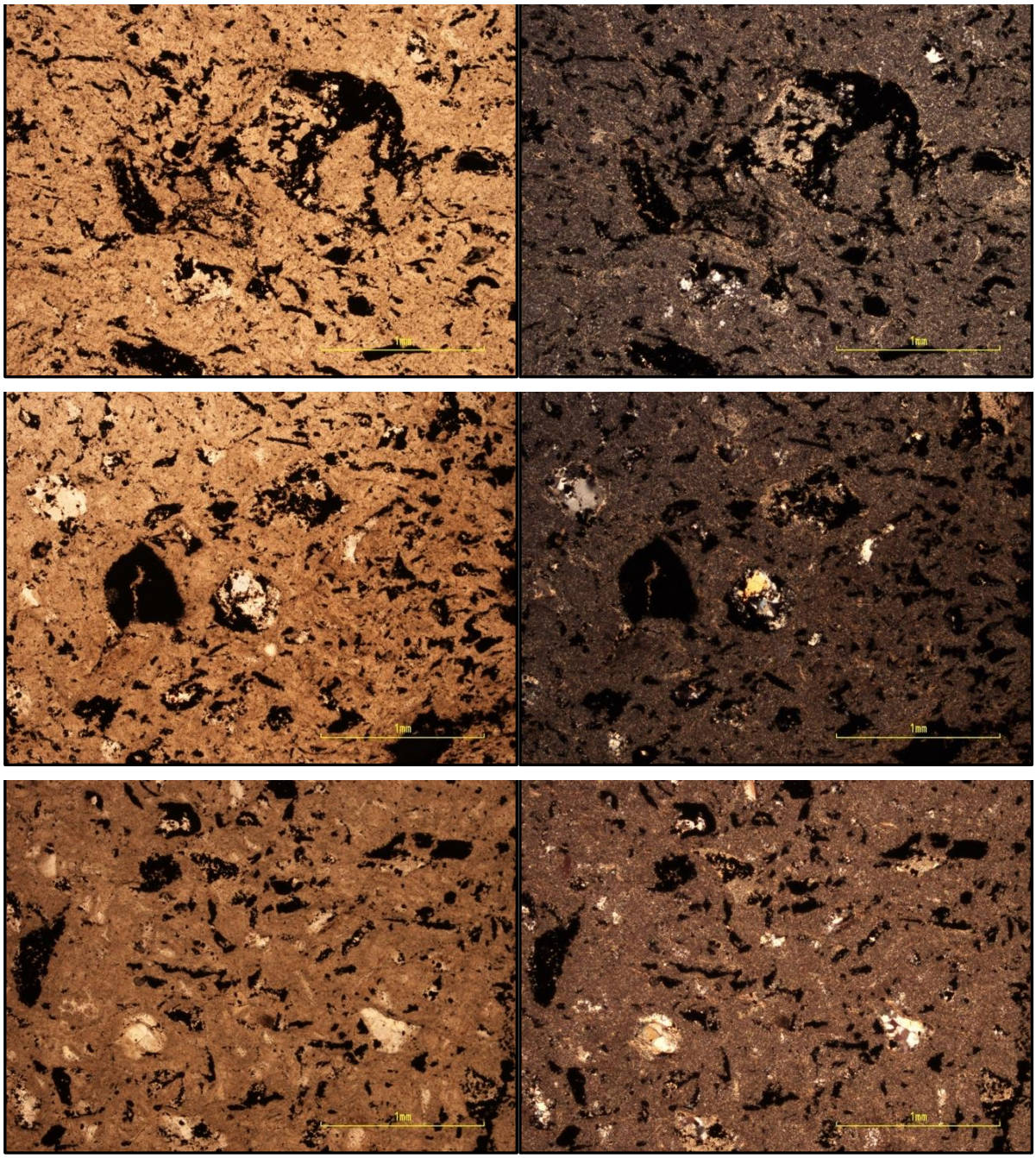

KT 201 [24°34'13,8" S; 28°26'18,1" E]:

KT 202.1 [24°34'6,9" S; 28°26'44,9" E]:

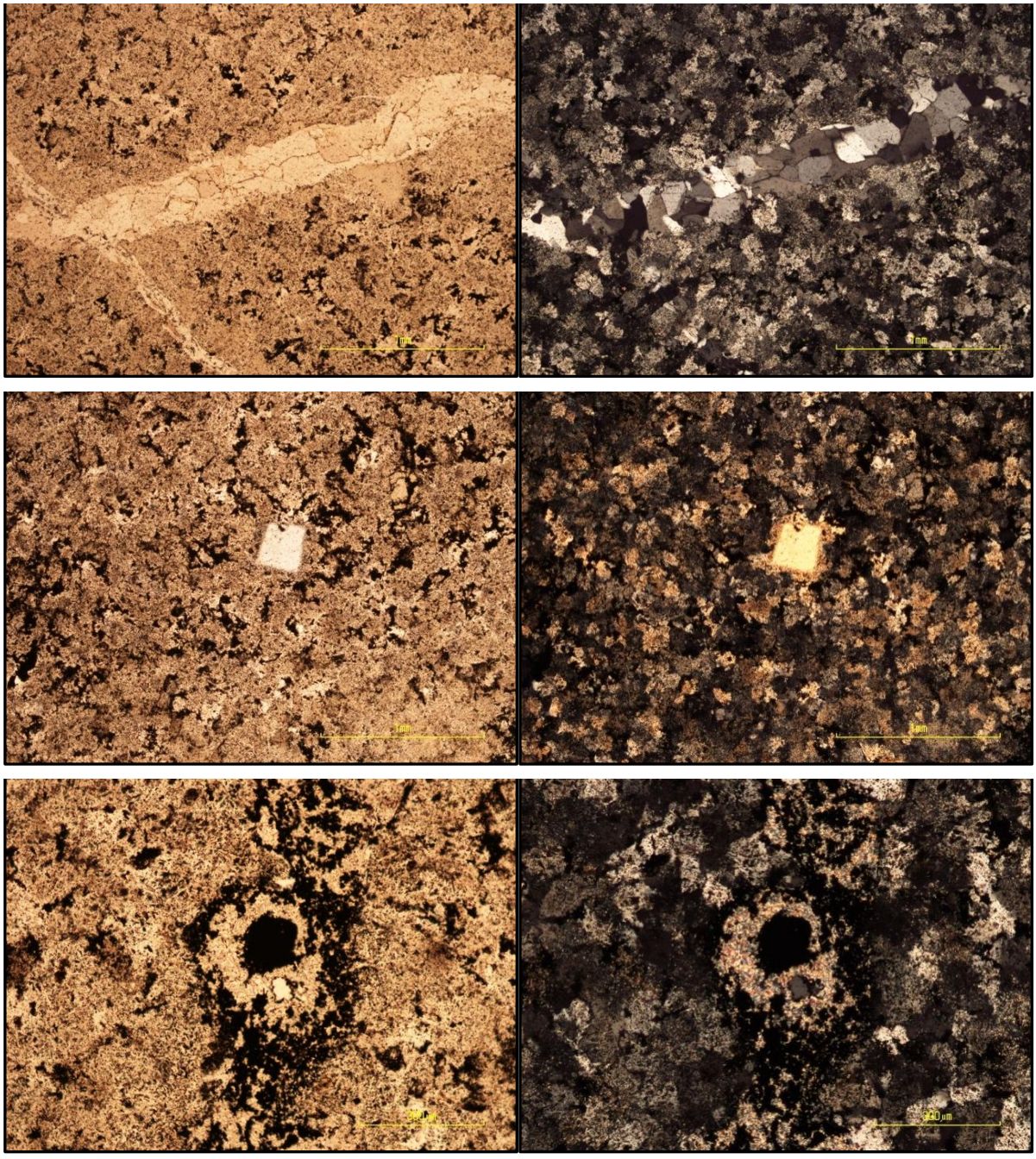

KT 210 [24°34'40,7" S; 28°27'17,5" E]:

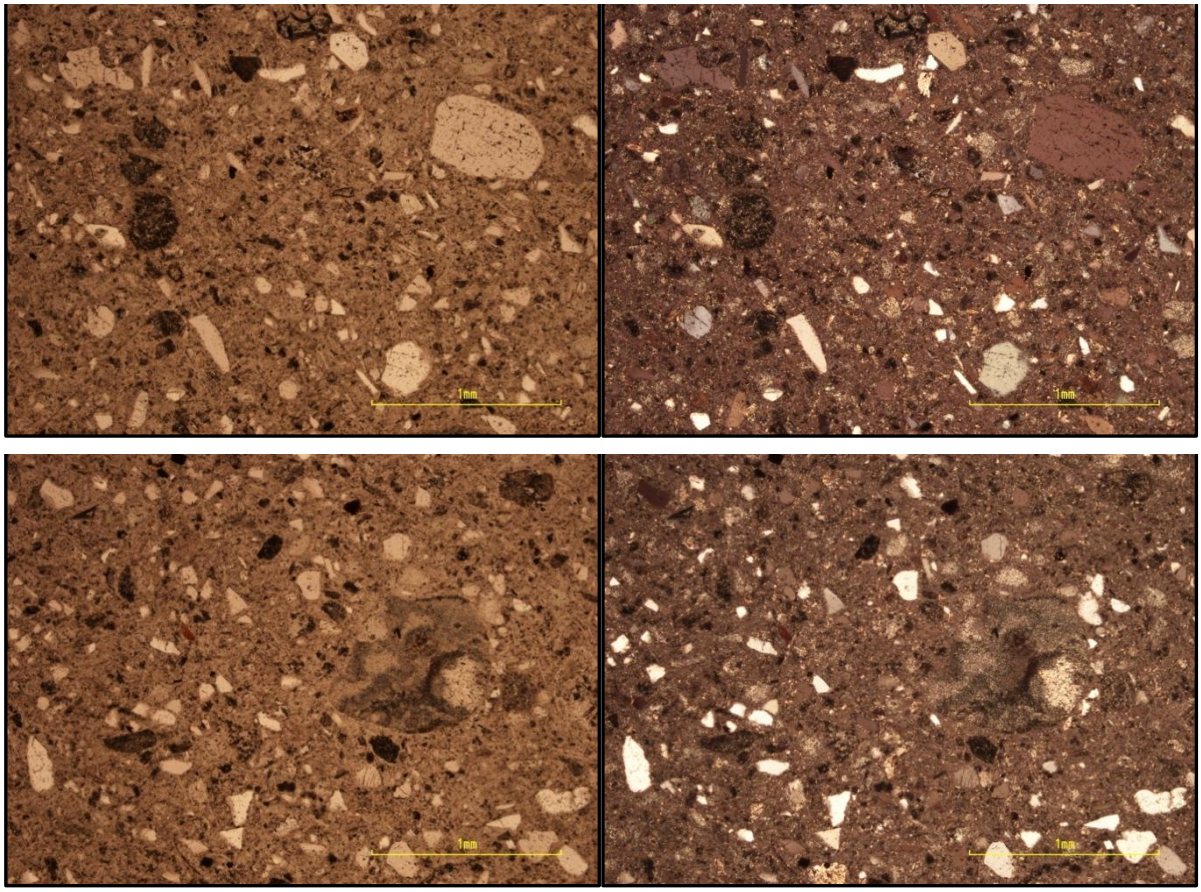

KTP 2 [24°36'31,7" S; 28°25'52,3" E]:

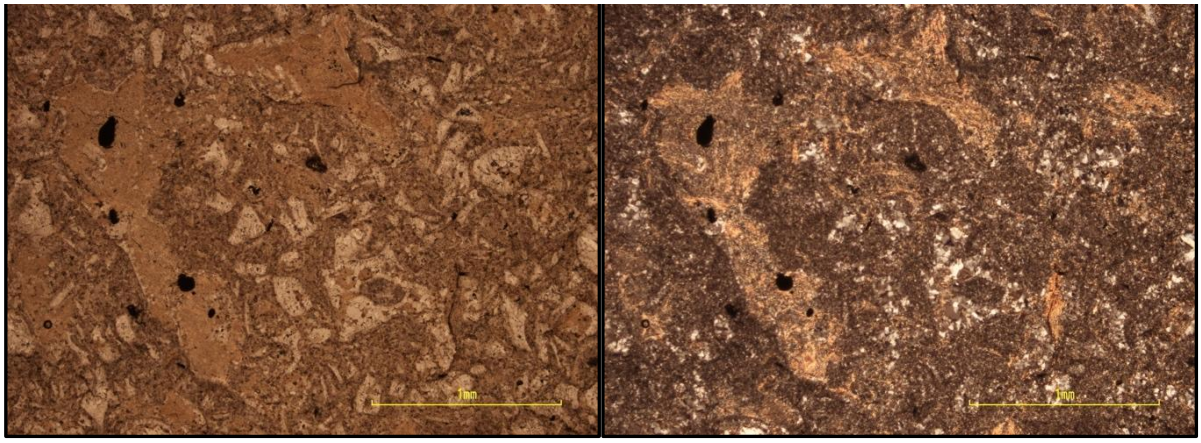

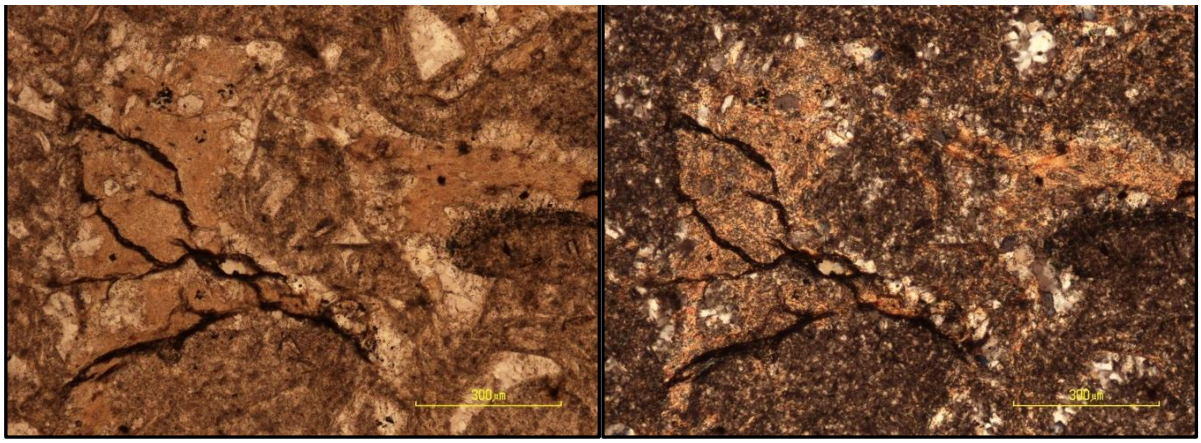

PYR 1A [24°36'31,6" S; 28°25'51,9" E]:

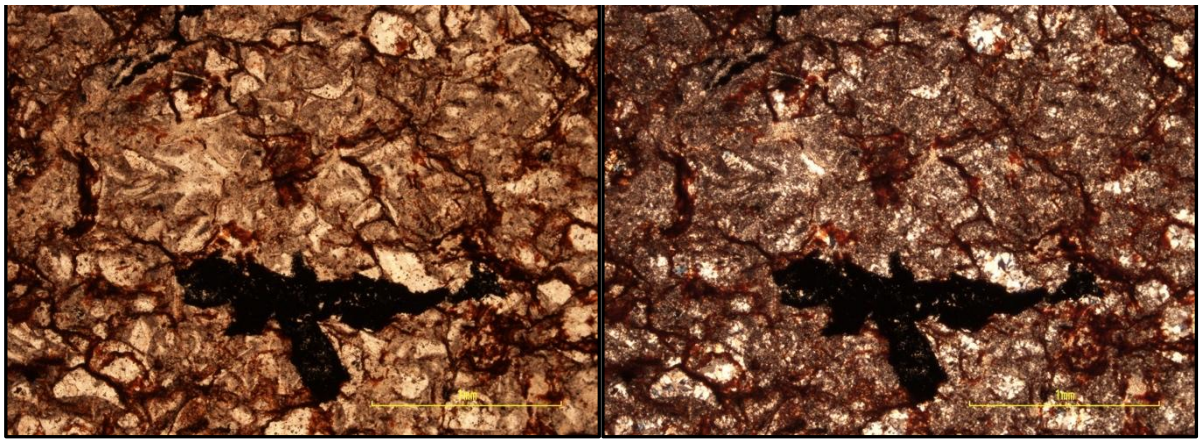

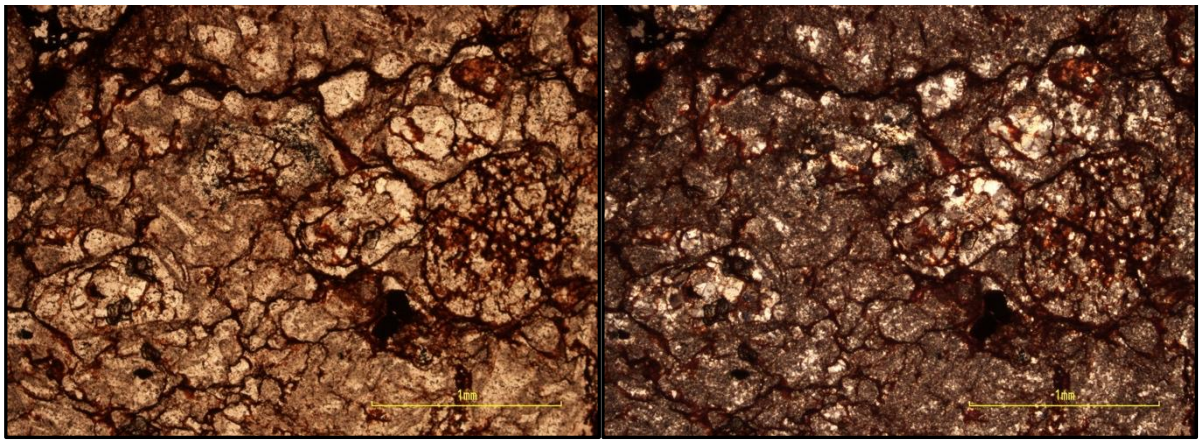

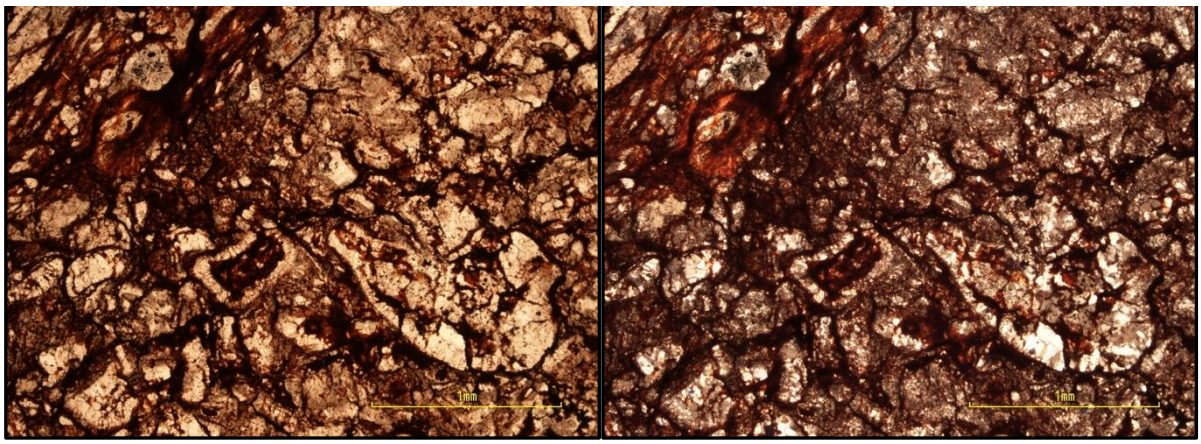

Sample PYR 1B [24°36'31,6" S; 28°25'51,9" E]:

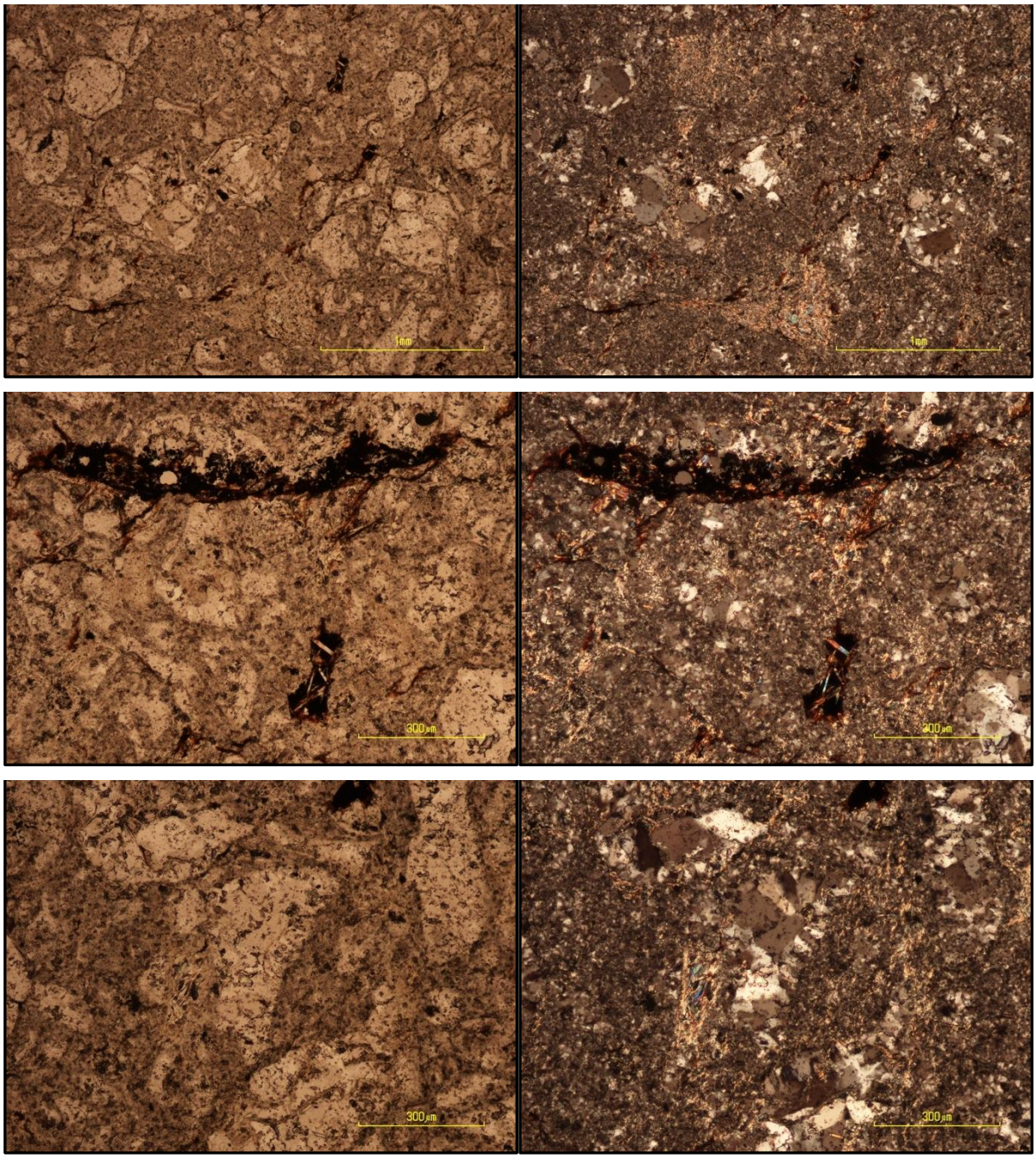

PYR 2 [24°36'32,2" S ; 28°25'53,0" E]:

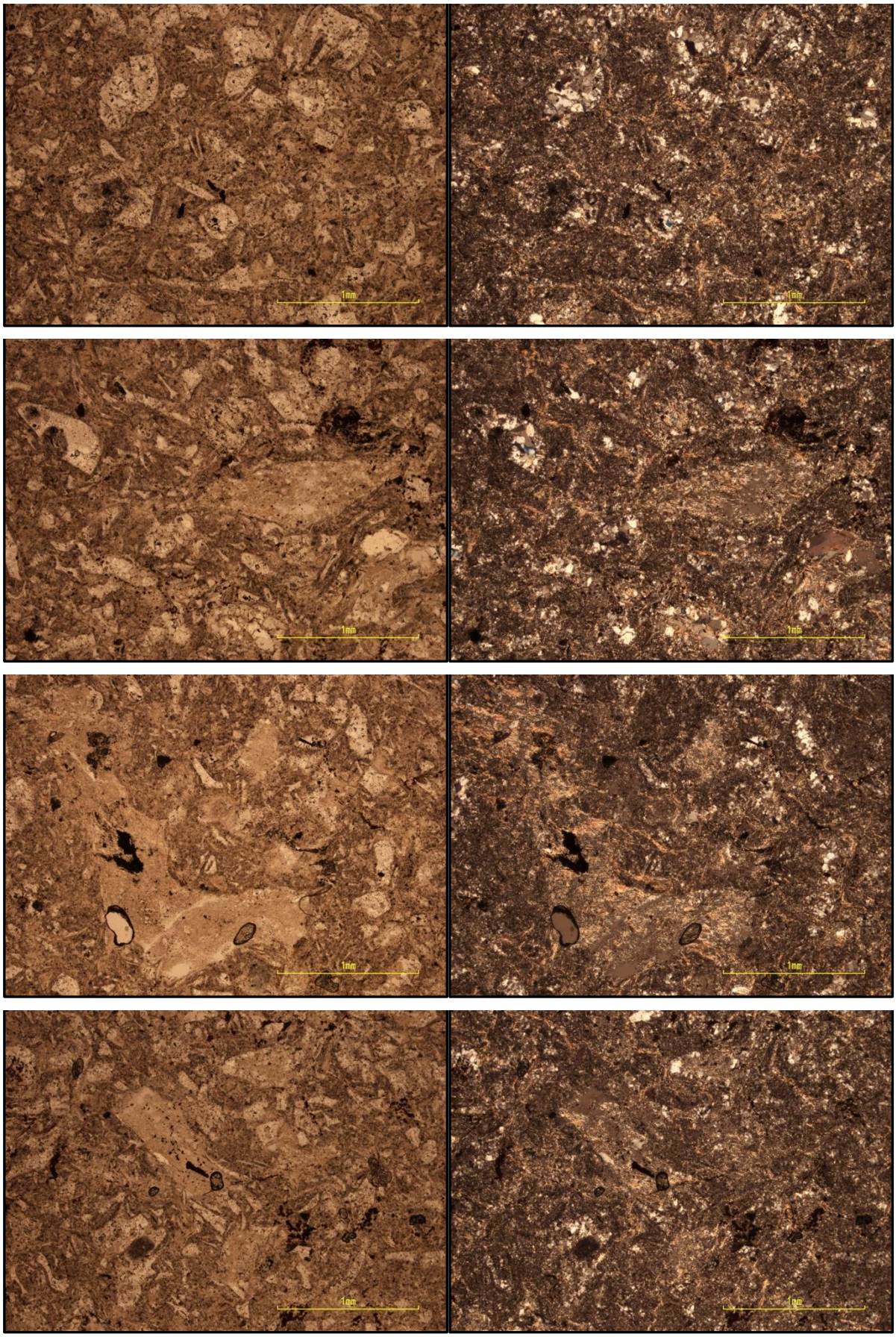

Appendix B

Raw data of the GSD plagioclase diameter sizes

No.	Rock Sample	Formation	Latitude	Longitude	Sam Regi	Thin	#	Plag length (mm)	Plag width (mm)	Plag width (um)
1	RG 7	Dullstroom	S 25°23'02.0"	E 29°58'54,2"	Dullstroom	1	1	0,148	0,052	52
2						7	1	0,127	0,029	29
3							2	0,088	0,023	23
4							3	0,087	0,027	27
5						8	1	0,124	0,031	31
6							2	0,096	0,031	31
7							3	0,1	0,027	27
8							4	0,114	0,027	27
9							5	0,09	0,03	30
10	RG 46	Dullstroom	S 25°23'53.3"	E 30°00'37.1"	Dullstroom	1	1	0,09	0,027	27
11							2	0,247	0,02	20
12							3	0,106	0,023	23
13							4	0,18	0,021	21
14							5	0,067	0,034	34
15							6	0,082	0,022	22
16							7	0,078	0,021	21
17							8	0,135	0,023	23
18							9	0,094	0,013	13
19							10	0,053	0,015	15
20						5	1	0,139	0,02	20
21							2	0,101	0,023	23
22							3	0,112	0,018	18
23							4	0,06	0,031	31
24							5	0,04	0,026	26
25							6	0,121	0,027	27
26							7	0,13	0,013	13
27							8	0,075	0,018	18
28							9	0,11	0,029	29
29						19	1	0,073	0,018	18
30							2	0,155	0,017	17
31							3	0,061	0,008	8
32							4	0,113	0,013	13
33							5	0,104	0,018	18
34							6	0,111	0,02	20
35						23	1	0,13	0,013	13
36							2	0,066	0,024	24
37							3	0,04	0,017	17
38							4	0,142	0,018	18
39							5	0,08	0,013	13
40							6	0,029	0,016	16
41							7	0,069	0,012	12
1	LD 021	Damwal	S 25°24'55,1"	E 29°22'09,4"	Loskop Dam	2	1	0,387	0,214	214
2							2	0,765	0,186	186
3							3	0,934	0,278	278
4							4	0,336	0,064	64
5							5	0,096	0,038	38

6						5	1	0,375	0,129	129
7							2	0,223	0,032	32
8						10	1	0,602	0,242	242
9							2	0,383	0,081	81
10							3	0,235	0,108	108
11							4	0,216	0,127	127
12							5	0,299	0,145	145
13						16	1	0,563	0,249	249
14						22	1	0,407	0,248	248
15							2	0,636	0,231	231
16							3	0,518	0,364	364
17							4	0,183	0,048	48
18						24	1	0,623	0,404	404
19							2	0,215	0,114	114
20							3	0,232	0,119	119
21							4	0,238	0,115	115
22							5	0,191	0,141	141
23							6	0,216	0,132	132
24							7	0,293	0,162	162
25						27	1	0,481	0,115	115
26							2	0,2	0,16	160
27						32	1	0,422	0,171	171
28							2	0,475	0,235	235
29							3	0,143	0,065	65
30						35	1	1,133	0,444	444
31							2	0,306	0,184	184
32						42	1	1,774	0,472	472
33							2	0,32	0,172	172
34							3	0,64	0,273	273
35						43	1	0,521	0,163	163
36							2	0,401	0,168	168
37							3	0,435	0,163	163
38							4	0,51	0,315	315
39						51	1	0,536	0,229	229
40							2	0,553	0,354	354
41							3	0,581	0,157	157
42							4	0,354	0,164	164
43	RL 1	Damwal	S 25°23'44,0"	E 29°30'30,5"	Loskop Dam	2	1	0,943	0,516	516
44							2	0,837	0,465	465
45							3	1,278	0,297	297
46							4	0,435	0,308	308
47						9	1	0,253	0,158	158
48							2	0,529	0,257	257
49							3	0,324	0,196	196

50							4	0,275	0,232	232
51						13	1	0,988	0,605	605
52							2	0,321	0,192	192
53							3	0,494	0,264	264
54						16	1	0,75	0,226	226
55							2	0,709	0,334	334
56							3	0,97	0,862	862
57						37	1	0,212	0,047	47
58							2	0,4	0,291	291
59						45	1	0,649	0,105	105
60						50	1	1,124	0,437	437
61							2	0,793	0,257	257
62							3	0,499	0,194	194
63							4	0,524	0,281	281
64						70	1	0,671	0,365	365
65							2	0,862	0,422	422
66							3	1,958	0,503	503
67						78	1	0,648	0,331	331
68							2	0,165	0,046	46
69							3	0,156	0,083	83
70						81	1	0,94	0,129	129
71							2	0,349	0,178	178
72							3	0,522	0,177	177
1	LD 002	Kwaggasnek	S 25°25'16,6"	E 29°22'59,9"	Loskop Dam	5	1	0,37	0,174	174
2						15	1	0,632	0,261	261
3						17	1	0,788	0,369	369
4						23	1	0,577	0,337	337
5						25	1	0,407	0,287	287
6							2	0,566	0,226	226
7							3	0,616	0,222	222
8							4	0,448	0,256	256
9						28	1	0,53	0,337	337
10							2	0,726	0,547	547
11						30	1	0,924	0,429	429
12						35	1	1,288	0,774	774
13						42	1	0,369	0,279	279
14	LD 004	Kwaggasnek	S 25°25'14,0"	E 29°22'59,9"	Loskop Dam	1	1	1,833	0,635	635
15						11	1	1,234	0,328	328
1	SM 28.1	Schrikkloof	S 25°25'07,0"	E 29°31'32,1"	Loskop Dam-Selons Rivier Region	6	1	0,794	0,358	358
2						20	1	2,681	1,902	1902
3						24	1	2,255	1,02	1020
4						30	1	0,829	0,604	604
5							2	0,211	0,083	83

6						32	1	0,98	0,734	734
7						39	1	2,574	1,862	1862
8						41	1	0,926	0,517	517
9							2	0,265	0,137	137
10						43	1	1,774	1,219	1219
11							2	0,473	0,294	294
12						47	1	1,151	0,475	475
13						52	1	1,542	0,73	730
14							2	0,702	0,437	437
15	KTP 2	Schrikkloof	S 24°36'31,7"	E 28°25'52,3"	Kuthaba Lodge	1	1	0,388	0,114	114
16							2	0,166	0,062	62
17						10	1	0,291	0,109	109
18							2	0,455	0,174	174
19						16	1	0,21	0,048	48
20							2	0,129	0,028	28
21						20	1	0,678	0,351	351
22							2	0,16	0,059	59
23	KT 9	Schrikkloof	S 24°36'30,8"	E 28°26'00,4"	Kuthaba Lodge	9	1	2,226	1,48	1480
24						10	1	0,615	0,37	370
25						12	1	2,077	1,377	1377
26							2	0,496	0,136	136
27						17	1	1,317	0,115	115
28							2	0,284	0,134	134
29	KT 53	Schrikkloof	S 24°36'14,9"	E 28°25'53,9"	Kuthaba Lodge	3	1	1,192	0,544	544
30						7	1	1,979	1,081	1081
31						12	1	0,262	0,129	129
32						13	1	1,817	0,946	946
33						19	1	0,239	0,215	215
34							2	0,397	0,32	320
35	KT 57	Schrikkloof	S 24°36'30,2"	E 28°25'38,5"	Kuthaba Lodge	9	1	0,366	0,259	259
36						11	1	0,37	0,269	269
37							2	0,224	0,16	160
38						17	1	0,909	0,412	412
39						19	1	0,255	0,136	136
40						21	1	1,606	0,477	477
41						26	1	0,674	0,394	394
42						27	1	1,207	0,492	492
43						30	1	0,355	0,302	302
44							2	0,216	0,109	109
45							3	0,541	0,384	384
46							4	0,42	0,316	316
47						32	1	0,344	0,161	161
48						33	1	0,386	0,263	263
49							2	0,803	0,462	462

50							3	0,824	0,549	549
51						34	1	0,675	0,285	285
52							2	0,178	0,101	101
53							3	0,11	0,074	74
54	KT 201	Schrikkloof	S 24°34'13,8"	E 28°26'18,1"	Kuthaba Lodge	2	1	0,213	0,137	137
55						7	1	1,739	1,624	1624
56						10	1	2,541	1,266	1266
57							2	0,625	0,469	469
58						14	1	0,821	0,699	699
59						16	1	1,602	1,138	1138
60	KT 202.1	Schrikkloof	S 24°34'6,9"	E 28°26'44,9"	Kuthaba Lodge	17	1	0,401	0,358	358
61						19	1	0,406	0,275	275
62	KT 210	Schrikkloof	S 24°34'40,7"	E 28°27'17,5"	Kuthaba Lodge	1	1	0,61	0,4	400
63							2	0,231	0,14	140
64							3	0,338	0,1	100
65							4	0,251	0,233	233
66							5	0,203	0,071	71
67							6	0,159	0,035	35
68							7	0,106	0,044	44
69							8	0,116	0,045	45
70						13	1	0,376	0,201	201
71							2	0,125	0,082	82
72							3	0,183	0,122	122
73							4	0,119	0,086	86
74						15	1	0,301	0,128	128
75							2	0,163	0,057	57
76							3	0,265	0,131	131
77							4	0,093	0,057	57
78							5	0,071	0,038	38
79							6	0,177	0,101	101
80						17	1	0,207	0,13	130
81							2	0,099	0,031	31
82							3	0,106	0,045	45
83							4	0,161	0,079	79
84							5	0,137	0,057	57
85						19	1	0,215	0,089	89
86							2	0,3	0,102	102
87							3	0,153	0,071	71
88							4	0,146	0,036	36
89							5	0,235	0,039	39
90							6	0,198	0,08	80
91						20	1	0,453	0,105	105
92							2	0,147	0,05	50
93							3	0,181	0,072	72

94							4	0,109	0,038	38
95						26	1	0,286	0,082	82
96							2	0,172	0,039	39
97							3	0,145	0,04	40
98							4	0,135	0,023	23
99							5	0,191	0,065	65
100						28	1	0,521	0,375	375
101							2	0,212	0,103	103
102							3	0,204	0,077	77
103							4	0,199	0,081	81
104							5	0,098	0,034	34
105	PYR 1A	Schrikkloof	S 24°36'31,6"	E 28°25'51,9"	Kuthaba Lodge	15	1	0,295	0,197	197
106							2	0,281	0,099	99
107							3	0,285	0,128	128
108						17	1	0,328	0,178	178
109	PYR 1B	Schrikkloof	S 24°36'31,6"	E 28°25'51,9"	Kuthaba Lodge	1	1	0,531	0,123	123
110							2	0,235	0,058	58
111							3	0,33	0,093	93
112						22	1	0,461	0,281	281
113							2	0,175	0,053	53
114						29	1	0,258	0,069	69
115							2	0,208	0,124	124
116							3	0,133	0,037	37
117	PYR 2	Schrikkloof	S 24°36'32,2"	E 28°25'53,0"	Kuthaba Lodge	3	1	0,879	0,221	221
118							2	0,21	0,1	100
119							3	0,195	0,063	63
120							4	0,217	0,105	105
121						5	1	0,329	0,07	70
122							2	0,171	0,105	105
123						7	1	0,407	0,175	175
124							2	0,162	0,08	80
125							3	0,156	0,051	51
126							4	0,238	0,106	106
127						9	1	0,271	0,201	201
128							2	0,234	0,035	35
129							3	0,278	0,095	95
130						21	1	0,991	0,327	327
131							2	0,184	0,071	71